SOME STUDIES ON HEAT TRANSFER IN CIRCULATING FLUIDIZED BEDS

MD. NAWSHER ALI MORAL

SOME STUDIES ON HEAT TRANSFER IN CIRCULATING FLUIDIZED BEDS

Thesis submitted in partial fulfilment of
the requirements for the degree

of

DOCTOR OF PHILOSOPHY
IN
ENGINEERING

BY
MD. NAWSHER ALI MORAL

Under the guidance of
PROF. P. K. NAG

DEPARTMENT OF MECHANICAL ENGINEERING
INDIAN INSTITUTE OF TECHNOLOGY
KHARAGPUR, INDIA
DECEMBER, 1990

CERTIFICATE

This is to certify that the thesis entitled "SOME STUDIES ON HEAT TRANSFER IN CIRCULATING FLUIDIZED BEDS", submitted by Mr. Md. Nawsher Ali Moral for the award of the degree of Doctor of Philosophy in Engineering to the Indian Institute of Technology, Kharagpur, is a record of bonafide work carried out by him under my supervision and guidance. The thesis has fulfilled the requirements according to the regulations of this Institute and in my opinion, has reached the necessary standard for submission. The results, embodied in this thesis, have not been submitted to any other University or Institute for award of any degree or diploma.

(Dr. P. K. Nag)
Professor

Mechanical Engineering Department
Indian Institute of Technology,
Kharagpur - 721 302, INDIA

ACKNOWLEDGEMENT

I would like to express my sincere thanks to Prof. P.K. Nag, who inspite of having a tight and busy schedule found time to go through my work and guide me. His technical expertise, valuable suggestions, kind encouragement and unfailing help have inspired me a great deal and influenced the course of the investigation.

My thanks are extended to Prof. B.C. Majumdar, Head of Mechanical Engineering Department, who, allowed me to use all kinds of facilities for carrying out the work. I would like to thank Prof. S.K. Som for providing me all the facilities of Steam Laboratory.

I am grateful to Prof. P. Basu, Professor of Mechanical Engineering, TUNS, Halifax, Canada and Prof. A.S. Gupta, Professor of Mathematics, I.I.T. Kharagpur, India for their valuable suggestions to carry out my work.

I wish to express thanks to Mr. K.K. Chatterjee and other staff of Steam Laboratory for helping me in various stages of my investigation.

My appreciation is extended to the Government of India for awarding the scholarship and to Indian Institute of Technology (IIT) Kharagpur for providing facilities during my stay and study here.

Finally I thank the Government of Bangladesh and the authority of Bangladesh Institute of Technology (BIT) Khulna, Bangladesh to depute me for the period of study in India.

Date :

(Md. Nawsher Ali Moral)

CONTENTS

PREFACE

Circulating fluidized bed (CFB) is an essential mode of gas-solid contact with high gas-solid contact efficiency, high gas throughput and high flexibility of solid handling. In boiler technology CFB combustion is gradually getting more recognized and the capacity is approaching to large scale utility boilers. Pressurized CFB combustion programs are also in progress. Application of CFB concept to iron ore reduction is under progress in several countries. Several new catalytic processes are also under development. However, it is felt that CFB applications so far established are still in the primitive stage.

The rapid commercial success of this technology drew attention of many researchers. Since the commercialization of this process outpaced fundamental research, a number of important gaps in the understanding of this process remained. The lack of information in those areas inhibits an optimum exploitation of this technology. The present work is expected to be an attempt in this direction.

(Md. Nawsher Ali Moral)

LIST OF TABLES

LIST OF FIGURES

LIST OF PHOTOGRAPHS

NOMENCLATURE

A	cross-sectional area of fin, m^2
A_T	total heat transfer area, m^2
A_F	area of fins, m^2
A_{UF}	area of unfinned surface, m^2
A_b	cross-sectional area of the bed, m^2
A_{ht}	area of heat exchange surface, m^2
A_{sb}	cross-sectional area of slow bed, m^2
A_1	cross-sectional area of pipe at upstream, m^2
A_2	cross-sectional area of pipe at down stream, m^2
A_p	area of packet, m^2
$A_o, A_1,$	constants
a, b, c	constants
B_o, B_1	constants
c_{pg}	specific heat of gas, kJ/kg K
c_{ps}	specific heat of solid particle, kJ/kg K
c_c	specific heat of cluster, kJ/kg K
c_D	valve aperture discharge coefficient
c	coefficient of discharge
d	diameter of pin fin, m
d_b, D	bed diameter, m
$d_p, \bar{d}_p$	mean particle size, m
d_o	diameter of orificemeter, m
D_b	bubble diameter, m

D_c	cluster diameter, m
D_i	diameter of dilute core, m
D_T	diameter of immersed tube, m
D_l	diameter of high pressure tapping, m
e_g	gas emissivity
e_p	particle emissivity
e_w	wall emissivity
e'	effective emissivity
E	velocity of approach factor, $\frac{1}{(1 - m^2)^{1/2}}$
E_h	entrainment flux at a height h above dilute / dense interface, kg/m^2s
E_o	entrainment flux at dense bed surface (dense/ dilute interface), kg/m^2s
E_α	entrainment flux above TDH , kg/m^2s
f_p	solid friction factor
f_g	gas friction factor
F_{p-w}	particle-to-wall view factor
g	acceleration due to gravity, $9.81\ m/s^2$
G_s, G	solid circulation rate, kg/m^2s
h, h_o	average overall heat transfer coefficient, W/m^2K
h_E	equivalent heat transfer coefficient, W/m^2K
h_W	wall heat transfer coefficient, W/m^2K
h_t	heat transfer coefficient between fin tip and surrounding emulsion, $W/m^2\ K$
h_H	homogeneous heat transfer coefficient, W/m^2K
h_r	radiative heat transfer coefficient, W/m^2K
h_e	experimental heat transfer coefficient, W/m^2K
h_T	predicted heat transfer coefficient, W/m^2K

h_L	heat transfer coefficient for lean phase, W/m^2K
h_D	heat transfer coefficient for dense phase, W/m^2K
h_{gc}	heat transfer coefficient for gas convection, W/m^2K
h_{wp}	wall heat transfer coefficient for packed bed, W/m^2K
h_{wb}	effective heat transfer coefficient of finned tube related to bare tube surface, W/m^2K
h_{wf}	total heat transfer coefficient for finned tube based on total area, W/m^2K
H	depth of packed bed, m
H_{mf}	bed height at minimum fluidization condition, m
Δh_o	pressure drop across the orificemeter, cm of water
Δh_L	pressure drop across the test section, cm of water
I	bed inventory, kg
I_1	solid inventory in dilute phase region, kg
I_2	solid inventory in the acceleration region, kg
I_3	solid inventory in the dense phase region, kg
I_{sb}	solid inventory in slow bed, kg
I	current, ampere
I	modified Bessel function
k	thermal conductivity of fin material, W/mK
k'	experimentally determined constant
k_a	apparent thermal conductivity of packed, bed, W/mK
k_c	thermal conductivity of cluster, W/mK

k_e	effective thermal conductivity of the homogeneous gas particle medium, W/mK
k_f	thermal conductivity of fluid, W/mK
k_g	thermal conductivity of gas, W/mK
k_s	thermal conductivity of solid, W/mK
k_{ew}	effective thermal conductivity of particle cluster near the wall W/mK
l_e	thickness of emulsion, m
l_g	gas layer thickness, m
L	height of fin from the wall, m
L_f, FL	length of fin, m
L_h	vertical height of heat transfer probe, m
L_m	distance between the pressure tappings across the test section, m
L_H	length of heater, m
L_s	static bed height, m
L_t	effective length of the test section, m
L_1	height of dilute phase region, m
L_3	height of dense phase region, m
L_{sb}	height of slow bed, m
L_h/D	dimensionless probe height
m_a	actual volume flow rate of air, m^3/s
m_1	ratio of orifice area to pipe area
m, m'	fin parameter
M_{SB}	mass of solids in slow bed, kg
M_{den}	mass of solids in dense phase region, kg
M_{dil}	mass of solids in dilute phase region, kg
M, N	dimensionless parameters

N_f, FN	number of fins
P	perimeter, m
Δp	pressure drop across the orifice meter, cm. of water
ΔP_{den}	pressure loss across the dense phase region, N/m^2
ΔP_{dil}	pressure loas across the dilute phase region, N/m^2
ΔP_R	pressure loss across the riser, W/m^2
ΔP_{cyc}	pressure loss across the primary cyclone, W/m^2
ΔP_v	pressure loss across the solids control valve, W/m^2
ΔP_{SB}	slow bed pressure loss, W/m^2
q"	heat flux, W/m^2
Q_T	total heat transfer, W
Q_F	heat transfer from finned surface, W
Q_{UF}	heat transfer from unfinned surface, W
r	radius of riser column, m
R_r	dimensionless radiation parameter
S	gap between the adjacent fins, m
t	thickness of fin, m
t_r	residence time, s
t_c	cluster residence time, s
T_b	bed temperature, K
T_s, T_w	surface or wall temperature, K
ΔT_f	temperature differential, K
U_o	superficial velocity, m/s

U_T	terminal velocity, m/s
U_p	particle velocity, m/s
U_g	gas velocity, m/s
U_f	interstitial gas velocity in dilute phase region (U_o/ε), m/s
U_{mf}	velocity at minimum fluidization, m/s
U_{mb}	velocity at minimum bubbling , m/s
U_{ms}	velocity at minimum slugging, m/s
U_{sr}	slug rise velocity, m/s
U_k	velocity corresponding to onset of turbulent fluidization, m/s
U_{tr}	transport velocity, m/s
V	voltage, volt
W_s	solid mass flux, kg/s
x_i	weight fraction of particles
x_c	fraction of wall surface covered by particle
x/L	dimensionless fin parameter
Z	a combined multiplier, product of Re, D and β

Dimensionless Groups

Ar	Archimedes number , $\rho_g(\rho_s - \rho_g) g d_p^3 / \mu_g^2$
Nu_e	experimental Nusselt number , $h_e d_p / kg$
Nu_T	predicted Nusselt number , $h_T d_p / kg$
$(Nu_p)_e$	experimental particle Nusselt number, $h_e d_p / kg$
$(Nu_p)_T$	predicted particle Nusselt number , $h_T d_p / kg$

Nu_{gc}	gas-particle Nusselt number, $h_{gc} d_p /kg$
Nu_{wp}	total Nusselt number, $d_p h_{wp} /kg$
Pr	Prandtl number, $\mu_g c_{pg} /kg$
Re	Reynolds number, $U_o d_p \rho_g /\mu_g$
Re_p	particle Reynolds number, $U_o d_p \rho_g /\mu g$
Re_{mf}	Reynolds number at minimum fluidization condition, $U_{mf} d_p \rho_g /\mu g$

Greek Letters

η_f	efficiency of fin
ρ_f, ρ_g	density of gas, kg/m^3
ρ_h	bed density at the fin tip, kg/m^3
ρ_s	density of solid, kg/m^3
$\bar{\rho}$	average suspension density, kg/m^3
ρ_{sus}	suspension density, kg/m^3
ρ_w	solid concentration at the wall, kg/m^3
ρ_e	density of emulsion, kg/m^3
ρ_c	density of cluster, kg/m^3
ρ_w	density of water, kg/m^3
ρ_a	density of air, kg/m^3
μ, μ_g, μ_f	viscosity of gas, kg/ms
ε	average voidage at a cross-section
ε_c	cluster porosity or cluster voidage
ε_{mf}	void fraction at minimum fluidization condition

ε_h	dilute phase voidage at a distance h above dense/dilute interface
ε_{den}	voidage in dense phase region
ε_{ave}	average voidage of the dense phase region
ε_4	voidage at transition region
δ_c	fraction of wall surface covered by cluster
$\bar{\tau}$	average residence time of packets, s
τ_p	thermal time constant
σ	Stefan - Boltzmann constant, 5.67×10^{-8} W/m^2K^4
θ_o	temperature difference, K

BIO-DATA

The author was born in July, 1951 in the district of Khulna, Bangladesh. He graduated in Mechanical Engineering with First Class from Bangladesh University of Engineering and Technology (BUET), Dhaka, Bangladesh in January 1974. He joined as a Lecturer in the Department of Mechanical Engineering in Bangladesh Institute of Technology (BIT), Khulna, Bangladesh in February 1974. In 1984 he obtained M. Eng. in Energy Technology from Asian Institute of Technology (AIT), Bangkok, Thailand. In the same year he attended a computerized energy management training program in WEM, Hampshire, U.K. At present he is working as an Associate Professor of Mechanical Engineering at BIT, Khulna, Bangladesh.

LIST OF PUBLICATIONS BASED ON PRESENT WORK

1. Nag, P.K., M. Nawsher Ali Moral and Basu, P., 'Effect of Fins on Heat Transfer in Fast Fluidized Beds', Proc. 10th National Conference on Heat and Mass Transfer, Srinagar, India, p. 429-435, Aug. 23-25, (1989).

2. Nag, P.K. and M. Nawsher Ali Moral, 'Heat Transfer in Circulating Fluidized Beds', Indian Journal of Technology, Vol. 28, p. 129-132, April, (1990).

3. Nag, P.K. and M. Nawsher Ali Moral, 'The Influence of Rectangular Fins on Heat Transfer in Circulating Fluidized Beds', Journal of the Institute of Energy, U.K., Vol. LXIII No. 456, p. 143-147, September, (1990).

4. Nag, P.K. and M. Nawsher Ali Moral, 'Prediction of Heat Transfer in Circulating Fluidized Beds', Proc., 3rd International Conference on Circulating Fluidized Beds, Nagoya, Japan, October 15-18, (1990).

5. Nag, P.K. and M. Nawsher Ali Moral, 'Effect of Probe Size on Heat Transfer at the Wall in Circulating Fluidized Beds', International Journal of Energy Research, John Wiley and Sons, Ltd. U.K., Vol. 14, (1990).

6. Nag, P.K. and M. Nawsher Ali Moral, 'Effect of Fins on Heat Transfer in Circulating Fluidized Beds', Journal of Regional Centre for Energy, Heat and Mass Transfer for Asia and Pacific, Madras, India, Vol. 12, No. 2, p. 123-130, (1990).

7. Basu, P., D. Lawrence, M.N. Ali Moral and P.K. Nag, 'An Experimental Investigation into the Effect of Fins on Heat Transfer in Circulating Fluidized Beds', Int. J. Heat Mass Transfer, (accepted for publication).

8. Nag, P.K. and M. Nawsher Ali Moral, 'An Experimental Study of the Effect of Pin Fins on Heat Transfer in Circulating Fluidized Beds', The Canadian Journal of Chemical Engineering. (communicated).

9. Nag, P.K., M.N. Ali Moral and Basu, P., 'A Mathematical Model of Heat Transfer from Bed to Finned Surfaces in a Circulating Fluidized Beds', Int. J. Heat Mass Transfer. (Communicated).

P.T.O

9. Nag, P.K., and M.Nawsher Ali Moral, 'An experimental study of the effect of Pin Fins on heat transfer in circulating fluidized beds', Int. J. of Energy Research, John wiley and sons, Ltd, U.K., Vol. 17, P. 863-872, 1993.

10. Mohammad Ali and M. Nawsher Ali, 'Finite Element Analysis of Saminar Convection Heat Transfer and Flow of the fluid bounded by V-corrugated vertial plates of different corrugation frequencies. Indian Journal of Engineering & aterials Science, Vo. 1, August 1994, P. 181-188.

11. Md. Nawsher Ali Moral, 'Producer gas from Agricultural Wastes', Presented in the First paper meet of Mechanical Engineering Div. held on 27-28 Oct. '94 at BIT, Khulna.

12. Nag, P.K., M. Nawsher Ali Moral and Basu, P., 'A Mathematical Model of Heat Transfer from Bed to Finned Surfaces in a Circulating Fluidized Beds', Int. J. Heat Mass Transfer. (Communicated).

ABSTRACT

Experimental investigations were made to study the effect of fin and vertical probe height on hydrodynamics and heat transfer in circulating fluidized beds (CFB). The experiments were conducted in a 100 mm I.D., 5.15 m tall CFB unit. Air was supplied by a high pressure centrifugal blower. The distributor plate used was straight hole orifice type having 12.4 % open area. The test section was located at 2.75 m above the distributor and electric tape heater was used as the source of heat. The temperatures of the inside wall and the bed at about the midpoint in the test section were measured with copper constantan thermocouples. Five plain and five finned test sections have been examined, three of which had rectangular fins and two had pin fins.

Local sand of mean diameter 310 μm was used as the bed material. Measurements covered a range of superficial air velocity from 5.6 to 12.5 m/s, suspension density from 18 to 76 kg/m^3 and bed temperature from 330 to 365 K. Three bed inventories of 20, 26 and 32 kg and five heat fluxes in the range of 3580 to 7876 W/m^2 were used.

One empirical model was developed with the help of dimensional analysis to predict heat transfer in a hot CFB to bare tube surfaces. One analytical model has been developed for the prediction of heat transfer to finned surfaces in a CFB both for long and short fins. An empirical equation has been developed correlating the parameters Nu_p , Re_p and L_h/D to estimate heat transfer from the probes of different vertical heights. In addition one expression for calculating particle residence time has also been derived.

The results predicted from the models and correlations have been compared with the present experimental results as well as those of other investigators, and good agreement is observed. With the use of fins, the heat transfer coefficient was found to decrease by a maximum of 32 %., but the total heat transfer got enhanced by about 103 % due to the additional surface area provided by the fins. Heat transfer coefficient was found to decrease and particle residence time was found to increase with the increase of vertical height of the probe.

CHAPTER - I

INTRODUCTION

Increasing world demand for more energy together with the oil embargo by OPEC in 1973-74 resulted in exploring new, cheaper and readily available sources of energy. This realisation evoked massive research and development activities all over the world since the middle of 1970's. The potential sources of energy can broadly be divided into two classes, the renewable energy and the non-renewable energy. In one hand the renewable energy is site effective, on the other hand the technology is not fully developed or is costly to harness. Solar energy would become popular only if direct energy conversion methods, simple, practicable and utility oriented for large scale application on low cost projections are made available. Although bio-mass is an old and established technology, but its application is limited due to inadequate concentration and some unpleasant properties of the raw materials. Geothermal and hydro energies are being considerably exploited and used in certain areas. The development of wind and tidal energies are not yet so promising. Nuclear energy is being utilized but there are many arguments against its large scale application due to the problem of waste disposal and environmental hazard. So the dependable source of energy is the non-renewable energy

source that means the fossil fuels. The reserves of oil and gas are limited, and unless otherwise new oil fields are discovered, the present reserve will be depleted within a few decades. Under these circumstances a number of measures have been suggested towards future energy use. Efficient energy conversion technique is one such measure. The technique of fluidization is one of the efficient means of energy utilization.

In the process of meeting the growing demand for electric power and heat, coal has been playing an important role worldwide. Also among the fossil fuels, reserves of coal are much more abundant than others. So peoples are depending increasingly upon coal day by day, rather than on other fossil fuels. On the other hand, the quality of coal is gradually degrading. The fluidized bed combustion is a novel and more efficient method of burning such low grade coal. It offers a method of burning insensitive to fuel quality, capable of reducing sulphur and nitric oxide emission, providing the best hope for the development of coal fired gas turbine and combined cycle operation [17].*

Circulating fluidized bed (CFB) combustion systems have been developed only since the mid 1970's. Till then almost all fluidized bed combustion efforts, particularly

---

* Numbers in parantheses indicate the references given at the end of the thesis.

in the UK and USA, were directed toward the bubbling bed. The oil crisis in 1973-74 caught several countries that were heavily dependent on the imported crude off balance, and intensive research into alternate fuels commenced to meet the growing energy demand. Finland, Sweden and West Germany in particular, started CFB programs at this time. The world's first commercial CFB boiler went into service at Pihlava, Finland in 1979 [2]. The pioneering company was Ahlstrom, and the aim was to convert an oil-fired unit into a CFB boiler producing 20 t/h of steam from woodwaste. Successful operation of this unit led to the startup in 1981, of a 90 t/h (steam) CFB boiler at Kauttua, Finland, that was designed to burn coal, woodwaste and peat.

Lurgi, drawing on previous mineral processing experience in CFB units, followed suit in 1982 with an 84 MW (thermal) CFB combustor at Leunen, Germany. This plant was designed to burn coal washery rejects with ash content of upto 55 % and appears to have been a resounding success [3]. In the relatively short span of its commercial life, the CFB boiler along with its 'bubbling' counterpart, has established itself as a reliable and attractive option for industrial boilers to supply process steam. Now it is competing as a utility boiler. Few CFB utility boilers in the 100-150 MWe range are already in operation, and some are in various stages of construction [2,4].

One of the main advantages of fluidized bed combustion is that flame stability is assured by the quantity of hot particles resident in the system — the bed acts as a thermal ballast. For fluidized bed combustors it is necessary to keep the particles below their ash fusion point, while from an acid gas emission point of view it is desirable to operate at a temperature below about 950°C. These constraints combine to limit operation in both bubbling bed and CFB systems to a temperature range of 800-900°C [5].

Early experience with bubbling bed combustors showed that unburned carbon losses could be as high as 10-15 % [6]. The main reason for this appears to have been that coal fines were too rapidly entrained from the bed. Bulk fines recycling is inherent in the CFB system, because solids loadings in the cyclone are high and the solids behave more as clusters than individuals. Under these conditions fines are unable to escape easily by virtue of their size alone. These factors combine to extend the residence time of fines in the CFB system to the point where losses of unburned carbon rarely exceed 2 % under normal condition [2].

Staged combustion is a characteristic feature of all CFB boilers. Figure 1.1 shows the combustion zones together with the entry points of primary and secondary air.

Primary air is fed from below through the distributor, and this stream contains about 50-60 % of the stoichiometric requirements. Secondary air is admitted from the side at a certain height, at this level the furnace environment changes from reducing to oxidizing. Fuel devolatilization and ignition occur in the lower oxygen lean environment. The probability of NO_x formation at this point is reduced. This strategy is more effective when the fuel contains a high level of volatile organic compounds. The main reason is the single-pass nature of gas flow through the system, vis-a-vis the recirculating nature of solids flow. Because staged combustion primarily affects the gas phase, the effectiveness of the strategy is enhanced when a greater proportion of fuel-bound nitrogen is released in the form of volatilized organic compound.

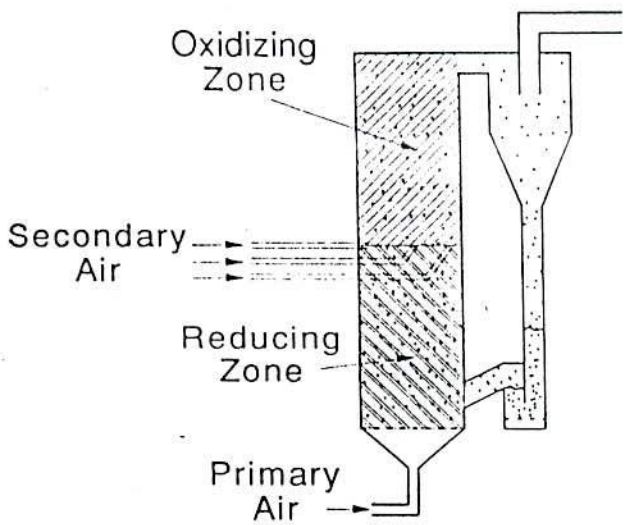

FIG. 1.1 STAGED COMBUSTION IN CFB

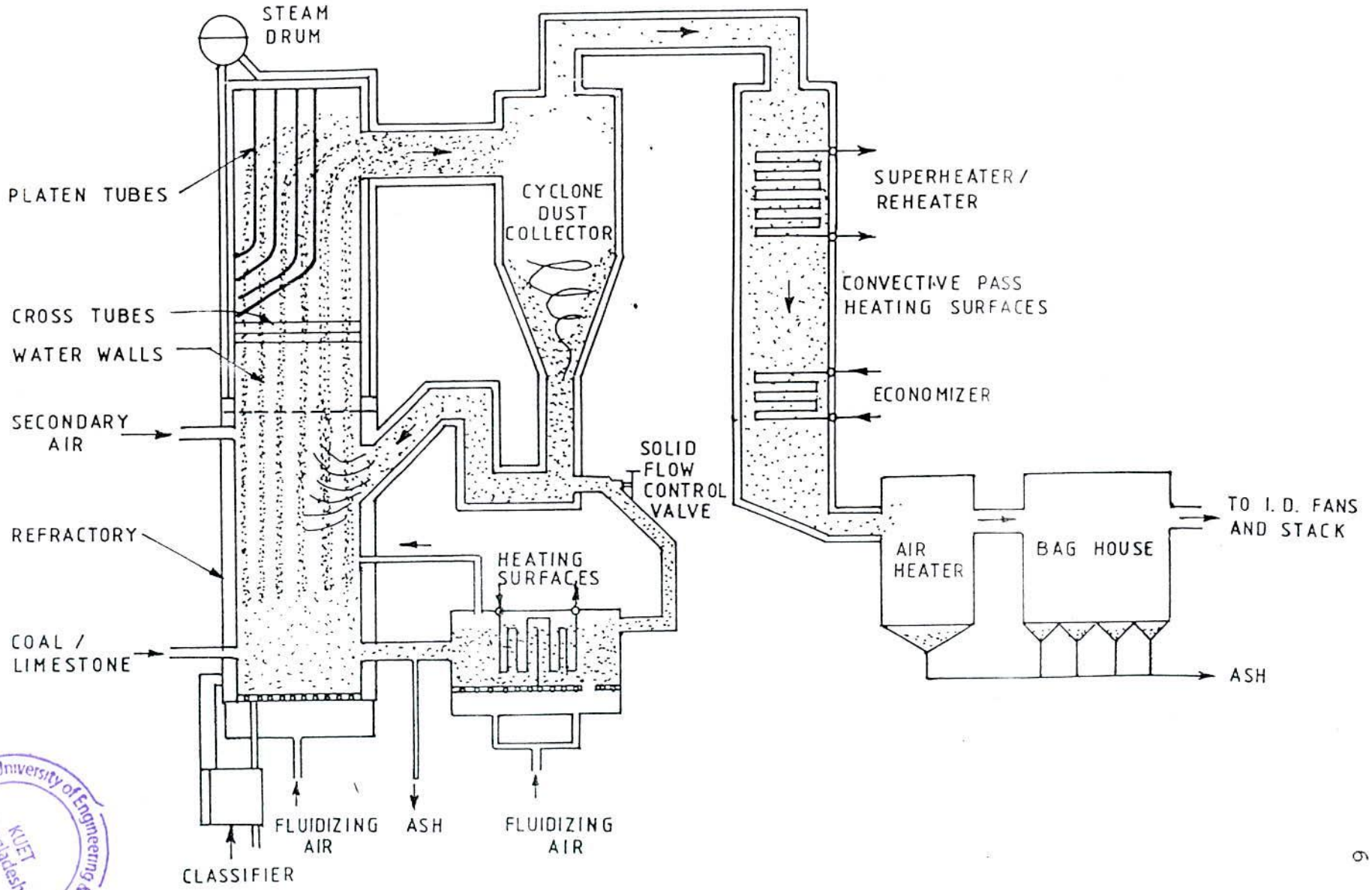

FIG. 1.2 DETAILS OF A TYPICAL CFB BOILER

Figure 1.2 shows details of a CFB boiler. The advantages of the same are as follows :

(a) Fuel flexibility :

The CFB boiler can efficiently burn a wide variety of fuels including low grade solid fuels rich in ash and moisture. It has the flexibility of burning different types of fuels in the same boiler, simultaneously and separately, without substantial change in capacity and efficiency. Examples of fuels fired in CFB units are bituminous coal, anthracite, anthracite culm, coarse coal rejects, coal washery tailings, peat, wood chips, wood waste, petroleum coke, oil shale etc.

(b) High combustion efficiency :

Superior mixing in the CFB and the large reaction space afford high combustion efficiencies for a wide variety of fuels under different operating conditions. For its Lunen boiler, in operation since 1982, Lurgi reports an efficiency of 99 % . Firing a mixture of bark, coal and waste paper, Ahlstrom's boiler at Hylte Bruk in Sweden has registered an efficiency of 98-99.5 % with oxygen level in the flue gas at 2-3 % . Ahlstrom's Kauttua Pyroflow boiler gave a combustion efficiency of 98.5 % when the boiler was at 50 % load with excess air maintained at 20 % .

(c) Efficient sulphur removal :

SO_2 formed by oxidation of sulphur in fuel ,

$$S + O_2 = SO_2 + 9260 \text{ kJ/kg}$$

enters into chemical reactions with moisture catalyzed by sunlight to form acids. For limestone directly fed into the CFB furnace as bed material, the following endothermic reactions occur

$$CaCO_3 = CaO + CO_2 - 1830 \text{ kJ/kg } CaCO_3$$
$$MgCO_3 = MgO + CO_2 - 1183 \text{ kJ/kg } MgCO_3$$

In a sufficiently oxidizing environment, the porous calcined limestone reacts as given below :

$$CaO + SO_2 + \frac{1}{2} O_2 = CaSO_4 + 15141 \text{ kJ}$$
$$MgO + SO_2 + \frac{1}{2} O_2 = MgSO_4 + \text{Heat}$$

$CaSO_4$ and $MgSO_4$ (gypsum) retain the sulphur in the solid form, rather than allowing it to escape as gaseous SO_2.

Thermodynamically, the formation of $CaSO_4$ is favoured at lower temperatures. The rate of formation is maximized at about 850^oC. At temperatures exceeding 900^oC, the sulphur capture is greatly reduced. This is one of the reasons why fluidized bed combustion processes are constrained to the $800 - 900^oC$ temperature range.

Good contact between gas and solid and the long contact time in the CFB combustor afford better sulphur capture at a given Ca/S ratio. Industrial CFB boilers show 90 % S capture at Ca/S ratio of 1.5 - 2.

(d) Low NO_x emission :

Owing to relatively low combustion temperature and the staged combustion, NO_x emission can be kept down to the range of 100-300 ppm [4]. Staged combustion is highly effective in limiting NO_x formation. It has been found that NO concentrations can be diminished progressively (by reduction to molecular nitrogen or possibly to nitrous oxide, N_2O) as combustion gases pass up the CFB chamber and into the hot cyclone. The most reasonable explanation appears to be that, despite the generally oxidizing environment higher up in the system, NO is catalytically reduced on the surface of uncombusted carbon particles. Nitrogen oxide emission levels respond to a number of other system parameters as well. Flue gas recirculation depresses NO_x and the introduction of ammonia or urea has been suggested for effective NO_x reduction.

(e) Simpler fuel handling and feed system :

In contrast to the conventional pulverized coal fired boiler, CFB boilers receive solid fuels in fairly coarse sizes. This simplifies the upstream feed preparation. But perhaps the main advantages of the CFB boiler is the

need for only one (industrial boiler) or few (utility boiler) feed points. The high degree of lateral solid mixing in turbulent zone at the bottom ensures uniform feed distribution within the bed. Besides the large height corrects any maldistribution.

(f) High heat release rates :

Lurgi, Ahlstrom and Gotaverken report running their boilers at gas velocities around 6-8 m/s. This results in high heat release rates (about 5 MW (th)/m^2), and so needs less floor area.

(g) Capability for good turndown and load following :

The relatively high fluidizing gas velocity and the use of staged combustion permit a fairly good turndown ratio by simply reducing the proportionate amounts of fuel and air. The turndown ratio of upto 5:1 has been achieved (20 % load).

CFB boilers respond quickly to load changes. The given load can be readily adjusted by changing the ratio of primary and secondary air and by controlling the solid circulation rate.

(h) High availability :

The availability records of CFB boilers are highly impressive. It is more than 90 % . During 2.5 years of operation Ahlstrom's Kemira plant logged in 20,457 hours.

The fundamental advantage of a fluidized system is that it tends to maintain a uniform temperature throughout the bed. Close temperature control is possible even when there is evolution or absorption of large quantities of heat inside the system, because the solid particles in a fluidized bed act as reservoirs and carriers of heat. Their violently turbulent motion enables them to absorb heat from the fluid in one part of the system and to release it to the fluid in another, thus tending to equalize the temperature and to eliminate hot and cold spots within the system.

The major disadvantages of CFB's are however, (i) erosion of reactor walls depending on velocity, reactor design and materials, (ii) attrition of particles, (iii) difficulty of immersing internals due to the possible erosion and (iv) complexities of the hydrodynamics [7].

Dwindling reserves of high quality coal and the imperative need for abatement at atmospheric pollution have spurred the development of CFB technology for steam generation. The heat transfer mechanisms of fluidized bed boilers are quite different from the usual in boiler engineering. In conventional fossil fuel steam generator, the physical mechanisms of heat transfer are restricted to radiation and gas convection. In fluidized bed boilers other mechanisms occur and not all in these mechanisms is fully understood yet. Empirical data on heat transfer to surfaces in fluidized beds are scarce. Not only the in-bed heat

transfer differs appreciably from the usual, also the transfer processes in and after the freeboard are quite unconventional due to much lower gas temperature, low gas velocities and heavy dust load. Designers of fluidized bed steam generating system need design data and procedures to handle these features. This asks for an understanding of the physical mechanisms controlling heat transfer in this type of steam generator. An accurate understanding of the heat transfer to the bed walls and to immersed surfaces is required for proper design of circulating fluidized bed boilers. It is also necessary to know how the heat transfer coefficient depends on various design and operating parameters. The process of heat exchange between the system and the heat transfer surfaces is intimately associated with the process of heat transfer between the fluidized solid and the fluidizing gas, the rate at which the particles mix inside the bed and the general behaviour and geometry of the fluidized system. There is now considerably renewed interest in large fluidized bed boilers for the efficient production of energy. This necessitates not only an optimum economic design but also a design that incorporates the essential features necessary for control of gaseous and solid pollutants. The development of fluidized bed boilers for the combustion of sulphur containing coal has particular promise. CFB combustors have gained popular acceptance recently because they have demonstrated that they can

burn a wide variety of fuels efficiently and in an environmentally acceptable manner. In the current energy climate, where fuel supplies cannot always be guaranteed over the long term, a combustor may also require that a single combustion unit can handle widely different fuels over a load range without a substantial loss in performance. The circulating fluidized bed has shown this capability [8].

The circulating fluidized bed boiler is outstanding in its fuel flexibility, low pollutant emission and adaptibility to load change, and has become a subject of world wide attention as an improved new type of coal combustion boiler [9,10]. To maintain the combustion temperature at an optimum level it is necessary for the walls of a CFB furnace to absorb a desired fraction of the heat input to the furnace. While the heat input is proportional to the bed cross-section, the heat absorption is proportional to the perimeter of the furnace, height remaining constant. Thus with the increase in the capacity of the boiler, the heat input and, hence, the required amount of heat absorption increases, but the wall area available for heat extraction does not increase in the same proportion. So large CFB boilers are required to have additional heating surfaces across the furnace or external heat exchangers. Both options are costly and increase the risk of tube erosion. Finned tubes are widely used in heat exchangers including the economizers of boilers to enhance the total heat transfer rate. In modern

boilers, panel wall tubes are welded to each other by flat fins. These fins are only partially effective, because only one side of the fins is available for heat transfer. The other side faces the insulated casing of the boiler. The heat absorption by each wall tube may be greatly increased if additional heating surfaces can be provided by welding to each tube, vertical fins projecting into the furnace.The present exploratory work examines if the overall heat transfer can be increased by using such projected fins on the walls of a circulating fluidized bed. Experiments were carried out at room temperatures, but covering other operating conditions relevant to commercial boilers such that at least the knowledge of convective component of heat transfer in actual boilers can be gained through this work.

Although fluidized bed is comparatively an old technology but the circulating bed is a recent development. The bottom section of a circulating fluidized bed below the secondary air inlet operates either in bubbling or turbulent bed regime, whereas at the top it is either in the fast bed or pneumatic transport regime, depending on the superficial velocity used. Grace [11], Glicksman [12] and many other workers have observed that the heat transfer coefficient is less at the fast bed than that in the bubbling bed due to lower bed density. Inspite of tremendous progress of commercialization of this technology, there is a serious dearth of information in some important areas of design.

Therefore, there are many areas of fundamental interest where there is much yet to be done. Research on CFB systems is being conducted at a brisk pace all around the world since about 1980. It is, however, lagging behind the pace at which its commercial application has been progressing. The main research areas are heat transfer as a function of important design parameters, combustion mechanisms, hydrodynamics of high velocity fluidization, influence of fuel properties etc. [13,14].

The present investigation has been carried out to study not only the effect of operating variables but also some experimental techniques to augment heat transfer by using fins. The effects of vertical probe height, fin size and geometry on heat transfer and hydrodynamics in circulating fluidized beds have also been studied.

1.1 Objectives of the Study

The main objectives of the present investigation are devoted to heat transfer in circulating fluidized beds as given below :

(1) Study of the effect of fins of rectangular and pin shapes on hydrodynamics and heat transfer in a CFB.

(2) Study of the effect of vertical probe height on heat transfer in a CFB .

(3) Development of an empirical model with the help of dimensional analysis to predict heat transfer in a hot CFB to bare tube surfaces.

(4) Development of a mathematical model for the prediction of heat transfer to finned surfaces in a CFB, both for long and short fins.

In addition, to form a base of the present work, the unfinned surface was studied first in a CFB and the results were compared with those of others available in literature.

CHAPTER - II

LITERATURE REVIEW

2.1 Introduction

Since the developments in petroleum industry in the early 1940's, fluidization has become a widely accepted technique for bringing about heat and mass transfer in chemical and process industries and later to effect the combustion of fossil fuels for power generation and process heat [15].

The history of development of fluidization technique has been provided by Zenz and Othmer [16], Jahnig [17] and Squires [18,19].

Different aspects of fluidization have been discussed by Kunii and Levenspiel [20], Yates [21], Davidson, Clift and Harrison [22], Van Swaaij and Afgan [23], Radovanovic [24], Geldart [25] and Howard [26]. Pell [27] explained the design aspects of heat transfer in gas fluidized beds.

For a detailed account of hydrodynamics in circulating fluidized beds (CFB) one can note the reviews of Grace [15], Yerushalmi and Avidan [28], Geldart and Rhodes [29] Kwauk et al [30], Matsen [31] and Horio [32].

The fundamentals of heat transfer in fluidized beds have been elucidated by Gelperin and Einstein [33].

Baskakov [34] and Botterill [35]. Gutfinger and Abauf [36] and Saxena et al [37] reviewed the bubbling bed heat transfer literatures. Heat transfer in CFB has been reviewed by Grace [11] and Glicksman [12]. Wu et al [38] and Basu et al [39,40] have compared data of various investigators. Leckner [41] discussed the mechanism of heat transfer with applications to CFB boilers in his comprehensive review.

The CFB as a combustor with its fuel flexibility and environmental compatibility is regarded as the 'second generation fluidized bed'. A historical account of the development of fluidized bed combustion has been given by Hoy and Kaya [42], and Kullendorff and Andersson [43]. Dry and LaNauze [2] elaborated the mechanisms of combustion and heat release in a fluid bed steam generator.

Most of the current activities in different areas of circulating fluidized bed technology have been reported in the proceedings of 1st, 2nd and 3rd International Conferences on CFB [13,14,44].

2.2 History of Development of Fluidized Beds

The first large scale, commercially significant use of fluidized beds was by Fritz Winkler for the gasification of powdered coal. The patent for this process was awarded in 1922 and the first gas producer started smooth operations in

1926 [20]. The combined effort of ESSO engineers together with the engineers of M.W. Kellogg Company and Standard Oil Company of Indiana, USA culminated in the first commercial fluid catalytic cracking (FCC) unit, and the SOD Model-I was built at Standard Oil's Baton Rouge refinery and it went into smooth operation in 1942. To reduce the heavy load on dust collectors, upflow beds were replaced by downflow fluidized beds, leading to SOD Model-II units. More than thirty FCC units of this type were built to produce aviation gasoline during World War - II.

In 1944 Dorr-Oliver Company acquired rights to ESSO's fluidization know-how for use in fields outside the petroleum industry. Concentrating on noncatalytic reactions of gas with solid they developed the Fluosolids system for the roasting of sulphide ores. The first such unit was constructed in 1947 in Canada. In 1952 at Berlin, New Hampshire, Dorr - Oliver introduced this type of roaster for producing SO_2 from sulphide ores. Following the very rapid acceptance by engineering organizations worldwide, CFB combustion technologies are being increasingly utilized by a wide range of end users including steam generation for process and power generation applications. Figure 2.1 shows how the major CFB technologies have progressed over the last decade , and it is clear that scale-up developments are being led by Lurgi and Ahlstrom. Ahlstrom currently has the largest unit in operation, but Lurgi has a number of larger units at various stages of design and construction [2].

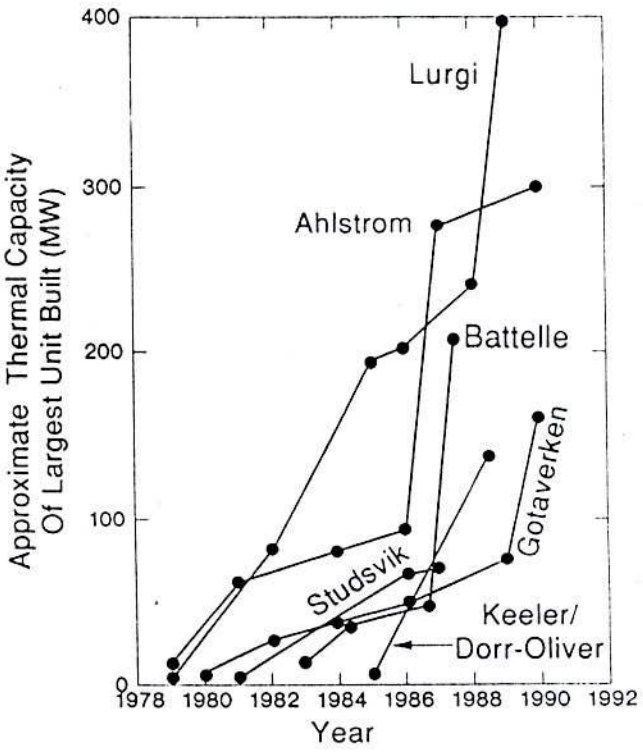

FIG. 2.1 CFB UNIT CAPACITY GROWTH

2.3 Applications of Fluidized Beds

Circulating fluidization is a growing new technology in many fields where good fluid-solid contact is required. Combustion and power generation, catalytic reactions, drying, waste incineration and iron ore prereduction are good examples of some of its applications.

2.2.1 Current commercial status of CFB boilers

Till 1989 there are six major commercial CFB combustion technologies [2], each having certain distinctive features as given below :

(a) Ahlstrom/Pyropower CFB system :

Ahlstrom, the first to build a commercial CFB boiler, and Pyropower, its US subsidiary, have more than 40 plants in operation (upto July 1990). Its simple, robust design features a water-wall riser with refractory lining in the lower region, and a vertical hot cyclone solid re-injection is carried out with the aid of a loop seal. The largest CFB boiler rated at 110 MWe is in operation at Nucla, Colorado. It consists of a twin combustion chamber, 7m x 7.3m x 37m tall. It is covered by EPRI program and represents a focal point for the American utility industry.

(b) Lurgi CFB boiler :

Lurgi of Germany commissioned their first utility boiler of 96 MWe at Duisburg and a 150 MWe unit is soon to be started. Lurgi's first CFB boiler (1982) at Lunen supplies process steam to an aluminium plant. The Lurgi design is simpler than the Ahlstrom's. About 16 Lurgi CFB boilers are in operation and another 16 are likely to come on stream during the next few years.

(c) Gotaverken CFB system :

Gotaverken of Sweden offers a design similar to Ahlstrom's. They began extensive pilot work early in 1980, and in 1983 placed the first commercial boiler in operation. About 11 Gotaverken boilers are now in operation.

(d) Keeler / Dorr-Oliver CFB boiler :

The Keeler Boiler Company, which was taken over by Dorr-Oliver, has recently entered the CFB market with boiler contracts at Decatur, IL and Ceder Rapids, IA. These plants based on coal, produce around 200 t/h of steam in each boiler. The distinguishing feature is the inclusion of a full length vortex finder in the hot cyclone.

(e) Studsvik CFB system :

Studsvik Energieteknik AB of Sweden is a government-based research and development company. A 2.5 MW(th) prototype CFB boiler was installed in 1978. The technology developed has been licenced by Babcock and Wilcox in USA, Babcock Hitachi in Japan and Ensaldo in Italy. At least seven boilers are in operation. It is characterized by the use of a labyrinth collector rather than a hot cyclone.

(f) Battelle MSFB system :

The multisolid fluid bed system was developed by Battelle Memorial Institute in Columbus, Chio. Eight commercial units are in operation, the largest being at Idemitsu refinery in Japan having a steam capacity of 300 t/h.

2.4 Heat Transfer in Fluidized Beds

One of the reasons fluid beds have such wide application is their excellent heat transfer characteristics. Particles entering the fluidized bed rapidly reach the bed temperature. Particles within the bed are uniformly at the same temperature. Gas entering the bed reaches the bed temperature within a few centimeters [27]. The high heat transfer rates are mainly due to the large surface area of solids available for the contacting operation rather than high heat transfer coefficient.

The mechanism of heat transfer in a fluidized bed is quite different from the usual system. It is very complicated because of the dependence of bed behaviour on a large number of variables. Heat transfer to the walls of a CFB is due to conduction from clusters of particles falling along the walls, thermal radiation and convection to uncovered surface areas.

Grace [11] regarded the circulating bed as intermediate between a dense fluidized bed and a dilute pneumatic conveying. He divided the overall surface-to-suspension heat transfer coefficient into three separate, approximately additive components accounting for convective transfer due to particles, gas phase convection and radiation. So the overall heat transfer coefficient can be written as

$$h_o = h_{pc} + h_{gc} + h_{rad}$$

2.4.1 Heat transfer in bubbling beds

The majority of the experimental and theoretical efforts has been toward an understanding of the mechanisms of heat transfer in fluidized beds by unsteady state conduction to moving solid particles at temperatures such that radiation can be neglected ($\lesssim$ 900 K) and with particle sizes ($\lesssim$ 1 mm) sufficiently small so that gas convection can also be neglected for non-pressurised system [37].

Dow and Jakob [45], Leva et al [46], Levenspiel and Walten [47] and Wasen and Ahluwalia [48] observed that the principal resistance to heat transfer is a fluid film, and the fluidized particles scour the film to reduce the resistance to heat transfer, that is why, they found high values of heat transfer rates in their experiments. Main feature of thin film model has been shown in Fig. 2.2 .

Van Heerden et al [49] proposed the first model accounting for the thermal resistance of the thin gas film as well as the layer of emulsion with its solids flowing parallel to the wall. This model indicates that the heat transfer coefficient between bed and wall should be large for short heat exchange sections and smaller for long sections.

In contrast with film models, Mickley and Fairbanks [50] observed the unsteady heating of elements by a small group of particles moving as individual unit called the 'packet (or cluster) of emulsion phase' as the vehicle

for heat transfer. These packets are viewed to rest on the surface for a short time, only to be swept away and replaced by fresh emulsion from the main region of the bed. The principal features of the model are shown in Fig. 2.3.

Mickley and Fairbanks were the first to physically model the heat transfer from a fluidized bed to an immersed surface as a transient renewal process [51]. In this model the heat transfer coefficient continually increases as the residence time decreases. Experiments by Dunsky et al [52] in stirred bed found that heat transfer coefficient approaches a constant upper limit as the residence times are decreased. This model has been modified by the introduction of a contact resistance in series between the heat transfer surface and the particles by Baskakov [53], Patel [54], Yoshida [55], Kubie and Broughton [56] and Wunschmann and Schlunder [57]. Zabrodsky [58] earlier introduced an equivalent of contact resistance viz., thermal resistance of an additional gas film gap between the heat transfer surface and the first row of particles. The contact resistance at the bed-wall interface is attributed to various effects e.g., Kubie and Broughton [56] modelled voidage variations in the bed near the wall, and Wunschmann and Schlunder [57] considered the reduced mean free path of the gas molecules.

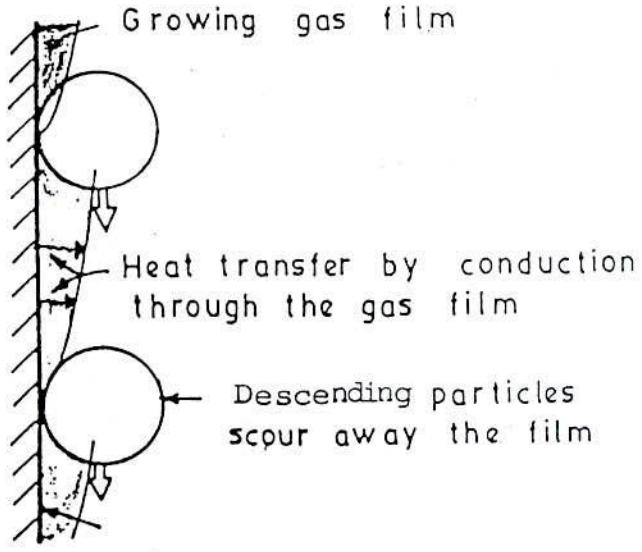

FIG. 2.2 MAIN FEATURE OF A THIN-FILM MODEL

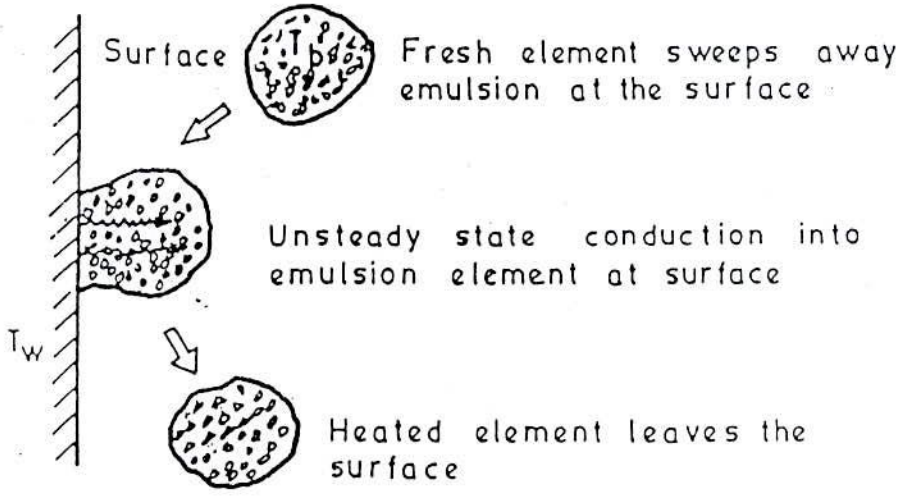

FIG.2.3 MAIN FEATURES OF THE EMULSION CONTACT PACKET MODEL

Botterill and Williams [59] were the first to numerically model the thermal behaviour of discrete particles adjacent to a heat transfer surface. They focussed on the aspect of this model dealing with the mechanism of contact of the emulsion with the heat transfer surface, instead of assuming mean properties of emulsion, they considered the separate roles played by the emulsion gas and the solids. The unsteady state conduction equations were solved numerically for various fluid and solid properties to give isotherms for different contact times. The results of these calculations show that the solids with their large heat capacity provide an effective heat sink, so that heat transfer is primarily in the region around the contact points of particles with the surface. Because of this, the heat flux can be taken to be proportional to the number of contact points per unit surface.

Botterill et al [60] then extended this analysis to a double layer of touching particles. As may be expected, for very short contact time hardly any heat enters the second layer. For large contact time the double layer treatment is perfect.

Ziegler and Brazelton [61] observed that absorption of heat by the fluidized particles rather than reduction of film resistance was the principal mechanism of heat removal

at a surface. They developed a model somewhat similar to that of Botterill and Williams [59]. Thus a particle is viewed to move to the wall region where it is suddenly bathed by fluid at the wall temperature. It absorbs heat from the gas by unsteady state conduction while the gas temperature remains unchanged and particle wall contact is ignored.

Gabor [62] has proposed theories describing heat transfer process at the surface based on semi-infinite 'packets of dense phase' composed of alternating flat layers of gas and solids. Other authors have considered particles having asperities on their surfaces [63], or single particles with allowance for the region near the point of contact where the mean free path of the gas is comparable to the gap width [64,65].

Kolar et al [66] verified the modified alternate-slab model of Gabor [67] for the prediction of radiative contribution to the total heat transfer. They assumed the radiative and conductive components to be additive and expressed the total heat transfer coefficient, h_w as

$$h_w = (h_{wce} + h_{wre})(1 - f_o) + f_o\, h_{wrb}$$

where f_o is the fractional heat transfer surface area exposed to bubbles and h_{wce}, h_{wre} and h_{wrb} are the heat transfer coefficients of conduction and radiation

through emulsion phase and radiation through bubble phase respectively. They used the correlation of Yoshida et al [68] to calculate h_{wrb} and the alternate-slab model of Gabor [69] as modified by Kolar et al [67] was used in its extended form to calculate h_{wce} and h_{wre}.

2.4.2 Heat transfer in circulating fluidized beds

Kiang et al [70] obtained data from a CFB unit of 10 cm in diameter and 3.7m tall for cracking catalyst having mean particle size of 53 micron. Heat transfer measurements were made using four miniature heaters 1.9 cm long at different levels of the bed. Their results for 53 micron particles are found considerably lower than that of Basu and Nag [39] for 87 micron particles.

Kobro and Brereton [8] studied the load control and fuel flexibility in CFB combustors. They reported heat transfer results collected from a 3m long steel pipe having 0.2m in diameter, which achieved control in a unique way using a combination of an uncooled particle storage zone and a controlled return of circulating solids to the combustor. Sand particles having mean diameters of 170 and 250 microns and bed bulk temperatures of 298K and 1123K were used. They measured the heat transfer coefficients for a 10 cm long active surface with velocity range from 6 to 12 m/s and reported the results in the range of 70 - 280 W/m^2K. They

became successful to prove the use of CFB technology in the pilot scale of Studsvik / Babcock and Wilcox boiler.

Subbarao and Basu [71] reported heat transfer results for 25 mm probe, 130 and 260 micron sand particles at room temperature. They found increasing heat transfer coefficient with increasing suspension density and further added that as the bed density increases the effect of particle size appears to be distinct. Stromgberg [72] earlier observed similar things and also found in his experiment a decrease in heat transfer coefficient with the increase in column diameter.

Basu et al [73] experimentally verified the effect of operating variables on bed to wall heat transfer in a CFB. They found positive dependence of heat transfer coefficient on suspension density and negative dependence on superficial velocity. Earlier, Fraley et al [74] also reported similar effects of the variables on heat transfer coefficient. Wu et al [75] observed the effect on heat transfer of fluidization velocity independent of suspension density.

Feugier et al [76] measured the average heat transfer coefficient to a water cooled jacket surrounding a 15 cm diameter, 7m high bed. They observed the heat transfer coefficient to be a strong function of particle diameter.

Basu and Nag [39] reported results for 87 and 227 micron sand particles and compared data from various sources. They found strong dependence of heat transfer coefficient on suspension density and weak dependence on bed inventory.

Andersson et al [77] presented heat transfer data for a 2.5 MW CFB combustor with a bed cross-section of 70 cm x 70 cm and 8.5 m high. They used 240 micron Olivin sand as the bed material. One centimeter diameter water cooled probes were installed flush with the walls. Over the temperature range of the data (1200 K), the increase in the overall heat transfer coefficient corresponds closely to the increase in the radiation heat transfer from the particles at the bulk bed temperature to the wall.

Furchi et al [78] reported results for the local heat transfer coefficient in a CFB unit of 72 mm I.D, 6m high, where the gas-solid suspension flows under fast fluidization condition. Glass spheres of 109, 196 and 269 micron were tested at temperatures upto 250^{o}C. The local heat transfer coefficients for all the cases were observed to vary inversely with the height of the bed. Pressure gradient along the bed height was found to a strong function of solid inventory in the system.

Heat transfer in CFB has been reviewed by Glicksman [12]. He considered the probes to be small when the typical transient time of particles past the length of the probe is small compared to the thermal time constant of the particles. Under these criteria, the small probes having 1 to 2 cm in diameter do not experience any significant temperature change when particles of 100 micron or larger move across it. From the data of Subbarao and Basu [71] and Basu et al [39, 73] he found that the measured heat transfer coefficient increases roughly as the square root of the suspension density. He also noted that Kiang's [70] result for 53 micron particles are considerably lower than that of Basu et al [73] for 87 micron particles. The heat transfer coefficients obtained for small surfaces represent an upper limit to the values for large heat transfer surfaces.

The results of Andersson et al taken from a 70 cm x 70 cm bed fall below those of Basu, Subbarao and Kiang taken on a bed of 10 centimeters diameter. This suggests that as bed size is increased there is a lower ratio of the wall solids fraction to the cross-sectional averaged solids fractions [12]. He found that the heat transfer to the surfaces of a circulating bed are closely related to the bed hydrodynamics. He further added that the heat transfer is a function of the average cluster displacement before break up,

the heat transfer coefficient varies inversely with the displacement raised to the power between 1/4 and 1/2.

Sekthira et al [79] studied heat transfer in a CFB unit having seven 10 cm high sections of 8.8 cm I.D. steel tubes with 15 cm I.D. water jackets. The data for 300 and 500 micron sand particles showed that heat transfer coefficients depend strongly on suspension density and have almost no effect on gas velocities and bed temperatures. The heat transfer coefficient decreases as the height above the distributor increases.

Wu et al [38,80,81] reported heat transfer data obtained from 1530 mm probe, 188 micron sand particle at 277°C [80], 22 mm probe, 171 micron sand particle at 35°C [81] and from tube and membrane wall at temperatures of 340 - 880°C for the sand particles of 222 to 299 micron [38]. Most of the data were taken using the CFB combustion unit at university of British Columbia. The details of the equipment are provided by Wu et al [80]. From these works they concluded that at the same volume-averaged solid density, there was no discernible effect of superficial gas velocity on heat transfer. At high temperature and low suspension density, radiation played a significant role. They also added that heat transfer coefficients varied significantly with lateral position of the tube. The magnitude of heat transfer coefficient is higher for small heat transfer surface probes and there is a moderate influence of particle size on heat transfer coefficient.

Basu [40] investigated the heat transfer in high temperature fast beds. He reported the results for four particle sizes, two heat transfer probes and temperatures in the range of 30-900°C. He compared the results from various sources and gave a critical analysis of the same. The heat transfer coefficients were found to increase with the increase of suspension density in all the cases and finer particles showed higher heat transfer coefficient. For very dilute beds, the particles contribute to increased radiation. He modified the model of Basu and Nag [39] where the maximum number of design and operating parameters were considered.

Dry and LaNauze [2] studied combustion and heat transfer in fluidized beds. He reported many advantages of CFB combustor and gave a picture of current commercial status of CFB boilers. In competition with bubbling beds, the CFB boiler often demonstrates superior carbon burn-out efficiency. The key to this combustion technique is the hydrodynamic behaviour of the fluidized bed. They described the mode of heat transfer in CFB by way of radiation and convection between dense packets of solids and vessel wall. Dense clusters or streamers tend to form on vertical surfaces. More often than not they move downward under gravity as a 'sheet' of solids before being broken up and reformed, sweeping the heat transfer surfaces. The design, construction and operation of a fluidized bed combustor has been discussed

in the book edited by Sens and Wilkinson [82].

Leckner [41] reviewed the heat transfer situation in CFB boilers on the basis of published works during the period of 1988-89. He covered mainly the area of thermal boundary layers and heat transfer mechanisms with special emphasis on the application of CFB heat transfer in boilers. It has been stated that radiation and heat transport by particles across the boundary layer are the principal mechanisms of heat transfer in CFB boilers.

Bi et al [83] investigated the effects of vertical length of heat transfer surface and the orientation of heat probes in a 186 mm diameter CFB unit with three heat probes having different lengths. They observed that local heat transfer coefficients and their radial profiles are influenced by both the vertical length and the orientation of the probes. In the central dilute region, the heat transfer coefficients decrease from the bottom to the top of the probes and the values of the coefficients obtained for downward probe are higher than those measured for upward one. In the dense region near the bed wall the trend is the opposite.

Zheng et al [84] studied heat transfer in circulating fluidized beds in two cold model test units. They measured heat transfer coefficients for 140 micron quartz sand and 443 micron resin at gas velocities from 3.7 to 5.8 m/s and for solid circulation mass fluxes from 2 to

50 kg/m^2s. Copper sphere probes of 5, 11, 15 and 18 mm in diameter cooled by liquid nitrogen were used to measure local heat transfer coefficients in the riser. A 3.7 m long 10mm O.D. electrically heated vertical tube was employed for measurement of local and length averaged heat transfer coefficients. The heat transfer coefficients were found to increase with the increase of suspension density and decrease slightly with increasing particle size. They further added that the particle convection component relative to gas convection component is nearly constant for different sizes of probes, particles and for different hydrodynamic parameters in the bed at a given suspension density.

Liu De-Chang et al [85] reported the heat transfer coefficient for a horizontal tube in a fast fluidized bed at room temperature. From the experimental observations they found the correctness of two-zone hydrodynamic model of CFB. They also reported the increase of heat transfer coefficient from bed centre to bed wall zones and a change along the height of the riser column.

2.4.3 Gas convection

For small particles of the size range (50-500)micron, gas convective heat transfer is small compared to particle convection [11]. It is important in the case of large particle diameter, high operating pressures and at very high gas

velocities. Direct measurement of gas convective component is difficult. Although the presence of particles may alter the turbulence characteristics of the gas somewhat, gas convective component may be estimated based on correlations for gas alone flowing through the column at the same superficial gas velocity and with the same physical properties.

Several investigators have attempted to correlate the convective component of heat transfer process. Wen and Miller [86] developed a correlation for predicting heat transfer coefficient from dilute phase which is of the form

$$h_{gc} = \left(\frac{k_g c_{ps}}{d_p c_{pg}}\right)\left(\frac{\rho_{sus}}{\rho_s}\right)^{0.3} \left(\frac{U_T}{g d_p}\right)^{0.21} Pr$$

Baskakov and Suprun [87] have estimated it by using the analogy between heat and mass transfer. In a later publication Baskakov et al. [88] suggested the best fit correlation

$$Nu_{gc} = \frac{h_{gc} d_p}{k_g} = 0.009 \; Ar^{1/2} \; Pr^{1/3}$$

and stressed the need to account for the effect of surface, size and shape in any future development of the correlation.

Gabor [89] proposed a heat transfer model to predict heat transfer rate from an immersed surface to bed for gas flow through the bed less than or equal to that required for minimum fluidization. The basis of the model is

that all heat transfer is normal to the heater and can be defined by an effective thermal conductivity for an orthorhombic array of spherical particles and that all the heat is removed by the gas flow. He derived the following equation to calculate total heat transfer coefficient (h_w) by solving a boundary value problem

$$h_w = \sqrt{\frac{4\ K_e\ c_{ps}\ G}{\pi\ L_H}} + \frac{K_e}{2r_2}$$

He also measured heat transfer between an electrically heated vertical tube and an air-fluidized bed. Three cylindrical heaters each 29 mm in diameter having lengths of 51, 102, and 203 mm. were used. In each measurement the heater was positioned axially in the column about 64 mm above the sintered stainless-steel air distributor plate. Heat transfer data were taken over a range of air fluidizing velocities from 0.031 m/s to U_{mf}. The experimental data were generally in good agreement with the values predicted from his proposed model.

Botterill and Denloye [90] proposed a modification to the model of Gabor [60] with $K_a = K_e$ by allowing for a zone of increased voidage and thickness d/a adjacent to the surface. Decker and Glicksman [91] simplified this two-zone model and obtained an analytical solution for h_{gc} with comparable accuracy, provided particular constants were used in the calculations. They have considered

the simple approach of taking any additional wall resistance in series with the bed resistance in the same manner as with the particle convective component, so that

$$h_{gc} = \frac{1}{\left(\frac{1}{h_{av}}\right) + \left(\frac{1}{h_{wp}}\right)}$$

where h_{av} can be estimated from the Gabor's [89] model.

Botterill and Denloye [92] extended their experimental study to gas flow rate above incipient fluidization beyond the maximum for the surface-to-bed heat transfer coefficient. In confirmity with Zabrodsky [58] and other workers they concluded that the contribution to heat transfer by gas convection increased with particle size and gas pressure.

Sathi et al [93] measured the heat transfer coefficient between a smooth vertical tube immersed in a fluidized bed of sand, silicon and alumina as a function of bed temperature and fluidizing velocity. They found that the heat transfer coefficient increased with the decrease in particle size and increase in bed temperature at a certain fluidizing velocity. Kiang et al [70], Fraley et al [74] and Martin [65] have all suggested equations for the convective heat transfer coefficient. Grace [11] reviewed the published data and correlations for heat

transfer in contact with circulating beds and showed that these models may differ from each other and from experimental data by more than hundred percent.

2.4.4 Radiation

For operations in high temperature fluidized bed such as combustion, the potential contribution of thermal radiation to heat transfer is an essential design parameter. It is an important mode of heat transfer in fast beds especially at high temperature ($> 700^{o}C$) and low bed density ($< 30\ kg/m^{3}$) [40]. Kharchenko and Mokhorin [94] proposed that there is no significant radiant heat transfer contribution in high temperature fluidized beds upto 1270 K. Ilchenko and Makhorin [95] and Botterill [96] concluded that radiation component is insignificant at temperatures below approximately 873K. In some other experimental study, these workers [95,96] observed that the heat transfer coefficient tends to increase with temperature primarily because of the increased contribution by radiation in the range of temperature 673-1673 K. Zabrodsky [97] argued that the radiative contribution to heat transfer is not prominant upto temperatures of about 1400K. Dunsky and Tamarin [98] and Gelperin and Einstein [33] contend that the radiation contribution is insignificant at temperatures below 1273K in fluidized beds.

Yoshida et al [68] estimated the radiation component both theoretically and experimentally. They assumed that heat is transferred by radiation from the bed through bubbles on the heat exchange surface and that radiant heat transfer affects the emulsion effective thermal conductivity. Their conclusion was that upto temperatures nearly 1000°C radiation is insignificant compared to the total heat transfer coefficient and is affected by the emissivity of the wall surface.

Vedamurthy and Sastri [99] estimated the radiative contribution by assuming packets of particles 3 d_p thick which move from the core of the bed to the heat transfer surface separated by a gas film 0.5 d_p thick for a given residence time. The packet consists of layers of solid and gaseous elements which radiate as black bodies. Heat is transferred from the packet to the wall by conduction through the gas film and radiation through the transparent film. The analysis was carried out for 0.5 - 3 mm ash particles at temperatures from 800-1100°C and at air velocities (1.25 - 8) U_{mf}. It can be seen from the calculations of Vedamurthy and Sastri [99] that radiation contributed between 17-30 % of the total heat transfer. They also carried out another experimental study on the influence of bed parameters on heat transfer in a fluidized bed combustor [100]. They burnt Leco coal of size range from 3.15 to 6.3 mm in

an inert bed of coal ash. The bed temperature varied from 850 to 950°C, superficial velocities varying from 0.2 to 0.4 m/s. They found the maximum overall heat transfer coefficient from bed-to-wall to be 120 W/m^2K, the radiation contribution of which was 20 to 40 percent.

Basu [101] reported the effect of combustion of coal in heat transfer rate to an immersed surface in a fluidized bed. He observed that the heat transfer coefficient increases with carbon content in the bed, except when the mean size of carbon particle is much larger than that of the inert bed material. He found 5 to 10 percent contribution of radiation heat transfer component on the overall heat transfer of the system.

Flamant [102] concluded from his investigation that radiation plays a significant role on heat transfer at temperature above 700°C. The theoretical and experimental investigations demonstrate the validity of the semi - transparent medium concept to account for the combined heat transfer by radiation and conduction between a wall and a fluidized bed. The governing parameter is the conduction to radiation interaction parameter N. If $N > 5$, the radiative heat exchange is limited at the surface boundaries between the wall and the emulsion only. If $N < 5$, an interaction occurs between the radiation and the conduction through the dense phase, and the radiative transfer increases when N decreases.

2.5 Heat Transfer from Finned Surfaces in Fluidized Beds

The performance characteristics of finned tubes in fluidized beds are not much known. Only few pioneering experiments have been reported in the literature. But no work in circulating fluidized bed on finned surface has been reported yet.

Petrie et al [103] published experimental data for bundles of horizontal finned tubes operating in a fluidized calciner. They investigated heat transfer from a steam - heated bundle of 19 tubes (D_T = 19 mm) immersed in a 0.305-m-diameter fluidized bed. The tubes were arranged on a 57 mm centre-to-centre triangular pitch. Tubes with no fins, tubes with 197 fin/m and tubes with 433 fins/m were used in the experiments. The height of the fin was 10 mm. Two sizes of sands, 497 and 530 micron were used as bed material. The air mass velocity (G) was used in the range of 0.186-0.384 kg/m^2s . The effects of air mass velocity and particle size on heat transfer rate were studied. Heat transfer from finned tube heat exchanger was represented by an effectiveness factor of the finned surface (ϕ) defined by

$$\phi = \frac{Q}{h_{wb} A_t (T_w - T_b)}$$

They found that the effectiveness factor for the finned tubes increased with the increase in fluidization velocity. It decreased with increase in the particle diameter. With an

increase in fin count, i.e., increase in the number of fins per unit length or decrease of fin gap, the effectiveness factor is decreased. However, the increased area more than compensated for the decreased effectiveness factor over the range of variables studied. Heat transfer coefficients based on actual fin area were found to be upto 50 % of those for bare tubes. By using finned tubes with a surface area of some 15 times greater than that of the base tube, a six or seven fold gain in heat transfer flux could be obtained compared with that using plain tubes of the same diameter.

Bartel et al [104] investigated heat transfer from a single horizontal steel tube with discontinuous fins to an air fluidized bed. Tubes having 172 mm length were mounted horizontally at 0.203 m above a perforated steel distributor plate. All the tubes were 16 mm in diameter and had 315 fins/m. The static height of the bed above the distributor plate was kept at 0.56 m. A 172 mm long electrical resistance rod heater was inserted in the tubes. Experimental variables were fin height, fin thickness, air fluidization velocity and particle diameter. They observed that the total rate of heat transfer from a single horizontal discontinuous finned tube continued to increase with fin height, although it leveled off when the height increased from 9 to 25.4 mm.

Investigations carried out by experimental/semiempirical studies of Genetti and coworkers [104,105] assumed a particle mode of heat transfer. With suitable assumptions, a boundary value problem was formulated to describe the temperature in the particle while it is near the hot tube surface. Gamma distribution functions were utilized to predict the mean particle residence time. A heat transfer model was used to predict heat transfer in a thin rectangular fin attached to the heated tube. The heat transfer rate into the fin and convection coefficient was determined, and then a suitable correlation was found for a given tube-fin configuration. Similar studies have been conducted by Ziegler et al [106] whose results agreed well with those of Genetti et al. Ziegler also found that the shorter the particle contact time, the higher the predicted heat transfer coefficient.

Professor Elliott's [107] first experiment using a built-up finned tube bundle immersed in a shallow fluidized bed at a depth of 80 mm gave somewhat surprising heat transfer coefficients which were significantly in excess of the existing data, all of which had been obtained in deep fluidized bed.

Gelperin et al [108] have reported the results of measurements of heat transfer between horizontal tubes with transverse rectangular copper and duraluminium fins (δ = 4mm) and a fluidized bed of quartz sand (d_p = 350 μm). Within the range of experiments they found the optimum gap (s) between

the fins to be 6 mm. With such a gap the effective heat transfer coefficient, related to the smooth tube surface area, reached its maximum value. The measurement of temperature over the fin height shows that the difference between a fluidized bed and some point of a fin becomes negligible at a distance about 10 mm from the base of copper fin and at a distance of 6 mm for duraluminium fin.

Bartel and Genetti [109] studied the effects of fin height, centre-to-centre distance between the tubes, particle diameter and fluidization velocity on heat transfer rate from a horizontal bundle of seven serrated finned tubes in an staggered array. It was observed that the rate of heat transfer increased with increase in fin height, but the rate leveled off for a fin height of about 25 mm, and further increase in fin height resulted in little increase in heat transfer rate. The heat transfer rate was sensitive to tube spacing for a bundle of short finned tubes. But the rate of heat transfer for tubes with 22 mm fins were found to be independent of centre-to-centre tube distance. The probable reason was that when a bundle of short finned tubes were expanded, particles could move easily into the region between the tubes as the resistance encountered by the particles in moving from the tips of the fins toward the centre tube was relatively small, and as a result, the rate of heat transfer was increased. However, with long fins, increasing the centre-to-centre tube distance did not increase the rate of heat transfer

noticeably, implying that the resistance to particle movement from the fin tips to the centre of the tube was not changed and was the principal resistance. The heat transfer coefficients increased with decrease in particle diameter for all fin heights (3 - 22mm). The heat transfer coefficients increased with increase in air mass velocity, but in most cases a maximum value was reached and further increase in air mass velocity decreased with heat transfer rate.

Natusch and Blenke [110] studied the effect of transverse rectangular fin on heat transfer. Both the tube and fins were made of copper. The tube was 25 mm in diameter, the height of fins ranged from 7.5 to 37.5 mm with 0.5 to 2mm thickness and a gap from 2 to 10 mm. Some close size fractions of glass beads (d_p = 400 - 800 μm) were fluidized with air. No effect of fin thickness on total heat transfer coefficient (h_w) has been observed in their experiments. For the calculation of heat transfer coefficient for a fin the authors suggested the following empirical correlation

$$h_{wf} = h_w \exp\left(\frac{-0.27\ l}{S + \beta l + 3.8}\right)$$

where, $$\beta = \frac{0.37}{0.36 + N} + 0.247$$

The equation is valid for $N > 6$ and $400 < d_p < 800$ μm

Gelperin et al [111] studied the effect of transverse fin profile. The experiments were performed with fins of rectangular, parabolic, triangular and trapezoidal profiles. The cylindrical body of the tube was 24 mm in diameter, the fins were 4 mm high in all of the cases. The distance between the fin bases (spacing) ranged from 0 to 12 mm for the fins of triangular profile, and from 2 to 12 mm for other cases. The cylindrical bodies of finned probes were made of brass. Quartz sand of mean diameter 350 μm was fluidized with air. The authors measured the effective heat transfer coefficient (h_{wb}). In all the cases the lowest h_{wb} were found for the rectangular profile and the highest were observed for triangular profile and at higher superficial velocities, for parabolic profile.

Priebe and Genetti [112] studied heat transfer from a horizontal bundle of extended surface tubes to an air fluidized bed about 2.44m tall with an inside cross-section of 0.356 by 0.165 m. The distributor plate consisted of two layers of 200-mesh stainless steel wire cloth sandwiched between two perforated steel plates. Micarta plates, located on opposite sides of the column, held the heater and tube assemblies. Escoa finned tubes were used to study the effects of heat flux and fin spacing on the heat transfer coefficients. The results show that, when fin spacing is more than ten particle diameters, the heat transfer coefficient is nearly constant, indicating very little particle hindrance.

When fin spacing was reduced from ten particle diameters, the heat transfer coefficient began to fall rapidly until the fin spacing was two particle diameters. Heatron spined tubes were used in a general study to determine the effect of spine height, spines per turn, spine material and air mass velocity on heat transfer coefficients. The heat transfer coefficients were greater for copper spines than that for stainless-steel spines. Heat transfer coefficients were slightly larger for the same tube with fewer spines per turn. There were no clear trends with respect to spine height.

Genetti and Kratovil [113] studied the effect of fin height (6-10.5 mm), fin spacing (197-709 m^{-1}), particle diameter (173, 262 and 551 μm) and air fluidization mass velocity (G = 0.135 - 0.949 $kg/m^2 s$) on the total heat transfer coefficient between a horizontal bundle of electrically heated tubes with helical fins, and a rectangular air fluidized bed (0.355 x 0.165 mm). The distributor plate consisted of two layers of 200-mesh stainless steel wire cloth sandwiched between two perforated steel plates. The results revealed that the heat transfer coefficient (h_w) increased with decreasing particle size. The sensitivity of h_w on particle size diminished as the fin spacing decreased and as the fin height increased. With decrease in fin height (from 10.5 to 6 mm) the heat transfer coefficients increased. Particle motion in and out of the fin space was hindered with long

fins. The heat transfer coefficients increased with increase in fin spacing (from 1 to 4.7 mm).

Chen and Withers [114] investigated the potential for use of finned tube to increase the heat transfer duty per unit bed volume in fluidized bed. They used the cylindrical bed vessel, built out of acrylic plastic, was of 0.14 m I.D. and 1.22 m high. Electric cartridge heaters, used as heat source, were centered within the inner diameter of various test sections. Glass spheres of three different sizes (127, 254 and 610 μm) were used as bed material. Wolverine Trufin type with integral spiral fins were used in this investigation. They defined a figure of merit $(hA)_{finned}/(hA)_{bare}$ as capacity function. The results indicate that for a given fin geometry the capacity function increases, reaches a maximum and then decreases with the increase of fin gap. They observed that fin density (fin per meter) has a stronger effect than fin height on the ratio of heat transfer coefficients (h_f/h_b). They concluded that increasing fin count i.e. decreasing fin gap causes a definite decrease in the ratio of heat transfer coefficients. An increase of (20-30)% in the maximum value of heat transfer coefficient was observed as fin density decreased from 748 to 354. In the range of experimental facilities they found a substantial increase of the order of (20-190) percent heat transfer capability over plain tubes. Finally, they concluded that when the fin tube performance, defined by the ratio of effective heat

transfer coefficient compared to that obtained on a plain tube under identical conditions (h_f/h_b), is unity, exceeds unity or is even just a substantial fraction of unity, one may expect the finned tube to provide higher heat transfer duty per unit length than a plain tube.

Saxena et al [37] reviewed some studies on finned tube heat transfer in fluidized beds. The primary conclusions drawn by them relating to horizontal finned heat exchange tubes are the following :

(i) Fins increase the rate of heat transfer to tubes. Their effectiveness increases, reaches a maximum and then decreases with decreasing spacing distance and increasing fin height.

(ii) An increase in tube-to-tube spacing in a bundle of short-finned tubes, which reduces the resistance to particle movement between the tubes, increases the total heat transfer coefficient. However, an increase in tube-to-tube spacing for a bundle of long finned tubes does not noticeably increase the heat transfer rate, implying that the resistance to particle movement between the fins predominates.

(iii) Correlations developed for finned tube heat transfer are for the most part based on the model by Ziegler et al [106] which considers heat transfer only to the first particle layer near a heat transfer surface. This type

of model is limited to short residence time where the heat has not had sufficient time to penetrate further particle depth.

Staub and coworkers [115] studied modelling of the flow behaviour along with finned tube performance in the turbulent flow regime. In their study they summarized preliminary data to validate the scaling of turbulent bed behaviour from room temperature to high temperature conditions. Wood et al [116] also conducted measurements related to the extent of its splash zone influence on tube heat transfer coefficients in horizontal banks of both bare and finned tubes. The tests were conducted with beds of silica (0.93 mm dia.), fluidized with air at atmospheric pressure and room temperature in a 0.3 m x 0.3 m cross-section.

Krause and Peters [117] carried out experiments on heat transfer from horizontal serrated finned tube in an air fluidized bed of uniformly sized particles. The apparatus used was made of plexiglass with inside dimensions, 33 cm wide by 30.5 cm long and a height of 1.8 m above the distributor plate. Heat was supplied by a 12.5 cm long, 1700 watt cartridge heater. Escoa serrated finned tubes were used in a study on the effect of fin length (4.76 - 17.46 mm), fin spacing (3 fins per centimeter), air fluidization mass velocity (1 - 24 times G_{mf}) on heat transfer coefficient. They introduced the term heat transfer capacity function (Ω) defined by $\Omega = (h_{fin} A_T)/(h_{bare} A_{tube})$ and stated

that the capacity function is a direct measure of the heat transfer capability for a finned tube relative to a bare tube under the same fluidization condition. The capacity function can be increased by a factor of approximately six times, depending on flow conditions and fin geometry. They concluded that when the ratio of h_{fin}/h_{bare} approaches unity or even a fraction of unity, finned tube will provide a higher heat transfer capacity per unit length than bare tube. The results revealed that the tube with shorter fins provides the best heat transfer when compared to bare tube of similar geometry and identical flow conditions. It also indicates that particles penetrate into the surfaces between the fins by an interactive relationship that depends on both fin height and fin spacing.

Glicksman [51] reviewed some studies on finned tube heat transfer in fluidized bed. He showed that almost all of the data available for finned surfaces relate to particles with diameter of 0.6 mm or less. Staub et al [115] presented data for particles of diameter in the range 0.65 to 2.6 mm. In most findings he found the heat transfer coefficients for finned surfaces are reduced by 30 to 50 percent of the bare tube surface. He further added that many investigators [103, 109, 114] concluded that even with this reduction in heat transfer coefficient and the inclusion of fin efficiency, fins still can provide increased overall heat transfer.

2.6 Factors Affecting the Heat Transfer in Circulating Fluidized Beds

The process of heat exchange between a fluidized bed and the heat transfer surface is intimately associated with the process of heat transfer between the fluidized solids, and the fluidizing gas, the rate at which the particles mix inside the bed, the general behaviour and geometry of the fluidized system. Consequently, the factors which control the heat transfer characteristics of the system include the variables which determine the fluidizing properties of the bed as given below :

(i) Properties of fluidized and fluidizing materials,

(ii) Operating conditions, and

(iii) Bed geometry

2.6.1 Influence of physical properties of fluidized and fluidizing materials

The thermal conductivity of the solid has practically no influence on heat transfer coefficient [63] where as the thermal conductivity of fluidizing gas has the greatest influence on heat transfer coefficient in a fluidized bed [118, 119]. Wen and Leva [120] established a correlation where $h \alpha k_g^{0.6}$. Gelperin and Einstein [33] reported that the increase in heat transfer coefficient with the temperature of the fluidized bed largely results from the increase in gas thermal conductivity with bed temperature

and not just from increased thermal radiation.

The effect of solid heat capacity on heat transfer coefficient is revealed from the investigations of many workers. Dow and Jakob [45] suggested a correlation where the dependence of h on the solid heat capacity was observed. In fact, all the correlations are of the form of $h \alpha (\rho_s c_{ps})^n$. The value of n varies from 0.25 [45] to 0.8 [121]. But Wunder and Mersmann [122] have presented a model where no influence of solid heat capacity was admitted. Specific heat of fluid does not affect the heat transfer at moderate pressure. But at high pressures h is found to be increasing with c_{pg}. This dependence is revealed clearly in fluidization by liquids [119] when the specific heat of the fluids and of the solid particles are comparable.

2.6.2 Influence of operating variables

Heat transfer coefficient has a strong dependence on the fluid velocity, particularly in fluidized bed. Kobro and Brereton [8], Basu and Nag [39] and many others have reported that the heat transfer coefficient decreases with increase in superficial velocity in circulating fluidized beds. Wu et al [80] have reported that fluidizing velocity has only marginal effect on bed-to-wall heat transfer coefficient once the bed density was established. Wunder and Mersmann [122] observed that for very fine solid particles,

the highest value of heat transfer coefficient reaches upto two orders of magnitude above comparable values for fixed bed or single phase gas flow. The steep increase in heat transfer coefficient from fixed bed to fluidized bed is the result of a fundamental change in the heat transfer mechanism induced by the solid motion.

The effect of particle size on heat transfer coefficient is quite significant. Baskakov [123] varied the particle size by more than three orders and revealed that heat transfer coefficient decreases with increase in particle size. Wunder and Mersmann [122] have reported from the published works a relationship between the particle diameter and maximum heat transfer coefficient as $h_{max} \alpha d_p^{0.4}$ which is valid only for $0.05 < d_p < 2$ mm. Decker and Glicksman [124] have observed that heat transfer coefficient decreases with increase in particle size for small particles. Mickley and Trilling [125] worked with five different particle sizes from 70-451 μm, Kobro and Brereton [8] performed experiments with two particle sizes (170 and 250 μm), Basu and Nag [39] experimented with two particle sizes (87 and 227 μm). All of these investigators observed that heat transfer coefficient decreases with increase in particle size. The data of Wu et al [80] and Sekthira et al [79] showed that for long heat transfer surfaces the effect of particle size is not so prominant in heat

transfer study. The shape and surface of the solid particles are found to be influencing the heat transfer rate. It is found to be higher for round and smooth particles [122].

2.6.3 Influence of bed geometry

Controversial data have been presented by different authors on the influence of bed dimension on heat transfer. Majority of the data agree with the fact that the heat transfer coefficient does not depend on bed height. Analysis of Dow and Jakob [45] shows that decreasing heat transfer coefficient with increasing bed height is a combined effect of surface height and a number of other factors. Gelperin and Einstein [33] showed that the dependence of heat transfer coefficient on bed diameter cannot be assessed either qualitatively or quantitatively. The data of Mickley and Trilling [125] on 0.1 m and 0.025 m diameter beds did not indicate any effect of column diameter. The data of Stromberg [72] suggest that the heat transfer coefficient decreases with increase in column diameter. Glicksman [12] reported that a small active heat transfer probe would give an upper limit to the heat transfer in a circulating fluidized bed. Wu et al [38] reviewed some relevant studies and from their own data concluded that, depending on the vertical length of heat transfer surface, one will obtain very different average heat transfer coefficients which will differ by upto 200 percent.

2.6.4 Influence of distributor design

The distributor has a strong influence on the size and frequency of the bubbles in a fluidized bed. This in turn, affects the combustion of coal in the bed. The distributor affects the attrition of the bed material [35]. A poorly designed distributor may lead to low combustion efficiency, agglomeration or can produce channelling in the bed. Wen [126] suggested that in order to reduce dumping, the orifice diameter should not be more than 3 to 8 times the particle diameter. Grewal and Saxena [127] performed experiments and studied the effect of distributor design on heat transfer from an immersed horizontal tube in a fluidized bed. They used two different distributors. The first one had 7.7 percent opening and the holes were in square array. The second one had 37.5 percent opening and the holes were in triangular array. They observed that for small values of $(G - G_{mf})$, the values of total heat transfer coefficient (h_w) for the second distributor were larger than those for the first distributor. As the value of $(G - G_{mf})$ was increased, the first distributor gave higher values of h_w. With further increase in $(G - G_{mf})$, the differences in the values of h_w for the two distributors diminished and the trend became reverse. They explained the effect of distributor design on total heat transfer coefficient on the basis of its effect on the initial bubble size and frequency.

2.7 Hydrodynamics

Glicksman [12] stated that the important hydrodynamic factors in circulating fluidized beds are the fraction of the wall covered by particles and gas, i.e., voidage phenomena and the average contact time of the particles at the wall.

2.7.1 Voidage

The pioneer work in this field by Yerushalmi and his co-workers [128,129,130] at city college of New York (CCNY) was later reviewed by Yerushalmi and Avidan [28]. Continuing research at CCNY, principally by Weinstein and his associates [131] has confirmed that the structure of the dense phase in a fast fluidized bed consists of a dilute core and a dense wall region, first reported by Gajdos and Bierl [132]. Further confirmation was provided by Hartge et al [133] employing fibre optic probes. The state of high velocity fluidization was also critically reviewed by Geldart and Rhodes [29]. They concluded that the nonuniform radial solid concentration distribution is typical of all flowing gas-solid system at velocities from incipient fluidization to dilute phase pneumatic transport. Matsen [134] stated that in a dense-phase flow, the circulation fluxes are in the range of 150-1460 kg/m^2s, average densities in the riser are 160-240 kg/m^3, the voidages are 0.85 - 0.9 and superficial solid velocities are 3-5 m/s. Radial density profile measured by Saxton and Worley [135] in a large riser show

considerable nonuniformities with densities at the wall 10 to 20 times those in the centre of the vertical pipe. Soo et al [136] showed that at conveying velocities in a 5 inch (125 mm) diameter horizontal pipe, small particles travel much more slowly at the walls than in the centre of the tube, moreover solid concentrations were higher at the wall. Horio et al [137] measured particle velocities in the free board of a bed fluidized at 0.3 to 0.5 m/s and found that particles travelled downwards at the wall. Morooka came to a similar conclusion and in addition found that particle concentration increased greatly in the region of the wall. In both the studies of solid hold-up, voidages were greater than 0.98. Abed [138] fluidized FCC up to 0.55 m/s and measured higher voidages (upto 0.79) on the bed axis than at the wall (0.6). The observation of Grace and Harrison [139] and Farrokhalaee and Clift [140] in small experimental units and that of Whitehead et al [141] and Abed [142] in large industrial size beds showed that all bubbling fluidized beds are non-uniform. Visual observation and Video tape [19] show fast beds to comprise of dense clusters or strands and a gas phase continum with dispersed solids [143]. Measurements with pitot tubes, capacitance probes and X-rays [131, 132, 144] suggest that these wall layers are intermittent and extend typically 10-20 mm into the column. Particles generally move up through the core of the bed and flow down the wall in the form of streamers which are called clusters. These streamers are

continuously formed, dissolved and reformed [40]. The thickness of streamer sliding down the wall was measured by Rhodes et al [145] and Horio et al [146] as several millimeters. Bolton and Davidson [147] observed that the velocity of the falling film is about 0.5 m/s and the particle hold-up in the falling streamer is more than twice that in the riser core. Li and Kwauk [148] noted two regions in the S-shapped axial voidage profile in fast fluidization:a dilute phase region at the top and a dense phase region at the bottom. Between these two regions there exists a transition zone in which is located the inflection point of voidage. Li et al [149] further extended the studies and identified three operating regions of axial voidage profiles in fast fluidized beds on the basis of the relation between the solids rate (G_s) and the saturation carrying capacity of the flowing gas (K^*). When the solid flow rate through the bed is equal to the saturation carrying capacity of the gas (K^*), at the operating velocity, the voidage profile will be 'S' shaped . There will be a dense phase region at the bottom and a dilute phase region at the top. When the solid flow rate is less than K^* only dilute flow exists, and when the solid flow exceeds K^* the dense phase extends to the top of the bed. Yang [150], Rhodes and Geldart [151] and few other investigators have shown that the zones or regimes comprise of a relatively dilute core of solids in the middle and a dense region of

generally down-flowing solids near the wall.

The radial non-uniformity of voidage at least for small cross-section reactors, is now generally accepted [11]. There is, however, a need of data on large diameter units. Some investigators feel the assumption of cluster is not necessary to explain the high gas-solid slip velocity. Although it can be explained by the downflow of solids in the reactor annulus, video pictures demonstrate the existance of long solid agglomerates. There is a general agreement on the existence of a dense bed at the bottom and a relatively dilute region at the top of CFB.

2.7.2 Residence time

It is a very important parameter for the study of heat transfer in circulating fluidized beds, but there is a serious scarcity of information about the particle residence time in the available literature. In many of the theoretical models the heat transfer process is postulated to be governed by the residence time of the particle or emulsion phase on heat transfer surface. To date applications of these theories have been hampered by lack of definitive information regarding the actual residence time in fluidized beds. Mickley and Fairbanks [152] and later Baskakov [123] attempted to measure residence time by recording the temperature fluctuation at the surface of small test heaters.

Koppel et al [153] measured the residence time on the Vessel's external wall by taking photograph of the particles through a transparent wall. Ozkaynak and Chen [154] measured residence time of the emulsion phase on the surface of an internal tube under normal fluidized condition. A fast response capacitance probe was used which permitted direct indication of emulsion and void phase contact at the surface of the test tube. Measurements were obtained for four different types of glass spheres over a wide range of fluidizing air velocities. At low excess air flow rate their data were close to those recorded by Mickley and Fairbanks [152] while at high excess flow rates the results approached those recorded by Baskakov [123]. Finally, they concluded that a definitive explanation of the various trends cannot be given in view of the limited understanding of the residence phenomenon on surfaces of submerged tubes.

Any correlation of residence time is scarce in the published literature. Subbarao [155] derived an expression of cluster residence time based on his cluster model. The correlation suggested by Subbarao [155] for the average cluster residence time on the wall is as follows :

$$t_c = \frac{\rho_{sus} D_b}{\rho_s^{1/3} (1 - \varepsilon_c)^{1/3} U_o^{1/3} W_s^{2/3}}$$

The stable bubble diameter, D_b can be calculated from the following expression

$$D_b = \frac{2\ U_T^2}{g}$$

If $\frac{2U_T^2}{g} > D_{bed}$, then bubble diameter is taken to be equal to the bed diameter. It assumes that small spherical clusters detach themselves from the wall or loose their identify after traversing a length equivalent to the diameter of the cluster (typically 10 mm). Thus for a given operating condition, it gives the lower limit of residence time. The residence time on the wall is less than the time the strand takes to traverse the length of the heat transfer surface and the time it takes to dissolve.

Glicksman [12] derived an expression for residence time considering the wall friction which was estimated from the measured maximum fall velocity. For a small probe located on an adiabatic wall, the residence time, t_r may be approximated as

$$t_r = \frac{L}{V_{max}}$$

This analysis does not take account of the time the cluster takes to be dissolved. It is possible that the cluster may loose its identity before it traverses the entire length of the heat transferring surface. Under these circumstances the above relation will give the upper limit of residence time.

He assumed that clusters swept to the wall start accelerating downward from rest till it reaches a maximum velocity, V_{max}. Except in cases where the clusters break-up before traversing the entire length of heat transferring surfaces, the residence time can be calculated by the equation of motion which follows [12]

$$L = \frac{V_{max}^2}{g} \left(e^{-gt_r/V_{max}} - 1 \right) + V_{max}\, t_r$$

Beyond the acceleration distance (which is about 15 cm) the residence time, t_r can be estimated from the free fall velocity (U_T) by substituting its value for V_{max}, i.e.,

$$t_r = \frac{L}{U_T}$$

2.8 Models of Fluidized Beds

Heat transfer in a circulating fluidized bed depends on a large number of variables. Several investigators have attempted to correlate these parameters. Mickley and Fairbanks [50] developed the first physical model of heat transfer from a bubbling bed by introducing the packet theory. Martin [65] developed a heat transfer model (for bubbling bed) based on kinetic theory of gases. Subbarao and Basu [156] suggested a heat transfer model for CFB with the concept of clusters in the lean phase. Basu and Nag [39] extended

this model by including a wall resistance in series with the homogeneous semi-infinite medium of particles. Glicksman [12] developed a mechanistic model with the concept of cluster and wall resistance. Sekthira, Lee and Genetti [79] developed a CFB model based on particle theory of Ziegter et al [106]. Chen et al [157] developed a model for high temperature in CFB. Suleyman Biyikli et al [158] developed a phenomenological model for heat transfer in the free board of a fluidized bed. Mahalingam and Kolar [159] developed a heat transfer model for the membrane wall of a high temperature circulating fluidized bed. Nag and Moral [160] developed an empirical model based on dimensional analysis of the parameters relevant to CFB heat transfer with the concept of cluster theory of Mickley and Fairbanks [50].

The important hydrodynamic models are developed by Rhodes and Geldart [161], Yang [150], Kunii and Levenspiel [162] and Heng Zhang et al [163].

2.8.1 Heat transfer models

(a) Bubbling bed models

Mickley and Fairbanks [50] developed the first physical model of heat transfer from a fluidized bed by introducing the packet theory, where a packet of particles from the bed at temperature T_b is swept into contact with the heat transfer surface at a temperature T_w and gives up

heat by unsteady state diffusion, then the rate of heat transfer (Q) is given by

$$Q = \frac{A_p}{\sqrt{\pi}} \sqrt{k_e \rho_e c_{ps}} \; t_r^{-1/2} \quad (T_b - T_w)$$

where, A_p is the area of the packet in contact with the heat transfer surface, k_e and ρ_e are the effective thermal conductivity and density of packet of emulsion respectively. Thus the local instantaneous heat transfer coefficient is given by

$$h_{wi} = \left(\frac{k_e \rho_e c_{ps}}{\pi t_r} \right)^{1/2}$$

Now the time averaged local heat transfer coefficient h_w should reflect the variation of h_{wi} with contact time as well as the variation of contact time from one packet to another. Thus h_w is given by

$$h_w = \int_0^{\alpha} h_{wi} \; I(t_r) \; dt_r$$

where $I(t_r)$ is the fraction of surface occupied by packets of age between t_r and $t_r + dt_r$. On substitution, the time averaged local heat transfer coefficient is given by

$$h_w = \left(\frac{k_e \rho_e c_{ps}}{\pi t_r} \right)^{1/2}$$

where t_r is the proper characteristic contact time of packets defined by

$$(t_r)^{-1/2} = \int_0^{\alpha} t_r^{1/2} \, I\,(t_r)\, dt_r$$

Detailed analyses about the feasibility of application and modification of the model by other authors have been discussed in Art. 2.4.1.

Martin [64,65] has had considerable success predicting heat transfer in conventional fluidized bed with a model based on a controversial analogy between particle motion and molecular motion described by the kinetic theory of gases. In Martin's model, single particle transfer at the surface is said to be rate-controlling. Transfer in the gas between a surface and the particle which has reached the surface is estimated using a relationship due to Schlunder [164].

$$Nu_{sp} = \frac{h_{sp}\, d_p}{\lambda_g} = 4\left[(1+Kn)\ Ln\ (1 + \frac{1}{Kn}) - 1\right]$$

where, Kn = Knudsen number

$$= \frac{4}{d_p} \left(\frac{2}{\gamma} - 1 \right) \frac{\lambda_g \sqrt{2\pi RT/M}}{P(2c_{pg} - R/M)}$$

The accommodation coefficient, γ, for a gas can be calculated from [64]

$$\gamma = \left[1 + 10^{(0.6B - 1 - 1000/T)/B} \right]^{-1}$$

where, B = 2.8 for air, so that $\gamma = 0.9$ for air at a temperature of 298K. For most of the cases the thermal resistance within the particles can be ignored. Martin's predicted h_{pc} can then be predicted from the following correlation

$$\frac{h_{pc}\, d_p}{\lambda_g} = C\, Z \left[1 - \exp\left(- \frac{Nu_{sp}}{k\, Z}\right)\right]$$

where, $$Z = \frac{\rho_p\, c_{ps}}{6\, \lambda_g} \left(\frac{g\, d_p^3\, (C_{mf} - C)}{5\, C_{mf}\, C} \right)^{1/2}$$

k is a constant which should lie in the range 2-4 and C is the volumetric concentration of particles.

(b) CFB models

Subbarao and Basu [156] developed a heat transfer model for circulating fluidized bed with the concept of clusters in lean phase. They considered the heat transfer by transient conduction to clusters of particles and voids/bubbles as they came into contact alternatively with the heated surface. The concepts and equations developed by Subbarao [155] for the clusters in the lean phase are used in the heat transfer model

$$D_c = \left(\frac{W}{\rho_s\, U_o\, (1 - \epsilon_c)} \right)^{1/3} D_v$$

$$D_v = D_{bs} = \frac{2\,U_t^2}{g} \qquad \text{for } D_{bs} < D_t ,$$

$$\text{or, } (U_o - U_{mf})/U_{sr} < 0.2$$

$$D_v = D_t \qquad \text{for } D_{bs} > D_t$$

$$\text{or, } (U_o - U_{mf})/U_{sr} > 0.2$$

$$U_{sr} = 0.35\,(g\,D_t)^{0.5}$$

$$h = \left[\frac{4\,k_c\,c_c\,U_o}{\pi\,D_v}\left(\frac{W}{\rho_s U_o(1-\varepsilon_c)}\right)^{2/3}\rho_{sus}\right] x$$

$$\left[1 + \left(\frac{k_g\,c_{pg}\,\rho_g\,(\varepsilon - \varepsilon_c)\,U_o}{k_c\,c_c\,(1-\varepsilon_c)\,W}\right)^{0.5}\right]$$

For small column diameter, this model predicts that particle diameter has no effect on heat transfer coefficient.

Basu and Nag [39] extended the model of Subbarao and Basu [156] by including a wall resistance in series with the homogeneous semi-infinite medium of particles. Basically, these models were developed on the basis of packet theory of Mickley and Fairbanks, where they assumed that when the cluster is in contact with the gas film, heat will flow to the wall surface by conduction through the gas film and by radiative interchange between the cluster and the wall during the period of contact. When the dispersed phase or

void is in contact with the wall, heat will be transferred by convection to the wall surface and by radiative exchange between the wall and distant clusters through the intervening space. In developing the model they used the analysis of Mickley and Fairbanks [50] and Baskakov [53] for the prediction of heat transfer from the cluster and correlation of Wen and Miller [86] for heat transfer from dilute phase. Assuming both cluster and wall as gray surfaces the final correlation for the average heat transfer coefficient in a CFB combustor suggested by them is given below :

$$h = \frac{\delta_c}{\frac{d_p}{10\,K_{ew}} + \left(\frac{\pi\, t_r}{4\,K_c\,C_c\,\rho_c}\right)^{1/2}}$$

$$+ (1-\delta_c)\left(\frac{k_g}{d_p}\right)\left(\frac{c_{ps}}{c_{pg}}\right)\left(\frac{\rho_{sus}}{\rho_s}\right)^{0.3}\left(\frac{U_T^2}{g\,d_p}\right)^{0.21}$$

$$+ \sigma\, f_{c-w}\,(T_b + T_w)(T_b^2 + T_w^2)$$

They used the correlation of Subbarao [155] for predicting the cluster residen time (t_r).

Glicksman [12] developed a mechanistic model for heat transfer in a circulating fluidized bed. He assumed that the particles move up through the core of the bed and flow down the wall as cluster or streamer. He considered heat

transfer between the wall and a layer which is several particles diameter thick. When striking the wall the particles are at bulk temperature T_b while the wall is at T_w. For very short residence time, the heat transfer from the particles to the wall will be controlled by the interfacial or wall heat transfer resistance with the particles initially at a uniform bulk bed temperature, T_b. For bubbling bed heat transfer, Decker and Glicksman [124] developed a relation of the form

$$\frac{h_w d_p}{k_g} = 12 + 0.05 \text{ Re Pr}$$

The heat transfer beyond the first layer comes into action when the heat transfer surface is sufficiently long and needs to be considered only when the thermal time constant of the first layer of particles is smaller than their residence time on the wall. Assuming heat conduction between these particles and the wall is $k_g/24d_p$ times the projected area of the particles, he derived the thermal time constant τ_p as

$$\tau_p = \frac{c_{ps} d_p^2}{36 k_g}$$

Glicksman [12] analysed the model of Mickley and Fairbanks [50] and suggested a model which includes the wall resistance in series with a homogeneous semi-infinite collection of particles giving an overall heat transfer coefficient to the particle as

$$h_o = \left(\frac{1}{h_w} + \frac{1}{h_H} \right)^{-1}$$

where, h_H is an effective or homogeneous heat transfer coefficient for transient conduction to the homogeneous semi - infinite medium given as

$$h_H = \sqrt{\frac{K_c \rho_s C_{ps} (1 - \varepsilon)}{\pi t_r}}$$

and wall heat transfer coefficient 'h_w' was approximated from the correlation of Decker and Glicksman [124] as

$$h_w = \frac{12 k_g}{d_p}$$

for small particles and non-pressurised bed.

Sekthira, Lee and Genetti [79] developed a model which is an extension of the model for fluidized beds proposed by Ziegler et al [106] and Genetti and Knudsen [165] to apply to a circulating bed. They assumed that heat transfer in a CFB is guided by heat convection from individual particles to the neighbouring film. They further assumed that V_{max} is equal to the free fall velocity of individual particles. They finally derived an equation where particle Nusselt Number is found to be a function of suspension density

$$Nu_p = 0.293 \rho_{sus}^{1/4}$$

This model shows that heat transfer coefficient is proportional to the fourth root of suspension density which contradicts the analysis of Glicksman [12] who showed that heat transfer data of most investigators are proportional to the square root of suspension density.

Chen et al [157] proposed a theoretical model for simultaneous convection and radiation in a high temperature CFB. They assumed that in a circulating bed, heat transfer between the hot gas-solid media and the walls occur by both turbulent convection and thermal radiation. The radiative and convective transport occur simaltaneously throughout the suspension and would interact in a nonlinear manner to affect the transverse temperature and heat flux profiles. The effective heat transfer coefficient can be calculated from the following relationship

$$h = \frac{q}{T_w - T_B} \quad \text{at} \quad y = 0$$

where, $q = q_r + q_c$

T (at $y = 0, x$) $= T_w$

and T_B the mixed-mean bulk temperature defined by

$$T_B = \frac{\int_0^L \left[\alpha_p \rho_s c_{ps} U_p + (1-\alpha_p) \rho_g c_{pg} U_g\right] T \, dy}{\int_0^L \left[\alpha_p \rho_s c_{ps} U_p + (1-\alpha_p) \rho_g c_{pg} U_g\right] dy}$$

Suleyman Biyikli et al [158] developed a phenomenological model for heat transfer in free board of fluidized bed. Ismail and Chen [166] observed that solid particles are carried from the dense bed into the free board in periodic bursts, rather than in a continuous stream. This suggests that tubes located in the free board will be intermittently splashed by bursts of relatively dense gas emulsion and exposed to a convective flow of relatively lean gas-particle mixture between splashes. This hypothesis was supported by the capacitance measurements of particle contact on the surface of free board tubes as reported by Biyikli et al [167]. The convective heat flux would be the time average contributions for heat transfer from the lean and dense phases. The total convective heat transfer coefficient can be written as the sum of the average lean phase and dense phase coefficients weighted by the fraction of contact by each phase :

$$h = \frac{q}{T_b - T_w} = h_L f_L + h_D (1 - f_L)$$

The measurements of Biyikli et al [167] indicate that the residence time of the dense phase on the tube surface is short, typically of the order of tenths of seconds. During such contacts, transient conduction occurs between the dense phase and the tube surface. Since the Fourier conduction depth is much less than the nominal dense phase depth, this process can be approximated as transient conduction between two semi-infinite media. The resulting solution for the time average

heat transfer coefficient is

$$h_D = \frac{2}{\sqrt{\pi}} \sqrt{\frac{K_D \, (\rho_s \, c_{ps})_D}{\bar{\theta}_D}}$$

where, $\bar{\theta}_D$ is the root-mean residence time for a statistical number of dense phase contacts. The final form of the equation for the prediction of area-averaged heat transfer coefficient is

$$h = f_L \left[\frac{K_L}{D} \; a \left(\frac{\rho_{sL} \, U_{sym} \, D}{\mu_L} \right)^b \left(\frac{\mu_L \, c_{pL}}{K_L} \right)^{1/3} \right]$$

$$+ \quad (1 - f_L) \left(\frac{2}{\sqrt{\pi}} \sqrt{\frac{K_D (\rho_s \, c_{ps})_D}{\bar{\theta}_D}} \right)$$

The input parameters required are the physical properties of the gas and solid (ρ_g , k_g , c_{pg} , μ_g , ρ_s , c_{ps} , k_s), system variables (U_{sg} , U_{mf} , U_t , U_{sym} , D , d_p) and particle contact parameters (f_L , $\bar{\theta}_D$, $\bar{\theta}_p$, $\bar{\alpha}_D$, $\bar{\alpha}_L$).

Mahalingam and Kolar [159] developed a model incorporating particle convection and radiation components for the prediction of heat transfer between the vertical membrane wall and the suspension of a high temperature circulating fluidized bed. The particle convective component is modelled based on a downward moving emulsion layer of thickness varying according to an one-third power law expression derived

from CFB dynamics. The radiation component is calculated through the alternate slab model using the local values of the emulsion layer thickness and residence time. They derived the local particle convective (h_{pc}) component of the form

$$h_{pc} = \frac{1}{\left(\frac{d_p}{10\, k_g}\right) + \frac{1}{h_x}}$$

where, h_x, the local heat transfer coefficient is expressed as

$$h_x = \frac{K_e}{\delta_x} + 2\,\frac{K_e}{\delta_x} \sum_{i=1}^{\alpha} \exp\left(\frac{-\, i^2\, \pi^2\, \alpha_e\, t}{\delta_x^2}\right)$$

The local thickness of emulsion layer, δ_x is given as,

$$\delta_x = \left(\frac{3\, \mu_e\, (E_x - G_s)\, A}{g\, p\, \rho_e^2}\right)^{1/3}$$

and the contact time, t was estimated from the following relation

$$t = \frac{x}{\bar{V}_x}$$

The radiation component was calculated through the use of the alternative slab model in its extended form as developed by Kolar et al [67]. The total heat transfer coefficient, h_t was composed of two additive components, viz., the particle convective component h_{pc} and the radiative component, h_r.

2.8.2 Heat transfer model for finned tubes in bubbling beds

Genetti and Knudsen [165] extended the model of Ziegler et al [106] to apply for finned surface. The model by Ziegler et al [106] for predicting heat transfer coefficient from surface to fluidized bed was based on the so called 'particle mode mechanism', viz., the particles absorbing (or releasing) heat at the heat transfer surface and releasing (or absorbing) this energy to the gas in the bulk of the bed. They derived the following equation.

$$Nu_{wp} = \frac{h_w d_p}{k_f} = \frac{4\pi/\sqrt{3}}{\left(1 + \frac{6 k_f \bar{\tau}}{\rho_s c_{ps} d_p^2}\right)^2}$$

This model was modified by Genetti and Knudsen [165] by assuming that the temperature of the fluid around the particle is equal to the arithmatic mean of the wall and bulk bed temperature ($T_r = (T_b + T_w)/2$). After relating the number of particles at the surface to the particle fraction $(1-\varepsilon)$ and introducing dimensionless group, the final correlation suggested by them was in the following form

$$Nu_{wp} = \frac{10(1-\varepsilon)^{0.5}}{(1 + \lambda Re_p^{\gamma})^2}$$

where λ and γ are unknown functions of fin height and fin thickness. They calculated the total heat transfer coefficient

for finned surfaces from the following relation

$$h_w = \frac{Q}{(T_w - T_b)\ A_w}$$

To eliminate the dependence of h_w on thermal conductivity of the fin material, the heat transfer coefficient was redefined in terms of local conditions as follows

$$h_{wL} = \frac{Q_L}{A_{wL}\ (T_{fL} - T_b)}$$

which is a function only of the frequency of collisions between the particles and the fin surface. Further, it was assumed that the heat transfer coefficient was constant over the full length of the fin. To determine the values of the redefined h_w, the standard mathematical model was used to describe the heat conduction in a thin rectangular fin [168]

$$T-T_b = \frac{-(T_w-T_b)\left[(k\sqrt{R}/h_w)\sinh\sqrt{R}\ 1 + \cosh\sqrt{R}\ 1\right]}{k\sqrt{R}/h_w\cosh\sqrt{R}\ 1 + \sinh\sqrt{R}\ 1} \times$$

$$\left(\sinh\sqrt{R}\ x + (T_w-T_b)\cosh\sqrt{R}\ x\right)$$

To calculate the amount of heat entering the base of a single fin, it was required to take the derivative of T with respect to x and to multiply it by the factor $(-k\,\delta w)$ and

then evaluate it at $x = 0$. The total amount of heat lost by the finned tube is equal to the amount of heat lost through the fins plus the amount of heat lost through the bare tube.

$$\frac{Q}{T_w - T_b} = \frac{k\,\delta w\sqrt{R}\,(k\sqrt{R}\,\sinh\sqrt{R}\,l + h_w\cosh\sqrt{R}\,l)(A_t - A_b)}{(k\sqrt{R}\,\cosh\sqrt{R}\,l + h_w\sinh\sqrt{R}\,l)\left[2l(w+\delta) + w\,\delta\right]} + A_b h_w$$

This equation was solved to find h_w for each experimental value of $Q/(T_w - T_b)$. The values of h_w thus obtained were independent of the thermal properties of the fin material.

The model developed by Ziegler et al [106] and extended by Genetti and Knudsen [165] was modified by Priebe and Genetti [112] to give

$$Nu_{wp} = \frac{a(Q/A_t)^b\,(d_p/s)^c}{\left[1 + d(G/G_{mf})^2\right]^2}$$

The ratio G/G_{mf} was used rather than Reynolds Number, to account for differences in dynamics for different particle sizes. Values of a, b, c, d and e were found by cross plotting of the various parameters. The final correlation developed by them was of the form

$$Nu_{wp} = \frac{(30270\ d_p - 2.9)(Q/A_t)^{0.24}(d_p/s)^{-(0.55+232\ d_p)}}{\left[1 + (8.19 + 231s)/(G/G_{mf})^{0.164}\right]^2}$$

where, d_p is expressed in micron, s in millimeter and Q/A_t in W/m^2.

Krause and Peters [117] developed a finned tube model. By one dimensional steady-state heat balance about a typical rectangular fin element, they first developed an equation for temperature profile. For this case they found the heat input to each fin from the Fourier heat conduction equation

$$q = - k A \left.\frac{dT}{dx}\right|_{x = 0}$$

Differentiation of the temperature profile yields an expression for the heat transfer to all fins as follows :

$$\frac{Q_{total}}{\Delta T} = FN(\bar{h}\ P\ k\ A_{cs})\tanh(m.\ FLC) + A_{uf}\ \bar{h}$$

where the corrected fin length, $FLC = FL + \frac{t}{2}$

The convective heat transfer coefficient in the above equation can not be found explicitly, hence, it is necessary to assume an initial value for 'h' and place this equation in an iteration scheme until convergence is reached.

2.8.3 Hydrodynamic models

Rhodes and Geldart [161] proposed a hydrodynamic model for circulating fluidized beds. In developing the model they used the correlation of Wen and Chen [169] as given below

$$E = E_{\alpha} + (E_o - E_{\alpha}) \exp(-a h)$$

where E, E_{α} and E_o are the entrained flux at riser outlet, above TDH and at dense bed surface respectively, 'a' is the exponential constant and 'h' is the height of the bed.

The solid concentration in the dense phase region is estimated using a method recommended by Geldart based on the modified 'Two-phase Theory' of Toomy and Johnstone [170]. The mass of solid in dilute phase region is calculated by numerical integration over the height 'h^*'.

The mass of solid in the dilute-phase region

$$M_{dil} = \int_{h=o}^{h=h^*} \rho_s (1 - \varepsilon_h) A \, dh$$

The mass of solid in the dense-phase region,

$$M_{den} = \rho_s (1 - \varepsilon_{den}) A (L - h^*)$$

Then neglecting wall friction and acceleration effect, pressure loss across the dilute-phase

$$\Delta P_{dil} = \frac{M_{dil}\, g}{A}$$

Pressure loss across the dense-phase

$$\Delta P_{den} = \frac{M_{den}\, g}{A}$$

Hence, pressure loss across the riser is given by

$$\Delta P_R = \Delta P_{dil} + \Delta P_{den}$$

The pressure loss across the primary cyclone 'ΔP_{cyc}' is calculated on the assumption that the design pressure loss of 1200 N/m^2 occurs when the superficial gas velocity in the riser is 6 m/s and that for a cyclone pressure loss is directly proportional to the square of the volumetric gas flow rate, thus

$$\Delta P_{cyc} = 33.33\, U_o^2$$

The solid control valve pressure loss can be calculated from the following correlation

$$\Delta P_v = 4.2 \times 10^{-6} \left(\frac{G}{\pi\, D_o^2/4} \right)^2$$

A fluidized bed operated under minimum fluidization condition is commonly referred to as the slow bed. The pressure drop in the slow bed can be calculated from the following equation

$$\Delta P_{SB} = \frac{M_{SB}\, g}{A_{SB}}$$

If instead of a slow bed a stand pipe or hopper and L-valve are used, appropriate alternative expressions must be written for the pressure drop. Thus,

$$M_{SB} = M - M_{dil} - M_{den} - ME$$

The overall pressure balance then becomes,

$$(M-M_{dil}-M_{den}-ME)\frac{g}{A_{SB}} = \int_{h=o}^{h=h^*} \rho_s(1-\varepsilon_h)\,dh + (L-h^*)(1-\varepsilon_{den})\,g\,\rho_s + 33.33U_o^2 + 4.2 \times 10^{-6} \left(\frac{G}{\pi D_o^2/4}\right)^2$$

Yang [150] observed 3-types of voidage profile in the riser section of a CFB. These are dilute-phase pneumatic transport profile, fast (fluidized) bed profile and dense-phase transport. Employing unified theory for dilute phase pneumatic transport through continuity consideration Yang [150] expressed the voidage 'ε' as

$$\varepsilon = 1 - \frac{4\, W_s}{\rho_s\, \pi\, D^2\, U_p}$$

Beyond the particle acceleration region, the particle velocity was calculated by

$$U_p = U_f - U_T \sqrt{\left(1 + \frac{f_p\, U_p^2}{2gD}\right) \varepsilon^{4.7}}$$

Beyond the particle acceleration region the total pressure drop in a vertical conveying line was expressed as

$$\Delta P_{Tl} = \rho_s(1-\varepsilon)L_l g + \frac{2f_g\rho_f U_f^2 L_l}{D} + \frac{f_p\rho_s(1-\varepsilon)U_p^2 L_l}{2D}$$

The solid inventory in the dilute phase region was calculated from the relation

$$I_1 = \rho_s(1-\varepsilon)A_r L_l$$

The solid inventory in the acceleration region was obtained from

$$I_2 = \int_{U_{pl}}^{U_{p2}} \frac{\rho_s(1-\varepsilon)\, A_r\, U_p\, dU_p}{\frac{3}{4} C_{DS}\, \varepsilon^{-4.7}\, \frac{\rho_f(U_f - U_p)^2}{(\rho_s - \rho_f)d_p} - (g + \frac{f_p U_p^2}{2D})}$$

The solid recirculation rate (R) between the dilute core and dense wall region was expressed as

$$R = \frac{\pi}{4}(D^2 - D_i^2)\,\rho_s(1-\varepsilon_{mf})U_T$$

The average voidage measured experimentally can be related to the voidage in the dilute core and dense wall region as follows

$$\frac{D}{D_i} = \left(\frac{\varepsilon_c - \varepsilon_{mf}}{\varepsilon_{ave} - \varepsilon_{mf}}\right)^{0.5}$$

The pressure drop and the solid inventory in the dense phase region can be approximated by the following equation

$$\Delta P_{T3} = \rho_s (1 - \varepsilon_{ave}) L_3 ,$$

$$I_3 = \rho_s (1 - \varepsilon_{ave}) A_r L_3$$

The transition region between the dense and dilute phases of a fast bed is formulated based on the empirical entrainment model by Lewis et al [171]. The height of a transition region can be calculated as follows

$$H = \frac{1}{a} \text{Ln} \left(\frac{1 - \varepsilon_{ave}}{1 - \varepsilon_4} \right)$$

The empirical freeboard exponential constant 'a' proposed by Lewis et al [171] can be expressed in terms of the particle turbulent diffusion coefficient, α_p , as

$$ah = \frac{16}{D^2} \int_o^h \frac{\alpha_p}{(U_f - U_T)} \, dh$$

where h is the height in the transition region.
The total pressure drop and the solid inventory in the transition region can be obtained from

$$\Delta P_{T4} = \int_o^H \rho_s (1 - \varepsilon_4) g \, dh$$

$$I_4 = \int_o^H \rho_s (1 - \varepsilon_4) A_r \, dh$$

Yang [150] considered a cyclone pressure loss of 10 times the inlet velocity heads

$$\Delta P_c = 10\ \rho_f\ U_c^2$$

The pressure drop and solid inventory in the slow bed (return leg) was calculated from the following equations

$$\Delta P_{SB} = \rho_s(1 - \varepsilon_{mf})\ L_{SB}\ g$$

$$I_{SB} = \rho_s(1 - \varepsilon_{mf})\ L_{SB}\ A_{SB}$$

Leung et al [172] suggested the following correlation to calculate the pressure drop through the solid flow control device

$$\Delta P_v = \frac{1}{2\rho_s\ (1 - \varepsilon_{mf})} \left(\frac{W_s}{C_D\ A_o} \right)^2$$

The aperture coefficient, C_D is taken as 0.5 .

Kunii and Levenspiel [162] developed a flow model to represent the phenomena in the free board heights. They postulated that three distinct phases are present in the free board. In phase I fines are completely dispersed and carried upward in the gas stream. In phase 2 agglomerates ejected from the fluidized bed move upward and phase 3 represents agglomerates and thin wall layers of particles, which move upward. Finally, upward moving agglomerates progressively disperse and also may change direction to return to the bed.

Solving the differential equations for the flow situation described above gives the following expressions for the distribution of solid density and solid upflow in the free board.

$$\frac{\bar{\rho} - x\,\bar{\rho}^*}{\bar{\rho}_o - x\,\bar{\rho}^*} = e^{-a\,Z_f}$$

$$\frac{G_{su} - x\,G_s^*}{G_{suo} - x\,G_s} = e^{-aZ_f}$$

where $\bar{\rho}$, is the mean density of gas/solid mixture, G_s, G_s^* and (G_{su}, G_{suo}) are the net upflow flux of solids, saturation carrying capacity of upflowing gas and upflow of solids at height (Z_f and at $Z_f = 0$) respectively, 'a' is the decay constant which is proportional to superficial velocity and 'x' represents the fraction of solids in the fluidized bed which is entrainable. Finally, they suggested the total inventory of solids 'W' in the column of height 'H_t' as given by

$$\frac{W}{A_t\,\rho_s} = L_m(1 - \varepsilon_m) = L_{mf}(1 - \varepsilon_{mf})$$

$$= \frac{\varepsilon_{sd} - \varepsilon_{se}}{a} + H_t\,\varepsilon_{sd} - H_f(\varepsilon_{sd} - \varepsilon_s^*)$$

where, A_t = cross sectional area of column, m^2

ρ_s = density of solid, kg/m^3

L_m , L_{mf} = height of fixed bed, and of the bed at minimum fluidization condition, respectively, m

ε_m , ε_{mf} = void fraction in fixed bed and a bed at minimum fluidization condition respectively

ε_{sd} = volume fraction of solids at lower dense region

ε_{se} = volume fraction of solids at the exit of the vessel

$H_t = H_d + H_f$ = column height, m

ε^* = void fraction at saturated carrying capacity condition

* indicates the saturated carrying capacity condition.

Heng Zhang et al [163] developed a mathematical model for longitudinal voidage distribution by considering the randomness of particle motion in a circulating fluidized bed.

They considered the random particle motion in a fluidized bed similar to ecological diffusion process. Combining Brownian movement model and random walk theory with particle motion in a fast fluidized bed, they derived the corresponding Fokker-Plank equation as

$$\frac{\partial \varepsilon}{\partial t} = \frac{\partial (U_s \varepsilon)}{\partial Z} + D \frac{\partial^2 \varepsilon}{\partial Z^2}$$

where ε denotes voidage and the two terms on the right hand side represent moving and diffusion fluxes respectively.

Substituting $U_s = G/(1-\varepsilon)\rho_s$, the above equation takes the form of

$$\frac{G}{(1-\varepsilon)^2 \rho_s} \frac{d\varepsilon}{dZ} = D \frac{d^2\varepsilon}{dZ^2}$$

The solutions of the equation give voidage in the dense phase as

$$\varepsilon = \varepsilon^* + \frac{\varepsilon^* - \varepsilon_a}{2} e^{-(Z-Z_i)/A} \qquad \text{for } Z \geqslant Z_i$$

and voidage at in the dilute phase as

$$\varepsilon = \varepsilon^* - \frac{\varepsilon^* - \varepsilon_a}{2} e^{(Z-Z_i)/A} \qquad \text{for } Z \leqslant Z_i$$

where ε_a, ε^* and Z_i have been determined from Li's [173] empirical formulae

$$\varepsilon_a = 0.756 \left(\frac{18R_e + 2.7\ Re_s^{1.687}}{Ar} \right)^{0.0741}$$

$$\varepsilon^* = 0.924 \left(\frac{18Re + 2.7\ Re_s^{1.687}}{Ar} \right)^{0.02857}$$

$$Z_i = L - 175.4\ W \left[d_p g\ (\rho_s - \rho_f)/\rho_g \right]^{1.922} (U-W)^{-3.844}$$

where,

A_r = Archimedes number
Re_s = relative Reynolds number
L = effective height of column
W = $G / ((1-\varepsilon_a)(\rho_s - \rho_f))$
Z_i = location of inflection point

CHAPTER - III

THEORETICAL ASPECTS

3.1 Principle of Fluidization

The phenomenon of fluidization relates to a particular mode of contacting granular solids with fluids, either liquid or gas, passing through the solids at a velocity sufficiently high to cause the particles to separate and become freely supported by the fluid. By this operation the solids are transformed into a fluid like state through contact with liquid or gas. This method of contacting has a number of unusual characteristics, and fluidization engineering is concerned with efforts to take advantage of this behaviour and put it to good use.

When a fixed bed of finely divided particles is subjected to an evenly distributed upward, low velocity flow of gas, the gas passes through the bed without disturbing the particles. The gas merely percolates through the void spaces between stationary particles. However, if the velocity of the gas is steadily increased, a point will be reached at which the individual particle will be forced upwards by the flow so as to be suspended in the fluid stream. At this point, the drag force exerted on the particles will counterbalance the weight of the particle, the vertical component of the compressive force between adjacent particles

disappears, and the pressure drop through any section of the bed about equals the weight of the fluid and particles in that section. The bed is considered to be just fluidized and is referred to as an incipiently fluidized bed or a bed at minimum fluidization. With further increase in flow rate, large instabilities with bubbling and channeling of gas are observed. The bed expands to allow the additional flow of gas to pass through it in the form of bubbles. The bed becomes highly turbulent and the surface is no longer well defined but appears diffuse and bubbles of gas rise through the bed. The bubbling action gives rise to a high degree of particle mixing. A dense-phase fluidized bed is considered as long as there is fairly clearly defined upper surface of the bed. However, at a sufficiently high fluid flow rate, the terminal velocity of solid is increased, the upper surface of the bed disappears, entrainment becomes appreciable and solids are carried out of the bed with the fluid stream. This state is termed as lean-phase fluidized bed.

The minimum fluidization velocity U_{mf}, is a measure of the superficial gas velocity at which there is a transition from fixed to fluidized bed behaviour. It is best to determine U_{mf} experimentally for a given particulate material, with the preferred method involving extrapolation of the two straight line portions of a pressure drop-vs-superficial velocity plot [174]. This experimental determination can be made in a small laboratory unit and should be

independent of bed depth. If U_{mf} must be calculated, there are many correlations available. The more convenient of these, especially for the relatively coarse particles, originate from balancing the pressure drop from Ergun's packed bed correlation with the bed weight per unit area [15]. This leads to equations of the form

$$Re_{mf} = \frac{\rho_f \bar{d}_p U_{mf}}{\mu_f}$$

$$= \sqrt{C_1^2 + C_2 Ar} - C_1$$

various values of the empirical constants C_1 and C_2 have been suggested. The values $C_1 = 27.2$ and $C_2 = 0.0408$ have been proposed by Grace [174] as giving some improvement over the commonly adapted values in the literature.

For small and large particles the above equation reduces to

$$U_{mf} = \frac{7.5 \times 10^{-4}(\rho_s - \rho_f) g \bar{d}_p^2}{\mu_f} \quad \text{for} \quad (Ar < 10^{-3})$$

and

$$U_{mf} = 0.202 \sqrt{(\rho_s - \rho_f) g \bar{d}_p / \rho_f} \quad \text{for} \quad (Ar > 10^7)$$

Even in applications where the operating superficial gas velocity, U_o, is far in excess of U_{mf}, the minimum fluidization velocity is a key parameter in characterizing the

particulate material. A second important quantity is the bed voidage at minimum fluidization, ε_{mf}, such that

$$M = \rho_s H_{mf} A(1 - \varepsilon_{mf})$$

ε_{mf} typically lies in the range 0.4 to 0.6 with some increase tending to occur with decreasing particle size, decreasing breadth of particle size distribution and increasing particle angularity [15]. There appears to be a slight increase in ε_{mf} with increasing pressure [175] although the effect is a small one [176].

The gas flow rate through a fluidized bed is limited on one hand by U_{mf} and on the other by entrainment of solids by the gas. The upper limit to gas flow rate is approximated by the terminal or free fall velocity of the particles, which can be estimated from fluid mechanics by [20]

$$U_T = \left[\frac{4 g \bar{d}_p (\rho_s - \rho_g)}{3 \rho_g C_d} \right]^{1/2}$$

where C_d is the experimentally determined drag coefficient. For spherical particles the above equation can be expressed as

$$U_T = \left[\frac{g(\rho_s - \rho_g)\,\bar{d}_p^2}{18\,\mu}\right], \quad \text{for} \quad Re_p < 0.4$$

$$U_T = \left[\frac{4}{225}\,\frac{(\rho_s - \rho_g)^2\, g^2}{\rho_g\,\mu}\right]^{1/3} \cdot \bar{d}_p, \quad \text{for} \quad 0.4 < Re_p < 500$$

$$U_T = \left[\frac{3.1 g(\rho_s - \rho_g)\bar{d}_p}{\rho_g}\right]^{1/2}, \quad \text{for} \quad 500 < Re_p < 200000$$

In calculating U_T , one is to consider the smallest size of solids present in appreciable quantity.

3.2 Regimes of Fluidization

Gas-solid systems are mostly **hetero**geneous. Except for a limited range of conditions under which individual particle can be said to be uniformly dispersed, particles in gas-solid system aggregate, giving rise to several distinct flow regimes. The interaction of gas and solid in these flow regimes and the transitions between them depend intrinsically on the properties of the gas and solid and on the solid and gas rates , they are also influenced by the containing vessel [128]. Key features of the principal regimes are described in Table-3.1 [15] and fluidization regimes by velocity is shown in Fig.3.1 [27].

Table-3.1 Regimes of fluidization with increasing superficial gas velocity

	Regime	Velocity range
(a)	Fixed bed	$0 < U_o < U_{mf}$
(b)	Particulate fluidization	$U_{mf} < U_o < U_{mb}$
(c)	Bubbling fluidization	$U_{mb} < U_o < U_{ms}$
(d)	Slugging regime	$U_{ms} < U_o < U_k$
(e)	Turbulent regime	$U_k < U_o < U_{tr}$
(f)	Fast fluidization	$U_{tr} < U_o$

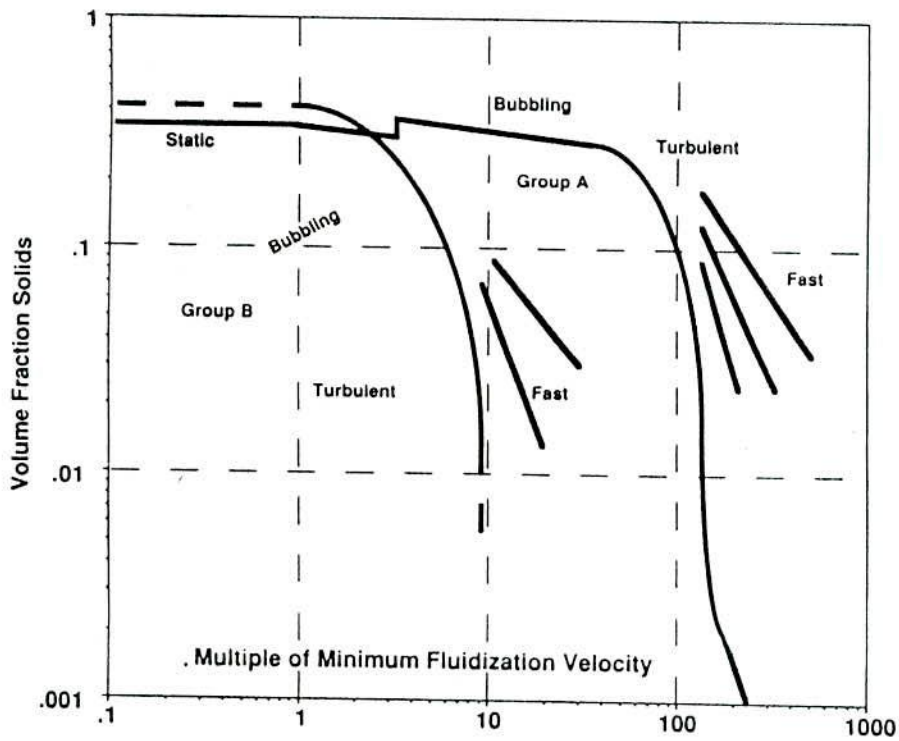

FIG. 3.1 FLUIDIZATION REGIMES BY VELOCITY

3.2.1 Appearance and principal features of the regimes of fluidization

(a) Fixed bed :

When a fluid flows upward through a bed of solid particles, it exerts upon them a frictional drag, which creates a corresponding pressure drop across the bed. So long as the drag force is smaller than the weight of the bed, the particles will remain essentially motionless, and the fluid will flow through the interstitial passages. This bed is termed as fixed bed. In fixed bed superficial velocity (U_o) is essentially less than minimum fluidization velocity (U_{mf}).

(b) Particulate fluidization :

With higher velocity, particles move apart, and a point is reached when the particles are all just suspended in the upward flowing gas or liquid. At this point the frictional force between a particle and fluid counterbalances the weight of the particle, the vertical component of the compressive force between adjacent particles disappears, and the pressure drop through any section of the bed about equals the weight of the fluid and particles in that section. In particulate fluidization the particles are uniformly dispersed within the fluid and the bed expands uniformly and found in quiescent state. Beyond the

quiescent state, when bubbles appear within the bed, the condition is called that of aggregative fluidization.

(c) Bubbling fluidization :

At gas velocities well in excess of that necessary to fluidize the bed, the bulk of the gas over and above that necessary to fluidize flows as bubbles, agitation becomes more violent and the movement of solids become more vigorous. In addition, the bed does not expand much beyond its volume at minimum fluidization. Void regions form near the distributor, grow mostly by coalescence and rise to the surface. The top surface is well defined with bubbles breaking through periodically. Bubble size increases as U_o increases . For type A [177] solids the minimum bubbling velocity, U_{mb} , exceeds U_{mf} and can be predicted by adapting the correlation developed by Geldart and Abrahamsen [178] as

$$U_{mb} = 33\, \bar{d}_p\, (\rho_g / \mu_g)^{0.1} , \quad (\text{SI unit})$$

For type B and D materials [177], U_{mb} predicted from the above relation is less than U_{mf}. In that case U_{mb} can be considered as U_{mf} .

(d) Slugging regime :

This regime may be bypassed altogether in beds of fine particles or in columns of large diameter. In the extreme case of channeling with gas fluidized beds of fine particles, the bed fails to fluidize at all. Also in deep, narrow gas fluidized beds there is a tendency for bubbles to grow and coalesce as they rise through the bed and so a slugging bed is formed. Voids fill most of the column cross-section, top surface rises and collapses with a reasonably regular frequency. Preconditions for slugging are that the bed depth to diameter (H/D) be at least 1.5 and that maximum stable bubble size be of order 'D' or greater [15]. If these conditions are satisfied, the superficial gas velocity corresponding to the onset of slugging is suggested by Stewart and Davidson [179] as

$$U_{ms} = U_{mf} + 0.07 \sqrt{gD}$$

(e) Turbulent regime :

Yerushalmi and Cankurt [130] described the turbulent regime as the process of dispersion. Large bubbles or slugs are dispersed in the solid phase, or, alternatively, the solids are dispersed in the gas. The net effect is the apparent breakdown of large bubbles and slugs into smaller voids which continually coalesce and

split, tracing tortuous passages as they rise through the bed. As U_k is approached, the solid, which in the bubbling fluid bed constitutes a continuous phase, also disperses, rearranging into distinct clusters and streamers of particles whose motion is mostly downwards and individual particles and small clusters are entrained upwards in the leaner gas phase. The structure of the turbulent fluidized bed has thus become considerably more homogeneous and is marked by strong interaction between its dense and lean phase. The turbulent regime extends from U_k to the transport velocity, U_{tr}.

The transition to turbulent fluidization is reflected in the fluctuations of both the dynamic pressure at any point in the bed and of the pressure drop across it. The transition is gradual and it can be characterized by two velocities: the velocity at which the pressure fluctuations peak, and the velocity at which the pressure fluctuations, having decayed from their peak value begin to level off (U_k). The transition to turbulent fluidization may be expected to show some dependence on bed diameter. There are few data on which to base prediction of the transition velocity, U_k, for the onset of turbulent fluidization. Grace [174] fitted the experimental results of Yerushalmi and Cankurt [130] by,

$$U_k = 7.0 \sqrt{\rho_s \bar{d}_p} - 0.77 \quad (\text{SI unit})$$

for $0.05 < \rho_s \bar{d}_p < 0.7$ kg/m^2 ,

air as the fluidizing gas, and a 0.152 m diameter column and 0.051 x 0.051 m 'two dimensional' column.

(f) Fast fluidized bed regime :

A circulating fluidized bed (CFB) may be defined as a high velocity fluidized bed where particles elutriated by the fluidizing gas are recovered and returned to the bottom of the bed at a rate sufficiently high so as to cause a minimum degree of solid refluxing in the column. The column can operate in turbulent, fast or lean phase transport bed regimes depending on gas and solid feed rates, but in case of CFB boilers the refluxing should be adequate to ensure axial temperature uniformity in the column.

The fast bed is often described by the core-annulus model in which there is the up flowing dilute gas stream in the core and the down flowing dense phase in the annulus with clusters or streamers, long slender solid agglomerates, continually forming, dissolving and reforming. The solid in the fast fluidized bed may typically occupy upto 25 % of the bed volume and is in a state of extreme turbulence marked by extensive refluxing of dense strands and packet of particles. Weinstein and his associates [131] at CCNY has confirmed that the

structure of the dense phase in a fast fluidized bed consists of a dilute core and a dense wall region. Further confirmation was provided by Hartge et al [133] employing fibre optic probes. Geldart and Rhodes [29] critically reviewed the high velocity fluidization and concluded that the non-uniform radial solids concentration distribution is typical of all flowing gas-solid systems at velocities from incipient fluidization to dilute phase pneumatic transport. Yerushalmi et al [128] observed that above the transport velocity lies the transport regime which encompasses a wide range of states from dilute-phase flow to the fast bed condition. As the velocity approaches U_{tr}, there is a sharp increase in the rate of particle carryover. Slip velocities are high in the fast bed. The large slip velocities arise from the characteristic aggregation of the solid in the fast bed into relatively large dense clusters of the particles [180]. If a cluster is sufficiently large it can not be sustained by the rising gas, it will fall back and will subsequently undergo disintegration by one mechanism or another. Hence the apparent high degree of solid back mixing occurs in the fast bed. The bed has got no upper surface. Particles are transported out through the top and must be replaced by adding solids at or near the bottom. At a fixed solid rate the bed becomes increasingly dilute as U_o is increased. Transport velicity may

be regarded as the boundary which divides vertical gas-solid flow regimes into two groups of state, and transport regime lies above it. There are insufficient data to allow correlation of the transport velocity U_{tr}, which makes the identification of onset of the fast fluidization regime difficult.

3.3 Theory of Heat Transfer in Fluidized Beds

The heat transfer rates between surface and circulating bed are much higher than in single gas flow. In order to explain this phenomenon and predict heat transfer rates for design purpose, many investigators worked on laboratory scale fluidized beds on tube-to-bed heat transfer and few theories have been proposed. The significant theories for modelling bed-to-wall heat transfer in fluidized beds are the following :

(a) Thin-film theory :

Dow and Jakob [45] and Levenspiel and Walten [47] observed that the principal resistance to heat transfer in a fluidized bed is offered by the fluid film and the moving fluidized particles scour the film to reduce the resistance to heat transfer.

(b) Packet theory :

Mickley and Fairbanks [50] observed unsteady heating of elements by a small group of particles moving as individual unit called the packet or cluster of emulsion phase as the vehicle for heat transfer. Initially a packet of particles from the dense-phase comes in contact with the surface and one dimensional transient conduction takes place until the packet is again replaced by a packet of fresh particles. The heat transfer in a packet is considered to be identical to transient conduction in a homogeneous semi-infinite medium initially at bed temperature with a sudden step increase in surface temperature.

(c) Particle theory :

Van Heerden et al [49], Ziegler and Brazelton [61] observed that particles from the bulk of the fluidized bed, having the bulk medium temperature move adjacent to the heat transfer surface, the individual particle receives energy primarily by convection from the fluid around the particle.

(d) Alternate slab model theory :

Gabor [62] proposed theories describing heat transfer process at the surface based on semi-infinite 'packets' of dense-phase composed of alternating flat layers of gas and solids.

Grace [11] regarded the circulating bed as intermediate between a dense fluidized bed and dilute pneumatic conveying. Heat is transmitted from the hot surface by gas bubbles, by packet of solid particles and by radiation, the three separate additive processes :

$$h = \delta_g h_{gc} + (1 - \delta_g) h_{pc} + h_{rad}$$

where δ_g is the fraction of the wall covered by gas bubbles. Since h_{gc} is generally much less than the particle convective component, h_{pc}, so h_{gc} can be estimated based on the correlations for gas alone flowing through the column and the same superficial velocity and with same physical properties. The radiative component, significant at high temperature, can be estimated by treating both wall and cluster as gray bodies and the intervening gas between the wall and the cluster as transparent to thermal radiation by [11]

$$h_{rad} = \frac{\sigma \left(T_{susp}^4 - T_{surf}^4 \right)}{\left[\left(\frac{1}{e_{surf}} \right) + \left(\frac{1}{e_{susp}} \right) - 1 \right] \left(T_{susp} - T_{surf} \right)}$$

For circulating bed equipment of industrial size and typical values of volumetric solids concentration, the

suspension will be opaque and the suspension emissivity is given approximately by Grace [174] considering multiple reflection as

$$e_{susp} = 0.5(1 + e_p)$$

The observations and suggestions for estimating the particle convective component, h_{pc}, of many workers have already been mentioned in Art. 2.4.

The observations of some investigators regarding the mechanism of heat transfer and the latest theoretically developed model applicable for heat transfer in circulating fluidized beds have already been discussed in Art. 2.4 and 2.8 respectively.

3.4 Working Formulae

3.4.1 Bed-to-wall heat transfer coefficient

The heat transfer coefficient, h is defined [20] as

$$Q = A_{ht}\, h\, \Delta T \qquad .. (3.1)$$

where Q is the rate of heat transfer, A_{ht} is the area of heat exchange surface and ΔT is the mean temperature difference between fluidized bed and exchange surface of height L_h, where

$$\Delta T = \int_{L=o}^{L=L_h} \frac{(T_w - T_b)}{L_h}\, dl \qquad .. (3.2)$$

The average heat transfer coefficient (h) was determined for each operating condition at steady state from the measured heat flux and the temperatures of the inside wall (T_w) and the bed suspension (T_b)

$$h = \frac{V I}{A_{UF} (T_w - T_b)} \qquad .. (3.3)$$

where V and I are the voltage and current respectively and A_{UF} is the total surface area of the unfinned test section. The total heat transfer from the finned surface was estimated from the equation

$$Q_T = A_F h (T_w - T_b)\eta_f + (A_T - A_F)h(T_w - T_b) \qquad .. (3.4)$$

where A_T is the total surface area including fins, A_F is the area of the fins and η_f is the fin efficiency. The heat input to the test section was maintained constant with the help of a variac.

3.4.2 Voidage

Glicksman [12] considered voidage as the volume fraction of the bed occupied by bubbles. The bed voidage (ε) at any cross-section of the test section has been estimated from the measured pressure drop (Δp_L) from a differential water filled u-tube manometer connected across it. If 'ε'

represents the voidage, then the fractional volume of the bed occupied by solid particles is equal to $(1-\varepsilon)$.

By force balance, we get

$$(\Delta p_L)\ A = (1-\varepsilon)\ \rho_s\ g\ A\ L_m \qquad .. (3.5)$$

Again we know that

$$\Delta p_L = \left(\frac{\Delta h_L}{100}\right)\rho_m\ g$$

where $\rho_m = 1000\ kg/m^3$ and $g = 9.81\ m/s^2$

Therefore, $\Delta p_L = 1000 \times \frac{\Delta h_L}{100} \times g$

or, $\Delta p_L = 10\ (\Delta h_L)\ g$

where Δh_L is in cm. of water

Substituting the expression of Δp_L in Eq.(3.5) we get,

$$\Delta p_L = (1-\varepsilon)\ \rho_s\ g\ L_m$$

or, $10(\Delta h_L)\ g = (1-\varepsilon)\ g\ \rho_s\ L_m$

or, $$\varepsilon = 1 - \frac{10\ \Delta h_L}{\rho_s L_m} \qquad .. (3.6)$$

where,

Δh_L = difference of height in manometric fluid, cm. of water

L_m = distance across which manometer is connected, m

3.4.3 Suspension density

The suspension density of the bed (ρ_{sus}) has been determined from the relation

$$\rho_{sus} = \rho_s(1 - \varepsilon) + \rho_g\varepsilon \qquad .. (3.7)$$

3.4.4 Superficial velocity

The superficial velocity (U_o) is defined as the volume rate of air flow per unit cross-section of the bed. So

$$U_o = \frac{\text{Volume flow of air through the bed}}{\text{Cross-sectional area of the bed}}$$

Rate of air flow through the bed (m_a)

Applying Bernouli's theorem to the upstream tapping (1) and to the orifice (2) (Fig.3.2) we can write

$$\frac{V_1^2}{2g} + H_1 = \frac{V_2^2}{2g} + H_2 \qquad .. (3.8)$$

Assuming that the pipe is running full and for the moment that no expansion of the fluid takes place, then

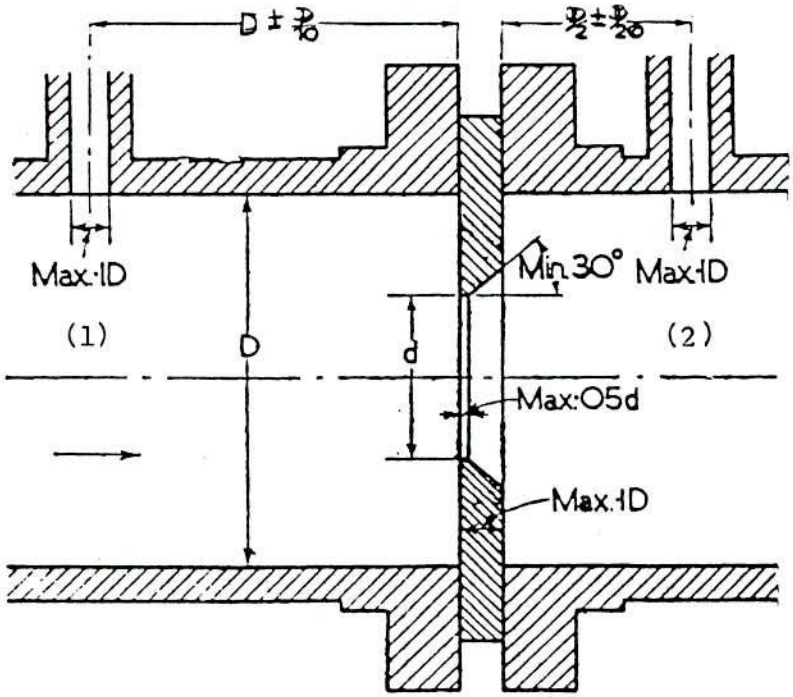

FIG. 3.2 ORIFICE PLATE WITH D AND D/2 TAPPINGS

$$A_1 V_1 = A_2 V_2$$

or, $$V_1 = \frac{A_2}{A_1} V_2 = m_1 V_2$$

where, $m_1 = A_2/A_1$

Now substituting the expression of V_1 to Eq.(3.8), we can write

$$V_2^2 = \frac{2g\,(H_1 - H_2)}{1 - m_1^2} \qquad .. (3.9)$$

where $(H_1 - H_2)$ is the difference of pressure heads between points (1) and (2) of Fig. 3.2 and expressed in meter of air. Now if we substitute $(H_1 - H_2)$ in terms

of (Δp) and expressed in cm. of water, then we can write

$$H_1 - H_2 = \left(\frac{\rho_w}{\rho_a}\right)\left(\frac{\Delta p}{100}\right)$$

where, Δp is the difference in height of manometric fluid (water) in cm. of water

$$H_1 - H_2 = \left(\frac{1000}{\rho_a}\right)\left(\frac{\Delta p}{100}\right) = \frac{10\ \Delta p}{\rho_a}$$

Now substituting the expression of (H_1-H_2) in Eq.(3.9), we can write

$$V_2 = \left[\frac{2g\ \left(\frac{10\ \Delta p}{\rho_a}\right)}{1 - m_1^2}\right]^{1/2} \quad m/s \qquad .. (3.10)$$

Theoretical mass flow rate (m_t) of air can be expressed as

$$m_t = \rho_a\ A_2\ V_2 \quad kg/s$$

or, $$m_t = \rho_a \left[\frac{\pi}{4}\left(\frac{d_o}{100}\right)^2\right]\left[\frac{2g \times 10\ \Delta p}{\rho_a(1-m_1^2)}\right]^{1/2} \times 3600 \quad kg/hr$$

$$= 3.96\ d_o^2 \sqrt{\Delta p\ \rho_a}\ \left(\frac{1}{\sqrt{1 - m_1^2}}\right) \quad kg/hr$$

$$= 3.96\ d_o^2\ E \sqrt{\Delta p\ \rho_a} \quad kg/hr \qquad .. (3.11)$$

where, $E = \frac{1}{\sqrt{1 - m_1^2}}$

d_o = diameter of orifice in cm.

Δp = difference in manometric fluid height in cm. of water

ρ_a = density of air

The actual mass flow rate (m_a) can now be expressed as

$$m_a = C \cdot Z \cdot m_t$$

$$m_a = C \cdot Z \cdot (3.96\ d_o^2\ E\ \sqrt{\Delta p\ \rho_a}) \quad kg/hr \qquad .. (3.12)$$

where,

C = coefficient of discharge

Z = velocity of approach factor

'C' and 'Z' were evaluated from B.S. code 1042 : 1943 [181] based on the following informations.

Pressure = 1 bar

Temperature = 30^oC

Inside diameter of pipe = 7.62 cm

diameter of orifice, d_o = 5.097 cm

density of air, ρ_a = 1.165 kg/m^3

$$E = \frac{1}{\sqrt{1 - m_1^2}} = \frac{1}{\sqrt{1 - (0.447)^2}}, \quad m_1 = 0.447$$

$$E = 1.118$$

From B.S. code, 1042 : 1943

Fig. D, S.7 and for $m_1 = 0.447$

$C = 0.605$ and $Z = 1.0$

Substituting the values of C and Z in Eq. (3.12) we get,

$$m_a = C.Z \left(3.96\, d_o^2\, E \sqrt{\Delta p\, \rho_a} \right) \quad kg/hr$$

or, $$m_a = 0.605 \times 1.0 \left[3.96\, d_a^2 \times (5.097)^2 \times 1.118 \times \sqrt{1.165} \times \sqrt{\Delta p} \right] \quad kg/hr$$

or, $$m_a = 75.11 \sqrt{\Delta p} \quad kg/hr$$

$$= \frac{75.11 \sqrt{\Delta p}}{3600} \times \frac{1}{1.165} \quad m^3/s$$

$$m_a = 0.0179 \sqrt{\Delta p} \quad m^3/s \qquad .. (3.13)$$

A_b , cross-sectional area of the bed $= \frac{\pi}{4} (D_b)^2$

$D_b = 100$ cm $= 0.1$ m

$\therefore \quad A_b = 7.854 \times 10^{-3} \ m^2$

Therefore, $$U_o = \frac{m_a}{A_b} = \frac{0.0179 \sqrt{\Delta p}}{7.854 \times 10^{-3}} \quad m/s$$

$$U_o = 2.28 \sqrt{\Delta p} \quad m/s \qquad .. (3.14)$$

where,

Δp is the pressure drop across the orificemeter, in cm of water.

3.4.5 Solid circulation rate

The solid circulation rate (G_s) can be defined as the circulation of solid particles per unit cross-section of the bed. Therefore,

$$G_s = \frac{\text{Circulation rate of solids (kg/s)}}{7.854 \times 10^{-3}\ m^2}$$

or, $$G_s = 127.3\ (W_s)\ \ kg/m^2 s \qquad .. (3.15)$$

where, W_s is the solid circulation in the bed per second

3.4.6 Fin effectiveness

It is defined as

$$\text{Fin effectiveness} = \frac{\text{Actual heat transfer through the fin}}{\text{Maximum heat transfer through the fin}}$$

Maximum heat transfer will occur when all the surfaces of the fin are at the same temperature as the base of the fin and the heat transfer coefficient over the entire surface of the fin will be the same as that over its base.

$$\text{Fin effectiveness} = \frac{Q_{actual}\,|_F}{A_T\ h_{UF}(\Delta T)_F} = \frac{q''|_F}{h_{UF}(\Delta T)_F} \qquad .. (3.16)$$

h_{UF} is to be evaluated at the same bed condition i.e. at the same bed density as that of h_F .

3.4.7 Particle Nusselt and Reynolds numbers

The particle Nusselt number (Nu_p) has been estimated on the basis of average heat transfer coefficient, the mean particle size and thermal conductivity of fluidizing gas (air). Thus

$$Nu_p = \frac{h\, d_p}{k_g} \qquad .. (3.17)$$

The particle Reynolds number (Re_p) has been estimated based on superficial velocity, mean particle size and the properties of fluidizing gas (air). Thus,

$$Re_p = \frac{U_o\, d_p\, \rho_g}{\mu_g} \qquad .. (3.18)$$

3.4.8 Residence time

The residence time (t_r) of the cluster has been evaluated using the correlation developed by Glicksman [12] as

$$h = \left(\frac{1}{h_W} + \frac{1}{h_H} \right)^{-1} \qquad .. (3.19)$$

where h, h_W and h_H are the overall, wall and homogeneous heat transfer coefficients respectively.

The correlation suggested by Basu and Nag [39] has been used to evaluate the wall heat transfer coefficient (h_W) as,

$$h_W = \frac{10\, K_{eW}}{d_p} \qquad .. (3.20)$$

For homogenous heat transfer coefficient (h_H), the correlation of Glicksman [12] has been used. Thus

$$h_H = \sqrt{\frac{K_c \rho_s C_{ps} (1 - \varepsilon)}{\pi t_r}} \qquad .. (3.21)$$

On substitution of Eq. (3.20) and (3.21) to Eq. (3.19) and after rearrangement the final expression for cluster residence time (t_r) can be written as

$$t_r = \frac{K_c \rho_s C_{ps}(1-\varepsilon)}{\pi} \left(\frac{1}{h} - \frac{d_p}{10 K_{eW}} \right)^2 \qquad .. (3.22)$$

'h' has been evaluated from Eq. (3.3) and the properties of fluid have been taken at the arithmetic mean of bed and surface temperatures.

CHAPTER - IV

PROPOSED HEAT TRANSFER MODELS

Two models and one correlation have been developed as given below :

(i) An empirical model for the prediction of heat transfer in a circulating fluidized bed for bare (unfinned) tube surface.

(ii) An analytical model for the prediction of heat transfer from bed to finned surfaces in a circulating fluidized bed.

(iii) An empirical correlation among the parameters Nu_p, Re_p and L_h/D to estimate heat transfer from the probes of different vertical heights.

4.1 Bare (unfinned) Tube Model

It is an empirical model [160] to predict heat transfer from bare (unfinned) tube surface in a circulating fluidized bed.

4.1.1 Introduction

The mechanism of heat transfer in a circulating fluidized bed is very complicated because of the dependence of the bed behaviour on a large number of variables. The process of heat exchange between the system and the heat transfer surfaces

is intimately associated with the process of heat transfer between the fluidized solid and the fluidizing gas, the rate at which the particles mix inside the bed and the general behaviour and geometry of the fluidized system. Since the fluidized bed represents a complex interaction of gas and solid, many factors will enter into the generalized correlation accounted for the bed to wall heat transfer coefficient. It is thus difficult to develop a fundamental model for prediction of heat transfer in these beds. Mickley and Fairbanks [50] developed the first physical model of heat transfer from a fluidized bed by introducing the packet theory. Subbarao and Basu [156] suggested a heat transfer model for circulating fluidized beds with the concept of clusters in the lean phase. Basu and Nag [39] extended this model by including a wall resistance in series with the homogeneous semi-infinite medium of particles. Grace [11] and Glicksman [12] have reviewed the various models of heat transfer and analyzed the influences of different variables that enter into the problem of predicting heat transfer. Sekthira et al [79] showed in their model that heat transfer coefficient is proportional to the fourth root of the suspension density in a circulating fluidized bed. All these models predict heat transfer coefficients which differ from one another and also from the experimental data, often by more than hundred percent [157]. Hence is the need for a comprehensive model for predicting heat transfer in a CFB incorporating all the concerned variables.

4.1.2 Model

To develop the model, the following assumptions are made.

(i) The physical properties of gas and solid are constant.

(ii) The shape of the solid particles is spherical.

(iii) In the bulk bed, the temperature and voidage of the bed are constant at any cross-section.

(iv) The particles are uniformly distributed and the circulating bed can be treated as a single phase continuum.

(v) Heat transfer is by transient conduction, gas convection and by radiation normal to the surface in the emulsion phase during its residence at the wall. The mechanism of heat transfer is such that the clusters from the bulk of the bed move to the heated surface and receive heat energy from the wall. The cluster is assumed to be at the arithmetic mean of bulk and wall temperatures $\left[T_c = (T_b + T_w)/2 \right]$.

(vi) Radiation from solids and gases occurs separately.

In this study, an empirical model based on dimensional analysis has been suggested. It has attempted to incorporate all the variables which affect heat transfer in a circulating fluidized bed. The variables considered for convective and conductive models of heat transfer are as follows :

1. Properties of fluidized material : Density (ρ_s), Thermal conductivity (K_s) and Specific heat (C_{ps}).

2. Properties of fluidizing gas : Density (ρ_g), Thermal conductivity (K_g), Specific heat (C_{pg}) and Viscosity (μ_g).

3. Operating conditions : Particle size (d_p), Size distribution and shape of particles (ϕ_s), Solid concentration in the bed (ρ_{sus}), Superficial velocity (U_o), Minimum fluidizing velocity (U_{mf}), Void fraction (ε), Particle Terminal Velocity (U_T), Void fraction (ε), Voidage at minimum fluidization (ε_{mf}), Feed or recycle rate of solids (G_s) and Temperature level (T).

4. Bed geometry : Bed diameter (d_b), Length of heat exchange surface (L_h) and Static bed height (L_s).

Nusselt number (Nu) incorporating the heat transfer coefficient (h) can be expressed as a function of other relevant dimensionless parameters. A dimensional analysis of the above variables yields a relationship [20] as given below :

$$\frac{h\, d_p}{k_g} = f\left[\frac{\mu_g\, C_{pg}}{k_g},\ \frac{U_o d_p \rho_g}{\mu_g},\ \frac{\rho_s}{\rho_g},\ \frac{C_{ps}}{C_{pg}},\ \frac{U_o}{U_{mf}},\ \frac{K_s}{k_g},\ \frac{d_b}{d_p},\ \frac{L_h}{d_b},\ \varepsilon,\ \varepsilon_{mf} \right] \quad .. (4.1)$$

Many of these terms and groups are interrelated, and these have been rearranged in fewer dimensionless groups as follows :

$$Nu = f\left[Pr , \frac{U_o d_p \rho_g}{\mu_g} , \frac{d_b}{d_p} , \frac{L_h}{d_b} , \frac{U_o}{U_{mf}} , \frac{\rho_s}{\rho_g} , \frac{C_{ps}}{C_{pg}} , \frac{K_s}{k_g} , \varepsilon \right] \quad .. (4.2)$$

For simplicity of analysis the parameters on the R.H.S. of Eq.(4.2) have been divided into two groups and designated by X and Y, where

$$X = \left(Pr , \frac{C_{ps}}{C_{pg}} , \frac{K_s}{k_g} , \frac{\rho_s}{\rho_g} , \varepsilon \right) \quad .. (4.3)$$

and

$$Y = \left(\frac{U_o d_p \rho_g}{\mu_g} , \frac{U_o}{U_{mf}} , \frac{d_b}{d_p} , \frac{L_h}{d_b} \right) \quad .. (4.4)$$

By definition, Archimedes number (Ar) is, Grace [15]

$$A_r = \frac{\rho_g(\rho_s - \rho_g) g d_p^3}{\mu_g^2}$$

or,
$$A_r = \left[\frac{g(\rho_s - \rho_g) d_p^2}{18 \mu_g} \right] \left[\frac{18 \rho_g d_p U_o}{\mu_g U_o} \right]$$

$$\text{or,} \qquad A_r = \frac{18\ U_T}{U_o} \left(\frac{\rho_g\ d_p\ U_o}{\mu_g} \right)$$

where terminal velocity, Pell [27]

$$U_T = \frac{g(\rho_s - \rho_g) d_p^2}{18\ \mu_g}$$

$$\text{or,} \qquad \frac{\rho_g\ d_p\ U_o}{\mu_g} = A_r \frac{U_o}{18\ U_T}$$

By introducing Archimedes number and terminal velocity Eq. (4.4) is expressed as

$$Y = \left(A_r \frac{U_o}{18\ U_T}, \frac{U_o}{U_{mf}}, \frac{d_b}{d_p}, \frac{L_h}{d_b} \right) \qquad .. (4.5)$$

If Nusselt number is substituted by Z, Eq. (4.2) takes the form of

$$Z = f(X, Y) \qquad .. (4.6)$$

where X represents the properties of fluidizing and fluidized materials and solid concentration in the bed, Y represents the operating conditions and geometry of the fluidized system and Z represents the heat transfer characteristics of the system. Now Z is expressed in the form of

$$Z = a + bX \qquad .. (4.7)$$

where 'a' and 'b' are constants which can further be expressed as

$$a = A_o + A_1 Y \qquad .. (4.8)$$

and

$$b = B_o + B_1 Y \qquad .. (4.9)$$

where A_o, A_1, B_o and B_1 are constants.

The radiative heat transfer between solid and gas present in the bed and the wall has been considered separately, with the two components added as given below :

$$h_r = x_c h_{sr} + (1-x_c) h_{gr} \qquad .. (4.10)$$

where, x_c is the fraction of the wall surface covered by particles, $(1-x_c)$ is the fraction of the surface covered by gas, and suffixes 'sr' and 'gr' stand for solid and gas radiative exchange with the wall respectively. The solid particles which are away from the wall or in contact with it are assumed to be at the bed temperature (T_b) and both the wall and particles are considered as gray surfaces. The radiative heat transfer coefficient between solid particles and the wall can thus be written as

$$h_{sr} = \sigma F_{P-W} \left(\frac{T_b^4 - T_w^4}{T_b - T_w} \right) \qquad .. (4.11)$$

where σ is the Stefan-Boltzmann constant, T_b and T_w are the bed and wall temperatures respectively, and F_{P-W}

is the particle-to-wall view factor, which can be estimated by considering the wall and solids as parallel planes from the following relationship

$$F_{P-W} = \frac{1}{\frac{1}{e_p} + \frac{1}{e_w} - 1} \qquad .. (4.12)$$

where e_p and e_w are the particle emissivity and wall emissivity respectively.

The temperature of the intervening gas between the solid and the wall is assumed to be at T_b. For radiative heat transfer between the gas and the wall, the heat transfer coefficient 'h_{gr}' is expressed as

$$h_{gr} = \sigma\, e' e_g \left(\frac{T_b^4 - T_w^4}{T_b - T_w} \right) \qquad .. (4.13)$$

where e_g is the gas emissivity and e' is the effective emissivity of the wall [182,183]. For gray wall, some of the radiation striking it is reflected back into the gas and then to the wall again. Hottel [184] suggested that it is fairly accurate to estimate the effective emissivity from the relation $e' = 0.5(1 + e_w)$.

Substituting Eqs. (4.11) and (4.13) in Eq.(4.10), the total radiant heat transfer coefficient is given by

$$h_r = \sigma \left[\frac{T_b^4 - T_w^4}{T_b - T_w} \right] \left[x_c F_{P-W} + (1-x_c) e' e_g \right] \quad .. (4.14)$$

In dimensionless form, let $R_r = \frac{h_r d_p}{k_g}$, then

$$R_r = \sigma \left[\frac{T_b^4 - T_w^4}{T_b - T_w} \right] \left[x_c F_{P-W} + (1-x_c) e' e_g \right] \frac{d_p}{k_g} \quad .. (4.15)$$

From Eqs. (4.7) to (4.9) and Eq. (4.15), the final expression for heat transfer is given by

$$Z = (A_o + A_1 Y) + (B_o + B_1 Y) X + R_r \quad .. (4.16)$$

where constants A_o, A_1, B_o and B_1 have been evaluated from the present experimental data of unfinned surface.

The experiments were performed in a circulating fluidized bed unit, the details of which have been described in Art. 5.1. Local sand of mean diameter (d_p) 310 micron was used as the bed material. Six superficial velocities ranging from 5.6 to 11.4 m/s were used. Three constant energy fluxes of 3580, 5519 and 7876 W/m^2 were employed for each air velocity, the bed temperature varying from 345 K to 365 K.

4.1.3 Evaluation of constants

By using the data of present experiments (Tables - A.4.1, A.4.2 , 6.27 to 6.29) and applying the technique of least squares, the values of the constants A_o , A_1 , B_o and B_1 have been evaluated (a sample calculation is given in Appendix - A) as follows :

$$A_o = 4.48050 \quad , \quad B_o = -8.0314 \times 10^{-7}$$

$$A_1 = 1.85178 \times 10^{-7} \quad , \quad B_1 = -4.6841 \times 10^{-14}$$

Substituting the values of A_o , A_1 , B_o and B_1 in Eq. (4.16), Z is expressed as ,

$$Z = (4.4805 + 1.85178 \times 10^{-7} Y) + (-8.0314 \times 10^{-7} - 4.6841 \times 10^{-14} Y) X + R_r \quad .. (4.17)$$

The values of 'X' and 'Y' are assumed to be the products of the non-dimensional parameters as given in Eqs. (4.3) and (4.5) respectively. Substituting these values in Eq. (4.17), Z is expressed as

$$Z = \left[4.4805 + 1.85178 \times 10^{-7} \left(Ar \frac{U_o}{18 U_T} \frac{U_o}{U_{mf}} \frac{d_b}{d_p} \frac{L_h}{d_b} \right) \right] + \left[-8.0314 \times 10^{-7} - 4.6841 \times 10^{-14} \left(Ar \frac{U_o}{18 U_T} \frac{U_o}{U_{mf}} \frac{d_b}{d_p} \frac{L_h}{d_b} \right) \right] \left[Pr \frac{C_{ps}}{C_{pg}} \frac{k_s}{k_g} \frac{\rho_s}{\rho_g} \varepsilon \right] + R_r \quad .. (4.18)$$

Using the properties of solid and gas at 381 K [185], and on rearranging, Eq.(4.18) takes the form as given below :

$$Z = 4.5 - 4.75\ Pr\varepsilon - (4.95\ Pr\varepsilon - 3.3)\,Ar\,\frac{U_o^2}{U_T U_{mf}}\,\frac{L_h}{d_b} \times 10^{-6} + R_r$$

$$Nu = 4.5 - 4.75M - N(4.95M - 3.3) + R_r \qquad .. (4.19)$$

where,

$$M = Pr\varepsilon, \quad N = Ar\,\frac{U_o^2}{U_T\,U_{mf}}\,\frac{L_h}{d_b} \times 10^{-6} \quad \text{and}$$

$$R_r = \sigma\left[\frac{T_b^4 - T_w^4}{T_b - T_w}\right]\left[x_c\,F_{P-W} + (1-x_c)\,e'e_g\right]\frac{d_p}{k_g}$$

Equation (4.19) is the final expression of heat transfer inferred by the proposed model, which includes all the three modes of heat transfer. The model is verified with the present experimental data as well as with those of Mickley and Trilling [125], Kobro and Brereton [8], Basu and Nag [39], and Sekthira et al [79] and good agreement is observed. Detail discussion on the model has been done in Article 7.8.

4.2 Finned Tube Model

An analytical model has been developed to predict heat transfer from bed to finned surfaces in a CFB.

Finned tubes are widely used in heat exchangers including the economizers of steam generators. In a CFB boiler, the heat absorption by each wall tube may be considerably increased if additional heating surface can be provided by welding vertical fins to each tube. The fluidized bed represents a complex interaction of gas and solid. In addition the radial variation of bed density complicates the development of a fundamental model for the prediction of heat transfer at the wall especially when fins are attached to the inner surface of the bed. Li et al [149], Tung et al [186] and many others have observed a dilute core of solids accompanied by a dense wall region in CFB. So the heat transfer coefficient along the fin surface varies as the fin extends from the wall towards the centre of the bed. Although few models have been developed for plain (unfinned) surfaces, but no model for the prediction of heat transfer for finned surface in a CFB has yet been published in literature. Here an analytical model has been proposed for predicting the same.

4.2.1 Development of model

The following assumptions are taken into consideration for developing the model.

(i) Heat transfer by radiation is assumed to be very small (cold bed) and it has not been considered.

(ii) Heat transfer is by particle convection and gas convection. The mechanism of heat transfer is such that the clusters from the bulk of the bed move to the heated surface and receive heat energy from the wall. The cluster is assumed to be at the arithmetic mean of bulk and wall temperatures ($T_c = (T_b+T_w)/2$).

(iii) The thickness of fin is small compared to its axial length.

(iv) The fin does not extend beyond the axis of the bed.

(v) The shape of the solid particles is spherical and the physical properties of gas and solid are constant.

(vi) The temperature varies in one direction only.

(vii) The material is homogeneous.

(viii) There is no energy source or sink within the fin.

(ix) The temperature of the surrounding fluid is uniform.

4.2.2 Mathematical formulation

To determine the temperature distribution along a fin, the governing energy equation is developed by performing an energy balance on a differential volume element in

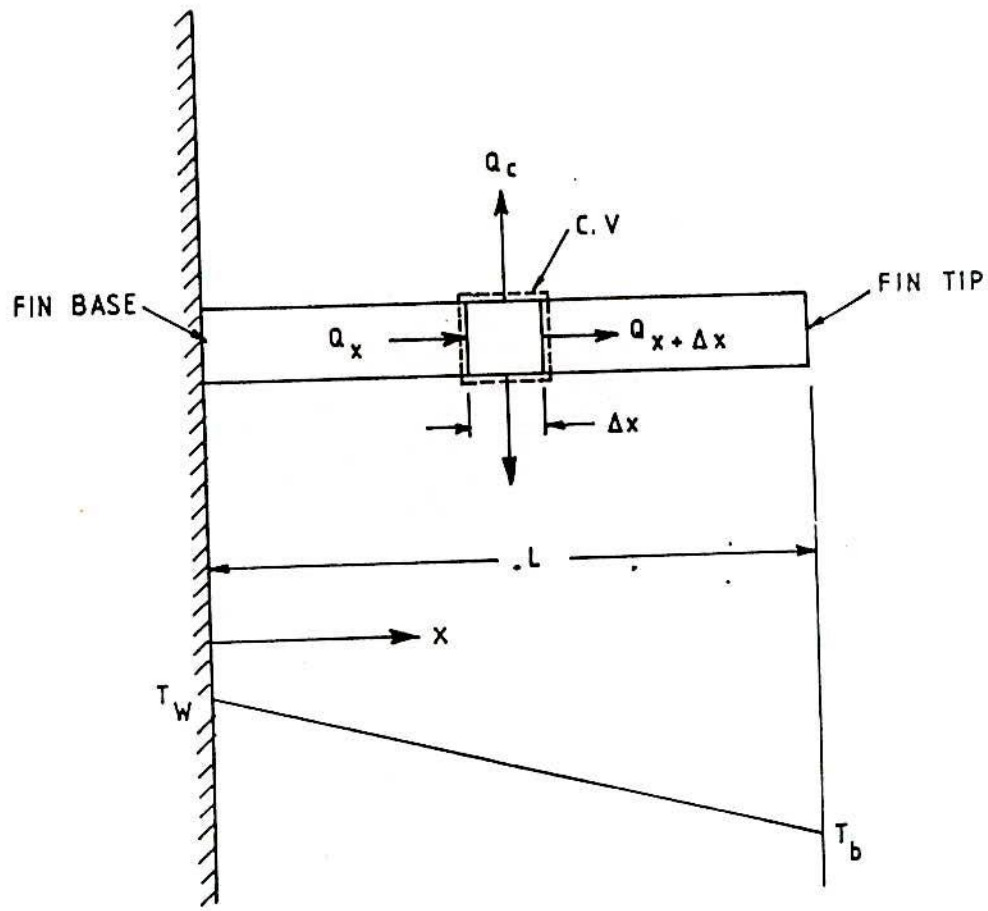

FIG. 4.1 NOMENCLATURE FOR THE DERIVATION OF ONE DIMENSIONAL FIN EQUATION

the fin. Figure 4.1 illustrates the geometry and coordinates for the development of the same.

Starting with the conventional equation of heat transfer from a finned surface,

$$\frac{d^2T}{dx^2} = \frac{Ph_x}{k\,A}\,(\,T(x) - T_b\,) \qquad .. (4.20)$$

equations have been developed which are applicable to CFB heat transfer for the following two cases

(i) Long fin

(ii) Short fin

4.3 Model I : Long Fin

It is assumed that the fin is sufficiently long so as to neglect the tip loss, but being long it will be subjected to radial distribution of suspension density in the fast bed. Glicksman [12] and Basu [40] observed that for small beds (< 15 cm diameter) heat transfer coefficient varies as the square root of suspension density. Therefore

$$h_x = k'\sqrt{\rho_x} \qquad .. (4.21)$$

where k' is an experimentally determined constant.

Now substituting the expression of h_x, the equation of temperature distribution for long fins takes the form of

$$\frac{d^2T}{dx^2} = \frac{P\, k' \sqrt{\rho_x}}{k\, A} \left(T(x) - T_b \right) \qquad .. (4.22)$$

4.3.1 Solution of equation

Equation (4.22) is a linear, second order differential equation with variable coefficient. To solve it, the equation has been transformed to an appropriate general Bessel's equation. For a longitudinal fin of rectangular profile having a constant thickness t , let x be the axial coordinate with its origin at the tip (Fig. 4.1). In the analysis of fin problem it is convenient to choose [187] without the loss of generality, $\frac{x}{L}\Big|_{tip} = 0$ and $\frac{x}{L}\Big|_{root} = 1$, so that the fin is considered to lie in the region $0 \leq \frac{x}{L} \leq 1$. It is assumed that the suspension density varies linearly with the radial distance from the wall within the short distance the fin extends into the bed. Therefore,

$$\frac{\rho_w + \rho_h}{2} \times L = \bar{\rho} \times L \qquad .. (4.23)$$

The distribution of suspension density along the fin surface is expressed as

$$\rho_x = \rho_h + \frac{x}{L} (\rho_w - \rho_h)$$

or, $$\rho_x = \rho_h + \frac{2x}{L} (\rho_w - \bar{\rho}) \qquad .. (4.24)$$

Inserting the expression of ρ_x , Eq. (4.22) takes the form of

$$\frac{d^2T}{dx^2} = \frac{Pk'}{kA} \sqrt{\rho_h + 2\frac{x}{L}(\rho_w - \bar{\rho})} \quad (T(x) - T_b) \qquad .. (4.25)$$

On substitution of $\theta(x) = T(x) - T_b$, Eq. (4.25) has been transformed to

$$\frac{d^2\theta}{dx^2} = C^2 (\sqrt{a + bx})\theta \qquad .. (4.26)$$

where $C^2 = \frac{P k'}{k A}$, $a = \rho_h$ and $b = \frac{2}{L}(\rho_w - \bar{\rho})$

The heat transfer area at the fin tip is generally small compared to its lateral area and hence, the tip loss is neglected for which $\frac{d\theta}{dx} = 0$ at $\frac{x}{L} = 0$ [187] . The mathematical formulation of the fin heat transfer then becomes

$$\frac{d^2\theta(x)}{dx^2} = C^2 \sqrt{(a + bx)}\ \theta \quad \text{in} \quad 0 \leq \frac{x}{L} \leq 1 \qquad .. (4.27)$$

$$\theta(x) = T_w - T_b = \theta_o \quad \text{at} \quad \frac{x}{L} = 1 \quad \text{(fin base)} \qquad .. (4.28)$$

$$\frac{d\theta(x)}{dx} = 0 \quad \text{at} \quad \frac{x}{L} = 0 \quad \text{(fin tip)} \qquad .. (4.29)$$

Let $U = a + bx$

Differentiating with respect to x

$$\frac{dU}{dx} = b$$

and $$\frac{d\theta}{dx} = \frac{d\theta}{dU} \cdot \frac{dU}{dx} = b \frac{d\theta}{dU}$$

Further differentiation gives

$$\frac{d}{dx}\left(\frac{d\theta}{dx}\right) = \frac{d}{dx}\left(b \frac{d\theta}{dU}\right)$$

or, $$\frac{d^2\theta}{dx^2} = b \cdot \frac{d^2\theta}{dU^2} \cdot \frac{dU}{dx} = b^2 \frac{d^2\theta}{dU^2}$$

Substituting the new parameter 'U' in Eq.(4.27), we get

$$\frac{d^2\theta(x)}{dx^2} = C^2 \sqrt{U}\, \theta$$

or, $$b^2 \frac{d^2\theta}{dU^2} - C^2 \sqrt{U}\, \theta = 0$$

or, $$\frac{d^2\theta}{dU^2} - \frac{C^2}{b^2} \sqrt{U}\, \theta = 0$$

or, $$\frac{d^2\theta}{dU^2} - m'^2 \sqrt{U}\, \theta = 0 \qquad \ldots (4.30)$$

where, $$m' = \frac{C}{b} = \frac{\left(\sqrt{Pk'/kA}\right)}{\frac{2}{L}\left(\rho_w - \bar{\rho}\right)}$$

Now Eq. (4.30) is written in the following form

$$\frac{d}{dU}\left(U^{\circ} \frac{d\theta}{dU} \right) - m'^{2} \sqrt{U}\, \theta = 0 \qquad .. (4.31)$$

Equation (4.31) is a form of Bessel's equation. Now comparing Eq. (4.31) with Eq. (3-126) of Ref. [188], (Table 3-1, P. 138), which is of the form $\frac{d}{dx}\left(x^{\alpha} \frac{dy}{dx} \right) + \gamma^2 x^{\beta} y = 0$ gives $\alpha = 0$, $\beta = \frac{1}{2}$, $\gamma = \pm$ im . The solution of Eq.(3-126) as given [188, 189] is

$$y(x) = x^{\nu/\mu} \, Z_{\nu}\left(|\gamma| \mu \, x^{1/\mu} \right)$$

where,

$$\nu = \frac{1 - \alpha}{\beta - \alpha + 2} \quad , \quad \mu = \frac{2}{\beta - \alpha + 2} \qquad \text{and}$$

$$\frac{\nu}{\mu} = \frac{1 - \alpha}{2}$$

The values of the parameters ν , μ and ν/μ for Eq. (4.31) have been evaluated as

$$\nu = \frac{2}{5} \quad , \quad \mu = \frac{4}{5} \qquad \text{and} \qquad \frac{\nu}{\mu} = \frac{1}{2}$$

So, for Eq. (4.31), the values of the parameters α , β , γ , ν , μ and ν/μ are as follows :

$$\alpha = 0 \, , \quad \beta = \frac{1}{2} \, , \quad \gamma = \pm \text{ im} \, , \quad \nu = \frac{2}{5} \, , \quad \mu = \frac{4}{5} \, ,$$

$$\frac{\nu}{\mu} = \frac{1}{2}$$

For non-integral values of ν ($\nu < 1$), the general solution of Eq. (4.31) [188,189] is

$$\theta(x) = C_1 U_x^{\nu/\mu} I_{-\nu}\left(|\gamma| \mu U_x^{1/\mu} \right) + C_2 U_x^{\nu/\mu} K_{-\nu}\left(|\gamma| \mu U_x^{1/\mu} \right) \quad .. (4.32)$$

where C_1 and C_2 are constants and the function $I_{-\nu}\left(|\gamma| \mu U_x^{1/\mu} \right)$ is the modified Bessel function of the first kind, of order ν , and the function $K_{-\nu}\left(|\gamma| \mu U_x^{1/\mu} \right)$ is the modified Bessel function of the second kind, of order ν .

The finiteness of tip temperature implies $C_2 = 0$, and for nonintegral ν ($\nu = \frac{2}{5}$) the solution of Eq.(4.32) simplifies to [187]

$$\theta(x) = C_1 U_x^{1/2} I_{-2/5}\left(\frac{4}{5} m' U_x^{5/4} \right) \quad .. (4.33)$$

using the first boundary condition (Eq. 4.28), i.e., at $\frac{x}{L} = 1$, $\theta(x) = T_w - T_b = \theta_o$, the constant C_1 of Eq. (4.33) is found to be

$$C_1 = \frac{\theta_o}{U_L^{1/2} I_{-2/5}\left(\frac{4}{5} m' U_L^{5/4} \right)}$$

where, $U_L = a + bL$

Therefore, the final solution of Eq. (4.31) is written as [187]

$$\theta(x) = \frac{\theta_o \, U_x^{1/2} \, I_{-2/5} \left(\frac{4}{5} m' \, U_x^{5/4} \right)}{U_L^{1/2} \, I_{-2/5} \left(\frac{4}{5} m' \, U_L^{5/4} \right)}$$

$$\text{or,} \quad \frac{\theta(x)}{\theta_o} = \frac{\sqrt{(a+bx)} \, I_{-2/5} \left[\frac{4}{5} m'(a+bx)^{5/4} \right]}{\sqrt{(a+bL)} \, I_{-2/5} \left[\frac{4}{5} m'(a+bL)^{5/4} \right]} \quad .. \quad (4.34)$$

Equation (4.34) is the final expression for temperature distribution along the fin length. For this case the heat input to each fin is from the Fourier's heat conduction law. Referring to Fig. 4.1.

$$Q_{fin} = - \left(- k A \frac{d\theta}{dx} \right)_{x=L} = k A \left. \frac{d\theta}{dx} \right|_{x=L} \quad .. \quad (4.35)$$

Differentiation of temperature profile as given by Eq. (4.34) yields an expression for the heat transfer from the whole fin surface. Now Eq. (4.34) is written as

$$\theta(x) = C_3 \sqrt{(a+bx)} \, I_{-2/5} \left(\frac{4}{5} m'(a+bx)^{5/4} \right)$$

where,

$$C_3 = \frac{\theta_o}{\sqrt{(a+bL)} \, I_{-2/5} \left(\frac{4}{5} m'(a + bL)^{5/4} \right)}$$

Differentiating the above equation, we get

$$\frac{d\theta}{dx} = C_3 \left[\sqrt{(a+bx)} \; \frac{d}{dx} \left[I_{-2/5} \left[\frac{4}{5} m'(a+bx)^{5/4} \right] \right] + I_{-2/5} \left[\frac{4}{5} m'(a+bx)^{5/4} \right] \frac{d}{dx} \left[\sqrt{(a+bx)} \right] \right] \quad .. \quad (4.36)$$

Let $\xi = \frac{4}{5} \left[m'(a + bx)^{5/4} \right]$

Therefore,

$$\frac{d\xi}{dx} = \left(\frac{4}{5} m' \right) \left(\frac{5}{4} \right) (a + bx)^{1/4} \; b = m'b(a+bx)^{1/4}$$

Now substituting the new parameter ξ in Eq. (4.36) it is found that

$$\frac{d\theta}{dx} = C_3 \left[\left[\sqrt{(a+bx)} \; \frac{d}{d\xi} \left(I_{-2/5}(\xi) \right) \frac{d\xi}{dx} \right] + \left[I_{-2/5}(\xi) \frac{d}{dx} \sqrt{(a+bx)} \right] \right]$$

or, $$\frac{d\theta}{dx} = C_3 \left[\sqrt{(a+bx)} \left[I_{(-2/5 \; +1)}(\xi) + \frac{-2/5}{\xi} I_{-2/5}(\xi) \right] \left[mb(a+bx)^{1/4} \right] + \left[I_{-2/5}(\xi) \right] \left[\frac{b}{2}(a+bx)^{-1/2} \right] \right]$$

$$\text{or,}\quad \frac{d\theta}{dx} = C_3 \left[(a+bx)^{1/2} \left[I_{3/5}\left(\frac{4}{5}(a+bx)^{5/4} \right) - \left(\frac{2}{5} x \frac{5}{4} \right) \left(\frac{1}{m'(a+bx)^{5/4}} \right) \left(I_{-2/5}\left(\frac{4}{5} m'(a+bx)^{5/4}\right) \right] \right.$$

$$\left[m'b(a+bx)^{1/4} \right] + \left[I_{-2/5}\left(\frac{4}{5} m'(a+bx)^{5/4} \right) \right]$$

$$\left. \left[\frac{b}{2}(a+bx)^{-1/2} \right] \right]$$

$$\text{or,}\quad \left.\frac{d\theta}{dx}\right|_{x=L} = C_3 \left[(a+bL)^{1/2} \left[I_{3/5}\left(\frac{4}{5}(a+bL)^{5/4} \right) \right. \right.$$

$$- \left(\frac{1}{2m'(a+bL)^{5/4}} \right) \left(I_{-2/5}\left(\frac{4}{5} m'(a+bL)^{5/4} \right) \right]$$

$$\left[m'b(a+bL)^{1/4} \right] + \left[I_{-2/5}\left(\frac{4}{5} m'(a+bL)^{5/4} \right) \right]$$

$$\left. \left[\frac{b}{2}(a+bL)^{-1/2} \right] \right]$$

$$\text{or,}\quad \left.\frac{d\theta}{dx}\right|_{x=L} = C_3 \left[(m'b(a+bL)^{3/4}) \left(I_{3/5}\left(\frac{4}{5} m'(a+bL)^{5/4}\right) \right) \right.$$

$$- \left(\frac{b}{2}(a+bL)^{-1/2} \right) \left(I_{-2/5}\left(\frac{4}{5} m'(a+bL)^{5/4} \right) \right.$$

$$\left. + \left(\frac{b}{2}(a+bL)^{-1/2} \right) \left(I_{-2/5}\left(\frac{4}{5} m'(a+bL)^{5/4} \right) \right) \right]$$

$$\text{or,} \quad \left.\frac{d\theta}{dx}\right|_{x=L} = \left[C_3 \, m'b(a+bL)^{3/4} \right] \left[I_{3/5}\left(\frac{4}{5} m'(a+bL)^{5/4} \right) \right] \quad \text{.. (4.37)}$$

Now inserting the expression of $\left.\frac{d\theta}{dx}\right|_{x=L}$ (fine base) from Eq. (4.37) to Eq. (4.35), it is found that

$$Q_{fin} = \left[kAC_3 m'b(a+bL)^{3/4} \right] \left[I_{3/5}\left(\frac{4}{5} m'(a+bL)^{5/4} \right) \right]$$

Substituting the expression of C_3 and m' in the above equation, we finally get

$$Q_{fin} = \frac{\left[kA \frac{C}{b} b \, \theta_o (a+bL)^{3/4} \right] \left[I_{3/5}\left(\frac{4}{5} m'(a+bL)^{5/4} \right) \right]}{(a+bL)^{1/2} \, I_{-2/5}\left(\frac{4}{5} m'(a+bL)^{5/4} \right)}$$

$$\text{or,} \quad Q_{fin} = \frac{kAC \, \theta_o (a+bL)^{3/4} \left[I_{3/5}\left(\frac{4}{5} m'(a+bL)^{5/4} \right) \right]}{(a+bL)^{1/2} \left[I_{-2/5}\left(\frac{4}{5} m'(a+bL)^{5/4} \right) \right]} \quad \text{.. (4.38)}$$

In more convenient form Eq. (4.38) has been expressed as

$$Q_{fin} = \frac{\left[\theta_o \, kAC \, U_x^{3/4} \right] \left[I_{3/5}\left(\frac{4}{5} m' \, U_x^{5/4} \right) \right]}{U_L^{1/2} \left[I_{-2/5}\left(\frac{4}{5} m' \, U_L^{5/4} \right) \right]} \quad \text{.. (4.39)}$$

where,

$$U_x = a + bx = \rho_h + 2\frac{x}{L}(\rho_w - \bar{\rho})$$

and $U_L = a + bL = \rho_h + 2\frac{L}{L}(\rho_w - \bar{\rho}) = \rho_w$

Now inserting the expressions, $C = \sqrt{Pk'/kA}$ and $U_L = \rho_w$ in Eq. (4.39) it is found that

$$Q_{fin} = \frac{\theta_o k A (\sqrt{Pk'/kA})(U_x^{3/4})\left[I_{3/5}(\frac{4}{5} m' U_x^{5/4})\right]}{\sqrt{\rho_w}\left[I_{-2/5}(\frac{4}{5} m' \rho_w^{5/4})\right]}$$

or, $$Q_{fin} = \frac{(\theta_o \sqrt{Pk'Ak})(U_x^{3/4})\left[I_{3/5}(\frac{4}{5} m' U_x^{5/4})\right]}{\sqrt{\rho_w}\left[I_{-2/5}(\frac{4}{5} m' \rho_w^{5/4})\right]} \quad .. (4.40)$$

If N_f is the number of fins, then the total heat transfer from the fins is finally given by

$$Q_F = \frac{(N_f\theta_o \sqrt{Pk'Ak})(U_x^{3/4})\left[I_{3/5}(\frac{4}{5} m' U_x^{5/4})\right]}{\sqrt{\rho_w}\left[I_{-2/5}(\frac{4}{5} m' \rho_w^{5/4})\right]} \quad .. (4.41)$$

The total heat transfer, Q_T from a finned surface is obtained by summing up the heat transfer through the fins and the unfinned portion such that

$$Q_T = Q_F + Q_{UF}$$

Substituting Q_F from Eq. (4.41) and dividing both sides by θ_o, the temperature difference between the wall and the bed, and A_T, the total heat transfer area including fins, the average overall heat transfer coefficient is obtained as

$$h_{T1} = \frac{N_f \sqrt{Pk'Ak}\ (U_x^{3/4}) \left[I_{3/5} \left(\frac{4}{5} m' U_x^{5/4} \right) \right]}{A_T \sqrt{\rho_w} \left[I_{-2/5} \left(\frac{4}{5} m' \rho_w^{5/4} \right) \right]} + \frac{A_{UF}}{A_T} \left(\frac{q''}{\theta_o} \right) \quad .. (4.42)$$

Equation (4.42) is the proposed heat transfer model for long fins in a CFB.

4.4 Model II : Short Fin

It is assumed that the fin is short enough so as to be unaffected by the radial voidage variation. However, the fin being short the heat loss from the tip needs to be considered. The mathematical formulation of the heat transfer for this case becomes

$$\frac{d^2\theta}{dx^2} - m^2\theta(x) = 0 \quad \text{in} \quad 0 \leq x \leq L \quad .. (4.43)$$

$$\theta(x) = T_w - T_b = \theta_o, \quad \text{at the fin base} \quad .. (4.44)$$

$$-k \frac{d\theta(x)}{dx} = h_t \theta(x), \quad \text{at the fin tip} \quad .. (4.45)$$

where, h_t is the heat transfer coefficient between the fin tip and the surrounding emulsion.

The solution of this problem Eq.(4.43) is well known [185,190]. The temperature distribution in the fin is given by

$$\frac{\theta(x)}{\theta_o} = \frac{T(x) - T_b}{T_w - T_b} = \frac{\cosh m(L-x) + (h_t/mk) \sinh m(L-x)}{\cosh mL + (h_t/mk) \sinh mL} \quad .. (4.46)$$

The heat flow rate through the fin is obtained by introducing this result into the equation

$$Q = - k A \left.\frac{d\theta(x)}{dx}\right|_{\text{fin base}} \quad .. (4.47)$$

which becomes

$$Q_{fin} = \theta_o \sqrt{PhkA} \left[\frac{\sinh mL + (h_t/mk) \cosh mL}{\cosh mL + (h_t/mk) \sinh mL} \right] \quad .. (4.48)$$

For N_f number of fins, it becomes

$$Q_F = (N_f \theta_o \sqrt{Phk A} \left[\frac{\sinh mL + (h_t/mk) \cosh mL}{\cosh mL + (h_t/mk) \sinh mL} \right] \quad .. (4.49)$$

where, $m = \sqrt{Ph/kA}$

The total heat transfer (Q_T) is

$$Q_T = Q_F + Q_{UF}$$

Substituting Q_F from Eq. (4.49) and dividing both sides by θ_o and A_T, the average overall heat transfer coefficient is obtained as

$$h_{T2} = \frac{N_f \sqrt{Phk\,A}}{A_T} \left[\frac{\sinh mL + (h_t/mk)\cosh mL}{\cosh mL + (h_t/mk)\sinh mL} \right] + \frac{A_{UF}}{A_T}\left(\frac{q''}{\theta_o}\right) \quad .. (4.50)$$

Equation (4.50) is the proposed heat transfer model for short fins in a CFB.

Heat transfer data in CFB with fins not being available, the heat transfer coefficients predicted from model I have been compared with those of present experiments only and good agreement is observed.

4.5 Empirical Correlation Among the Parameters Nu_p, Re_p and L_h/D

An empirical equation has been developed correlating the parameters Nu_p, Re_p and L_h/D to estimate heat transfer from probes of different vertical heights. Assuming a functional relationship among them as

$$Nu_p = k\,(Re_p)^m\,(L_h/D)^n \quad .. (4.51)$$

where, Nu_p = Particle Nusselt number, $h\,d_p/k_g$

Re_p = Particle Reynolds number, $U_o d_p \rho_g / \mu_g$

L_h = Vertical height of the probe

D = Diameter of the probe

k, m and n are constants

4.5.1 Evaluation of constants

To evaluate the constants of Eq. (4.51) experiments were performed here in the laboratory in a circulating fluidized bed unit with probes of four different vertical heights. The detailed description of experimental set-up and the procedure have been narrated in Articles 5.1 and 5.2.5 respectively. Using a computer package programme and the data of the present experiments [Tables 6.49 to 6.52], the average values of the slopes were computed to be $m = -0.25$ and $n = -0.5$. Now substituting the values of 'm' and 'n' in Eq. (4.51) and using the least square technique, the value of 'k' was computed to be 4.7. Then the final correlation becomes

$$Nu_p = 4.7 \left[Re_p \left(L_h / D \right)^2 \right]^{-0.25} \quad .. (4.52)$$

Equation (4.52) is the final empirical correlation. The predicted results from the correlation (a sample calculation is shown in Art. 6.9(h)) have been compared with those of present experiments as well as with those of Sekthira et al [79] and good agreement is observed.

CHAPTER - V

EXPERIMENTAL SET-UP AND PROCEDURE

5.1 Experimental Set-Up

The experimental work for the study of heat transfer in circulating fluidized beds was conducted in a circulating fluidized bed (CFB) unit specifically fabricated, installed and instrumented. The CFB unit comprised of 100 mm. I.D., 5.15 m high main column, made up of steel sections, along with a return leg, mainly of plexiglass, a cyclone and a bag filter (Fig. 5.1, Plate 1). Air was supplied by a high pressure centrifugal blower, and the air flow rate, controlled by a stop valve and a bypass arrangement, was measured by a standard orificemeter. The distributor plate used was straight hole orifice type having 12.4 % open area. A butterfly valve was located about mid-way in the return leg to measure the solid circulation rate in the column by closing the valve and measuring the volume of solids collected above it over a certain period of time. Entrained solids were recovered in a cyclone and returned to the bottom of the riser column. Solid return point from the return leg to the main column was located 0.5 m above the distributor. Static pressures were measured at 0.5 m intervals along the bed height. Fine wire mesh (BS 400) and cigarette filters were used at pressure tapping ends to minimize pressure fluctuations in the water filled U-tube manometers.

The test section (Fig. 5.2, Plate 2), 300 mm long was located 2.75 m above the distributor. A tape heater which was used as the source of heat was wrapped uniformly around it. It was then adequately insulated with glass wool and asbestos rope. Asbestos gaskets of 10 mm thickness were used at the flanges, and guard tape heaters were provided before and after the test section to prevent axial heat loss by conduction along the pipe wall. Electrical energy input to the heater was controlled by a variac and measured with a voltmeter and ammeter. The temperatures of the inside wall and the bed at about the mid-point in the test section were measured with copper-constantan thermocouples. The thermocouple wires were all connected to a multipoint switch and then to a digital D.C. microvoltmeter.

Local sand of mean diameter (d_p) 310 micron was used as the bed material. The properties and size distribution of sand particles are shown in Tables 5.1 and 5.2 respectively. The mean particle size is calculated from the reciprocal of $\Sigma(x_i/d_{pi})$, where x_i is the weight fraction of particles which has an average size of d_{pi} determined by standard sieve analysis. The experimental conditions are given in Table 5.3.

5.1.1 Test section

The details of the test section have been shown in Fig. 5.2 and its cross-sectional view has been shown in Fig. 5.3. The photograph of the same has been given in

Table - 5.1 : Properties of Sand Particles

1.	Mean particle size	:	d_p =	310 micron
2.	Density of sand	:	ρ_s =	2350 kg/m^3
3.	Minimum fluidization velocity	:	U_{mf} =	0.075 m/s
4.	Voidage at U_{mf}	:	ϵ_{mf} =	0.5
5.	Terminal velocity	:	U_T =	1.54 m/s

Table - 5.2 : Size Analysis of Sand Particles

Diameter range (μ_m)	Mean diameter (d_{pi}) (μm)	Weight fraction (X_i)
200 - 234	217.0	0.2500
234 - 285	259.5	0.1305
285 - 370	327.5	0.3180
370 - 556	463.0	0.2275
556 - 778	667.0	0.0740

Table - 5.3 : Experimental Conditions

Variable	Range
Fluidizing velocity, m/s	5.6 - 12.5
Bed temperature, K	330 - 365
Suspension density, kg/m^3	18 - 76
Heat flux, W/m^2	3580 - 7876
Bed inventory, kg	20 - 32
Vertical probe height, mm	85 - 300
Mode of heating	Electric heater
Fin geometry	Rectangular and pin shap

Plate 2. It has a dimension of 100 mm I.D. and 300 mm long.

Four more plain and five finned test sections have been used, three of which had rectangular fins and two had pin fins. The details of fins and their attachment with test section have been shown in Fig. 5.4.

(a) Test sections with rectangular fins :

The test sections were fitted with 2, 4 and 8 vertical rectangular fins of 246 mm x 23 mm x 6 mm, which were fitted symmetrically by screwing to the inside surface separately. The matching surfaces were machined accurately and special care was taken to ensure perfect thermal contact of the fin. The surface contact was checked by applying light before and after their use.

(b) Test sections with pin fins

The test sections were fitted with 16 and 32 number of pin fins of 6.35 mm O.D., 15 mm long, which were fitted inside the wall by screwing, located at 90° and 45° apart in columns respectively. In each case the fins were positioned at four equidistant rows.

(c) Test sections having different vertical heights :

Four test sections having 100 mm I.D. and 85, 127.5, 170 and 255 mm length were used to conduct the last part of the experiments. The photographs of these test sections have been shown in Plate-3.

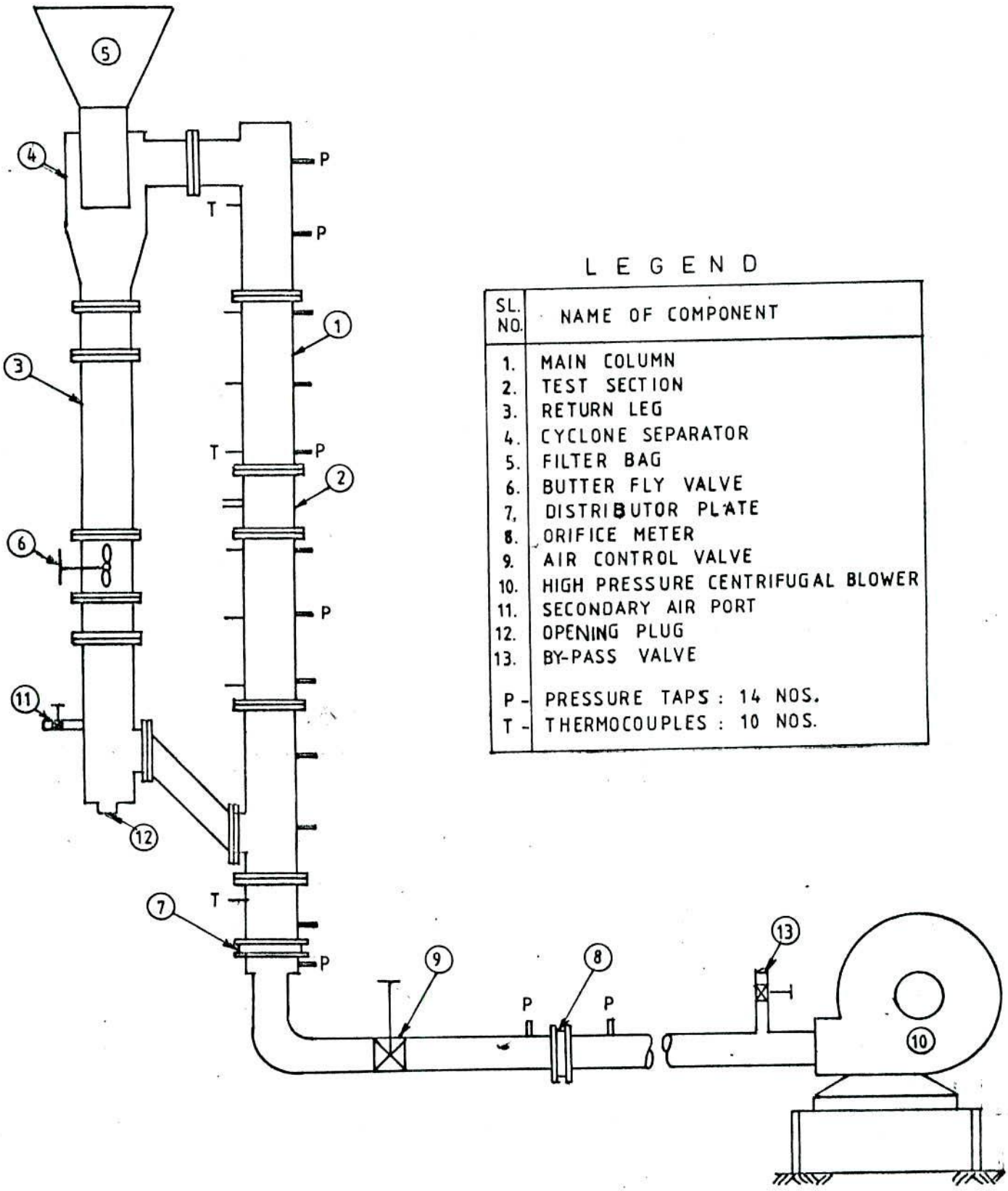

LEGEND

SL. NO.	NAME OF COMPONENT
1.	MAIN COLUMN
2.	TEST SECTION
3.	RETURN LEG
4.	CYCLONE SEPARATOR
5.	FILTER BAG
6.	BUTTER FLY VALVE
7.	DISTRIBUTOR PLATE
8.	ORIFICE METER
9.	AIR CONTROL VALVE
10.	HIGH PRESSURE CENTRIFUGAL BLOWER
11.	SECONDARY AIR PORT
12.	OPENING PLUG
13.	BY-PASS VALVE
P -	PRESSURE TAPS : 14 NOS.
T -	THERMOCOUPLES : 10 NOS.

FIG. 2 SCHEMATIC DIAGRAM OF EXPERIMENTAL SET-UP

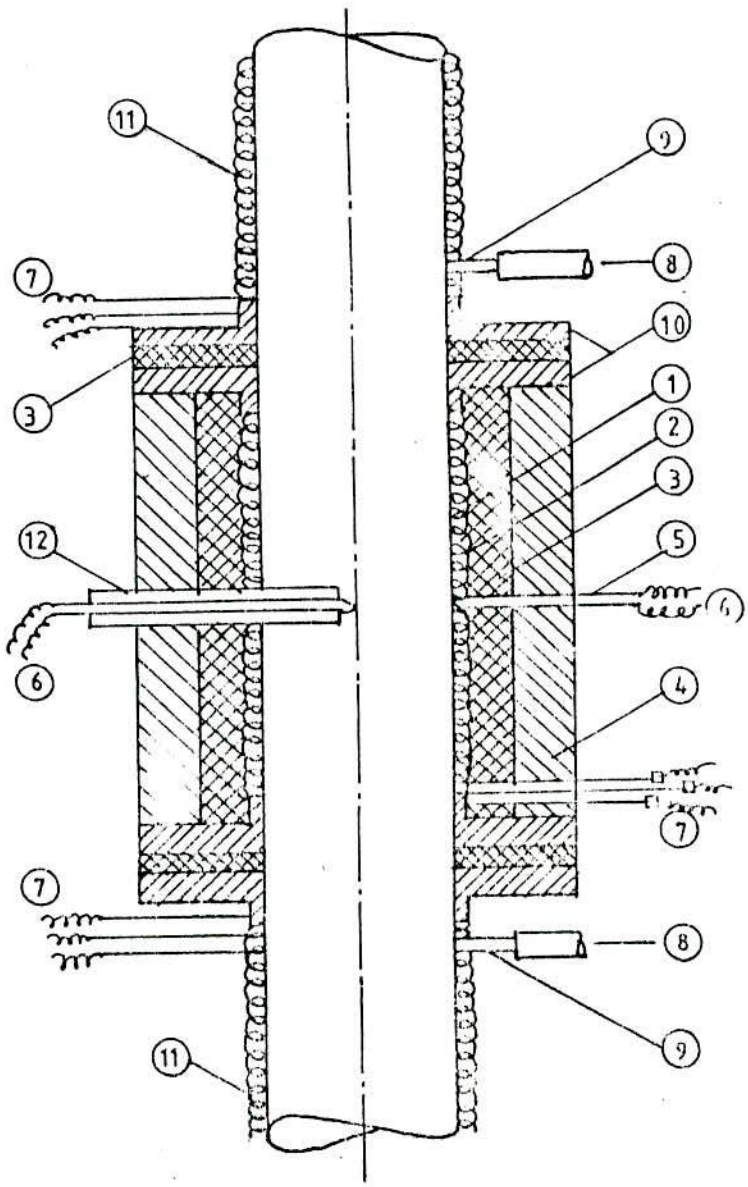

LEGEND

NO.	NAME OF PART
1	HEAT TRANSFER WALL
2.	MAIN HEATER
3.	ASBESTOS INSULATION
4.	GLASS WOOL INSULATION
5.	WALL THERMOCOUPLE
6.	TO MICROVOLTMETER
7.	TO MAIN SUPPLY
8.	TO MANOMETER
9	PRESSURE TAPPING
10.	FLANGES
11	GUARD HEATER
12.	BED THERMOCOUPLE

FIG. 5-2 TEST SECTION WITH INSTRUMENTATION AND GUARD HEATER

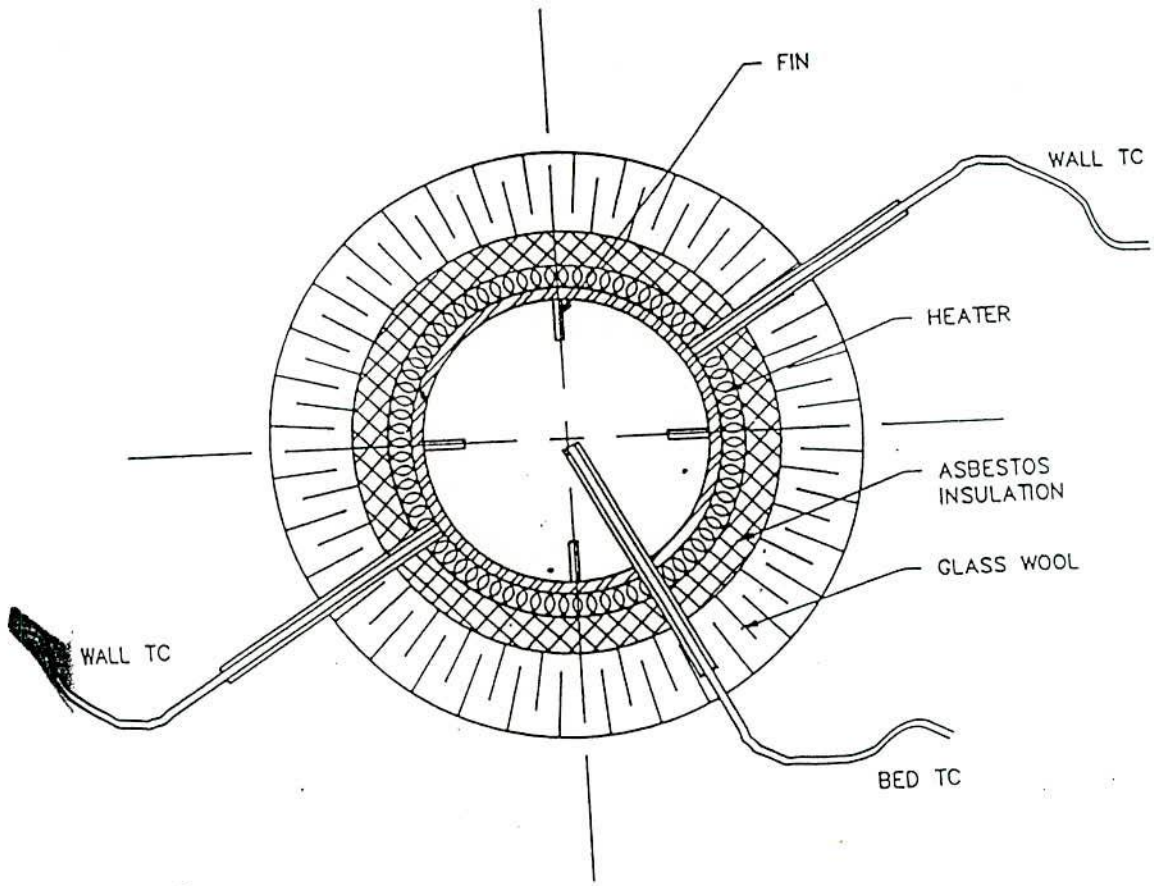

FIG 5.3 : CROSS-SECTION OF THE TEST SECTION

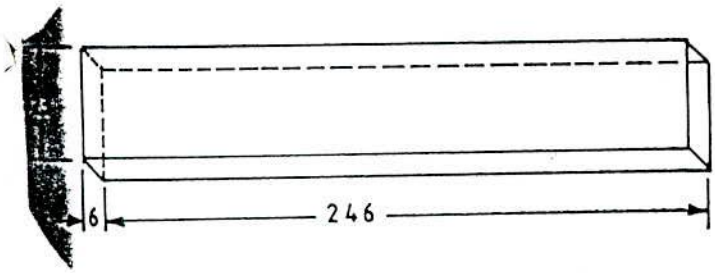

(a) Typical rectangular fin

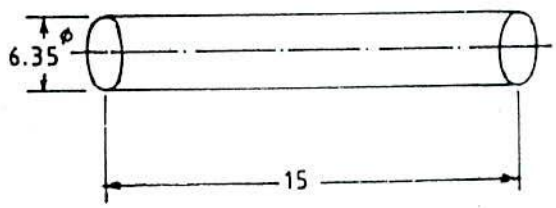

(b) Typical pin fin

ALL DIMENSIONS ARE IN mm
NOT TO SCALE

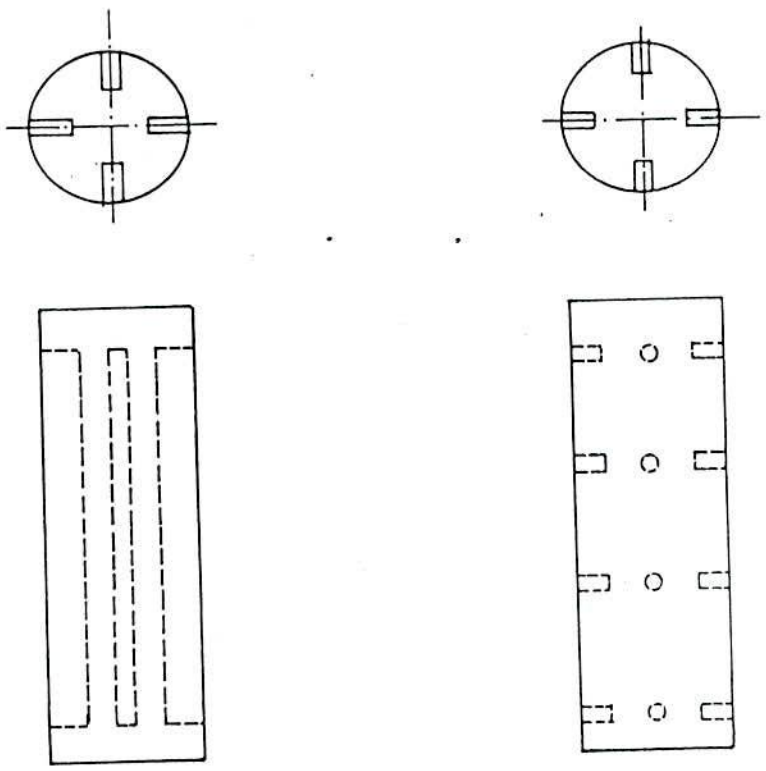

(c) Test section fitted with 4-rectangular fins

(d) Test section fitted with 16-pin fins

FIG. 5.4 DETAILS OF FINS AND THEIR ATTACHMENT WITH TEST SECTIONS

5.1.2 Blower

It was a high pressure, centrigugal type of blower. It was installed to supply air to the main column to fluidize the solid particles.

Specification of blower :

Air quantity	:	3000 to 4000 m^3/hr
Temperature	:	60^oC
Total pressure	:	1600 to 1900 mm of w.g.
Power consumption	:	22 to 27.44 kW (29.5 to 36.8 HP)
Motor rating	:	29.83 kW (40 HP) , 4 pole
Fan speed	:	3600 r.p.m.

5.1.3 Heat source

Electric tape heaters were used as the source of heat. Six heaters of different dimensions and capacities were used in the whole range of experiments. The first five were used as source heaters and the sixth one was used as the guard heater. The detailed specifications of each kind of heater are given in Appendix-B.

5.1.4 Distributor

It is located at the bottom of the main column. The distributor was made following the design outline given by Kunii and Levenspiel [20], Botterill [35] and Basu [191]. It is a straight hole orifice type of distributor having 12.4 % open area. The diagram is shown in Fig. C5.1 and the design details have been given in Appendix - C. A layer of fine wire mesh (B.S. 200) was used on the top of the distributor to prevent the smallest particle from passing through it. Two pressure tappings, one at the top and the other at the bottom of the distributor, were provided to measure the pressure drop across it.

5.1.5 Thermocouples

Copper-constantan thermocouples were used to measure both the bed and surface temperatures. Two thermocouples were embedded at 180° apart to the inner surface and located about the mid-position of the test section. The average of the two thermocouple readings was taken as the wall temperature in all the cases. For the bed temperature, the thermocouple was located in such a fashion that its tip lies at the central axis of the bed. Four thermocouples above the test sections and three below it were used to check the steady state condition of the riser column. All the thermocouple leads were connected to a multipoint switch and then

to a digital D.C. microvolt meter. Before use, the thermocouples were caliberated.

5.1.6 Air flow measurement

The rate of air flow through the bed was measured by using a standard orifice meter made to B.S. code 1043 : 1943 with D and D/2 tappings (Plate 4). Equation (3.13) was used to estimate the volume flow rate of air through the orifice meter.

5.1.7 Pressure drop measurement

Pressure tappings were provided at ten different locations along the height of the bed (Fig. 5.1) at equal intervals of 0.5 m to determine the axial voidage of the bed. These pressure tappings were connected to a water - filled U-tube manometer bank (Plate 5). Fine wire mesh (B.S. 400) and cigarette filters were used at pressure tapping ends to minimize pressure fluctuations in the manometers.

5.1.8 Return leg

A solid return leg, a major part of which is made of plexiglass, is connected to the main column through a cyclone separator at the top and a 45° inclined smooth passage at the bottom. The solid return point is about 0.5m above the distributor plate. The entrained solids first come

to the cyclone where these are separated from the gas and returned to the main column at the bottom. A bag filter made of canvas and covering the outlet of the cyclone catches the solids which do not separate in the cyclone, and sends these back to the main column. A butterfly valve is located at about the middle of the return leg, which is used to hold a column of sand and prevent air from flowing into the downcomer from the distributor (Plate-6).

5.1.9 Measurement of solid circulation rate

The butterfly valve shown in Plate 6 located at the middle of the return leg is used to measure and control the solid circulation rate in CFB loop. The solid circulation rate is measured by closing the valve and measuring the volume of solids collected above it over a certain period of time. At a steady velocity the butterfly valve was closed sharply, and with the help of a stop watch, the time was recorded to store a certain amount of solid above it. The average of at least five such readings was considered for estimating the recirculation rate by using Eq. (3.15).

5.1.10 Insulation

The test section was adequately insulated. The first layer of insulation was provided by asbestos rope of about 30 mm thick. The outer layer of insulation was provided with glass wool of about 120 mm thick. The top and

bottom of the test section was insulated by providing asbestos gaskets of about 10 mm thick in between the flanges to prevent axial heat conduction along the thickness of the pipe wall. The electrical equipment used in the experiment has been shown in Plate-7.

5.2 Experimental Procedure

The experiments were divided into three parts.

(i) Heat transfer from unfinned surface

(ii) Heat transfer from finned surfaces

(iii) Heat transfer from the probes of different vertical heights.

5.2.1 Heat transfer from unfinned surface

Prior to the starting of actual experiments, some trial runs were taken to have an idea about the control and measurement of the operating parameters.

The experiment was made first with unfinned surface. A known quantity of sand was fed into the main column through the top of the cyclone. The outlet of the cyclone was then covered by the bag filter. The switches of the main heater and guard heaters were then put on. A predetermined heat flux was set by controlling the variac after adjusting the supply voltage and current, read from the voltmeter and ammeter respectively. The switch of microvoltmeter was set on and allowed to warm up for

about ten minutes before taking any reading. The blower was then started and air was allowed to flow through the riser column with the help of air control valve. The air flow rate was slowly increased and the bed starts expanding and within a short period it attained the complete fluidization condition. When the air velocity was further increased and the terminal velocity was exceeded, the entrainment of solids began which was observed visually through the plexiglass column located at the bottom of the cyclone in the return leg. The desired air flow rate was maintained by adjusting the flow through orifice meter, which was ascertained from the pressure drop data across the orifice meter. The entrained solids were allowed to return to the main column by opening the butterfly valve and thus a continuous loop of emulsion was established. A 1250 watt electric tape heater was switched on to supply heat to the test section. The gas-particle emulsion while passing over the test section got heated till the steady state condition was reached. The bed took about three hours to attain this steady state condition, which could be ascertained from the constant readings of the thermocouples. Two pressure taps were provided, one at the top and the other at the bottom of the test section, to estimate the average bed suspension density. The pressure taps were connected to a water filled U-tube manometer.

The solid circulation rate was determined with the help of a stop watch and closing the butterfly valve to collect a desired amount of solid over it for a certain period of time. At steady state condition the following observations were made at certain intervals of time.

(i) The bed temperature, noted from the microvoltmeter reading.

(ii) The surface temperatures from two different points at the same level, noted from the microvoltmeter reading.

(iii) Manometer reading (connected across the orifice meter).

(iv) Manometer reading (connected across the test section).

(v) Manometer readings (ten pressure taps) connected along the bed height.

(vi) Data for solid circulation rate.

(vii) The ambient air temperature.

At least five data for each observation were recorded and average of which has been taken into consideration for any calculation. The experiments were repeated for six superficial velocities ranging from

5.6 to 11.4 m/s, three constant energy fluxes of 3580, 5519 and 7876 W/m^2 and for three bed inventories of 20 kg, 26 kg and 32 kg of local sand having mean diameter of 310 micron. When the observations for one bed inventory were completed, the sand was taken out of the bed through the opening plug (Fig. 5.1) and fresh measured quantity of solids were again loaded before starting the next experiment.

5.2.2 Heat transfer from rectangular finned surface

Three test sections fitted with rectangular fins have been examined. Experiments were first conducted with the test section having two vertical rectangular fins (246 mm x 23 mm x 6 mm) fitted inside the wall and located 180° apart, diametrically opposed to each other. The fins were tightly screwed to the wall, and special care was taken to ensure near perfect thermal contact of the fin with its base. Then these experiments were repeated for four and eight vertical rectangular fins of the same dimensions fitted inside the wall, located at 90° and 45° apart respectively. The fins were fitted to the wall with the same technique as explained earlier. Local sand of mean diameter of 310 micron was used as the bed material and it was fluidized in the same manner as described in Art. 5.2.1. When steady state

condition was reached the same data as recorded for unfinned surface were noted. The experiments were performed for six superficial velocities ranging from 5.6 to 11.4 m/s, for three heat inputs of 3580, 5519 and 7876 W/m^2 and for three bed inventories of 20 kg, 26 kg and 32 kg sand particles. When observations for one bed inventory were completed, the bed materials were taken out and a fresh measured amount was loaded for the next experiment.

5.2.3 Experiments with 1500 mm long rectangular fins

For this set of experiments four rectangular fins having length of 1500 mm and remaining other dimensions (23 mm breadth x 6 mm thick) the same as before were used. The fins were located at 90^o apart and extended from the test section along the main column. The experimental procedure was the same as described in Art. 5.2.1. The experiments were performed for 26 kg of local sand having 310 micron mean particle size and for 5519 W/m^2 constant heat flux. The observations were repeated for six superficial velocities ranging from 5.6 to 11.4 m/s. The same data as described in Art. 5.2.1 were recorded when steady state condition of the bed was reached.

5.2.4 Heat transfer from pin finned surface

Experiments were performed with two test sections. The first one was equipped with 16 number pin fins of 6.35 mm in diameter and 15 mm long. The fins were fitted by screwing to the inside surface of the test section in four rows and in four columns in such a manner that the columns were at 90^{o} apart and the rows were equidistant. The second one had 32 number of pin fins of the same dimensions and fitted in the same way to the inner surface of the test section as that of the first except that the columns of fins were at 45^{o} apart. The experiments were conducted in the same way as before. The experiments were performed for six superficial velocities ranging from 5.6 to 11.4 m/s, for three constant heat inputs of 3580, 5519 and 7876 W/m^2 and for three bed inventories of 20 kg, 26 kg and 32 kg of sand particles having a mean particle size of 310 micron. All the needed data were recorded as stated earlier.

5.2.5 Heat transfer from probes of different vertical heights

Here, four probes having vertical heights of 85, 127.5, 170 and 255 mm were tested. Four electric tape heaters of the same rating but having different lengths were used as the source of heat. The heaters having lengths of 1.22, 1.83, 2.44 and 3.66 meter were

wrapped uniformly around 85, 127.5, 170 and 255 mm long probes respectively. The heat transfer probes were installed one after another at the same height as previously mentioned, i.e., 2.75 m above the distributor. The experiments were performed for each probe independently following the same procedure as explained in Art. 5.2.1. Local sand of mean diameter of 310 micron was used as the bed material. The experiments were conducted for five superficial velocities ranging from 7.2 to 12.5 m/s, for two constant heat fluxes of 4500 and 6000 W/m^2 and for 32 kg of bed material. For steady state condition the required data were recorded.

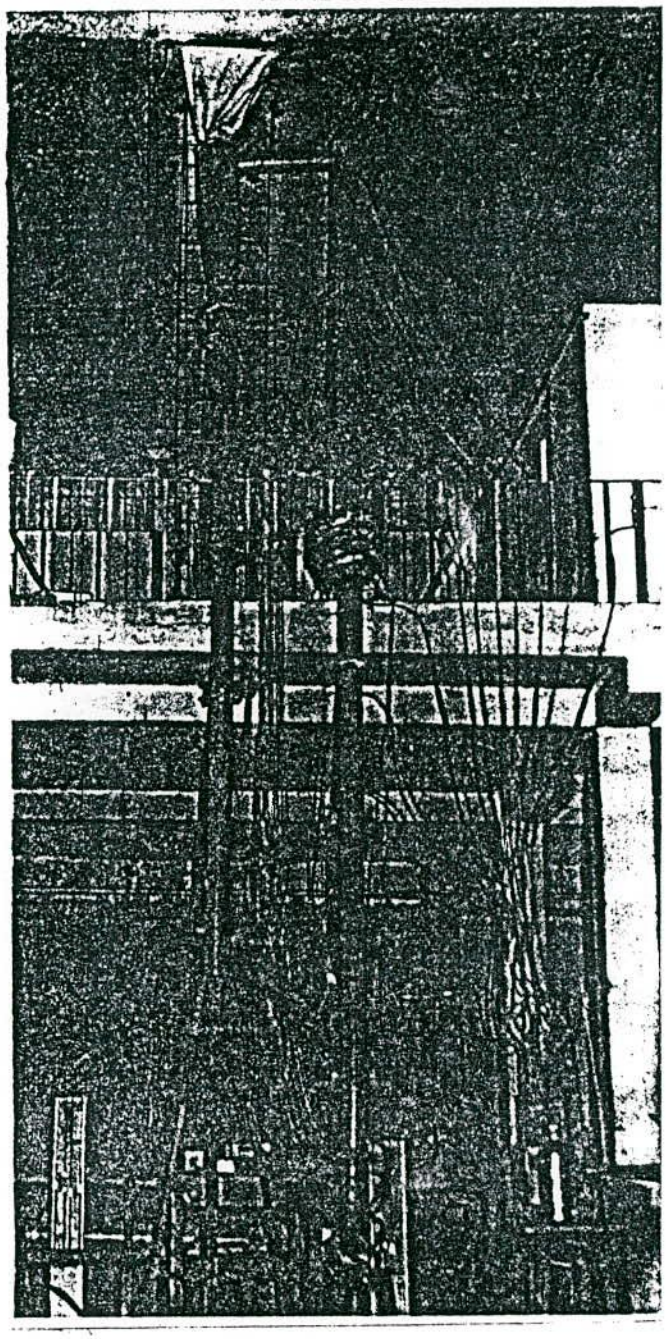

PLATE-1 SCHEMATIC DIAGRAM OF EXPERIMENTAL SET-UP

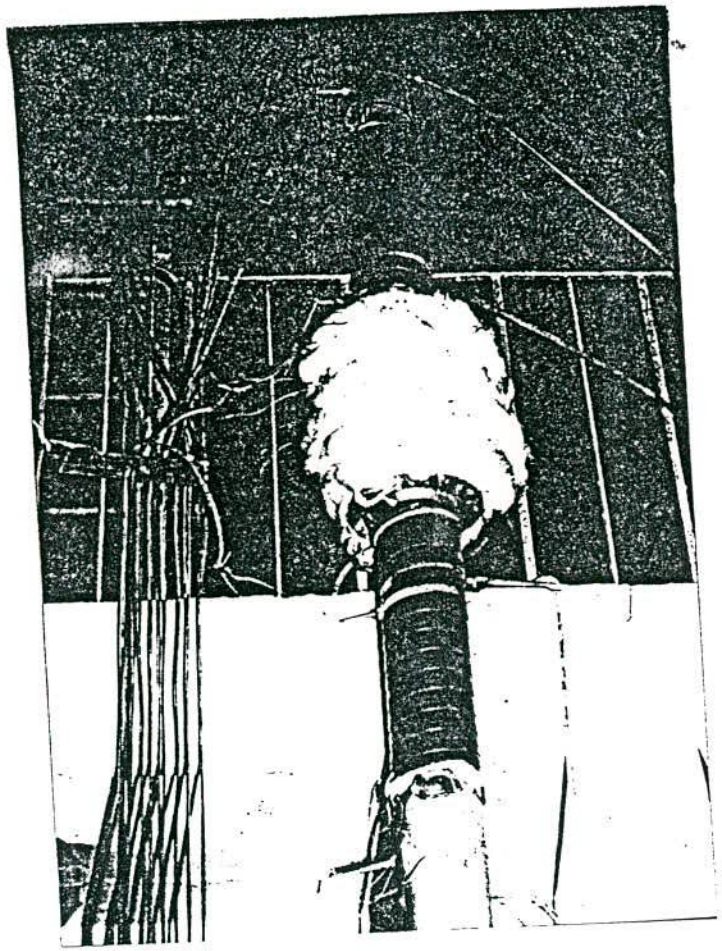

PLATE-2 INSULATED TEST SECTION WITH GUARD HEATERS

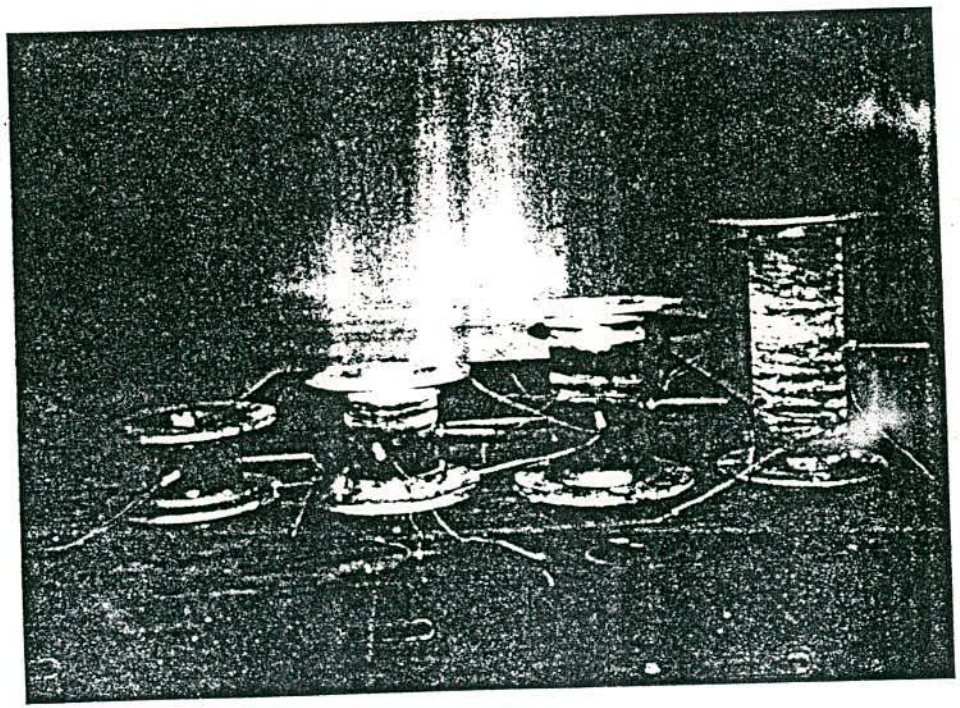

PLATE-3 PROBES OF DIFFERENT VERTICAL HEIGHTS

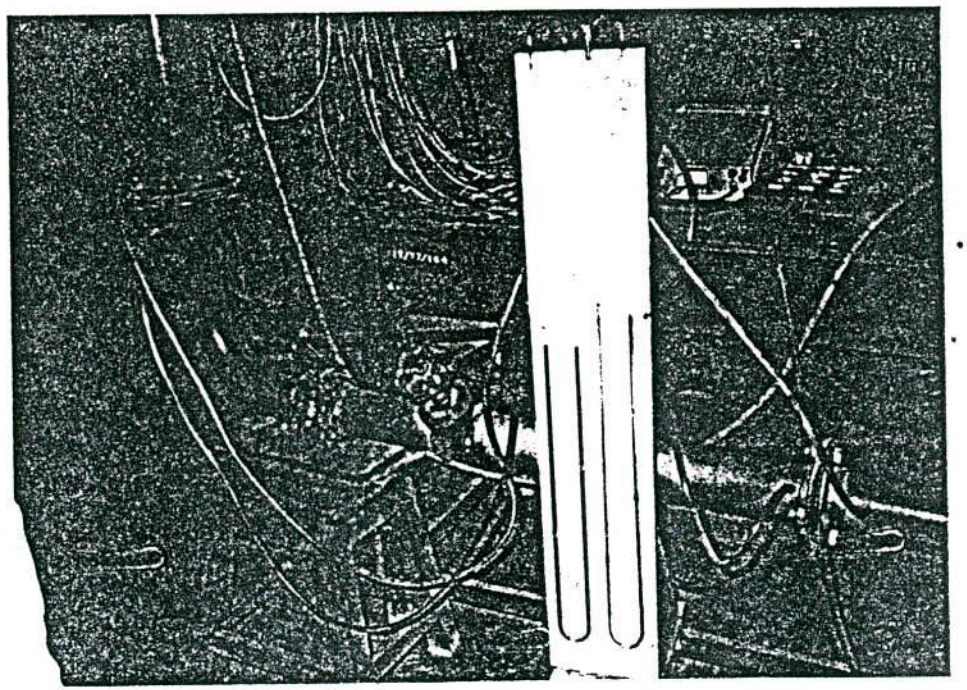

PLATE-4 AIR FLOW MEASUREMENT DEVICE

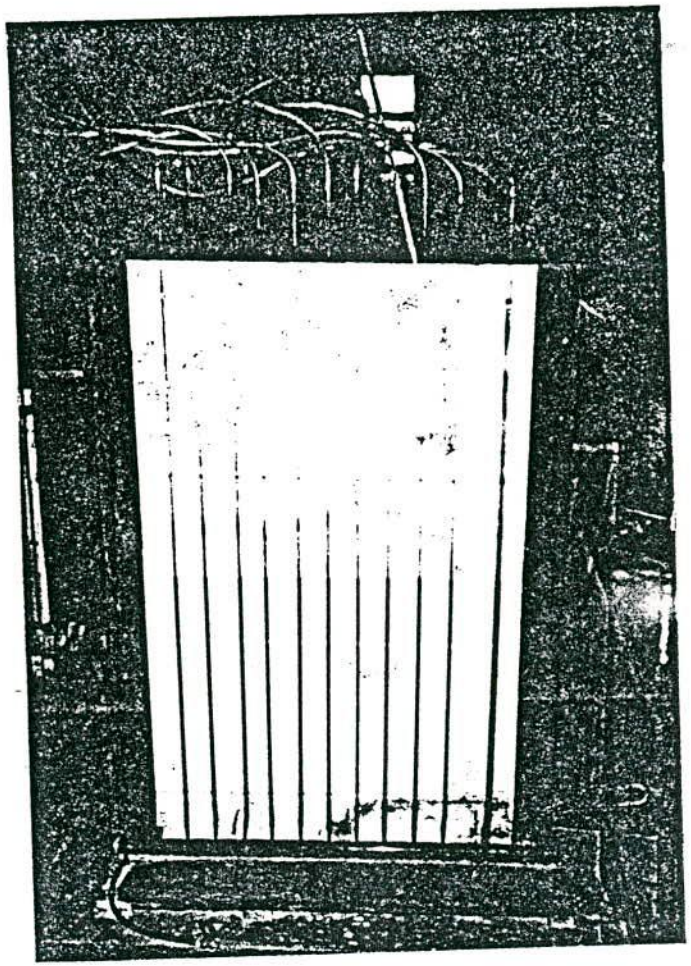

PLATE-5 U-TUBE MANOMETER BANK

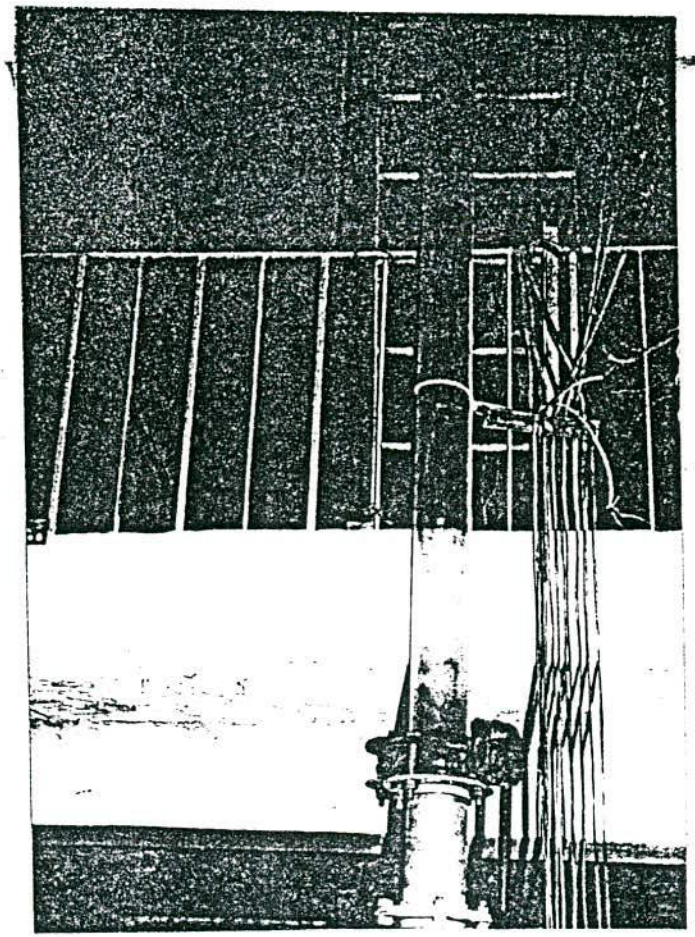

PLATE-6 BUTTERFLY VALVE FITTED TO RETURN LEG

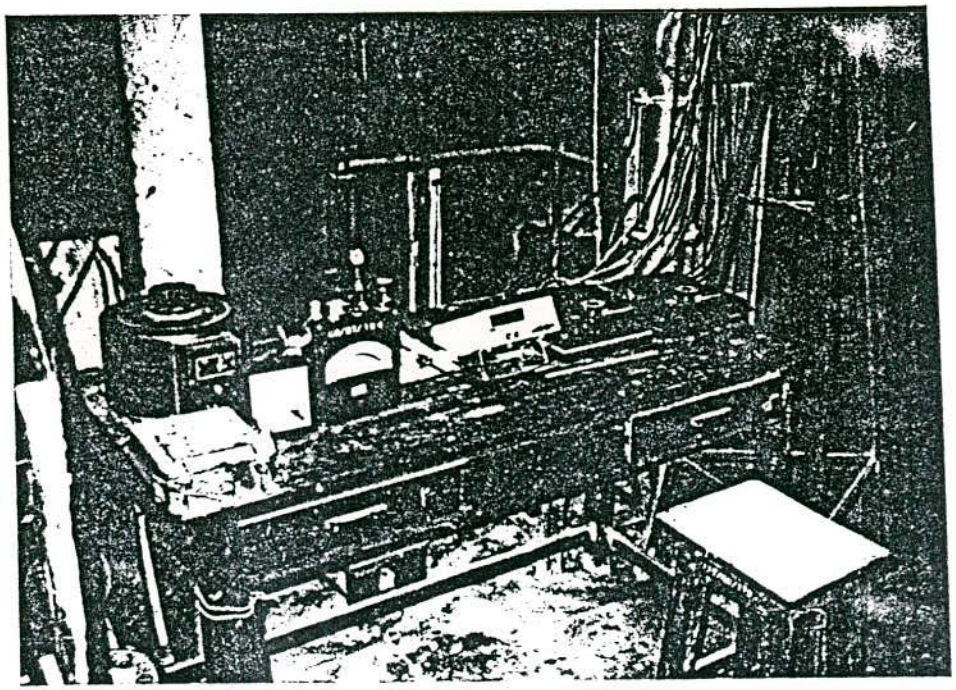

PLATE-7 ELECTRICAL EQUIPMENT USED IN THE EXPERIMENT

CHAPTER - VI

OBSERVATIONS AND RESULTS

The study of heat transfer in circulating fluidized beds is broadly divided into two categories. The first one is the laboratory scale experimental study and the other is the development of theoretical models suitable for predicting heat transfer in circulating fluidized beds. The experimental work was further divided into three parts. The first part deals with experiments with the bare (unfinned) heat transfer surface. In the second part, experiments were repeated for surfaces having fins of different sizes and geometries. In the third part experiments were performed with heat transfer probes of different vertical heights. The experimental data are shown in tabular form in Tables - 6.1 to 6.26. and the calculated results are shown in Tables - 6.27 to 6.52 from which Figs. 6.1 to 6.95 have been drawn.

6.1 Experimental Data for Heat Transfer and Hydrodynamic Study

The parameters in these tests were heat input, air flow rate, bed inventory, pressure drop across the test section, pressure drop along the bed height, solid circulation rate and temperatures of bed and surface. In the whole span of experiments the superficial velocity used was in the range of 5.6 to 12.5 m/s. For a particular set of reading all

the data were recorded at the same time.

6.1.1 Heat input

Experiments were performed for unfinned surface, two, four and eight rectangular finned surfaces and sixteen and thirty pin-finned surfaces. For all these cases the heat fluxes used were 3580, 5519 and 7876 W/m^2. Data were also taken for four probes of different vertical heights for which heat fluxes used were 4500 and 6000 W/m^2. The recorded data have been presented in Tables - 6.1 to 6.15 and 6.23 to 6.26.

6.1.2 Air flow measurement

In order to estimate the amount of air flowing through the bed to fluidize the solids, the manometer(connected across the orifice meter) readings as recorded have been presented in Tables - 6.1 to 6.15 and 6.23 to 6.26.

6.1.3 Bed inventory

The work was performed for three bed inventories of 20, 26 and 32 kg of sand for unfinned, two, four and eight rectangular finned and sixteen and thirty two number of pin-finned surfaces. For the experiments with probes of different vertical heights 32 kg bed inventory was used. The recorded data have been presented in Tables - 6.1 to 6.15 and 6.23 to 6.26.

6.1.4 Temperature measurement

Both surface and bed temperatures were measured by using copper constantan thermocouples located at suitable positions. The data have been presented in Tables - 6.1 to 6.15 and 6.23 to 6.26.

6.1.5 Measurement of pressure drop across the test section

To estimate solid concentration in the bed, the pressure drop data across the test section were taken with the help of a water filled U-tube manometer connected across it. The data have been presented in Tables - 6.1 to 6.15 and 6.23 to 6.26.

6.1.6 Measurement of pressure drop along the riser column

In order to estimate the axial voidage profile along the bed height, the pressure drop data at ten locations having equal intervals along the height of the bed were recorded and have been presented in Tables - 6.16 to 6.22.

6.1.7 Measurement of solid circulation rate

The solid circulation rates per unit cross sectional area of the bed for various superficial velocities were measured and have been shown in Tables - 6.1 to 6.15 and 6.23 to 6.26.

6.1.8 Experimental data for the probes of different vertical heights

The data of the study of the effect of vertical probe height on heat transfer have been presented in Tables 6.23 to 6.26.

6.2 Presentation of Results

The results of heat transfer and hydrodynamics of the present investigation have been calculated from the experimental data using the correlations derived in Art.3.4 and have been presented in Tables - 6.27 to 6.52 and Figs. 6.1 to 6.95. Heat transfer coefficients for bare (unfinned) and finned surfaces were calculated using equations (3.3) and (3.4) respectively. Voidages and suspension densities were determined by using Eqs. (3.6) and (3.7) respectively. The superficial velocities were estimated using Eq. (3.14), solid circulation rate from Eq. (3.15), fin effectiveness from Eq. (3.16), particle Nusselt number from Eq. (3.17), particle Reynolds number from Eq. (3.18) and cluster residence time from Eq. (3.22). Heat supplied was determined by using Eq. (3.1) . A sample calculation has been shown in Art. 6.9.

6.2.1 Heat transfer from bare (unfinned) surface

For the study of heat transfer from unfinned surface, experiments were performed for six superficial velocities of 5.6, 6.5, 7.2, 8.2, 9.1 and 11.4 m/s, three heat fluxes of

3580, 5519 and 7876 W/m^2 and three bed inventories of 20, 26 and 32 kg of sand. The results of heat transfer from unfinned surface were calculated and have been shown in Tables 6.27 to 6.29 from which Figs. 6.1, 6.2, 6.6, 6.10, 6.15, 6.18, 6.21, 6.25, 6.29, 6.33, 6.37 and 6.42 have been drawn.

6.2.2 Heat transfer in presence of finned surface

The effects of rectangular and pin fins on heat transfer in the CFB were evaluated in this study. At first 2, 4 and 8 rectangular finned surfaces were tested and later 16 and 32 number of pin finned surfaces were tested. Similar to the unfinned surface, six superficial velocities of 5.6, 6.5, 7.2, 8.2, 9.1 and 11.4 m/s, three heat fluxes of 3580, 5519, 7876 W/m^2 and three bed inventories of 20, 26 and 32 kg of sand were employed. The results estimated from the experimental data have been presented in Tables 6.30 to 6.41 from which Figs. 6.3 to 6.5, 6.7 to 6.9, 6.11 to 6.14, 6.16, 6.17, 6.19, 6.20, 6.22 to 6.24, 6.26 to 6.28, 6.30 to 6.32, 6.34 to 6.36, 6.38 to 6.41, 6.43 to 6.45(a) and 6.45(c) to 6.49 have been drawn.

6.2.3 Effects of suspension density on heat transfer coefficients

The study was performed in the range of suspension density from 18 to 76 kg/m^3. The calculated values of

suspension densities and heat transfer coefficients for finned and unfinned surfaces have been presented in Tables 6.27 to 6.41 from which Figs. 6.1 to 6.14 have been drawn.

6.2.4 Effect of superficial velocity on heat transfer coefficient

The superficial velocities used for finned and unfinned surfaces were in the range of 5.6 to 11.4 m/s. The relevant data are shown in Tables 6.27 to 6.41 from which Figs. 6.15 to 6.24 have been drawn.

6.2.5 Effect of heat input on heat transfer coefficient

Three heat fluxes of 3580, 5519 and 7876 W/m^2 were used for the finned and unfinned surfaces. The calculated results together with other relevant parameters are shown in Tables 6.27 to 6.41 from which Figs.6.25 to 6.36 have been drawn.

6.2.6 Effect of bed inventory on heat transfer coefficient

Three bed inventories of 20, 26 and 32 kg sand particles having 310 micron mean size were used. The estimated data are presented in Tables 6.27 to 6.41 and have been shown in Figs. 6.37 to 6.40.

6.2.7 Effect of bed temperature on heat transfer coefficient

The bed temperature of the present experiments lie in the range of 330 to 365 K for finned and unfinned surfaces, which have been presented in Tables 6.1 to 6.15 and 6.27 to 6.41 and shown in Figs. 6.41 to 6.45(a).

6.2.8 Effect of solid circulation rate on heat transfer coefficient

The solid circulation rate was in the range of 19 to 80 kg/m^2s . The data have been shown in Tables 6.1 to 6.15 and their effect on heat transfer have been presented in Figs. 6.45(b) and 6.45(c).

6.3 Performance of Fins in CFB

The fin performance has been evaluated from the experimental data as functions of h_F/h_{UF} and $A_F h_F/A_{UF} h_{UF}$ and presented in Tables 6.30 to 6.40 (equivalent heat transfer coefficient) and shown in Figs. 6.46 and 6.47.

6.4 Effectiveness of Fins in CFB

The fin effectiveness has been estimated for different conditions and shown in Tables 6.30 to 6.40 from which Figs. 6.48 and 6.49 have been drawn.

6.5 Effect of Fins on Bed Hydrodynamics

The results computed from experimental data to demonstrate the effect of fins on bed hydrodynamics are shown in Figs. 6.50 to 6.69.

6.6 Study of Heat Transfer from Probes of Different Vertical Heights

The study was performed with four probes having 85, 127.5, 170 and 255 mm vertical heights, two heat fluxes

of 4500 and 6000 W/m^2, five superficial velocities of 7.2, 8.8, 10.2, 11.4 and 12.5 m/s, and 32 kg sand of 310 micron mean size as the bed material. Results computed from the experimental data have been presented in Tables - 6.49 to 6.52 and plotted in Figs. 6.70 to 6.74.

6.7 Presentation of Experimental Results in Non-dimensional Form

The computed results from the experimental data in the non-dimensional form have been presented in Tables 6.27 to 6.41 and 6.49 to 6.52 and shown in Figs. 6.75 to 6.80.

6.8 Prediction from the Models

Two models and one correlation have been developed to predict heat transfer from a circulating fluidized bed.

6.8.1 Empirical model

Equation (4.19) is the final form of the empirical model for prediction of heat transfer from unfinned surface in a CFB. The results are shown in Tables 6.27 to 6.29 from which Figs. 6.81 to 6.87 have been drawn.

6.8.2 Mathematical model

Equations (4.42) and (4.50) represent the mathematical models for long and short fins respectively. The results calculated from Eq. (4.42) for 2, 4 and 8 rectangular finned and 16 and 32 number of pin finned surfaces

have been shown in Tables 6.30 to 6.41 from which Figs. 6.88 to 6.92 were plotted.

6.8.3 Empirical correlation

The empirical correlation (Eq.(4.52)) has been developed based on the experimental data of four heat transfer probes of different vertical heights. The results calculated from the correlation have been shown in Tables 6.49 to 6.52 from which Figs. 6.93 to 6.95 have been drawn.

6.9 Sample Calculations*

Diameter of the bed, d_b = 0.1 m

Diameter of particle, d_p = 310×10^{-6} m

Density of solid particle (sand), ρ_s = 2350 kg/m^3

Density of air, ρ_g = 0.9216 kg/m^3

Specific heat of solid, C_{ps} = 0.703 kJ/kg K

Distance between pressure tappings across the test section, L_m = 0.5 m

Prandtl number of air, Pr = 0.692

Thermal conductivity of gas, k_g = 0.03242 W/mK

Viscosity of gas, $\mu_g = 2.214 \times 10^{-5}$ kg/ms

Heat transfer area of unfinned surface, A_{UF} = 0.0816 m^2

Heat transfer area of a single rectangular fin = 0.013 m^2

Heat transfer area of a single pin fin = 0.000331 m^2

---

* All the calculations have been done using computer program, where accuracies upto eight places of decimals were considered which have not been recorded in Tables.

(a) Unfinned surface :

Referring to run no. 15 of Table 6.27

Bed inventory, $I = 20$ kg

Heat flux, $q'' = 7876\ W/m^2$

Bed temperature, $T_b = 355.65$ K

Surface temperature, $T_w = 414.63$ K

Pressure drop across the orifice meter, $\Delta p = 10$ cm of water

Pressure drop across the test section, $\Delta h_L = 3.0$ cm of water

(i) Experimental

heat transfer coefficient, $h_e = \dfrac{q''}{T_w - T_b}$

$$= \frac{7876}{414.63 - 355.65} = 133.53\ W/m^2K$$

(ii) Voidage, $\varepsilon = 1 - \dfrac{10\ \Delta h_L}{\rho_s\ L_m} = 1 - \dfrac{10 \times 3.0}{2350 \times 0.5}$

$$= 0.9745$$

(iii) Suspension density, $\rho_{sus} = \rho_s(1-\varepsilon)$

$$= 2350(1 - 0.9745)$$

$$= 60\ kg/m^3$$

(iv) Superficial velocity, $U_o = 2.28\sqrt{\Delta p}$

$$= 2.28\sqrt{10} = 7.2\ m/s$$

(v) Experimental Nusselt Number, $Nu_e = \dfrac{h_e d_p}{k_g}$

$$= \frac{133.53 \times 310 \times 10^{-6}}{0.03242}$$

$$= 1.28$$

(vi) Particle Reynolds number, $Re_p = \frac{U_o d_p \rho_g}{\mu_g}$

$$= \frac{7.2 \times 310 \times 10^{-6} \times 0.9216}{2.214 \times 10^{-5}} = 93.06$$

(b) Rectangular finned surface :

Referring to run no. 25 of Table 6.33 for four vertical rectangular finned surface.

Size of fin = 24.6 cm x 2.3 cm x 0.6 cm

Bed inventory, I = 26 kg

Heat transfer area of a single fin

$= 2 \times 0.246 \times 0.023 + 0.246 \times 0.006 + 2 \times 0.023 \times 0.006$

$= 0.013 \text{ m}^2$

Total heat transfer area when four rectangular fins are attached, (A_T) :

$A_T = (0.0816 + 4 \times 0.013) - 4 \times 0.006 \times 0.246$

$= 0.1277 \text{ m}^2$

Pressure drop across the orificemeter, Δp = 6 cm of water

Heat flux, q'' = 5519 W/m^2

Bed temperature, T_b = 349.8 K

Surface temperature, T_w = 395.13 K

Pressure drop across the test section,

$$\Delta h_L = 3.2 \text{ cm of water}$$

(i) Experimental heat transfer coefficient,

$$h_e = \frac{5519}{395.13 - 349.8} = 121.75 \text{ W/m}^2\text{K}$$

(ii) Voidage, $\varepsilon = 1 - \frac{10 \times 3.2}{2350 \times 0.5} = 0.9728$

(iii) Suspension density, $\rho_{sus} = (1 - 0.9728) \times 2350$

$$= 64 \text{ kg/m}^3$$

(iv) Superficial velocity, $U_o = 2.28\sqrt{6} = 5.6 \text{ m/s}$

(v) Experimental Nusselt number, $Nu_e = \frac{121.75 \times 310 \times 10^{-6}}{0.03242}$

$$= 1.16$$

(vi) Particle Reynolds number, $Re_p = \frac{5.6 \times 310 \times 10^{-6} \times 0.9216}{2.214 \times 10^{-5}}$

$$= 72.08$$

(vii) Equivalent heat transfer coefficient, $h_E = h_e\left(\frac{A_T}{A_{UF}}\right)$

$$= 121.75 \times \frac{0.1277}{0.0816} = 190.53 \text{ W/m}^2$$

(viii) Fin effectiveness $= \left.\frac{q''}{\theta_o}\right|_F \times \frac{1}{h_{UF}}$

h_{UF} $(\rho_{sus} = 64 \text{ kg/m}^3) = 133.0 \text{ W/m}^2\text{K}$

$\therefore$ Fin effectiveness $= \frac{5519}{395.13 - 349.8} \times \frac{1}{133.0}$

$$= 0.9154$$

(c) Pin finned surface :

Referring to run no. 18 of Table 6.40 for 32 pin finned surface

Size of fin = 6.35 mm dia x 15 mm long

Bed inventory, I = 32 kg

Heat transfer area of a single pin fin

$$= \pi dl + \frac{\pi}{4} d^2$$

$$= \pi \times (6.35 \times 10^{-3}) \times 15 \times 10^{-3} + \frac{\pi}{4} \times (6.35 \times 10)$$

$$= 0.000331 \text{ m}^2$$

Heat transfer area when 32 pin fins are attached,

$$A_T = 0.0816 + (0.000331 \times 32) - 32 \times \frac{\pi}{4}(6.35 \times 10^{-3})^2$$

$$= 0.0912 \text{ m}^2$$

Heat flux, $q'' = 5519 \text{ W/m}^2$

Bed temperature, $T_b = 341.46$ K

Surface temperature, $T_w = 402.98$ K

Pressure drop across the orificemeter,

$\Delta p = 25$ cm of water

Pressure drop across the test section,

$\Delta h_L = 1.45$ cm of water

(i) Experimental heat transfer coefficient,

$$h_e = \frac{5519}{402.98 - 341.46} = 89.71 \text{ W/m}^2\text{K}$$

(ii) Voidage, $\varepsilon = 1 - \frac{1.45 \times 10}{2350 \times 0.5} = 0.9877$

(iii) Suspension density, $\rho_{sus} = (1 - 0.9877) \times 2350$

$= 29 \ kg/m^3$

(iv) Superficial velocity, $U_o = 2.28\sqrt{25} = 11.4 \ m/s$

(v) Experimental Nusselt number, $Nu_e = \frac{89.71 \times 310 \times 10^{-6}}{0.03242}$

$= 0.86$

(vi) Particle Reynolds number,

$$Re_p = \frac{11.4 \times 310 \times 10^{-6} \times 0.9216}{2.214 \times 10^{-5}} = 147.14$$

(vii) Equivalent heat transfer coefficient,

$$h_E = h_e\left(\frac{A_T}{A_{UF}}\right) = 89.71 \times \frac{0.0912}{0.0816} = 100.26 \ W/m^2K$$

(viii) Fin effectiveness $= \left.\frac{q''}{\theta_o}\right|_F \times \frac{1}{h_{UF}}$

h_{UF} $(\rho_{sus} = 29 \ kg/m^3) = 101.0 \ W/m^2K$

Fin effectiveness $= \left(\frac{5519}{402.98 - 341.46}\right) \times \frac{1}{101.0}$

$= 0.8882$

(d) Prediction from empirical model (Eq. (4.19)) :

Referring to data no. 37 of Table 6.27 for unfinned surface

Bed inventory, $I = 32$ kg

Heat flux, $q'' = 3580 \ W/m^2$

Diameter of smallest particle size $= d_{pm} = 217 \times 10^{-6}$ m

Superficial velocity, U_o = 5.6 m/s

Bed temperature, T_b = 347.89 K

Surface temperature, T_w = 373.51 K

Voidage, ε = 0.9677

Suspension density, ρ_{sus} = 76 kg/m^3

Particle size, d_p = 310 x 10^{-6} m

Particle density, ρ_s = 2350 kg/m^3

Experimental heat transfer coefficient, h_e = 139.76 W/m^{2}K

Thermal conductivity of gas, k_g = 0.03242 W/mK

Diameter of the bed, d_b = 0.1 m

Vertical length of test section, L_h = 0.3 m

Experimental Nusselt number, Nu_e = 1.34

Prandtl number, Pr = 0.692

Fraction of the wall surface covered by particles,

$$x_c = 1 - \varepsilon = 1 - 0.9677 = 0.0323$$

Fraction of the wall surface covered by gas,

$$(1 - x_c) = 0.9677$$

Stefan-Boltzmann constant, σ = 5.67 x 10^{-8} W/m^{2}K^4

Emissivity of particle, e_p = 0.76

Emissivity of wall, e_w = 0.24

Emissivity of gas, e_g = 0.036

Effective emissitity, $e' = 0.5(1 + e_w) = 0.62$

Particle-to-wall view factor,

$$F_{p-w} = \frac{1}{\left(\frac{1}{e_p} + \frac{1}{e_w} - 1\right)} = 0.2231$$

Archimedes number, Grace [15]

$$Ar = \frac{\rho_g (\rho_s - \rho_g)\, g\, d_p^3}{\mu_g^2}$$

$$= \frac{0.9216\ (2350 - 0.9216) \times 9.81 \times (310 \times 10^{-6})^3}{(2.214 \times 10^{-5})^2}$$

$$= 1291.02$$

Velocity at minimum fluidization condition, Grace [15]

$$U_{mf} = \frac{7.5 \times 10^{-4} (\rho_s - \rho_g)\ (d_p)^2\, g}{\mu}$$

$$= \frac{7.5 \times 10^{-4} (2350 - 0.9216) \times (310 \times 10^{-6})^2 \times 9.81}{2.214 \times 10^{-5}}$$

$$= 0.075 \quad m/s$$

Terminal velocity, Kunii [20]

$$U_T = \frac{4}{225} \left(\frac{(\rho_s - \rho_g)^2\, g^2}{\rho_g\, \mu_g} \right)^{1/3} d_{pm}$$

$$= \left(\frac{4}{225} \times \frac{(2350 - 0.9216)^2 \times (9.81)^2}{0.9216 \times 2.214 \times 10^{-5}} \right)^{1/3} \times 217 \times 10^{-6}$$

$$= 1.54 \ m/s$$

The empirical model is

$$Nu = 4.5 - 4.75M - N(4.95M - 3.3) + R_r$$

where, $M = Pr\varepsilon$, $N = Ar \frac{U_o^2}{U_T U_{mf}} \frac{L_h}{d_b} \times 10^{-6}$

$$R_r = \sigma \left(\frac{T_b^4 - T_w^4}{T_b - T_w} \right) \left(x_c F_{p-w} + (1-x_c) e' e_g \right) \frac{d_p}{k_g}$$

Now, $M = Pr\,\varepsilon = 0.692 \times 0.9677 = 0.6696$

$$N = Ar \frac{U_o^2}{U_T U_{mf}} \frac{L_h}{d_b} \times 10^{-6}$$

$$= 1291.02 \times \frac{(5.6)^2}{1.54 \times 0.075} \times \frac{0.3}{0.1} \times 10^{-6}$$

$$= 1.0516$$

$$R_r = \sigma \left(\frac{T_b^4 - T_w^4}{T_b - T_w} \right) \left(x_c F_{p-w} + (1-x_c) e' e_g \right) \frac{d_p}{k_g}$$

$$= 5.67 \times 10^{-8} \left(\frac{(347.89)^4 - (373.51)^4}{347.89 - 373.51} \right) \times$$

$$(0.0323 \times 0.2231 + (0.9677 \times 0.62 \times 0.036)) \times \frac{310 \times 10^{-6}}{0.03242}$$

$$= 0.0029$$

$$(Nu)_T = 4.5 - 4.75M - N(4.95M - 3.3) + R_r$$

$$= 4.5 - 4.75 \times 0.6696 - 1.0516(4.95 \times 0.6696 - 3.3) + 0.0029$$

$$= 1.31$$

$$\% \quad \text{Error} = \frac{(Nu)_T - (Nu)_e}{(Nu)_T} = \frac{1.31 - 1.34}{1.31}$$

$$= -2.26\ \%$$

(e) Prediction from the mathematical model (Eq.(4.42)) for long rectangular fin :

Referring to data no. 40 of Table 6.32 for 2-rectangular finned surface

Size of fin = 24.6 cm x 2.3 cm x 0.6 cm

Bed inventory, I = 32 kg

Heat flux, q" = 3580 W/m^2

Superficial velocity, U_o = 8.2 m/s

Bed temperature, T_b = 350.48 K

Surface temperature, T_w = 385.02 K

Number of fins, N_f = 2

Area of a single rectangular fin = 0.013 m^2

Total heat transfer area when two fins are attached to the test section, (A_T)

$$A_T = 0.0816 + 2 \times 0.013 - 2 \times 0.001476 = 0.1046\ m^2$$

Area of unfinned portion, $A_{UF} = 0.0816 - 2 \times 0.001476$

$$= 0.07865\ m^2$$

Cross-sectional area of a rectangular fin

$$A = L_f t = \frac{24.6}{100} \times \frac{0.6}{100} = 1.476 \times 10^{-3}\ m^2$$

Perimeter of the fin, $P = 2 L_f$, Kreith [190]

$$= 2 \times \frac{24.6}{100} = 0.492 \text{ m}$$

Average voidage, $\varepsilon = 0.977$

Average suspension density, $\bar{\rho} = 54 \text{ kg/m}^3$

Temperature difference, $\theta_o = 385.02 - 350.48 = 34.54 \text{ K}$

Experimentally determined constant, $K' = 17.26 \text{ (W/m}^2\text{)(}\sqrt{\text{m}^3}\text{ kg)}$

Thermal conductivity of fin material (steel)

$$k = 66.5 \text{ W/mK}$$

$$C = \sqrt{\frac{Pk'}{k A}} = \frac{0.492 \times 17.26}{66.5 \times 1.476 \times 10^{-3}}$$

$$= 9.3014 \left(\text{K} / \sqrt{\text{m.kg}} \right)^{1/2}$$

Voidage at the fin tip, Tung et al [186],

$$\varepsilon_h = \varepsilon^{(\phi^2 + 0.191)}$$

at the fin tip, $\phi = x/L = 0$

Therefore, $\varepsilon_h = (0.977)^{0.191} = 0.9956$

Solid concentration at the fin tip

$$\rho_h = (1 - \varepsilon_h)\rho_s = (1 - 0.9956) \times 2350$$

$$= 10.24 \text{ kg/m}^3$$

From Eq.(4.23), solid concentration near the wall,

$$\rho_w = 2\bar{\rho} - \rho_h = 2 \times 54 - 10.24 = 97.76 \text{ kg/m}^3$$

Now, $b = \frac{2}{L}(\rho_w - \bar{\rho}) = \frac{2 \times 100}{2.3}(97.76 - 54.0)$

$$= 3805.22 \text{ kg/m}^4$$

Therefore, $m' = \frac{C}{b} = \frac{9.3014}{3805.22} = 2.444 \times 10^{-3}$

From Eq. (4.39), U_x is defined as

$$U_x = \rho_h + 2 \frac{x}{L} (\rho_w - \bar{\rho})$$

at the fin root $\frac{x}{L} = 1$

Therefore, $U_x = 10.24 + 2(97.76 - 54)$

$= 97.76 \ kg/m^3$

The final model (Eq. 4.42) for the long fin is given by

$$h_{Tl} = \frac{N_f \sqrt{Pk'Ak} \ (U_x^{3/4}) \left[I_{3/5}(\frac{4}{5} m' U_x^{5/4}) \right]}{A_T \sqrt{\rho_w} \left[I_{-2/5} (\frac{4}{5} m' \rho_w^{5/4}) \right]} + \frac{A_{UF}}{A_T} (\frac{q''}{\theta_o})$$

The argument of Bessel function in the numerator

$$= \frac{4}{5} m' U_x^{5/4}$$

$$= \frac{4}{5} \times 2.444 \times 10^{-3} \times (97.76)^{5/4} = 0.601$$

The argument of Bessel function in the denominator

$$= \frac{4}{5} m' \rho_w^{5/4}$$

$$= \frac{4}{5} \times 2.444 \times 10^{-3} \times (97.76)^{5/4} = 0.601$$

For these small arguments, the Bessel functions converge very rapidly [188] and for the present case it converges

to the 3rd term of the series. So, we have considered the power series as

$$I(x) = \frac{(x/2)^{\nu}}{\Gamma(\nu+1)}\left[1 + \frac{(x/2)^2}{1!\,(\nu+1)} + \frac{(x/2)^2}{2!\,(\nu+1)(\nu+2)}\right]$$

Using Fig. 2.6 of Myers [192] the gamma functions have been calculated as follows

when $\nu = \frac{3}{5}$

$$\Gamma(\nu+1) = \Gamma\left(\frac{3}{5}+1\right) = \Gamma(1.60) = 0.909$$

when $\nu = -\frac{2}{5}$

$$\Gamma(\nu+1) = \Gamma\left(-\frac{2}{5}+1\right) = \Gamma(-0.4+1)$$
$$= -0.4\,\Gamma(-0.4) = -0.4\left(\frac{1}{-0.4}\right)\Gamma(0.6)$$
$$= \frac{1}{0.6}\,\Gamma(1.6) = \frac{0.909}{0.60} = 1.515$$

Now, $I_{3/5}(0.601) = \frac{(0.601/2)^{3/5}}{0.909}\left[1 + \frac{(0.601/2)^2}{1!\,(\frac{3}{5}+1)} + \frac{(0.601/2)^4}{2!\,(\frac{3}{5}+1)(\frac{3}{5}+2)}\right]$

$$= 0.5662$$

and

$$I_{-2/5}(0.601) = \frac{(0.601/2)^{-2/5}}{1.515}\left[1 + \frac{(0.601/2)^{2}}{1!\,(-\frac{2}{5}+1)} + \frac{(0.601/2)^{4}}{2!\,(-\frac{2}{5}+1)(-\frac{2}{5}+2)}\right]$$

$$= 1.2326$$

Therefore, on substitution in the final model

$$h_{T1} = \left[\frac{2 \times (\sqrt{0.492 \times 17.26 \times 1.476 \times 10^{-3} \times 66.5}) \times 0.5662}{0.1046 \times \sqrt{97.76} \times 1.2326} \times (97.76)^{3/4}\right]$$

$$+ \left(\frac{0.07865}{0.1046} \times \frac{3580}{34.54}\right)$$

$$= 102.51 \ W/m^2K$$

$$\text{Percent error} = \frac{h_{T1} - h_e}{h_{T1}} \times 100$$

$$= \frac{102.51 - 103.63}{102.51} \times 100$$

$$= -1.09\ \%$$

(f) Prediction from the mathematical model (Eq. 4.42) for long pin fin :

Referring to data no. 17 of Table 6.37 for 16 pin finned surface

size of fin = 6.35 mm O.D. x 15 mm long

Bed inventory, I = 20 kg

Heat flux, q" = 7876 W/m^2

Temperature differential, θ_o = 416.98 - 341.55 = 75.43

Superficial velocity = 9.1 m/s

Total heat transfer area when 16 pin fins are attached,

$$A_T = 0.0816 + (0.000331236 \times 16) - 16 \times 0.000032$$
$$= 0.0864 \ m^2$$

Unfinned portion of heat transfer surface,

$$A_{UF} = 0.0816 - 16 \times 0.000032 = 0.0811 \ m^2$$

Cross-sectional area of the pin,

$$A = \frac{\pi}{4} \left(\frac{6.35}{1000} \right)^2 = 0.000032 \ m^2$$

Perimeter of the fin, $P = \pi d$ = 0.02 m

Number of fins N_f = 16

k' = 17.26 $\frac{W}{m^2} \sqrt{m^3/kg}$

k = 66.5 W/mK

ε = 0.9838

$\overline{\rho}$ = 38 kg/m^3

$\varepsilon_h = e^{(\phi^2+0.191)}$ (From Tung et al [186])

at the fin tip $\phi = \frac{x}{L} = 0$

Therefore, $\varepsilon_h = (0.9838)^{0.191} = 0.998$

$$\rho_h = (1 - \varepsilon_h)\rho_s = (1 - 0.998) \times 2350$$
$$= 4.7 \text{ kg/m}^3$$

$$\rho_w = 2\bar{\rho} - \rho_h = 2 \times 33 - 4.7 = 71.3 \text{ kg/m}^3$$

Now, $b = \frac{2}{L}(\rho_w - \bar{\rho}) = \frac{2 \times 1000}{15}(71.3 - 38)$
$$= 4440 \text{ kg/m}^4$$

$$C = \frac{Pk'}{kA} = \left[\left(\frac{0.02 \times 17.26}{66.5 \times 0.000032} \right) \right]^{1/2}$$

$$= 12.74 \left(\frac{K}{\sqrt{m\ kg}} \right)^{1/2}$$

$$m' = \frac{C}{b} = \frac{12.74}{4440} = 2.868 \times 10^{-3} \frac{1}{m} \left(\frac{K}{\sqrt{m\ kg}} \right)^{1/2}$$

and $U_x = \rho_h + 2\frac{x}{L}(\rho_w - \bar{\rho}) = 4.7 + 2(71.3 - 38)$

$= 71.3 \text{ kg/m}^3$ (at the fin root $\frac{x}{L} = 1$)

The model (Eq. 4.42) for long fin is

$$h_{Tl} = \frac{N_f \sqrt{Pk'\ Ak}\ (U_x^{3/4}) \left[I_{3/5} \left(\frac{4}{5} m'\ U_x^{5/4} \right) \right]}{A_T \sqrt{\rho_w} \left[I_{-2/5} \left(\frac{4}{5} m'\ \rho_w^{5/4} \right) \right]} + \frac{A_{UF}}{A_T} \left(\frac{q''}{\theta_o} \right)$$

The argument of Bessel function in the numerator

$$= \frac{4}{5} m' U_x^{5/4}$$

$$= \frac{4}{5} \times 2.868 \times 10^{-3} \times (71.3)^{5/4} = 0.49$$

The argument of Bessel function in the denominator

$$= \frac{4}{5} m' \rho_w^{5/4}$$

$$= \frac{4}{5} \times 2.868 \times 10^{-3} \times (71.3)^{5/4} = 0.49$$

The gamma functions have been calculated as before using Fig. 2.6 of Myers [192] as

$$\Gamma(\nu + 1) = \Gamma(\frac{3}{5} + 1) = \Gamma(1.6) = 0.909$$

and

$$\Gamma(\nu + 1) = \Gamma(-\frac{2}{5} + 1) = \Gamma(-0.4 + 1) = 1.515$$

Now, $$I_{3/5}(0.49) = \frac{(0.49/2)^{3/5}}{0.909} \left[1 + \frac{(0.49/2)^2}{1!\,(\frac{3}{5} + 1)} + \frac{(0.49/2)^4}{2!\,(\frac{3}{5} + 1)(\frac{3}{5} + 2)} \right] = 0.49$$

and

$$I_{-2/5}(0.49) = \frac{(0.49/2)^{-2/5}}{1.515}\left[1 + \frac{(0.49/2)^{2}}{1!\,(-\frac{2}{5}+1)}\right.$$

$$\left. + \frac{(0.49/2)^{4}}{2!\,(-\frac{2}{5}+1)(-\frac{2}{5}+2)}\right] = 1.27$$

Therefore, on substitution

$$h_{T1} = \frac{16 \times \left[\sqrt{0.02 \times 17.26 \times 0.000032 \times 66.5}\right](71.3)^{3/4} \times 0.49}{0.0864 \times \sqrt{71.3} \times 1.27}$$

$$+ \frac{0.0811}{0.0864} \times \frac{7876}{75.43}$$

$$= 103.57 \ \ W/m^2K$$

$$\text{Percentage error,} = \frac{h_{T1} - h_e}{h_{T1}} \times 100$$

$$= \frac{103.57 - 104.41}{103.57} \times 100$$

$$= -0.81\ \%$$

(g) Residence time (t_r) predicted from the expression derived in Eq. (3.22) which is given below

$$t_r = \left(k_c \rho_s C_{ps} \frac{1-\varepsilon}{\pi}\right)\left(\frac{1}{h} - \frac{d_p}{10k_{ew}}\right)^2$$

Referring to data no. 40 of Table 6.52

Thermal conductivity of gas, k_g = 0.03242 W/mK

Density of solid, ρ_s = 2350 kg/m^3

Specific heat of solid, C_{ps} = 0.703 kJ/kg K

Voidage, ε = 0.9884

$k_{ew} = k_c = k_g$, Basu and Nag [39]

= 0.03242 W/mK

$$t_r = \left(\frac{0.03242 \times 2350 \times 0.703 \times (1-0.9894)}{3.14} \right) \times \left(\frac{1}{94.98} - \frac{310 \times 10^{-6}}{10 \times 0.03242} \right)$$

$$= 16.625 \times 10^{-3} \text{ sec.}$$

(h) Prediction from empirical correlation (Eq. 4.52) :

The empirical correlation is

$$Nu_p = 4.7 \left[Re_p \left(\frac{L_h}{D}\right)^2 \right]^{-0.25}$$

Referring to data no. 40 of Table 6.52 for 255 mm vertical probe

Bed inventory, I = 32 kg

Heat flux, q" = 6000 W/m^2

Bed temperature, T_b = 345.71 K

Surface temperature, T_w = 408.88 K

Superficial velocity, U_o = 12.5 m/s

Vertical probe height, L_h = 255 mm

Diameter of the probe, D = 0.1 m

Particle diameter, d_p = 310×10^{-6} m

Experimental particle Nusselt number, $(Nu_p)_e$ = 0.91

Experimental heat transfer coefficient, h_e = 94.98 W/m^2K

Particle Reynolds number,

$$Re_p = \frac{U_o\, d_p\, \rho_g}{\mu_g} = \frac{12.5 \times 310 \times 10^{-6} \times 0.9216}{2.214 \times 10^{-5}}$$

$$= 161.18$$

$$\frac{L_h}{D} = \frac{255}{100} = 2.55$$

$$(Nu_p)_T = 4.7 \left[161.18\ (2.55)^2\right]^{-0.25} = 0.8258$$

$$= 0.83$$

$$\text{Percent error} = \frac{(Nu_p)_T - (Nu_p)_e}{(Nu_p)_T} \times 100$$

$$= \frac{0.8258 - 0.9082}{0.8258} \times 100$$

$$= -9.97\ \%$$

DATA SHEET

Table - 6.1 : Experimental Observations on CFB Heat Transfer for Unfinned Surface

d_p = 310 μm , d_b = 100 mm, kg = 0.03242 W/mk, ρ_s = 2350 kg/m^3, ρ_g = 0.9218 kg/m^3, μg = 2.214 x 10^{-5} kg/ms, A_{ht} = 0.0816 m^2, L_m = 0.5 m, Pr = 0.692, e_p = 0.76, e_g = 0.036, e_w = 0.24

Serial number of runs	Bed inventory (I) kg	Heat flux (q") W/m^2	Pressure drop across the orificemeter(Δp) cm of water	Bed temperature (T_b) K	Surface temperature (T_s) K	Pressure drop across the test section (Δh_L), cm of water	Solid circulation rate (G_s) kg/m^{2}s
1	20	3580	6.0	350.24	376.80	3.50	19.61
2		3580	8.0	346.25	372.57	3.10	27.02
3		3580	10.0	345.54	373.03	3.00	44.21
4		3580	13.0	344.84	373.51	2.50	64.40
5		3580	16.0	345.07	375.86	2.00	76.21
6		3580	25.0	345.07	381.97	1.25	79.32
7		5519	6.0	354.71	395.60	3.50	19.61
8		5519	8.0	352.36	392.78	3.10	27.02
9		5519	10.0	348.83	389.96	3.00	44.21
10		5519	13.0	348.36	392.54	2.50	64.40
11		5519	16.0	348.60	395.36	2.00	76.21
12		5519	25.0	347.19	403.59	1.25	79.32
13		7876	6.0	361.52	419.10	3.50	19.61
14		7876	8.0	358.70	416.75	3.10	27.02
15		7876	10.0	355.65	414.63	3.00	44.21
16		7876	13.0	354.24	416.75	2.50	64.40
17		7876	16.0	354.71	420.27	2.00	76.21
18		7876	25.0	357.53	437.66	1.25	79.32

DATA SHEET

Table - 6.2 : Experimental Observations on CFB Heat Transfer for Unfinned Surface

d_p = 310 μm , d_b = 100 mm, kg = 0.03242 W/mk, ρ_s = 2350 kg/m^3, ρ_g = 0.9218 kg/m^3, μg = 2.214 x 10^{-5} kg/ms, A_{ht} = 0.0816 m^2, L_m = 0.5 m, Pr = 0.692, e_p = 0.76, e_g = 0.036, e_w = 0.24

Serial number of runs	Bed inventory (I) kg	Heat flux (q") W/m^2	Pressure drop across the orificemeter(Δp) cm of water	Bed temperature (T_b) K	Surface temperature (T_s) K	Pressure drop across the test section (Δh_L), cm of water	Solid circulation rate (G_s) kg/m^{2}s
19	26	3580	6.0	349.07	375.63	3.70	20.15
20		3580	8.0	348.36	373.74	3.40	27.20
21		3580	10.0	347.19	373.98	3.10	51.81
22		3580	13.0	348.36	377.27	2.70	66.97
23		3580	16.0	348.36	379.85	2.10	78.86
24		3580	25.0	348.60	385.02	1.50	79.78
25		5519	6.0	356.35	396.77	3.70	20.15
26		5519	8.0	351.18	391.60	3.40	27.20
27		5519	10.0	352.36	393.48	3.10	51.81
28		5519	13.0	351.68	395.60	2.70	66.97
29		5519	16.0	350.95	398.89	2.10	78.86
30		5519	25.0	345.78	401.71	1.50	79.78
31		7876	6.0	363.64	420.27	3.70	20.15
32		7876	8.0	358.47	414.40	3.40	27.20
33		7876	10.0	358.00	416.75	3.10	51.81
34		7876	13.0	360.11	422.86	2.70	66.97
35		7876	16.0	359.88	427.79	2.10	78.86
36		7876	25.0	358.94	438.60	1.50	79.78

DATA SHEET

Table - 6.3 : Experimental Observations on CFB Heat Transfer for Unfinned Surface

d_p = 310 μm , d_b = 100 mm, kg = 0.03242 W/mk, ρ_s = 2350 kg/m^3, ρ_g = 0.9218 kg/m^3, μg = 2.214 x 10^{-5} kg/ms, A_{ht} = 0.0816 m^2, L_m = 0.5 m, Pr = 0.692, e_p = 0.76, e_g = 0.036, e_w = 0.24

Serial number of runs	Bed inventory (I) kg	Heat flux (q") W/m^2	Pressure drop across the orificemeter(Δp) cm of water	Bed temperature (T_b) K	Surface temperature (T_s) K	Pressure drop across the test section (Δh_L), cm of water	Solid circulation rate (G_s) kg/m^{2}s
37	32	3580	6.0	347.89	373.51	3.80	20.90
38		3580	8.0	348.60	374.92	3.60	29.32
39		3580	10.0	347.89	374.45	3.25	57.31
40		3580	13.0	348.13	376.80	3.00	68.42
41		3580	16.0	348.60	380.09	2.20	76.71
42		3580	25.0	347.42	382.91	1.60	79.93
43		5519	6.0	360.35	401.47	3.80	20.90
44		5519	8.0	355.18	394.42	3.60	29.32
45		5519	10.0	352.59	393.25	3.25	57.31
46		5519	13.0	352.59	396.54	3.00	68.42
47		5519	16.0	353.06	400.77	2.20	76.71
48		5519	25.0	352.83	407.35	1.60	79.93
49		7876	6.0	364.58	421.45	3.80	20.90
50		7876	8.0	360.35	416.26	3.60	29.32
51		7876	10.0	358.94	416.75	3.25	57.31
52		7876	13.0	359.64	421.92	3.00	68.42
53		7876	16.0	359.41	426.15	2.20	76.71
54		7876	25.0	360.35	437.43	1.60	79.93

DATA SHEET

Table - 6.4 : Experimental Observations on CFB Heat Transfer for 2 - Rectangular Finned Surface

d_p = 310 μm , d_b = 100 mm, kg = 0.03242 W/mk, ρ_s = 2350 kg/m^3, ρ_g = 0.9218 kg/m^3, μg = 2.214 x 10^{-5} kg/ms, A_{ht} = 0.1046 m^2, L_m = 0.5 m, Pr = 0.692, e_p = 0.76, e_g = 0.036, e_w = 0.24

Serial number of runs	Bed inventory (I) kg	Heat flux (q") W/m^2	Pressure drop across the orificemeter(Δp) cm of water	Bed temperature (T_b) K	Surface temperature (T_s) K	Pressure drop across the test section (Δh_L), cm of water	Solid circulation rate (G_s) kg/m^2s	Bare tube heat transfer coefficient, W/m^2K
1	20	3580	6.0	345.07	373.51	3.25	19.32	135.00
2		3580	8.0	344.37	373.27	3.00	26.72	130.00
3		3580	10.0	346.01	377.50	2.85	45.15	127.00
4		3580	13.0	345.78	381.50	2.40	62.90	118.00
5		3580	16.0	347.19	384.08	1.80	75.80	105.00
6		3580	25.0	343.90	389.02	1.10	79.19	92.50
7		5519	6.0	350.48	394.19	3.25	19.32	135.00
8		5519	8.0	350.71	394.66	3.00	26.72	130.00
9		5519	10.0	351.65	398.65	2.85	45.15	127.00
10		5519	13.0	350.48	400.30	2.40	62.90	118.00
11		5519	16.0	349.77	409.70	1.80	75.80	105.00
12		5519	25.0	349.54	414.63	1.10	79.19	92.50
13		7876	6.0	356.82	418.86	3.25	19.32	135.00
14		7876	8.0	355.41	417.22	3.00	26.72	130.00
15		7876	10.0	355.88	418.39	2.85	45.15	127.00
16		7876	13.0	355.18	422.63	2.40	62.90	118.00
17		7876	16.0	359.17	435.55	1.80	75.80	105.00
18		7876	25.0	359.17	451.53	1.10	79.19	92.50

DATA SHEET

Table - 6.5 : Experimental Observations on CFB Heat Transfer for 2 - Rectangular Finned Surface

d_p = 310 μm , d_b = 100 mm, kg = 0.03242 W/mk, ρ_s = 2350 kg/m^3, ρ_g = 0.9218 kg/m^3, μg = 2.214 x 10^{-5} kg/ms, A_{ht} = 0.1046 m^2, L_m = 0.5 m, Pr = 0.692, e_p = 0.76, e_g = 0.036, e_w = 0.24

Serial number of runs	Bed inventory (I) kg	Heat flux (q") W/m^2	Pressure drop across the orificemeter(Δp) cm of water	Bed temperature (T_b) K	Surface temperature (T_s) K	Pressure drop across the test section (Δh_L), cm of water	Solid circulation rate (G_s) kg/m^2s	Bare tube heat transfer coefficient, W/m^2k
19	26	3580	6.0	349.30	378.21	3.35	21.15	138.00
20		3580	8.0	347.66	376.09	3.20	25.92	134.00
21		3580	10.0	346.01	374.92	2.95	48.81	129.00
22		3580	13.0	348.36	380.32	2.60	63.32	122.00
23		3580	16.0	352.59	388.31	1.90	77.93	108.00
24		3580	25.0	353.77	395.83	1.35	78.92	97.00
25		5519	6.0	354.47	398.42	3.35	21.15	138.00
26		5519	8.0	356.12	398.89	3.20	25.92	134.00
27		5519	10.0	354.24	399.13	2.95	48.81	129.00
28		5519	13.0	354.71	401.71	2.60	63.32	122.00
29		5519	16.0	352.36	406.64	1.90	77.93	108.00
30		5519	25.0	348.60	412.75	1.35	78.92	97.00
31		7876	6.0	358.00	416.75	3.35	21.15	138.00
32		7876	8.0	358.47	417.92	3.20	25.92	134.00
33		7876	10.0	361.29	423.33	2.95	48.81	129.00
34		7876	13.0	359.88	426.15	2.60	63.32	122.00
35		7876	16.0	361.76	438.60	1.90	77.93	108.00
36		7876	25.0	363.88	453.88	1.35	78.92	97.00

DATA SHEET

Table - 6.6 : Experimental Observations on CFB Heat Transfer for 2 - Rectangular Finned Surface

d_p = 310 μm , d_b = 100 mm, kg = 0.03242 W/mk, ρ_s = 2350 kg/m^3, ρ_g = 0.9218 kg/m^3, μg = 2.214 x 10^{-5} kg/ms, A_{ht} = 0.1046 m^2, L_m = 0.5 m, Pr = 0.692, e_p = 0.76, e_g = 0.036, e_w = 0.24

Serial number of runs	Bed inventory (I) kg	Heat flux (q") W/m^2	Pressure drop across the orificemeter(Δp) cm of water	Bed temperature (T_b) K	Surface temperature (T_s) K	Pressure drop across the test section (Δh_L), cm of water	Solid circulation rate (G_s) kg/m^2s	Bare tube heat transfer coefficient, W/m^2k
37	32	3580	6.0	347.42	375.63	3.65	20.88	143.50
38		3580	8.0	348.60	376.33	3.50	28.90	140.00
39		3580	10.0	350.95	379.62	3.10	58.10	131.50
40		3580	13.0	350.48	385.02	2.70	67.50	120.50
41		3580	16.0	350.48	386.20	2.10	74.90	111.50
42		3580	25.0	350.48	395.13	1.50	78.00	99.00
43		5519	6.0	356.35	397.95	3.65	20.88	143.50
44		5519	8.0	354.00	395.60	3.50	28.90	140.00
45		5519	10.0	355.41	398.42	3.10	58.10	131.50
46		5519	13.0	355.65	405.00	2.70	67.50	120.50
47		5519	16.0	353.53	407.35	2.10	74.90	111.50
48		5519	25.0	351.42	412.75	1.50	78.90	99.00
49		7876	6.0	358.70	416.04	3.65	20.88	143.50
50		7876	8.0	357.76	415.57	3.50	28.90	140.00
51		7876	10.0	361.29	423.80	3.10	58.10	131.50
52		7876	13.0	361.76	428.26	2.70	67.50	120.50
53		7876	16.0	358.23	435.08	2.10	74.90	111.50
54		7876	25.0	357.76	443.77	1.50	78.80	99.00

DATA SHEET

Table - 6.7 : Experimental Observations on CFB Heat Transfer for 4 - Rectangular Finned Surface

d_p = 310 μm , d_b = 100 mm, kg = 0.03242 W/mk, ρ_s = 2350 kg/m^3, ρ_g = 0.9218 kg/m^3, μg = 2.214 x 10^{-5} kg/ms, A_{ht} = 0.1277 m^2, L_m = 0.5 m, Pr = 0.692, e_p = 0.76, e_g = 0.036, e_w = 0.24

Serial number of runs	Bed inventory (I) kg	Heat flux (q") W/m2	Pressure drop across the orificemeter(Δ_p) cm of water	Bed temperature (T_b) K	Surface temperature (T_s) K	Pressure drop across the test section (Δh_L), cm of water	Solid circulation rate (G_s) kg/m^{2}s	Bare tube heat transfer coefficient, W/m^{2}k
1	20	3580	6.0	343.19	374.50	3.00	18.83	130.00
2		3580	8.0	343.62	374.85	2.80	24.72	126.00
3		3580	10.0	344.60	377.76	2.60	40.92	122.00
4		3580	13.0	344.23	381.85	2.15	65.15	112.00
5		3580	16.0	344.98	389.37	1.60	73.32	101.00
6		3580	25.0	343.57	391.25	1.00	76.91	90.00
7		5519	6.0	348.95	395.83	3.00	18.83	130.00
8		5519	8.0	347.78	393.72	2.80	24.72	126.00
9		5519	10.0	347.59	396.42	2.60	40.92	122.00
10		5519	13.0	347.07	399.13	2.15	64.15	112.00
11		5519	16.0	342.91	405.02	1.60	73.32	101.00
12		5519	25.0	343.76	415.60	1.00	76.91	90.00
13		7876	6.0	353.18	419.36	3.00	18.83	130.00
14		7876	8.0	352.95	417.34	2.80	24.72	126.00
15		7876	10.0	349.77	417.03	2.60	40.92	122.00
16		7876	13.0	350.01	422.23	2.15	64.15	112.00
17		7876	16.0	346.98	431.79	1.60	73.32	101.00
18		7876	25.0	347.24	447.58	1.00	76.91	90.00

DATA SHEET

Table - 6.8 : Experimental Observations on CFB Heat Transfer for 4 - Rectangular Finned Surface

d_p = 310 μm , d_b = 100 mm, kg = 0.03242 W/mk, ρ_s = 2350 kg/m^3, ρ_g = 0.9218 kg/m^3, μg = 2.214 x 10^{-5} kg/ms, A_{ht} = 0.1277 m^2, L_m = 0.5 m, Pr = 0.692, e_p = 0.76, e_g = 0.036, e_w = 0.24

Serial number of runs	Bed inventory (I) kg	Heat flux (q") W/m^2	Pressure drop across the orificemeter(Δp) cm of water	Bed temperature (T_b) K	Surface temperature (T_s) K	Pressure drop across the test section (Δh_L), cm of water	Solid circulation rate (G_s) kg/m^2s	Bare tube heat transfer coefficient, W/m^2k
19	26	3580	6.0	342.77	373.23	3.20	20.21	133.00
20		3580	8.0	341.86	375.18	2.90	26.34	128.00
21		3580	10.0	340.96	374.50	2.70	50.91	124.00
22		3580	13.0	340.42	375.08	2.35	60.84	117.00
23		3580	16.0	340.37	383.92	1.80	78.10	105.00
24		3580	25.0	339.55	387.42	1.20	78.63	93.00
25		5519	6.0	349.80	395.13	3.20	20.21	133.00
26		5519	8.0	348.27	395.13	2.90	26.34	128.00
27		5519	10.0	347.03	394.35	2.70	50.91	124.00
28		5519	13.0	346.98	398.09	2.35	60.84	117.00
29		5519	16.0	346.06	405.23	1.80	78.10	105.00
30		5519	25.0	345.62	414.42	1.20	78.63	93.00
31		7876	6.0	354.19	418.63	3.20	20.21	133.00
32		7876	8.0	351.89	418.04	2.90	26.34	128.00
33		7876	10.0	348.79	421.54	2.70	50.91	124.00
34		7876	13.0	348.98	426.15	2.35	60.84	117.00
35		7876	16.0	348.55	441.66	1.80	78.10	105.00
36		7876	25.0	349.30	447.42	1.20	78.63	93.00

DATA SHEET

Table - 6.9 : Experimental Observations on CFB Heat Transfer for 4 - Rectangular Finned Surface

d_p = 310 μm , d_b = 100 mm, kg = 0.03242 W/mk, ρ_s = 2350 kg/m^3, ρ_g = 0.9218 kg/m^3, μg = 2.214 x 10^{-5} kg/ms, A_{ht} = 0.1277 m^2, L_m = 0.5 m, Pr = 0.692, e_p = 0.76, e_g = 0.036, e_w = 0.24

Serial number of runs	Bed inventory (I) kg	Heat flux (q") W/m^2	Pressure drop across the orificemeter(Δp) cm of water	Bed temperature (T_b) K	Surface temperature (T_s) K	Pressure drop across the test section (Δh_L), cm of water	Solid circulation rate (G_s) kg/m^{2}s	Bare tube heat transfer coefficient, W/m^{2}k
37	32	3580	6.0	342.42	372.83	3.35	20.41	138.00
38		3580	8.0	343.57	375.74	3.25	29.10	135.00
39		3580	10.0	342.00	375.63	2.80	57.24	126.00
40		3580	13.0	341.88	376.82	2.60	65.23	122.00
41		3580	16.0	341.57	379.17	2.00	75.13	109.00
42		3580	25.0	341.29	386.48	1.40	79.10	96.00
43		5519	6.0	346.81	391.77	3.35	20.41	138.00
44		5519	8.0	346.91	391.86	3.25	29.10	135.00
45		5519	10.0	346.27	393.01	2.80	57.24	126.00
46		5519	13.0	346.63	396.33	2.60	65.23	112.00
47		5519	16.0	344.77	402.30	2.00	75.13	109.00
***								
49		7876	6.0	348.79	412.31	3.35	20.41	138.00
50		7876	8.0	348.39	412.78	3.25	29.10	135.00
51		7876	10.0	349.23	417.03	2.80	57.24	126.00
52		7876	13.0	349.23	419.59	2.60	65.23	122.00
53		7876	16.0	348.08	430.97	2.00	75.13	109.00
54		7876	25.0	347.99	440.63	1.40	79.10	96.00
***								
49		5519	25.0	344.37	410.83	1.40	96.00	79.10

DATA SHEET

Table -6.10 : Experimental Observations on CFB Heat Transfer for 8 - Rectangular Finned Surface

d_p = 310 μm , d_b = 100 mm, kg = 0.03242 W/mk, ρ_s = 2350 kg/m^3, ρ_g = 0.9218 kg/m^3, μg = 2.214 x 10^{-5} kg/ms, A_{ht} = 0.1743 m^2, L_m = 0.5 m, Pr = 0.692, e_p = 0.76, e_g = 0.036, e_w = 0.24

Serial number of runs	Bed inventory (I) kg	Heat flux (q") W/m^2	Pressure drop across the orificemeter(Δp) cm of water	Bed temperature (T_b) K	Surface temperature (T_s) K	Pressure drop across the test section (Δh_L), cm of water	Solid circulation rate (G_s) kg/m^2s	Bare tube heat transfer coefficient, W/m^2k
1	20	5519	6.0	352.34	414.05	2.35	18.95	117.00
2		5519	8.0	352.81	417.13	2.10	39.18	111.50
3		5519	10.0	352.15	417.85	1.95	56.61	109.00
4		5519	13.0	348.53	418.35	1.70	63.56	103.00
5		5519	16.0	347.24	425.75	1.25	71.72	94.00
6		5519	25.0	346.84	440.39	0.90	76.83	87.00

DATA SHEET

Table - 6.11 : Experimental Observations on CFB Heat Transfer for 16 - Pin Finned Surface

d_p = 310 μm , d_b = 100 mm, kg = 0.03242 W/mk, ρ_s = 2350 kg/m^3, ρ_g = 0.9218 kg/m^3, μg = 2.214 x 10^{-5} kg/ms, A_{ht} = 0.0864 m^2, L_m = 0.5 m, Pr = 0.692, e_p = 0.76, e_g = 0.036, e_w = 0.24

Serial number of runs	Bed inventory (I) kg	Heat flux (q") W/m^2	Pressure drop across the orificemeter(Δp) cm of water	Bed temperature (T_b) K	Surface temperature (T_s) K	Pressure drop across the test section (Δh_L), cm of water	Solid circulation rate (G_s) kg/m^2s	Bare tube heat transfer coefficient, W/m^2k
1	20	3580	6.0	340.61	370.22	3.20	18.83	134.00
2		3580	8.0	339.43	371.39	2.70	26.91	125.00
3		3580	10.0	338.73	370.92	2.60	51.32	124.00
4		3580	13.0	336.85	369.98	2.20	62.41	116.00
5		3580	16.0	336.85	372.57	1.90	73.81	113.00
6		3580	25.0	335.67	376.80	1.20	77.95	97.00
7		5519	6.0	343.43	389.49	3.20	18.83	134.00
8		5519	8.0	342.72	391.13	2.70	26.91	125.00
9		5519	10.0	342.02	392.07	2.60	51.32	124.00
10		5519	13.0	342.49	392.78	2.20	62.41	116.00
11		5519	16.0	338.73	393.25	1.90	73.81	113.00
12		5519	25.0	338.02	399.36	1.20	77.95	97.00
13		7876	6.0	349.07	412.99	3.20	18.83	134.00
14		7876	8.0	347.19	413.46	2.70	26.91	125.00
15		7876	10.0	345.54	414.63	2.60	51.32	124.00
16		7876	13.0	344.60	417.45	2.20	62.41	116.00
17		7876	16.0	341.55	416.98	1.90	73.81	113.00
18		7876	25.0	341.08	428.50	1.20	77.95	97.00

DATA SHEET

Table - 6.12 : Experimental Observations on CFB Heat Transfer for 16- Pin Finned Surface

d_p = 310 μm , d_b = 100 mm, kg = 0.03242 W/mk, ρ_s = 2350 kg/m^3, ρ_g = 0.9218 kg/m^3, μg = 2.214 x 10^{-5} kg/ms, A_{ht} = 0.0864 m^2, L_m = 0.5 m, Pr = 0.692, e_p = 0.76, e_g = 0.036, e_w = 0.24

Serial number of runs	Bed inventory (I) kg	Heat flux (q^1) W/m^2	Pressure drop across the orificemeter(Δp) cm of water	Bed temperature (T_b) K	Surface temperature (T_s) K	Pressure drop across the test section (Δh_L), cm of water	Solid circulation rate (G_s) kg/m^{2}s	Bare tube heat transfer coefficient, W/m^{2}k
19	26	3580	6.0	339.90	369.51	3.35	18.90	138.00
20		3580	8.0	338.73	369.04	2.90	28.12	130.00
21		3580	10.0	338.96	369.75	2.75	50.32	128.00
22		3580	13.0	338.26	370.44	2.50	65.71	123.00
23		3580	16.0	337.79	371.63	2.00	76.22	114.00
24		3580	25.0	336.26	375.63	1.35	78.55	100.00
25		5519	6.0	342.72	388.08	3.35	18.90	138.00
26		5519	8.0	343.55	389.96	2.90	28.12	130.00
27		5519	10.0	337.44	389.49	2.75	50.32	128.00
28		5519	13.0	335.32	384.55	2.50	65.71	123.00
29		5519	16.0	336.85	387.84	2.00	76.22	114.00
30		5519	25.0	334.97	395.60	1.35	78.55	100.00
31		7876	6.0	345.78	409.25	3.35	18.90	138.00
32		7876	8.0	342.14	407.82	2.90	28.12	130.00
33		7876	10.0	341.43	408.17	2.75	50.32	128.00
34		7876	13.0	342.96	412.05	2.50	65.71	123.00
35		8876	16.0	343.22	416.75	2.00	76.22	114.00
36		7876	25.0	343.19	426.97	1.35	78.55	100.00

DATA SHEET

Table -6.13 : Experimental Observations on CFB Heat Transfer for 16- Pin Finned Surface

d_p = 310 μm , d_b = 100 mm, kg = 0.03242 W/mk, ρ_s = 2350 kg/m^3, ρ_g = 0.9218 kg/m^3, μg = 2.214 x 10^{-5} kg/ms, A_{ht} = 0.0864 m^2, L_m = 0.5 m, Pr = 0.692, e_p = 0.76, e_g = 0.036, e_w = 0.24

Serial number of runs	Bed inventory (I) kg	Heat flux (q") W/m^2	Pressure drop across the orificemeter(Δp) cm of water	Bed temperature (T_b) K	Surface temperature (T_s) K	Pressure drop across the test section (Δh_L), cm of water	Solid circulation rate (G_s) kg/m^2s	Bare tube heat transfer coefficient, W/m^2k
37	32	3580	6.0	336.80	366.22	3.40	19.81	139.00
38		3580	8.0	336.26	366.46	3.25	30.17	135.00
39		3580	10.0	334.19	364.58	2.95	55.24	129.00
40		3580	13.0	334.15	366.22	2.70	65.86	125.00
41		3580	16.0	332.67	368.10	2.05	75.92	115.00
42		3580	25.0	330.79	369.28	1.50	79.15	102.00
43		5519	6.0	339.93	386.20	3.40	19.81	139.00
44		5519	8.0	337.34	381.50	3.25	30.17	135.00
45		5519	10.0	339.15	383.61	2.95	55.24	129.00
46		5519	13.0	335.49	385.66	2.70	65.86	125.00
47		5519	16.0	336.97	390.05	2.05	75.92	115.00
48		5519	25.0	344.56	403.35	1.50	79.15	102.00
49		7876	6.0	350.95	413.93	3.40	19.81	139.00
50		7876	8.0	347.87	410.40	3.25	30.17	135.00
51		7876	10.0	347.92	412.14	2.95	55.24	129.00
52		7876	13.0	345.24	415.57	2.70	65.86	125.00
53		7876	16.0	346.06	418.39	2.05	75.92	115.00
54		7876	25.0	342.77	423.96	1.50	79.15	102.00

DATA SHEET

Table - 6.14 : Experimental Observations on CFB Heat Transfer for 32 - Pin Finned Surface

d_p = 310 μm , d_b = 100 mm, kg = 0.03242 W/mk, ρ_s = 2350 kg/m^3, ρ_g = 0.9218 kg/m^3, μg = 2.214 x 10^{-5} kg/ms, A_{ht} = 0.0912 m^2, L_m = 0.5 m, Pr = 0.692, e_p = 0.76, e_g = 0.036, e_w = 0.24

Serial number of runs	Bed inventory (I) kg	Heat flux (q") W/m2	Pressure drop across the orificemeter(Δp) cm of water	Bed temperature (T_b) K	Surface temperature (T_s) K	Pressure drop across the test section (Δh_L), cm of water	Solid circulation rate (G_s) kg/m^{2}s	Bare tube heat transfer coefficient, W/m^{2}k
1	20	5519	6.0	342.22	388.67	3.00	18.19	130.00
2		5519	8.0	342.07	390.92	2.65	25.46	125.00
3		5519	10.0	341.78	391.13	2.55	43.44	123.00
4		5519	13.0	341.48	392.57	2.25	59.95	117.50
5		5519	16.0	339.41	394.59	1.80	74.50	110.00
6		5519	25.0	337.41	399.69	1.20	78.57	97.00
7	26	5519	6.0	344.06	390.13	3.15	18.13	132.50
8		5519	8.0	344.28	390.81	2.90	27.23	128.00
9		5519	10.0	343.52	391.98	2.70	58.11	125.00
10		5519	13.0	343.19	393.32	2.40	70.21	120.00
11		5519	16.0	340.96	392.97	1.95	75.60	113.00
12		5519	25.0	339.95	402.63	1.35	77.83	100.00
13	32	5519	6.0	345.19	392.57	3.20	19.23	134.00
14		5519	8.0	344.42	388.17	3.10	28.25	132.00
15		5519	10.0	343.52	388.13	2.90	58.04	130.00
16		5519	13.0	342.72	392.95	2.60	71.46	124.00
17		5519	16.0	342.21	395.95	2.00	74.70	114.00
18		5519	25.0	341.46	402.98	1.45	78.88	101.00

DATA SHEET

Table - 6.15 : Experimental Observations on CFB Heat Transfer for 1500 mm Long 4-Rectangular Finned Surface

d_p = 310 μm , d_b = 100 mm, kg = 0.03242 W/mk, ρ_s = 2350 kg/m^3, ρ_g = 0.9218 kg/m^3, μg = 2.214 x 10^{-5} kg/ms, A_{ht} = 0.1277 m^2, L_m = 0.5 m, Pr = 0.692, e_p = 0.76, e_g = 0.036, e_w = 0.24

Serial number of runs	Bed inventory (I) kg	Heat flux (q") W/m^2	Pressure drop across the orificemeter(Δp) cm of water	Bed temperature (T_b) K	Surface temperature (T_s) K	Pressure drop across the test section (Δh_L), cm of water	Solid circulation rate (G_s) kg/m^{2}s	Bare tube heat transfer coefficient, W/m^{2}k
1	26	5519	6.0	344.06	390.43	3.10	17.44	132.00
2		5519	8.0	348.20	396.21	2.85	25.86	127.00
3		5519	10.0	348.55	388.56	2.55	49.59	120.50
4		5519	13.0	348.08	405.03	2.25	58.75	114.50
5		5519	16.0	345.85	409.69	1.80	76.26	105.50
6		5519	25.0	345.26	418.35	1.15	77.15	93.00

DATA SHEET

Table - 6.16 : Data of Pressure Differential Along the Height of the Riser Column for Unfinned Surface

d_p = 310 μm , d_b = 100 mm , ρ_s = 2350 kg/m^3 , L_m = 0.5 m

Serial No. of runs	Bed inventory (I) kg	Superficial velocity (U_o) m/s	Value of Δh_L (cm. of water) between the consecutive pressure tappings along the column above the distributor at a height								
			1.1m	1.6m	2.1m	2.6m	3.1m	3.6m	4.1m	4.6m	5.1m
1	20	5.6	4.5	4.0	3.52	3.52	3.5	3.51	3.25	2.9	3.0
2		6.5	4.05	4.0	3.0	3.0	3.1	3.1	2.9	2.9	3.0
3		7.2	4.0	3.52	3.0	3.0	3.0	3.0	2.82	2.75	2.9
4		8.2	3.0	3.0	3.0	2.4	2.5	2.6	2.73	2.7	2.82
5		9.1	2.23	2.11	2.1	2.11	2.0	2.11	1.87	1.85	2.11
6		11.4	1.52	1.3	1.3	1.3	1.25	1.2	1.3	1.3	1.2
7	26	5.6	4.5	4.2	3.75	3.65	3.7	3.6	3.5	3.45	3.52
8		6.5	4.25	4.0	3.52	3.4	3.4	3.52	3.3	3.28	3.15
9		7.2	4.0	3.52	3.25	3.0	3.1	3.0	2.9	2.82	2.9

(contd...)

DATA SHEET

Table - 6.16 : Data of Pressure Differential Along the Height of the Riser Column for Unfinned Surface

d_p = 310 μm , d_b = 100 mm , ρ_s = 2350 kg/m^3 , L_m = 0.5 m

Serial No. of runs	Bed inventory (I) kg	Superficial velocity (U_o) m/s	Value of Δh_L (cm. of water) between the consecutive pressure tappings along the column above the distributor at a height								
			1.1m	1.6m	2.1m	2.6m	3.1m	3.6m	4.1m	4.6m	5.1m
10	26	8.2	3.25	3.25	2.6	2.52	2.7	2.6	2.55	2.52	2.82
11		9.1	2.5	2.25	2.11	2.25	2.1	2.11	2.25	2.11	2.25
12		11.4	1.5	1.3	1.6	1.52	1.5	1.3	1.3	1.3	1.2
13	32	5.6	4.7	4.25	3.85	3.75	3.8	3.75	3.75	3.6	3.65
14		6.5	4.25	4.0	3.52	3.52	3.6	3.52	3.52	3.4	3.4
15		7.2	4.1	3.65	3.25	3.25	3.25	3.1	3.0	2.9	2.82
16		8.2	3.25	3.25	2.9	2.9	3.0	3.0	3.0	2.82	2.81
17		9.1	2.75	2.5	2.11	2.11	2.2	2.11	2.25	2.11	2.25
18		11.4	1.75	1.52	1.6	1.53	1.6	1.35	1.35	1.3	1.3

DATA SHEET

Table - 6.17 : Data of Pressure Differential Along the Height of the Riser Column for 2-Rectangular Finned Surface

d_p = 310 μm , d_b = 100 mm , ρ_s = 2350 kg/m^3 , L_m = 0.5 m

Serial No. of runs	Bed inventory (I) kg	Superficial velocity (U_o) m/s	D Value of Δh_L (cm. of water) between the consecutive pressure tappings along the column above the distributor at a height								
			1.1m	1.6m	2.1m	2.6m	3.1m	3.6m	4.1m	4.6m	5.1m
19	20	5.6	4.4	4.05	3.6	3.52	3.25	3.1	3.0	2.95	3.0
20		6.5	4.0	3.9	3.3	3.25	3.0	2.9	2.9	2.8	2.8
21		7.2	3.9	3.52	3.2	3.0	2.85	2.8	2.75	2.75	2.7
22		8.2	3.2	3.0	2.75	2.6	2.4	2.25	2.25	2.1	2.2
23		9.1	2.4	2.25	2.11	1.95	1.8	1.75	1.60	1.75	1.6
24		11.4	1.65	1.65	1.6	1.5	1.1	1.16	1.05	1.16	1.2
25	26	5.6	4.5	4.0	3.8	3.6	3.35	3.25	3.25	3.2	3.3
26		6.5	4.2	3.8	3.4	3.52	3.2	3.1	3.2	3.0	3.05
27		7.2	4.05	3.8	3.52	3.4	2.95	3.0	2.9	2.75	2.8

(contd...)

DATA SHEET

Table - 6.17 : Data of Pressure Differential Along the Height of the Riser Column for 2-Rectangular Finned Surface

d_p = 310 μm , d_b = 100 mm , ρ_s = 2350 kg/m^3 , L_m = 0.5 m

Serial No. of runs	Bed inventory (I) kg	Superficial velocity (U_o) m/s	Value of Δh_L (cm. of water) between the consecutive pressure tappings along the column above the distributor at a height								
			1.1m	1.6m	2.1m	2.6m	3.1m	3.6m	4.1m	4.6m	5.1m
28	26	8.2	3.1	3.0	2.6	2.8	2.6	2.5	2.4	2.55	2.55
29		9.1	2.6	2.5	2.2	2.11	1.9	1.8	1.75	1.6	1.8
30		11.4	1.9	1.8	1.65	1.6	1.35	1.3	1.2	1.35	1.2
31	32	5.6	4.7	4.2	3.9	3.9	3.65	3.6	3.5	3.6	3.52
32		6.5	4.25	4.0	4.0	3.8	3.5	3.4	3.5	3.4	3.4
33		7.2	4.2	3.75	3.6	3.45	3.1	3.0	3.0	3.4	2.75
34		8.2	3.25	3.1	3.0	3.0	3.0	2.7	2.6	2.6	2.5
35		9.1	2.7	2.6	2.4	2.35	2.1	2.0	2.15	2.1	2.2
36		11.4	1.8	1.7	1.65	1.65	1.5	1.5	1.35	1.3	1.3

DATA SHEET

Table - 6.18 : Data of Pressure Differential Along the Height of the Riser Column for 4-Rectangular Finned Surface

d_p = 310 μm , d_b = 100 mm , ρ_s = 2350 kg/m^3 , L_m = 0.5 m

Serial No. of runs	Bed inventory (I) kg	Superficial velocity (U_o) m/s	Value of Δh_L (cm. of water) between the consecutive pressure tappings along the column above the distributor at a height								
			1.1m	1.6m	2.1m	2.6m	3.1m	3.6m	4.1m	4.6m	5.1m
37	20	5.6	4.3	4.05	3.85	3.65	3.0	2.9	2.95	3.0	3.0
38		6.5	4.05	4.0	3.7	3.52	2.8	2.6	2.9	2.8	2.9
39		7.2	4.0	3.45	3.45	3.0	2.6	2.6	2.5	2.6	2.7
40		8.2	3.0	2.9	2.8	2.6	2.15	2.1	2.25	2.13	2.12
41		9.1	2.25	2.25	2.4	2.23	1.6	1.55	1.6	1.76	1.75
42		11.4	1.5	1.3	1.35	1.5	1.0	1.05	1.18	1.06	1.17
43	26	5.6	4.5	4.25	4.2	3.75	3.2	3.2	3.25	3.35	3.4
44		6.5	4.3	4.05	3.85	3.65	2.9	2.8	2.9	2.9	2.8
45		7.2	4.0	3.65	3.45	3.4	2.7	2.7	2.8	2.75	2.8

(contd...)

DATA SHEET

Table - 6.18 : Data of Pressure Differential Along the Height of the Riser Column for 4-Rectangular Finned Surface

d_p = 310 μm , d_b = 100 mm , ρ_s = 2350 kg/m^3 , L_m = 0.5 m

Serial No. of runs	Bed inventory (I) kg	Superficial velocity (U_o) m/s	Value of Δh_L (cm. of water) between the consecutive pressure tappings along the column above the distributor at a height								
			1.1m	1.6m	2.1m	2.6m	3.1m	3.6m	4.1m	4.6m	5.1m
46	26	8.2	3.4	3.4	2.9	2.8	2.35	2.2	2.45	2.25	2.2
47		9.1	2.52	2.52	2.4	2.4	1.8	1.75	1.8	1.95	1.95
48		11.4	1.6	1.35	1.4	1.55	1.2	1.27	1.3	1.25	1.25
49	32	5.6	4.7	4.25	3.88	3.85	3.35	3.25	3.2	3.4	3.39
50		6.5	4.3	4.05	4.0	3.75	3.25	3.2	3.1	3.3	3.25
51		7.2	4.2	3.8	3.6	3.4	2.8	2.7	2.9	2.8	2.75
52		8.2	3.4	3.4	3.25	3.0	2.6	2.5	2.6	2.4	2.38
53		9.1	2.82	2.58	2.5	2.48	2.0	2.1	2.0	2.1	2.2
54		11.4	1.8	1.7	1.65	1.6	1.4	1.3	1.3	1.3	1.3

DATA SHEET

Table - 6.19 : Data of Pressure Differential Along the Height of the Riser Column for 8-Rectangular Finned Surface

d_p = 310 μm , d_b = 100 mm , ρ_s = 2350 kg/m^3 , L_m = 0.5 m

Serial No. of runs	Bed inventory (I) kg	Superficial velocity (U_o) m/s	Value of Δh_L (cm. of water) between the consecutive pressure tappings along the column above the distributor at a height								
			1.1m	1.6m	2.1m	2.6m	3.1m	3.6m	4.1m	4.6m	5.1m
55	20	5.6	4.5	4.3	4.0	2.95	2.35	2.4	2.35	2.3	2.25
56		6.5	4.4	4.0	3.25	2.6	2.1	2.1	2.2	2.05	2.0
57		7.2	4.1	3.75	3.0	2.4	1.95	2.0	1.88	1.77	1.75
58		8.2	3.1	3.0	2.6	2.1	1.7	1.75	1.6	1.65	1.55
59		9.1	2.5	2.5	2.1	1.6	1.25	1.25	1.2	1.25	1.25
60		11.4	2.0	1.75	1.55	1.25	0.94	0.95	0.94	0.95	0.9

DATA SHEET

Table - 6.20 : Data of Pressure Differential Along the Height of the Riser Column for 16-Pin Finned Surface

d_p = 310 μm , d_b = 100 mm , ρ_s = 2350 kg/m^3 , L_m = 0.5 m

Serial No. of runs	Bed inventory (I) kg	Superficial velocity (U_o) m/s	Value of Δh_L (cm. of water) between the consecutive pressure tappings along the column above the distributor at a height								
			1.1m	1.6m	2.1m	2.6m	3.1m	3.6m	4.1m	4.6m	5.1m
61	20	5.6	4.5	4.0	3.5	3.4	3.0	3.1	3.1	3.0	2.9
62		6.5	4.0	3.5	3.25	3.1	2.7	2.6	2.6	2.7	2.75
63		7.2	3.9	3.2	3.2	2.9	2.6	2.5	2.6	2.6	2.7
64		8.2	3.1	3.0	3.0	2.6	2.2	2.1	2.1	2.2	2.25
65		9.1	2.5	2.25	2.25	2.25	1.9	1.75	1.88	1.75	1.6
66		11.4	1.52	1.3	1.35	1.5	1.2	1.2	1.25	1.3	1.1
67	26	5.6	4.5	4.1	4.1	3.75	3.35	3.3	3.25	3.1	3.1
68		6.5	4.3	4.11	3.75	3.3	2.9	2.8	2.75	2.9	2.81
69		7.2	4.0	3.8	3.7	3.1	2.75	2.75	2.9	2.7	2.7

(contd...)

DATA SHEET

Table - 6.20 : Data of Pressure Differential Along the Height of the Riser Column for 16-Pin Finned Surface

d_p = 310 μm , d_b = 100 mm , ρ_s = 2350 kg/m^3 , L_m = 0.5 m

Serial No. of runs	Bed inventory (I) kg	Superficial velocity (U_o) m/s	Value of Δh_L (cm. of water) between the consecutive pressure tappings along the column above the distributor at a height								
			1.1m	1.6m	2.1m	2.6m	3.1m	3.6m	4.1m	4.6m	5.1m
70	26	8.2	3.3	3.2	3.2	2.75	2.5	2.58	2.4	2.5	2.6
71		9.1	2.5	2.3	2.3	2.4	2.0	2.0	2.05	2.05	2.11
72		11.4	1.25	1.25	1.3	1.5	1.35	1.3	1.25	1.25	1.2
73	32	5.6	4.65	4.11	4.0	3.8	3.4	3.4	3.3	3.1	3.1
74		6.5	4.2	3.75	3.5	3.59	3.25	3.25	3.15	3.0	3.0
75		7.2	4.1	3.75	3.4	3.25	2.95	2.85	2.95	2.9	2.9
76		8.2	3.5	3.3	3.3	3.0	2.7	2.5	2.6	2.6	2.7
77		9.1	2.82	2.7	2.5	2.3	2.05	2.1	2.05	2.12	2.1
78		11.4	1.7	1.6	1.5	1.65	1.5	1.5	1.2	1.25	1.2

DATA SHEET

Table - 6.21 : Data of Pressure Differential Along the Height of the Riser Column for 32-Pin Finned Surface

d_p = 310 μm , d_b = 100 mm , ρ_s = 2350 kg/m^3 , L_m = 0.5 m

Serial No. of runs	Bed inventory (I) kg	Superficial velocity (U_o) m/s	Value of Δh_L (cm. of water) between the consecutive pressure tappings along the column above the distributor at a height								
			1.1m	1.6m	2.1m	2.6m	3.1m	3.6m	4.1m	4.6m	5.1m
79	20	5.6	4.5	4.1	3.75	3.4	3.0	3.0	2.85	2.7	2.55
80		6.5	4.0	3.9	3.0	3.1	2.65	2.6	2.6	2.55	2.5
81		7.2	3.9	3.85	3.1	2.8	2.55	2.4	2.3	2.25	2.2
82		8.2	3.1	3.0	2.6	2.6	2. 5	2.2	2.2	2.1	2.1
83		9.1	2.45	2.4	2.25	2.1	1.8	1.8	1.7	1.6	1.6
84		11.4	1.6	1.5	1.45	1.5	1.2	1.2	1.18	1.18	1.18
85	26	5.6	4.5	4.15	4.0	3.5	3.15	3.1	2.9	2.95	2.7
86		6.5	4.35	4.0	3.45	3.25	2.9	2.95	2.75	2.75	2.55
87		7.2	4.1	3.6	3.1	3.15	2.7	2.55	2.7	2.5	2.5

(contd...)

DATA SHEET

Table - 6.21 : Data of Pressure Differential Along the Height of the Riser Column for 32-Pin Finned Surface

d_p = 310 μm , d_b = 100 mm , ρ_s = 2350 kg/m^3 , L_m = 0.5 m

Serial No. of runs	Bed inventory (I) kg	Superficial velocity (U_o) m/s	Value of Δh_L (cm. of water) between the consecutive pressure tappings along the column above the distributor at a height								
			1.1m	1.6m	2.1m	2.6m	3.1m	3.6m	4.1m	4.6m	5.1m
88	26	8.2	3.25	3.15	2.7	2.7	2.4	2.25	1.95	1.95	1.75
89		9.1	2.6	2.45	2.5	2.25	1.95	1.95	1.75	1.75	1.55
90		11.4	1.6	1.5	1.55	1.6	1.35	1.25	1.2	1.18	1.18
91	32	5.6	4.7	4.2	3.9	3.75	3.2	3.35	3.3	3.25	3.2
92		6.5	4.55	4.05	3.6	3.45	3.1	3.0	2.9	2.7	2.7
93		7.2	4.1	3.75	3.4	3.2	2.9	2.75	2.75	2.55	2.5
94		8.2	3.25	3.1	3.0	2.9	2.6	2.6	2.55	2.4	2.25
95		9.1	2.8	2.7	2.5	2.2	2.0	1.95	2.0	2.05	1.88
96		11.4	1.75	1.6	1.5	1.6	1.45	1.45	1.35	1.3	1.35

DATA SHEET

Table - 6.22 : Data of Pressure Differential Along the Height of the Riser Column for 1500 mm Long 4-Rectangular Finned Surface

d_p = 310 μm , d_b = 100 mm , ρ_s = 2350 kg/m^3 , L_m = 0.5 m

Serial No. of runs	Bed inventory (I) kg	Superficial velocity (U_o) m/s	Value of Δh_L (cm. of water) between the consecutive pressure tappings along the column above the distributor at a height								
			1.1m	1.6m	2.1m	2.6m	3.1m	3.6m	4.1m	4.6m	5.1m
97	26	5.6	4.49	4.3	4.05	3.9	3.1	3.35	3.25	3.15	3.15
98		6.5	4.3	4.05	3.9	3.6	2.85	3.05	2.88	2.75	2.75
99		7.2	3.9	3.9	3.75	3.5	2.55	2.7	2.59	2.58	2.58
100		8.2	3.45	3.18	3.0	2.7	2.25	2.25	2.3	2.28	2.27
101		9.1	2.4	2.4	2.45	2.25	1.8	1.7	1.55	1.58	1.57
102		11.4	1.55	1.52	1.52	1.5	1.18	1.25	1.2	1.23	1.23

DATA SHEET

Table - 6.23 : Experimental Observations on CFB Heat Transfer for 85 mm Vertical Probe

d_p = 310 μm , d_b = 100 mm, kg = 0.03242 W/mk, ρ_s = 2350 kg/m^3, ρ_g = 0.9218 kg/m^3, μg = 2.214 x 10^{-5} kg/ms, c_{p_s} = 0.703 kJ/kgK, L_m = 0.5 m, L_h = 85 mm, L_H = 1.22 m, L_h/D = 0.85, A_{ht} = 0.0267 m^2

Serial number of runs	Bed inventory (I) kg	Heat flux (q") W/m^2	Pressure drop across the orificemeter(Δp) cm of water	Bed temperature (T_b) K	Surface temperature (T_s) K	Pressure drop across the test section (Δh_L), cm of water	Solid circulation rate (G_s) kg/m^2s
1	32	4500	10	335.30	363.52	3.10	57.30
2		4500	15	334.69	364.13	2.30	66.39
3		4500	20	335.67	366.39	1.80	76.40
4		4500	25	335.44	368.48	1.60	77.89
5		4500	30	335.23	368.81	1.25	78.30
6		6000	10	336.94	374.21	3.10	57.30
7		6000	15	336.76	376.49	2.30	66.39
8		6000	20	336.38	377.74	1.80	76.40
9		6000	25	336.33	378.70	1.60	77.89
10		6000	30	335.44	380.11	1.25	78.30

DATA SHEET

Table - 6.24 : Experimental Observations on CFB Heat Transfer for 127.5 mm Vertical Probe

d_p = 310 μm , d_b = 100 mm, kg = 0.03242 W/mk, ρ_s = 2350 kg/m^3, ρ_g = 0.9218 kg/m^3, μg = 2.214 x 10^{-5} kg/ms, L_h = 127.5 mm, L_m = 0.5 m, L_H = 1.83 m, L_h/D = 1.275 , c_{p_s} = 0.703 kJ/kgK, A_{ht} = 0.04 m^2

Serial number of runs	Bed inventory (I) kg	Heat flux (q") W/m^2	Pressure drop across the orificemeter(Δp) cm of water	Bed temperature (T_b) K	Surface temperature (T_s) K	Pressure drop across the test section (Δh_L), cm of water	Solid circulation rate (G_s) kg/m^{2}s
11	32	4500	10	337.39	366.72	3.10	57.30
12		4500	15	336.87	370.85	2.30	66.39
13		4500	20	337.01	375.04	1.80	76.40
14		4500	25	336.54	376.14	1.60	77.89
15		4500	30	336.36	376.89	1.25	78.30
16		6000	10	338.38	377.08	3.10	57.30
17		6000	15	340.02	385.47	2.30	66.39
18		6000	20	339.74	388.84	1.80	76.40
19		6000	25	339.88	390.45	1.60	77.89
20		6000	30	339.74	392.86	1.25	78.30

DATA SHEET

Table - 6.25 : Experimental Observations on CFB Heat Transfer for 170 mm Vertical Probe

d_p = 310 μm , d_b = 100 mm, kg = 0.03242 W/mk, ρ_s = 2350 kg/m^3, ρ_g = 0.9218 kg/m^3, μg = 2.214 x 10^{-5} kg/ms, L_h = 170 mm, L_m = 0.5 m, L_H = 2.44 m, L_h/D = 1.70 , c_{p_s} = 0.703 kJ/kgK, A_{ht} = 0.0534 m^2

Serial number of runs	Bed inventory (I) kg	Heat flux (q") W/m^2	Pressure drop across the orificemeter(Δp) cm of water	Bed temperature (T_b) K	Surface temperature (T_s) K	Pressure drop across the test section (Δh_L), cm of water	Solid circulation rate (G_s) kg/m^{2}s
21	32	4500	10	338.02	372.90	3.10	57.30
22		4500	15	337.72	377.20	2.30	66.39
23		4500	20	337.51	379.55	1.80	76.40
24		4500	25	338.26	381.99	1.60	77.89
25		4500	30	338.07	383.99	1.25	78.30
26		6000	10	339.69	390.45	3.10	57.30
27		6000	15	340.02	392.19	2.30	66.39
28		6000	20	339.88	397.20	1.80	76.40
29		6000	25	340.05	397.43	1.60	77.89
30		6000	30	339.90	399.90	1.25	78.30

DATA SHEET

Table - 6.26 : Experimental Observations on CFB Heat Transfer for 255 mm Vertical Probe

d_p = 310 μm , d_b = 100 mm, kg = 0.03242 W/mk, ρ_s = 2350 kg/m^3, ρ_g = 0.9218 kg/m^3, μg = 2.214 x 10^{-5} kg/ms, L_h = 255 mm, L_m = 0.5 m, L_H = 3.66 m, L_h/D = 2.55, c_{p_s} = 0.703 kJ/kgK, A_{ht} = 0.08 m^2

Serial number of runs	Bed inventory (I) kg	Heat flux (q") W/m^2	Pressure drop across the orificemeter(Δp) cm of water	Bed temperature (T_b) K	Surface temperature (T_s) K	Pressure drop across the test section (Δh_L), cm of water	Solid circulation rate (G_s) kg/m^2s
31	32	4500	10	340.49	381.29	3.10	57.30
32		4500	15	341.41	385.96	2.30	66.39
33		4500	20	341.29	388.67	1.80	76.40
34		4500	25	343.41	389.77	1.60	77.89
35		4500	30	342.23	392.33	1.25	78.30
36		6000	10	348.41	403.05	3.10	57.30
37		6000	15	348.34	405.56	2.30	66.39
38		6000	20	348.11	407.14	1.80	76.40
39		6000	25	347.50	408.41	1.60	77.89
40		6000	30	345.71	408.88	1.25	78.30

RESULT SHEET

Table - 6.27 : Experimental Results on CFB Heat Transfer for Unfinned Surface

d_p = 310 μm, d_b = 100 mm, k_g = 0.03242 W/m K, ρ_s = 2350 kg/m^3, ρ_g = 0.9218 kg/m^3, μ_g = 2.214 x 10^{-5} kg/ms, A_{ht} = 0.0816 m^2, L_m = 0.5 m, Pr = 0.692 , e_p = 0.76, e_g = 0.035, e_w = 0.24,

Sl. No. of runs	Bed inventory (I) kg	Heat flux (q") W/m^2	Superficial velocity (U_o) m/s	Bed temperature (T_b) K	Voidage (ε)	Suspension density (ρ_{sus}) kg/m^3	Experimental heat transfer coefficient (h_e) W/m^{2}K	Predict heat transfer coefficient (h_T) W/m^{2}K	Reynolds number (Re)	Experimental Nusselt number (Nu_e)	Predicted Nusselt number (Nu_T)	% Error
1	20.0	3580.0	5.6	350.24	.9702	70.00	134.81	134.84	72.08	1.29	1.29	.02
2			6.5	346.25	.9736	62.00	136.02	131.10	83.23	1.30	1.25	-3.75
3			7.2	345.54	.9745	60.00	130.21	129.00	93.06	1.25	1.23	-0.93
4			8.2	344.84	.9787	50.00	124.87	122.00	106.10	1.19	1.17	-2.35
5			9.1	345.07	.9830	40.00	116.29	113.41	117.71	1.11	1.08	-2.54
6			11.4	345.07	.9894	25.00	97.03	90.24	147.14	.93	.86	-7.53
7	20.0	5519.0	5.6	354.71	.9702	70.00	134.97	134.87	72.08	1.29	1.29	-0.07
8			6.5	352.36	.9736	62.00	136.54	131.14	83.23	1.31	1.25	-4.12
9			7.2	348.83	.9745	60.00	134.20	129.03	93.06	1.28	1.23	-4.01

(contd...)

RESULT SHEET

Table - 6.27 : Experimental Results on CFB Heat Transfer for Unfinned Surface

d_p = 310 um, d_b = 100 mm, k_g = 0.03242 W/m K, ρ_s = 2350 kg/m^3, ρ_g = 0.9218 kg/m^3, μ_g = 2.214 x 10^{-5} kg/ms, A_{ht} = 0.0816 m^2, L_m = 0.5 m, Pr = 0.692 , e_p = 0.76, e_g = 0.035, e_w = 0.24,

Sl. No. of runs	Bed inventory (I) kg	Heat flux (q") W/m^2	Superficial velocity (U_o) m/s	Bed temperature (T_b) K	Voidage (ε)	Suspension density (ρ_{sus}) kg/m^3	Experimental heat transfer coefficient (h_e) W/m^{2}K	Predict heat transfer coefficient (h_T) W/m^{2}K	Reynolds number (Re)	Experimental Nusselt number (Nu_e)	Predicted Nusselt number (Nu_T)	% Error
10			8.2	348.36	.9787	50.00	124.92	122.03	106.10	1.19	1.17	-2.37
11			9.1	348.60	.9830	40.00	118.02	113.44	117.71	1.13	1.08	-4.04
12			11.4	347.19	.9894	25.00	97.85	90.27	147.14	.94	.86	-8.41
13	20.0	7876.0	5.6	361.52	.9702	70.00	136.80	134.92	72.08	1.31	1.29	-1.39
14			6.5	358.70	.9736	62.00	135.69	131.18	83.23	1.30	1.25	-3.44
15			7.2	355.65	.9745	60.00	133.53	129.07	93.06	1.28	1.23	-3.45
16			8.2	354.24	.9787	50.00	126.00	122.07	106.10	1.20	1.17	-3.22
17			9.1	354.71	.9830	40.00	120.13	113.48	117.71	1.15	1.09	-5.86
18			11.4	357.53	.9894	25.00	98.28	90.32	147.14	.94	.86	-8.81

RESULT SHEET

Table - 6.28 : Experimental Results on CFB Heat Transfer for Unfinned Surface

d_p = 310 μm, d_b = 100 mm, k_g = 0.03242 W/m K, ρ_s = 2350 kg/m^3, ρ_g = 0.9218 kg/m^3, μ_g = 2.214 x 10^{-5} kg/ms, A_{ht} = 0.0816 m^2, L_m = 0.5 m, Pr = 0.692 , e_p = 0.76, e_g = 0.035, e_w = 0.24,

Sl. No. of runs	Bed inventory (I) kg	Heat flux (q") W/m^2	Superficial velocity (U_o) m/s	Bed temperature (T_b) K	Voidage (ε)	Suspension density (ρ_{sus}) kg/m^3	Experimental heat transfer coefficient (h_e) W/m^{2}K	Predict heat transfer coefficient (h_T) W/m^{2}K	Reynolds number (Re)	Experimental Nusselt number (Nu_e)	Predicted Nusselt number (Nu_T)	% Error
19	26.0	3580.0	5.6	349.07	.9685	74.00	134.81	136.07	72.08	1.29	1.30	.92
20			6.5	348.36	.9711	68.00	141.06	133.27	83.23	1.35	1.27	-5.85
21			7.2	347.19	.9736	62.00	133.63	129.83	93.06	1.28	1.24	-2.93
22			8.2	348.36	.9770	54.00	123.85	123.98	106.10	1.18	1.19	.10
23			9.1	348.36	.9821	42.00	113.69	114.56	117.71	1.09	1.10	.76
24			11.4	348.60	.9872	30.00	98.28	94.30	147.14	.94	.90	-4.22
25	26.0	5519.0	5.6	356.35	.9685	74.00	136.54	136.10	72.08	1.31	1.30	-0.32
26			6.5	351.18	.9711	68.00	136.54	133.29	83.23	1.31	1.27	-2.44
27			7.2	352.36	.9736	62.00	134.20	129.86	93.06	1.28	1.24	-3.35

(contd...)

RESULT SHEET

Table - 6.28 : Experimental Results on CFB Heat Transfer for Unfinned Surface

d_p = 310 μm, d_b = 100 mm, k_g = 0.03242 W/m K, ρ_s = 2350 kg/m^3, ρ_g = 0.9218 kg/m^3, μ_g = 2.214 x 10^{-5} kg/ms, A_{ht} = 0.0816 m^2, L_m = 0.5 m, Pr = 0.692 , e_p = 0.76, e_g = 0.035, e_w = 0.24.

Sl. No. of runs	Bed inventory (I) kg	Heat flux (q") W/m^2	Superficial velocity (U_o) m/s	Bed temperature (T_b) K	Voidage (ε)	Suspension density (ρ_{sus}) kg/m^3	Experimental heat transfer coefficient (h_e) W/m^{2}K	Predict heat transfer coefficient (h_T) W/m^{2}K	Reynolds number (Re)	Experimental Nusselt number (Nu_e)	Predicted Nusselt number (Nu_T)	% Error
28			8.2	351.65	.9770	54.00	125.59	124.01	106.10	1.20	1.19	-1.28
29			9.1	350.95	.9821	42.00	115.12	114.59	117.71	1.10	1.10	-0.47
30			11.4	345.78	.9872	30.00	98.68	94.32	147.14	.94	.90	-4.62
31	26.0	7876.0	5.6	363.64	.9685	74.00	139.07	136.15	72.08	1.33	1.30	-2.14
32			6.5	358.47	.9711	68.00	140.82	133.33	83.23	1.35	1.27	-5.61
33			7.2	358.00	.9736	62.00	134.06	129.90	93.06	1.28	1.24	-3.20
34			8.2	360.11	.9770	54.00	125.52	124.05	106.10	1.20	1.19	-1.18
35			9.1	359.88	.9821	42.00	115.97	114.64	117.71	1.11	1.10	-1.16
36			11.4	358.94	.9872	30.00	98.86	94.38	147.14	.95	.90	-4.75

RESULT SHEET

Table - 6.29 : Experimental Results on CFB Heat Transfer for Unfinned Surface

d_p = 310 um, d_b = 100 mm, k_g = 0.03242 W/m K, ρ_s = 2350 kg/m^3, ρ_g = 0.9218 kg/m^3, μ_g = 2.214 x 10^{-5} kg/ms, A_{ht} = 0.0816 m^2, L_m = 0.5 m, Pr = 0.692, e_p = 0.76, e_g = 0.035, e_w = 0.24,

Sl. No. of runs	Bed inventory (I) kg	Heat flux (q") W/m^2	Superficial velocity (U_o) m/s	Bed temperature (T_b) K	Voidage (ε)	Suspension density (ρ_{sus}) kg/m^3	Experimental heat transfer coefficient (h_e) W/m^{2}K	Predict heat transfer coefficient (h_T) W/m^{2}K	Reynolds number (Re)	Experimental Nusselt number (Nu_e)	Predicted Nusselt number (Nu_T)	% Error
37	32.0	3580.0	5.6	347.89	.9677	76.00	139.76	136.68	72.08	1.34	1.31	-2.26
38			6.5	348.60	.9694	72.00	136.02	134.71	83.23	1.30	1.29	-0.97
39			7.2	347.89	.9723	65.00	134.81	131.07	93.06	1.29	1.25	-2.86
40			8.2	348.13	.9745	60.00	124.37	126.93	106.10	1.19	1.21	1.63
41			9.1	348.60	.9813	44.00	113.69	115.71	117.71	1.09	1.11	1.75
42			11.4	347.42	.9864	32.00	100.89	95.92	147.14	.96	.92	-5.18
43	32.0	5519.0	5.6	360.35	.9677	76.00	134.20	136.73	72.08	1.28	1.31	1.85
44			6.5	355.18	.9694	72.00	140.63	134.74	83.23	1.34	1.29	-4.37
45			7.2	352.59	.9723	65.00	135.75	131.10	93.06	1.30	1.25	-3.55

(contd...)

RESULT SHEET

Table - 6.29 : Experimental Results on CFB Heat Transfer for Unfinned Surface

d_p = 310 μm, d_b = 100 mm, k_g = 0.03242 W/m K, ρ_s = 2350 kg/m^3, ρ_g = 0.9218 kg/m^3, μ_g = 2.214 x 10^{-5} kg/ms, A_{ht} = 0.0816 m^2, L_m = 0.5 m, Pr = 0.692 , e_p = 0.76, e_g = 0.035, e_w = 0.24.

Sl. No. of runs	Bed inventory (I) kg	Heat flux (q") W/m^2	Superficial velocity (U_o) m/s	Bed temperature (T_b) K	Voidage (ε)	Suspension density (ρ_{sus}) kg/m^3	Experimental heat transfer coefficient (h_e) W/m^{2}K	Predict heat transfer coefficient (h_T) W/m^{2}K	Reynolds number (Re)	Experimental Nusselt number (Nu_e)	Predicted Nusselt number (Nu_T)	% Error
46			8.2	352.59	.9745	60.00	125.59	126.96	106.10	1.20	1.21	1.08
47			9.1	353.06	.9813	44.00	115.69	115.74	117.71	1.11	1.11	.04
48			11.4	352.83	.9864	32.00	101.23	95.96	147.14	.97	.92	-5.49
49	32.0	7876.0	5.6	364.58	.9677	76.00	138.49	136.77	72.08	1.32	1.31	-1.26
50			6.5	360.35	.9694	72.00	140.82	134.78	83.23	1.35	1.29	-4.48
51			7.2	358.94	.9723	65.00	136.24	131.14	93.06	1.30	1.25	-3.89
52			8.2	359.64	.9745	60.00	126.47	127.01	106.10	1.21	1.21	.42
53			9.1	359.41	.9813	44.00	118.01	115.78	117.71	1.13	1.11	-1.93
54			11.4	360.35	.9864	32.00	102.18	96.01	147.14	.98	.92	-6.43

RESULT SHEET

Table - 6.30 : Experimental Results on CFB Heat Transfer for 2 - Rectangular Finned Surface

d_p = 310 μm, d_b = 100 mm, k_g = 0.03242 W/mK, ρ_s = 2350 kg/m^3, ρ_g = 0.09218 kg/m^3, μg = 2.214 x 10^{-5} kg/ms

A_{ht} = 0.1046 m^2, L_m = 0.5 m, Pr = 0.692, e_p = 0.76, e_g = 0.036, e_w = 0.24

Serial number of runs	Bed inventory(I) kg	Heat flux (q") W/m^2	Superficial velocity (U_o), m/s	Bed temperature (T_b) K	Voidage (ε)	Suspension density (ρ_{sus}) kg/m^3	Experimental heat transfer coefficient (h_e) W/m^2K	Predicted heat transfer coefficient (h_T), W/m^2K	% Error	Equivalent heat transfer coefficient (h_E), W/m^2K	Reynolds number (Re)	Experimental Nusselt number (Nu_e)	Predicted Nusselt number (Nu_T)	Fin effectiveness
(1)	(2)	(3)	(4)	(5)	(6)	(7)	(8)	(9)	(10)	(11)	(12)	(13)	(14)	(15)
1	20.0	3580	5.6	345.07	.9723	65.00	125.90	121.43	-3.68	161.39	72.08	1.20	1.16	0.9326
2			6.5	344.37	.9745	60.00	123.85	118.93	-4.14	158.76	83.23	1.18	1.14	0.9527
3			7.2	346.01	.9757	57.00	113.69	110.69	-2.71	145.73	93.06	1.09	1.06	0.8952
4			8.2	345.78	.9796	48.00	100.22	98.65	-1.59	128.47	106.10	.96	0.94	0.8494
5			9.1	347.19	.9847	36.00	97.03	93.34	-3.95	124.38	117.71	.93	0.89	0.9241
6			11.4	343.90	.9906	22.00	79.34	75.84	-4.63	101.71	147.14	.76	0.73	0.8578
7	20.0	5519	5.6	350.48	.9723	65.00	126.26	121.70	-3.75	161.85	72.08	1.21	1.16	0.9353
8			6.5	350.71	.9745	60.00	125.59	120.24	-4.45	160.99	83.23	1.20	1.15	0.9661
9			7.2	351.65	.9757	57.00	117.43	113.50	-3.46	150.52	93.06	1.12	1.09	0.9246

(contd..)

RESULT SHEET

Table -6.30 : Experimental Results on CFB Heat Transfer for 2 - Rectangular Finned Surface

d_p = 310 μm, d_b = 100 mm, k_g = 0.03242 W/mK, ρ_s = 2350 kg/m^3, ρ_g = 0.09218 kg/m^3, μg = 2.214 x 10^{-5} kg/ms

A_{ht} = 0.1046 m^2, L_m = 0.5 m, Pr = 0.692, e_p = 0.76, e_g = 0.036, e_w = 0.24

Serial number of runs	Bed inventory(I) Kg	Heat flux (q") W/m^2	Superficial velocity (U_o), m/s	Bed temperature (T_b) K	Voidage (ε)	Suspension density (ρ_{sus}) kg/m^3	Experimental heat transfer coefficient (h_e) W/m^{2}K	Predicted heat transfer coefficient (h_T), W/m^{2}K	% Error	Equivalent heat transfer coefficient (h_E), W/m^{2}K	Reynolds number (Re)	Experimental Nusselt number (Nu_e)	Predicted Nusselt number (Nu_T)	Fin effectiveness
(1)	(2)	(3)	(4)	(5)	(6)	(7)	(8)	(9)	(10)	(11)	(12)	(13)	(14)	(15)
10	20	5519	8.2	350.48	.9796	48.00	110.78	106.59	-3.93	142.00	106.10	1.06	1.02	0.9388
11			9.1	349.77	.9847	36.00	92.10	89.63	-2.75	118.06	117.71	.88	0.86	0.8771
12			11.4	349.54	.9906	22.00	84.74	79.93	-6.08	108.68	147.14	.81	0.76	0.9166
13	20.0	7876	5.6	356.82	.9723	65.00	126.95	122.22	-3.87	162.73	72.08	1.21	1.17	0.9404
14			6.5	355.41	.9745	60.00	127.43	121.62	-4.78	163.35	83.23	1.22	1.16	0.9803
15			7.2	355.88	.9757	57.00	126.00	119.94	-5.05	161.51	93.06	1.20	1.15	0.9921
16			8.2	355.18	.9796	48.00	116.78	111.10	-5.11	149.69	106.10	1.12	1.06	0.9896
17			9.1	359.17	.9847	36.00	103.12	97.92	-5.31	132.19	117.71	.99	0.94	0.9821
18			11.4	359.17	.9906	22.00	85.28	80.30	-6.20	109.32	147.14	.82	0.77	0.9219

RESULT SHEET

Table -6.31 : Experimental Results on CFB Heat Transfer for 2 - Rectangular Finned Surface

d_p = 310 μm, d_b = 100 mm, k_g = 0.03242 W/mK, ρ_s = 2350 kg/m^3, ρ_g = 0.09218 kg/m^3, μg = 2.214 x 10^{-5} kg/ms

A_{ht} = 0.1046 m^2, L_m = 0.5 m, Pr = 0.692, e_p = 0.76, e_g = 0.036, e_w = 0.24

Serial number of runs	Bed inventory(I) kg	Heat flux (q") W/m^2	Superficial velocity (U_o), m/s	Bed temperature (T_b) K	Voidage (ε)	Suspension density (ρ_{sus}) kg/m^3	Experimental heat transfer coefficient (h_e) W/m^{2}K	Predicted heat transfer coefficient (h_T), W/m^{2}K	% Error	Equivalent heat transfer coefficient (h_E), W/m^{2}K	Reynolds number (Re)	Experimental Nusselt number (Nu_e)	Predicted Nusselt number (Nu_T)	Fin effectiveness
(1)	(2)	(3)	(4)	(5)	(6)	(7)	(8)	(9)	(10)	(11)	(12)	(13)	(14)	(15)
19	26.0	3580	5.6	349.30	.9715	67.00	123.85	120.26	-2.98	158.76	72.08	1.18	1.15	0.8975
20			6.5	347.66	.9728	64.00	125.90	121.24	-3.84	161.39	83.23	1.20	1.16	0.9396
21			7.2	346.01	.9749	59.00	123.85	118.73	-4.31	158.76	93.06	1.18	1.14	0.9601
22			8.2	348.36	.9779	52.00	112.02	108.39	-3.34	143.59	106.10	1.07	1.04	0.9182
23			9.1	352.59	.9838	38.00	100.22	96.26	-4.12	128.47	117.71	.96	0.92	0.9280
24			11.4	353.77	.9885	27.00	85.11	81.81	-4.03	109.09	147.14	.81	0.78	0.8774
25	26.0	5519	5.6	345.47	.9715	67.00	125.59	121.57	-3.31	160.99	72.08	1.20	1.16	0.9101
26			6.5	356.12	.9728	64.00	129.04	123.60	-4.40	165.41	83.23	1.23	1.18	0.9630
27			7.2	354.24	.9749	59.00	122.96	118.06	-4.15	157.62	93.06	1.18	1.13	0.9532

(contd...)

RESULT SHEET

Table - 6.31 : Experimental Results on CFB Heat Transfer for 2 - Rectangular Finned Surface

d_p = 310 μm, d_b = 100 mm, k_g = 0.03242 W/mK, ρ_s = 2350 kg/m^3, ρ_g = 0.09218 kg/m^3, μg = 2.214 x 10^{-5} kg/ms

A_{ht} = 0.1046 m^2, L_m = 0.5 m, Pr = 0.692, e_p = 0.76, e_g = 0.036, e_w = 0.24

Serial number of runs	Bed inventory(I) kg	Heat flux (q") W/m^2	Superficial velocity (U_o), m/s	Bed temperature (T_b) K	Voidage (ε)	Suspension density (ρ_{sus}) kg/m^3	Experimental heat transfer coefficient (h_e) W/m^{2}K	Predicted heat transfer coefficient (h_T), W/m^{2}K	% Error	Equivalent heat transfer coefficient (h_E), W/m^{2}K	Reynolds number (Re)	Experimental Nusselt number (Nu_e)	Predicted Nusselt number (Nu_T)	Fin effectiveness
(1)	(2)	(3)	(4)	(5)	(6)	(7)	(8)	(9)	(10)	(11)	(12)	(13)	(14)	(15)
28	26	5519	8.2	354.71	.9779	52.00	117.43	112.46	-4.42	150.52	106.10	1.12	1.08	0.9625
29			9.1	352.36	.9838	38.00	101.67	97.35	-4.44	130.32	117.71	.97	0.93	0.9414
30			11.4	348.60	.9885	27.00	86.03	82.50	-4.27	110.27	147.14	.82	0.79	0.8869
31	26.0	7876	5.6	358.00	.9715	67.00	134.06	127.94	-4.78	171.85	72.08	1.28	1.22	0.9714
32			6.5	358.47	.9728	64.00	132.47	126.18	-4.98	169.81	83.23	1.27	1.21	0.9886
33			7.2	361.29	.9749	59.00	126.95	121.06	-4.86	162.73	93.06	1.21	1.16	0.9741
34			8.2	359.88	.9779	52.00	118.85	113.53	-4.68	152.35	106.10	1.14	1.09	0.9742
35			9.1	361.76	.9838	38.00	102.49	97.97	-4.62	131.38	117.71	.98	0.94	0.9490
36			11.4	363.88	.9885	27.00	87.51	83.61	-4.66	112.17	147.14	.84	0.80	0.9021

RESULT SHEET

Table - 6.32 : Experimental Results on CFB Heat Transfer for 2 - Rectangular Finned Surface

d_p = 310 μm, d_b = 100 mm, k_g = 0.03242 W/mK, ρ_s = 2350 kg/m^3, ρ_g = 0.09218 kg/m^3, μg = 2.214 x 10^{-5} kg/ms

A_{ht} = 0.1046 m^2, L_m = 0.5 m, Pr = 0.692, e_p = 0.76, e_g = 0.036, e_w = 0.24

Serial number of runs	Bed inventory (I) kg	Heat flux (q") W/m^2	Superficial velocity (U_o), m/s	Bed temperature (T_b) K	Voidage (ε)	Suspension density (ρ_{sus}) kg/m^3	Experimental heat transfer coefficient (h_e) W/m^{2}K	Predicted heat transfer coefficient (h_T), W/m^{2}K	% Error	Equivalent heat transfer coefficient (h_E), W/m^{2}K	Reynolds number (Re)	Experimental Nusselt number (Nu_e)	Predicted Nusselt number (Nu_T)	Fin effectiveness
(1)	(2)	(3)	(4)	(5)	(6)	(7)	(8)	(9)	(10)	(11)	(12)	(13)	(14)	(15)
37	32.0	3508	5.6	347.42	.9689	73.00	126.95	123.67	-2.65	162.73	72.08	1.21	1.18	0.8847
38			6.5	348.60	.9702	70.00	129.10	124.76	-3.48	165.49	83.23	1.23	1.19	0.9222
39			7.2	350.95	.9736	62.00	124.87	120.09	-3.98	160.07	93.06	1.19	1.15	0.9496
40			8.2	350.48	.9770	54.00	103.63	102.51	-1.09	132.84	106.10	.99	0.98	0.8600
41			9.1	350.48	.9821	42.00	100.22	97.26	-3.05	128.47	117.71	.96	0.93	0.8989
42			11.4	350.48	.9872	30.00	80.18	79.01	-1.48	102.78	147.14	.77	0.76	0.8099
43	32.0	5519	5.6	356.35	.9689	73.00	132.68	127.98	-3.67	170.08	72.08	1.27	1.22	0.9246
44			6.5	354.00	.9702	70.00	132.68	127.45	-4.11	170.08	83.23	1.27	1.22	0.9477
45			7.2	355.41	.9736	62.00	128.33	122.69	-4.60	164.51	93.06	1.23	1.17	0.9759

(contd...)

RESULT SHEET

Table - 6.32 : Experimental Results on CFB Heat Transfer for 2 - Rectangular Finned Surface

d_p = 310 μm, d_b = 100 mm, k_g = 0.03242 W/mK, ρ_s = 2350 kg/m^3, ρ_g = 0.09218 kg/m^3, μg = 2.214 x 10^{-5} kg/ms

A_{ht} = 0.1046 m^2, L_m = 0.5 m, Pr = 0.692, e_p = 0.76, e_g = 0.036, e_w = 0.24

Serial number of runs	Bed inventory(I) kg	Heat flux (q") W/m^2	Superficial velocity (U_o), m/s	Bed temperature (T_b) K	Voidage (ε)	Suspension density (ρ_{sus}) kg/m^3	Experimental heat transfer coefficient (h_e) W/m2K	Predicted heat transfer coefficient (h_T), W/m^{2}K	% Error	Equivalent heat transfer coefficient (h_E), W/m^{2}K	Reynolds number (Re)	Experimental Nusselt number (Nu_e)	Predicted Nusselt number (Nu_T)	Fin effectiveness
(1)	(2)	(3)	(4)	(5)	(6)	(7)	(8)	(9)	(10)	(11)	(12)	(13)	(14)	(15)
46	32	5519	8.2	355.65	.9770	54.00	111.83	108.68	-2.90	143.36	106.10	1.07	1.04	0.9281
47			9.1	353.53	.9821	42.00	102.56	99.01	-3.58	131.46	117.71	.98	0.95	0.9198
48			11.4	351.42	.9872	30.00	89.98	86.38	-4.17	115.34	147.14	.86	0.83	0.9089
49	32.0	7876	5.6	358.70	.9689	73.00	137.36	131.50	-4.46	176.07	72.08	1.31	1.26	0.9572
50			6.5	357.76	.9702	70.00	136.24	130.12	-4.70	174.64	83.23	1.30	1.24	0.9731
51			7.2	361.29	.9736	62.00	126.00	120.93	-4.19	161.51	93.06	1.20	1.16	0.9581
52			8.2	361.76	.9770	54.00	118.43	113.64	-4.22	151.81	106.10	1.13	1.09	0.9828
53			9.1	358.23	.9821	42.00	102.49	98.96	-3.57	131.38	117.71	.98	0.95	0.9192
54			11.4	357.76	.9872	30.00	91.57	87.57	-4.57	117.38	147.14	.88	0.84	0.9250

RESULT SHEET

Table - 6.33 : Experimental Results on CFB Heat Transfer for 4 - Rectangular Finned Surface

d_p = 310 μm, d_b = 100 mm, k_g = 0.03242 W/mK, ρ_s = 2350 kg/m^3, ρ_g = 0.09218 kg/m^3, μg = 2.214 x 10^{-5} kg/ms

A_{ht} = 0.1277 m^2, L_m = 0.5 m, Pr = 0.692, e_p = 0.76, e_g = 0.036, e_w = 0.24

Serial number of runs	Bed inventory(I) kg	Heat flux (q") W/m^2	Superficial velocity (U_o), m/s	Bed temperature (T_b) K	Voidage (ϵ)	Suspension density (ρ_{sus}) kg/m^3	Experimental heat transfer coefficient (h_e) W/m^{2}K	Predicted heat transfer coefficient (h_T), W/m^{2}K	% Error	Equivalent heat transfer coefficient (h_E), W/m^{2}K	Reynolds number (Re)	Experimental Nusselt number (Nu_e)	Predicted Nusselt number (Nu_T)	Fin effectiveness
(1)	(2)	(3)	(4)	(5)	(6)	(7)	(8)	(9)	(10)	(11)	(12)	(13)	(14)	(15)
1	20.0	3580	5.6	343.19	.9745	60.00	114.37	110.07	-3.90	178.98	72.08	1.09	1.05	0.8798
2			6.5	343.62	.9762	56.00	114.63	108.91	-5.25	179.39	83.23	1.10	1.04	0.9097
3			7.2	344.60	.9779	52.00	107.97	103.59	-4.22	168.96	93.06	1.03	0.99	0.8850
4			8.2	344.23	.9817	43.00	95.15	92.67	-2.68	148.91	106.10	.91	0.89	0.8496
5			9.1	344.98	.9864	32.00	80.65	79.41	-1.55	126.21	117.71	.77	0.76	0.7985
6			11.4	343.57	.9915	20.00	75.08	69.84	-7.50	117.50	147.14	.72	0.67	0.8342
7	20.0	5519	5.6	348.95	.9745	60.00	117.72	112.06	-5.05	184.23	72.08	1.13	1.07	0.9055
8			6.5	347.78	.9762	56.00	120.13	112.17	-7.09	188.00	83.23	1.15	1.07	0.9534
9			7.2	347.59	.9779	52.00	113.02	106.59	-6.04	176.87	93.06	1.08	1.02	0.9264

(contd...)

RESULT SHEET

Table -6.33 : Experimental Results on CFB Heat Transfer for 4 - Rectangular Finned Surface

d_p = 310 μm, d_b = 100 mm, k_g = 0.03242 W/mK, ρ_s = 2350 kg/m^3, ρ_g = 0.09218 kg/m^3, μg = 2.214 x 10^{-5} kg/ms

A_{ht} = 0.1277 m^2, L_m = 0.5 m, Pr = 0.692, e_p = 0.76, e_g = 0.036, e_w = 0.24

Serial number of runs	Bed inventory(I) kg	Heat flux (q") W/m^2	Superficial velocity (U_o), m/s	Bed temperature (T_b) K	Voidage (ε)	Suspension density (ρ_{sus}) kg/m^3	Experimental heat transfer coefficient (h_e) W/m^{2}K	Predicted heat transfer coefficient (h_T), W/m^{2}K	% Error	Equivalent heat transfer coefficient (h_E), W/m^{2}K	Reynolds number (Re)	Experimental Nusselt number (Nu_e)	Predicted Nusselt number (Nu_T)	Fin effectiveness
(1)	(2)	(3)	(4)	(5)	(6)	(7)	(8)	(9)	(10)	(11)	(12)	(13)	(14)	(15)
10	20	5519	8.2	347.07	.9817	43.00	106.03	99.12	-6.97	165.93	106.10	1.01	0.95	0.9467
11			9.1	342.91	.9864	32.00	88.86	84.28	-5.43	139.06	117.71	.85	0.81	0.8798
12			11.4	343.76	.9915	20.00	76.82	70.87	-8.40	120.23	147.14	.73	0.68	0.8536
13	20.0	7876	5.6	353.18	.9745	60.00	119.02	112.83	-5.49	186.25	72.08	1.14	1.08	0.9155
14			6.5	352.95	.9762	56.00	122.32	113.47	-7.80	191.42	83.23	1.17	1.09	0.9708
15			7.2	349.77	.9779	52.00	117.10	109.01	-7.43	183.26	93.06	1.12	1.04	0.9599
16			8.2	350.01	.9817	43.00	109.06	100.92	-8.07	170.68	106.10	1.04	0.97	0.9738
17			9.1	346.98	.9864	32.00	92.86	86.66	-7.17	145.33	117.71	.89	0.83	0.9195
18			11.4	347.24	.9915	20.00	78.49	71.86	-9.22	122.83	147.14	.75	0.69	0.8721

RESULT SHEET

Table - 6.34 : Experimental Results on CFB Heat Transfer for 4 - Rectangular Finned Surface

d_p = 310 μm, d_b = 100 mm, k_g = 0.03242 W/mK, ρ_s = 2350 kg/m^3, ρ_g = 0.09218 kg/m^3, μg = 2.214 x 10^{-5} kg/ms

A_{ht} = 0.1277 m^2 L_m = 0.5 m, Pr = 0.692, e_p = 0.76, e_g = 0.036 , e_w = 0.24

Serial number of runs	Bed inventory(I) kg	Heat flux (q") W/m^2	Superficial velocity (U_o), m/s	Bed temperature (T_b) K	Voidage (ε)	Suspension density (ρ_{sus}) kg/m^3	Experimental heat transfer coefficient (h_e) W/m^{2}K	Predicted heat transfer coefficient (h_T), W/m^{2}K	% Error	Equivalent heat transfer coefficient (h_E), W/m^{2}K	Reynolds number (Re)	Experimental Nusselt number (Nu_e)	Predicted Nusselt number (Nu_T)	Fin effectiveness
(1)	(2)	(3)	(4)	(5)	(6)	(7)	(8)	(9)	(10)	(11)	(12)	(13)	(14)	(15)
19	26.0	3580	5.6	342.77	.9728	64.00	117.55	113.22	-3.82	183.95	72.08	1.12	1.08	0.8838
20			6.5	341.86	.9753	58.00	107.43	105.31	-2.02	168.13	83.23	1.03	1.01	0.8393
21			7.2	340.96	.9770	54.00	106.76	103.57	-3.08	167.07	93.06	1.02	0.99	0.8609
22			8.2	340.42	.9800	47.00	103.28	99.01	-4.31	161.63	106.10	0.99	0.95	0.8827
23			9.1	340.37	.9847	36.00	82.21	82.13	-0.10	128.66	117.71	0.79	0.79	0.7830
24			11.4	339.55	.9898	24.00	74.79	71.95	-3.95	117.04	147.14	0.72	0.69	0.8042
25	26.0	5519	5.6	349.80	.9728	64.00	121.75	115.71	-5.22	190.53	72.08	1.16	1.11	0.9154
26			6.5	348.27	.9753	58.00	117.78	111.44	-5.69	184.32	83.23	1.13	1.07	0.9201
27			7.2	347.03	.9770	54.00	116.61	109.41	-6.58	182.49	93.06	1.12	1.05	0.9404

(Contd....)

RESULT SHEET

Table - 6.34 : Experimental Results on CFB Heat Transfer for 4 - Rectangular Finned Surface

d_p = 310 μm, d_b = 100 mm, k_g = 0.03242 W/mK, ρ_s = 2350 kg/m^3, ρ_g = 0.09218 kg/m^3, μg = 2.214 x 10^{-5} kg/ms

A_{ht} = 0.1277 m^2 L_m = 0.5 m, Pr = 0.692, e_p = 0.76, e_g = 0.036 , e_w = 0.24

Serial number of runs	Bed inventory(I) kg	Heat flux (q") W/m^2	Superficial velocity (U_o), m/s	Bed temperature (T_b) K	Voidage (ε)	Suspension density (ρ_{sus}) kg/m^3	Experimental heat transfer coefficient (h_e) W/m^{2}K	Predicted heat transfer coefficient (h_T), W/m^{2}K	% Error	Equivalent heat transfer coefficient (h_E), W/m^{2}K	Reynolds number (Re)	Experimental Nusselt number (Nu_e)	Predicted Nusselt number (Nu_T)	Fin effectiveness
(1)	(2)	(3)	(4)	(5)	(6)	(7)	(8)	(9)	(10)	(11)	(12)	(13)	(14)	(15)
28			8.2	346.98	.9800	47.00	107.98	101.80	-6.07	168.98	106.10	1.03	0.97	0.9229
29			9.1	346.06	.9847	36.00	93.27	88.68	-5.17	145.96	117.71	0.89	0.85	0.8883
30			11.4	345.62	.9898	24.00	80.21	75.16	-6.72	125.52	147.14	0.77	0.72	0.8625
31	26.0	7876	5.6	354.19	.9728	64.00	122.23	115.99	-5.37	191.28	72.08	1.17	1.11	0.9190
32			6.5	351.89	.9753	58.00	119.06	112.20	-6.11	186.32	83.23	1.14	1.07	0.9301
33			7.2	348.79	.9770	54.00	108.25	104.45	-3.64	169.41	93.06	1.04	1.00	0.8730
34			8.2	348.98	.9800	47.00	102.06	98.28	-3.84	159.71	106.10	0.98	0.94	0.8723
35			9.1	348.55	.9847	36.00	84.59	83.54	-1.26	132.38	117.71	0.81	0.80	0.8056
36			11.4	349.30	.9898	24.00	80.28	75.2	-6.75	125.63	147.14	0.77	0.72	0.8632

RESULT SHEET

Table -6.35 : Experimental Results on CFB Heat Transfer for 4 - Rectangular Finned Surface

d_p = 310 μm, d_b = 100 mm, k_g = 0.03242 W/mK, ρ_s = 2350 kg/m^3, ρ_g = 0.09218 kg/m^3, μ_g = 2.214 x 10^{-5} kg/ms

A_{ht} = 0.1277 m^2 L_m = 0.5 m, Pr = 0.692, e_p = 0.76, e_g = 0.036 , e_w = 0.24

Serial number of runs	Bed inventory(I) kg	Heat flux (q") W/m^2	Superficial velocity (U_o), m/s	Bed temperature (T_b) K	Voidage (ε)	Suspension density (ρ_{sus}) kg/m^3	Experimental heat transfer coefficient (h_e) W/m^{2}K	Predicted heat transfer coefficient (h_T), W/m^{2}K	% Error	Equivalent heat transfer coefficient (h_E), W/m^{2}K	Reynolds number (Re)	Experimental Nusselt number (Nu_e)	Predicted Nusselt number (Nu_T)	Fin effectiveness
(1)	(2)	(3)	(4)	(5)	(6)	(7)	(8)	(9)	(10)	(11)	(12)	(13)	(14)	(15)
37	32.0	3580	5.6	342.42	.9715	67.00	117.73	114.25	-3.05	184.24	72.08	1.13	1.09	0.8531
38			6.5	343.57	.9723	65.00	111.28	109.81	-1.33	174.15	83.23	1.06	1.05	0.8243
39			7.2	342.00	.9762	56.00	106.46	104.07	-2.30	166.60	93.06	1.02	1.00	0.8449
40			8.2	341.88	.9779	52.00	102.45	100.32	-2.12	160.10	106.10	0.98	0.96	0.8397
41			9.1	341.57	.9830	40.00	95.21	91.51	-4.05	149.00	117.71	0.91	0.88	0.8735
42			11.4	341.29	.9881	28.00	79.22	76.65	-3.35	123.98	147.14	0.76	0.73	0.8252
43	32.0	5519	5.6	346.81	.9715	67.00	122.77	117.23	-4.72	192.12	72.08	1.17	1.12	0.8896
44			6.5	346.91	.9723	65.00	122.77	116.62	-5.27	192.12	83.23	1.17	1.12	0.9094
45			7.2	346.27	.9762	56.00	118.07	110.95	-6.42	184.78	93.06	1.13	1.06	0.9371

(contd....)

RESULT SHEET

Table -6.35 : Experimental Results on CFB Heat Transfer for 4 - Rectangular Finned Surface

d_p = 310 μm, d_b = 100 mm, k_g = 0.03242 W/mK, ρ_s = 2350 kg/m^3, ρ_g = 0.09218 kg/m^3, μg = 2.214 x 10^{-5} kg/ms

A_{ht} = 0.1277 m^2 L_m = 0.5 m, Pr = 0.692, e_p = 0.76, e_g = 0.036 , e_w = 0.24

Serial number of runs	Bed inventory(I) kg	Heat flux (q") W/m^2	Superficial velocity (U_o), m/s	Bed temperature (T_b) K	Voidage (ϵ)	Suspension density (ρ_{sus}) kg/m^3	Experimental heat transfer coefficient (h_e) W/m^{2}K	Predicted heat transfer coefficient (h_T), W/m^{2}K	% Error	Equivalent heat transfer coefficient (h_E), W/m^{2}K	Reynolds number (Re)	Experimental Nusselt number (Nu_e)	Predicted Nusselt number (Nu_T)	Fin effectiveness
(1)	(2)	(3)	(4)	(5)	(6)	(7)	(8)	(9)	(10)	(11)	(12)	(13)	(14)	(15)
46	32.0	5519	8.2	346.63	.9779	52.00	111.04	105.41	-5.34	173.77	106.10	1.06	1.01	0.9914
47			9.1	344.77	.9830	40.00	95.94	91.94	-4.35	150.13	117.71	0.92	0.88	0.8801
48			11.4	344.37	.9881	28.00	83.04	78.92	-5.23	129.96	147.14	0.79	0.76	0.8651
49	32.0	7876	5.6	348.79	.9715	67.00	123.99	117.96	-5.11	194.04	72.08	1.19	1.13	0.8985
50			6.5	348.39	.9723	65.00	122.32	116.36	-5.12	191.42	83.23	1.17	1.11	0.9061
51			7.2	349.23	.9762	56.00	116.17	109.82	-5.78	181.80	93.06	1.11	1.05	0.9220
52			8.2	349.23	.9779	52.00	111.94	105.95	-5.66	175.18	106.10	1.07	1.01	0.9175
53			9.1	348.08	.9830	40.00	95.02	91.40	-3.97	148.71	117.71	0.91	0.87	0.8718
54			11.4	347.99	.9881	28.00	85.02	80.09	-6.16	133.05	147.14	0.81	0.77	0.8856

RESULT SHEET

Table - 6.36: Experimental Results on CFB Heat Transfer for 8 - Rectangular Finned Surface

d_p = 310 μm, d_b = 100 mm, k_g = 0.03242 W/mK, ρ_s = 2350 kg/m^3, ρ_g = 0.09218 kg/m^3, μ_g = 2.214 x 10^{-5} kg/ms

A_{ht} = 0.1743 m^2 L_m = 0.5 m, Pr = 0.692, e_p = 0.76, e_g = 0.036 , e_w = 0.24

Serial number of runs	Bed Inventory(I) kg	Heat flux (q") W/m^2	Superficial velocity (U_o), m/s	Bed temperature (T_b) K	Voidage (ε)	Suspension density (ρ_{sus}) kg/m^3	Experimental heat transfer coefficient (h_e) W/m^{2}K	Predicted heat transfer coefficient (h_T), W/m^{2}K	% Error	Equivalent heat transfer coefficient (h_E), W/m^{2}K	Reynolds number (Re)	Experimental Nusselt number (Nu_e)	Predicted Nusselt number (Nu_T)	Fin effectiveness
(1)	(2)	(3)	(4)	(5)	(6)	(7)	(8)	(9)	(10)	(11)	(12)	(13)	(14)	(15)
1	20.0	5519	5.6	352.34	.9800	47.00	89.43	91.18	1.92	191.03	72.08	0.86	0.87	0.7644
2			6.5	352.81	.9821	42.00	85.81	86.92	1.29	183.28	83.23	0.82	0.83	0.7696
3			7.2	352.15	.9834	39.00	84.00	84.42	0.51	179.42	93.06	0.80	0.81	0.7706
4			8.2	348.53	.9855	34.00	79.05	79.30	0.31	168.85	106.10	0.76	0.76	0.7675
5			9.1	347.24	.9894	25.00	70.29	69.40	-1.29	150.15	117.71	0.67	0.66	0.7478
6			11.4	346.84	.9923	18.00	58.99	58.93	-0.10	126.01	147.14	0.56	0.56	0.6781

RESULT SHEET

Table - 6.37 : Experimental Results on CFB Heat Transfer for 16 - Pin Finned Surface

d_p = 310 μm, d_b = 100 mm, k_g = 0.03242 W/mK, ρ_s = 2350 kg/m^3, ρ_g = 0.09218 kg/m^3, μ_g = 2.214 x 10^{-5} kg/ms

A_{ht} = 0.0864 m^2 L_m = 0.5 m, Pr = 0.692, e_p = 0.76, e_g = 0.036 , e_w = 0.24

Serial number of runs	Bed inventory(I) kg	Heat flux (q") W/m^2	Superficial velocity (U_o), m/s	Bed temperature (T_b) K	Voidage (ε)	Suspension density (ρ_{sus}) kg/m^3	Experimental heat transfer coefficient (h_e) W/m^{2}K	Predicted heat transfer coefficient (h_T), W/m^{2}K	% Error	Equivalent heat transfer coefficient (h_E), W/m^{2}K	Reynolds number (Re)	Experimental Nusselt number (Nu_e)	Predicted Nusselt number (Nu_T)	Fin effectiveness
(1)	(2)	(3)	(4)	(5)	(6)	(7)	(8)	(9)	(10)	(11)	(12)	(13)	(14)	(15)
1	20	3580	5.6	340.61	.9728	64.0	120.91	120.59	-0.26	128.02	72.08	1.16	1.15	.9023
2			6.5	339.43	.9770	54.0	112.02	111.70	-0.28	118.6	83.23	1.07	1.07	.8961
3			7.2	338.73	.9779	52.0	111.20	110.82	-0.34	117.74	93.06	1.06	1.06	.8968
4			8.2	336.85	.9813	44.0	108.04	107.37	-0.62	114.40	106.1	1.03	1.03	.9314
5			9.1	336.85	.9838	38.0	100.22	99.64	-0.59	106.12	117.71	0.96	0.95	.8869
6			11.4	335.67	.9898	24.0	87.05	86.18	-1.01	92.17	147.14	0.83	0.82	.8974
7	20	5519	5.6	343.43	.9728	64.0	119.82	119.57	-0.21	126.87	72.08	1.15	1.14	.8942
8			6.5	342.72	.9770	54.0	114.01	114.57	-0.38	120.71	83.23	1.09	1.09	.9120
9			7.2	342.02	.9779	52.0	110.26	109.94	-0.29	116.74	93.06	1.05	1.05	.8892

(contd....)

RESULT SHEET

Table -6.37: Experimental Results on CFB Heat Transfer for 16 - Pin Finned Surface

d_p = 310 µm, d_b = 100 mm, k_g = 0.03242 W/mK, ρ_s = 2350 kg/m^3, ρ_g = 0.09218 kg/m^3, μ_g = 2.214 x 10^{-5} kg/ms

A_{ht} = 0.0864 m^2 L_m = 0.5 m, Pr = 0.692, e_p = 0.76, e_g = 0.036, e_w = 0.24

Serial number of runs	Bed inventory(I) kg	Heat flux (q") W/m^2	Superficial velocity (U_o), m/s	Bed temperature (T_b) K	Voidage (ϵ)	Suspension density (ρ_{sus}) kg/m^3	Experimental heat transfer coefficient (h_e) W/m^{2}K	Predicted heat transfer coefficient (h_T), W/m^{2}K	% Error	Equivalent heat transfer coefficient (h_E), W/m^{2}K	Reynolds number (Re)	Experimental Nusselt number (Nu_e)	Predicted Nusselt number (Nu_T)	Fin effectiveness
(1)	(2)	(3)	(4)	(5)	(6)	(7)	(8)	(9)	(10)	(11)	(12)	(13)	(14)	(15)
10	20	5519	8.2	342.49	.9813	44.0	109.74	108.97	-0.71	116.20	106.10	1.05	1.04	.9461
11			9.1	338.73	.9838	38.0	101.23	100.58	-0.64	107.18	117.71	0.97	0.96	.8958
12			11.4	338.02	.9898	24.0	89. 98	88.93	-1.18	95.27	147.14	0.86	0.85	.9276
13	20	7876	5.6	349.07	.9728	64.0	123.22	122.76	-0.38	130.46	72.08	1.18	1.17	.9195
14			6.5	347.19	.9770	54.0	118.85	118.12	-0.62	125.84	83.23	1.14	1.13	.9508
15			7.2	345.54	.9779	52.0	114.00	113.45	-0.48	120.70	93.06	1.09	1.08	.9193
16			8.2	344.60	.9813	44.0	108.11	107.44	-0.63	114.47	106.10	1.03	1.03	.9320
17			9.1	341.55	.9838	38.0	104.41	103.57	-0.81	110.55	117.71	1.00	0.99	.9240
18			11.4	341.08	.9898	24.0	90.09	89.04	-1.18	95.39	147.14	0.86	0.85	.9288

RESULT SHEET

Table - 6.38: Experimental Results on CFB Heat Transfer for 16 - Pin Finned Surface

d_p = 310 μm, d_b = 100 mm, k_g = 0.03242 W/mK, ρ_s = 2350 kg/m^3, ρ_g = 0.09218 kg/m^3, μ_g = 2.214 x 10^{-5} kg/ms

A_{ht} = 0.0864 m^2 L_m = 0.5 m, Pr = 0.692, e_b = 0.76, e_g = 0.036, e_w = 0.24

Serial number of runs	Bed inventory(I) kg	Heat flux (q") W/m^2	Superficial velocity (U_o), m/s	Bed temperature (T_b) K	Voidage (ε)	Suspension density (ρ_{sus}) kg/m^3	Experimental heat transfer coefficient (h_e) W/m^{2}K	Predicted heat transfer coefficient (h_T), W/m^{2}K	% Error	Equivalent heat transfer coefficient (h_E), W/m^{2}K	Reynolds number (Re)	Experimental Nusselt number (Nu_e)	Predicted Nusselt number (Nu_T)	Fin effectiveness
(1)	(2)	(3)	(4)	(5)	(6)	(7)	(8)	(9)	(10)	(11)	(12)	(13)	(14)	(15)
19	26	3580	5.6	339.90	.9715	67.0	120.91	120.74	-0.14	128.02	72.08	1.16	1.15	.8761
20			6.5	338.73	.9753	58.0	118.09	117.63	-0.39	125.04	83.23	1.13	1.12	.9084
21			7.2	338.96	.9766	55.0	116.29	115.77	-0.45	123.13	93.06	1.11	1.11	.9085
22			8.2	338.26	.9787	50.0	112.02	111.47	-0.49	118.60	106.10	1.07	1.07	.9107
23			9.1	337.79	.9830	40.0	105.79	105.08	-0.75	112.02	117.71	1.01	1.00	.9280
24			11.4	336.26	.9885	27.0	90.95	90.10	-0.94	96.30	147.17	0.87	0.86	.9095
25	26	5519	5.6	342.72	.9715	67.0	121.68	121.47	-0.18	128.84	72.08	1.16	1.16	.8818
26			6.5	343.55	.9753	58.0	118.91	118.40	-0.43	125.91	83.23	1.14	1.13	.9147
27			7.2	337.44	.9766	55.0	114.84	114.41	-0.38	121.60	93.06	1.10	1.09	.8972

(Contd....)

RESULT SHEET

Table - 6.38 : Experimental Results on CFB Heat Transfer for 16 - Pin Finned Surface

d_p = 310 μm, d_b = 100 mm, k_g = 0.03242 W/mK, ρ_s = 2350 kg/m^3, ρ_g = 0.09218 kg/m^3, μ_g = 2.214 x 10^{-5} kg/ms

A_{ht} = 0.0864 m^2 L_m = 0.5 m, Pr = 0.692, e_p = 0.76, e_g = 0.036, e_w = 0.24

Serial number of runs	Bed inventory(I) kg	Heat flux (q") W/m^2	Superficial velocity (U_o), m/s	Bed temperature (T_b) K	Voidage (ε)	Suspension density (ρ_{sus}) kg/m^3	Experimental heat transfer coefficient (h_e) W/m^{2}K	Predicted heat transfer coefficient (h_T), W/m^{2}K	% Error	Equivalent heat transfer coefficient (h_E), W/m^{2}K	Reynolds number (Re)	Experimental Nusselt number (Nu_e)	Predicted Nusselt number (Nu_T)	Fin effectiveness
(1)	(2)	(3)	(4)	(5)	(6)	(7)	(8)	(9)	(10)	(11)	(12)	(13)	(14)	(15)
28	26	5519	8.2	335.32	.9787	50.0	112.10	111.55	-0.49	118.69	106.10	1.07	1.07	.9114
29			9.1	336.85	.9830	40.0	108.23	107.29	-0.88	114.59	117.71	1.03	1.03	.9494
30			11.4	334.97	.9885	27.0	91.03	90.17	-0.95	96.38	147.14	0.87	0.86	.9103
31	26	7876	5.6	345.78	.9715	67.0	124.08	123.72	-0.29	131.38	72.08	1.19	1.18	.8992
32			6.5	342.14	.9753	58.0	119.91	119.34	-0.48	126.96	83.23	1.15	1.14	.9224
33			7.2	341.43	.9766	55.0	118.01	117.39	-0.53	124.95	93.06	1.13	1.12	.9220
34			8.2	342.96	.9787	50.0	114.0	113.33	-0.59	120.70	106.10	1.09	1.08	.9268
35			9.1	343.22	.9830	40.0	107.11	106.24	-0.82	113.41	117.71	1.02	1.02	.9396
36			11.4	343.19	.9885	27.0	94.01	92.98	-1.11	99.54	147.14	0.90	0.89	.9401

RESULT SHEET

Table - 6.39 : Experimental Results on CFB Heat Transfer for 16 - Pin Finned Surface

d_p = 310 μm, d_b = 100 mm, k_g = 0.03242 W/mK, ρ_s = 2350 kg/m^3, ρ_g = 0.09218 kg/m^3, μ_g = 2.214 x 10^{-5} kg/ms

A_{ht} = 0.0864 m^2 L_m = 0.5 m, Pr = 0.692, e_p = 0.76, e_g = 0.036, e_w = 0.24

Serial number of runs	Bed inventory (I) kg	Heat flux (q") W/m^2	Superficial velocity (U_o), m/s	Bed temperature (T_b) K	Voidage (ε)	Suspension density (ρ_{sus}) kg/m^3	Experimental heat transfer coefficient (h_e) W/m^{2}K	Predicted heat transfer coefficient (h_T), W/m^{2}K	% Error	Equivalent heat transfer coefficient (h_E), W/m^{2}K	Reynolds number (Re)	Experimental Nusselt number (Nu_e)	Predicted Nusselt number (Nu_T)	Fin effectiveness
(1)	(2)	(3)	(4)	(5)	(6)	(7)	(8)	(9)	(10)	(11)	(12)	(13)	(14)	(15)
37	32	3580	5.6	336.80	.9711	68.0	121.68	121.51	-0.13	128.84	72.08	1.16	1.16	.8754
38			6.5	336.26	.9723	65.0	118.55	118.43	-0.10	125.53	83.23	1.13	1.13	.8782
39			7.2	334.19	.9749	59.0	117.82	117.43	-0.33	124.75	93.06	1.13	1.12	.9133
40			8.2	334.15	.9770	54.0	111.60	111.32	-0.26	118.17	106.10	1.07	1.06	.8928
41			9.1	332.67	.9826	41.0	101.02	100.59	-0.43	106.96	117.71	0.97	0.96	.8784
42			11.[illegible]	330.79	.9872	30.0	93.00	92.27	-0.79	98.47	147.14	0.89	0.88	.9118
43	32	5519	5.6	339.93	.9711	68.0	119.27	119.26	-0.01	126.29	72.08	1.14	1.14	.8581
44			6.5	337.34	.9733	65.0	124.99	124.47	-0.42	132.34	83.23	1.20	1.19	.9258
45			7.2	339.15	.9749	59.0	124.13	123.35	-0.63	131.43	93.06	1.19	1.18	.9622

(Contd ....)

RESULT SHEET

Table - 6.39 : Experimental Results on CFB Heat Transfer for 16 - Pin Finned Surface

d_p = 310 μm, d_b = 100 mm, k_g = 0.03242 W/mK, ρ_s = 2350 kg/m^3, ρ_g = 0.09218 kg/m^3, μ_g = 2.214 x 10^{-5} kg/ms

A_{ht} = 0.0864 m^2 L_m = 0.5 m, Pr = 0.692, e_p = 0.76, e_g = 0.036 , e_w = 0.24

Serial number of runs	Bed inventory(I) kg	Heat flux (q") W/m^2	Superficial velocity (U_o), m/s	Bed temperature (T_b) K	Voidage (ε)	Suspension density (ρ_{sus}) kg/m^3	Experimental heat transfer coefficient (h_e) W/m^{2}K	Predicted heat transfer coefficient (h_T), W/m^{2}K	% Error	Equivalent heat transfer coefficient (h_E), W/m^{2}K	Reynolds number (Re)	Experimental Nusselt number (Nu_e)	Predicted Nusselt number (Nu_T)	Fin effectiveness
(1)	(2)	(3)	(4)	(5)	(6)	(7)	(8)	(9)	(10)	(11)	(12)	(13)	(14)	(15)
46	32	5519	8.2	335.49	.9770	54.0	110.00	109.81	-0.17	116.47	106.10	1.05	1.05	.8800
47			9.1	336.97	.9826	41.0	103.96	103.35	-0.59	110.08	117.71	0.99	0.99	.9040
48			11.4	344.56	.9872	30.0	93.87	93.08	-0.84	99.39	147.14	0.90	0.89	.9202
49	32	7876	5.6	350.95	.9711	68.0	125.06	124.68	-0.30	132.41	72.08	1.20	1.19	.8997
50			6.5	347.87	.9723	65.0	125.95	125.37	-0.46	133.36	83.23	1.20	1.20	.9330
51			7.2	347.92	.9749	59.0	122.63	121.94	-0.56	129.84	93.06	1.17	1.17	.9566
52			8.2	345.24	.9770	54.0	111.98	111.67	-0.28	118.56	106.10	1.07	1.07	.8958
53			9.1	346.06	.9826	41.0	108.89	107.97	-0.85	115.29	117.71	1.04	1.03	.9468
54			11.4	342.77	.9872	30.0	97.0	96.03	-1.02	102.71	147.14	0.93	0.92	.9510

RESULT SHEET

Table - 6.40: Experimental Results on CFB Heat Transfer for 32 - Pin Finned Surface

d_p = 310 μm, d_b = 100 mm, k_g = 0.03242 W/mK, ρ_s = 2350 kg/m^3, ρ_g = 0.09218 kg/m^3, μ_g = 2.214 x 10^{-5} kg/ms

A_{ht} = 0.0912 m^2 L_m = 0.5 m, Pr = 0.692, e_p = 0.76, e_g = 0.036, e_w = 0.24

Serial number of runs	Bed inventory(I) kg	Heat flux (q") W/m^2	Superficial velocity (U_o), m/s	Bed temperature (T_b) K	Voidage (ε)	Suspension density (ρ_{sus}) kg/m^3	Experimental heat transfer coefficient (h_e) W/m^{2}K	Predicted heat transfer coefficient (h_T), W/m^{2}K	% Error	Equivalent heat transfer coefficient (h_E), W/m^{2}K	Reynolds number (Re)	Experimental Nusselt number (Nu_e)	Predicted Nusselt number (Nu_T)	Fin effectiveness
(1)	(2)	(3)	(4)	(5)	(6)	(7)	(8)	(9)	(10)	(11)	(12)	(13)	(14)	(15)
1	2o	5519	5.6	341.22	.9745	6o.o	116.32	115.85	-o.4o	13o.o1	72.o8	1.11	1.11	.8948
2			6.5	342.o7	.9774	53.o	112.96	112.15	-o.72	126.25	83.23	1.o8	1.o7	.9o37
3			7.2	341.78	.9783	51.o	111.25	11o.42	-o.75	124.34	93.o6	1.o6	1.o6	.9o45
4			8.2	341.48	.98o9	45.o	1o1.o5	1oo.72	-o.33	112.94	1o6.1o	o.97	o.96	.8600
5			9.1	339.41	.9847	36.o	95.o	94.24	-o.82	1o6.18	117.71	o.91	o.9o	.8637
6			11.4	337.41	.9894	24.o	88.66	86.83	-2.11	99 .o9	147.14	o.85	o.83	.9140
7	26	5519	5.6	344.o6	.9732	63.o	119.82	119.25	-o.48	133.92	72.o8	1.15	1.14	.9o43
8			6.5	344.28	.9753	58.o	118.61	117.67	-o.8o	132.57	83.23	1.13	1.13	.9267
9			7.2	343.52	.977o	54.o	113.89	113.o8	-o.72	127.29	93.o6	1.o9	1.o8	.9112

(Contd ....)

RESULT SHEET

Table - 6.40: Experimental Results on CFB Heat Transfer for 32 - Pin Finned Surface

d_p = 310 μm, d_b = 100 mm, k_g = 0.03242 W/mK, ρ_s = 2350 kg/m^3, ρ_g = 0.09218 kg/m^3, μ_g = 2.214 x 10^{-5} kg/ms

A_{ht} = 0.0912 m^2 L_m = 0.5 m, Pr = 0.692, e_p = 0.76, e_g = 0.036, e_w = 0.24

Serial number of runs	Bed inventory(I) kg	Heat flux (q") W/m^2	Superficial velocity (U_o), m/s	Bed temperature (T_b) K	Voidage (ε)	Suspension density (ρ_{sus}) kg/m^3	Experimental heat transfer coefficient (h_e) W/m^{2}K	Predicted heat transfer coefficient (h_T), W/m^{2}K	% Error	Equivalent heat transfer coefficient (h_E), W/m^{2}K	Reynolds number (Re)	Experimental Nusselt number (Nu_e)	Predicted Nusselt number (Nu_T)	Fin effectiveness
(1)	(2)	(3)	(4)	(5)	(6)	(7)	(8)	(9)	(10)	(11)	(12)	(13)	(14)	(15)
10	26	5519	8.2	343.19	.9796	48.0	104.80	104.38	-0.40	117.13	106.10	1.00	1.00	.8733
11			9.1	340.96	.9834	39.0	98.03	97.29	-0.74	109.55	117.71	0.94	0.93	.8674
12			11.4	339.95	.9885	27.0	88.06	86.79	-1.46	98.42	147.14	0.84	0.83	.8806
13	32	5519	5.6	345.19	.9728	64.0	116.49	116.40	-0.08	130.20	72.08	1.11	1.11	.8614
14			6.5	344.42	.9736	62.0	122.77	121.75	-0.84	137.21	83.23	1.17	1.16	.9300
15			7.2	343.52	.9753	58.0	120.07	118.96	-0.93	134.19	93.06	1.15	1.14	.9236
16			8.2	342.72	.9779	52.0	106.03	105.91	-0.11	118.50	106.10	1.01	1.01	.8551
17			9.1	342.21	.9830	40.0	100.02	99.19	-0.84	111.79	117.71	0.96	0.95	.8774
18			11.4	341.46	.9877	29.0	89.71	88.55	-1.30	100.26	147.14	0.86	0.85	.8882

RESULT SHEET

Table - 6.41 : Experimental Results on CFB Heat Transfer for 1500 mm Long 4-Rectangular Finned Surface

d_p = 310 μm, d_b = 100 mm, k_g = 0.03242 W/m K, ρ_s = 2350 kg/m^3, ρ_g = 0.9218 kg/m^3, μ_g = 2.214 x 10^{-5} kg/ms, A_{ht} = 0.1277 m^2, L_m = 0.5 m, Pr = 0.692 , e_p = 0.76, e_g = 0.035, e_w = 0.24,

Sl. No. of runs	Bed inventory (I) kg	Heat flux (q") W/m^2	Superficial velocity (U_o) m/s	Bed temperature (T_b) K	Voidage (ε)	Suspension density (ρ_{sus}) kg/m^3	Experimental heat transfer coefficient (h_e) W/m^{2}K	Equivalent heat transfer coefficient (h_E)	Reynolds number (Re)	Experimental Nusselt number (Nu_e)	Fin effectiveness
1	26	5519	5.6	344.06	0.9736	62	119.03	186.28	72.08	1.14	.9018
2			6.4	348.20	0.9757	57	114.95	179.89	83.23	1.10	.9051
3			7.2	348.55	0.9783	51	110.36	172.71	93.06	1.06	.9159
4			8.2	348.08	0.9809	45	104.24	163.13	106.10	1.00	.9104
5			9.1	345.85	0.9847	36	90.71	141.96	117.71	0.87	.8598
6			11.4	345.26	0.9902	23	75.51	118.17	147.14	0.72	.8120

RESULT SHEET

Table - 6.42 : Voidage Along the Height of the Riser Column for Unfinned Surface

d_p = 310 μm , d_b = 100 mm , ρ_s = 2350 kg/m^3 , L_m = 0.5 m

Serial No. of runs	Bed inventory (I) kg	Superficial velocity (U_o) m/s	Voidage along the column above the distributor at a height								
			1.1m	1.6m	2.1m	2.6m	3.1m	3.6m	4.1m	4.6m	5.1m
1	20	5.6	0.9617	0.9660	0.9702	0.9702	0.9702	0.9702	0.9723	0.9753	0.9745
2		6.5	0.9655	0.9660	0.9745	0.9745	0.9736	0.9736	0.9753	0.9753	0.9745
3		7.2	0.9660	0.9702	0.9745	0.9745	0.9745	0.9745	0.9760	0.9766	0.9753
4		8.2	0.9745	0.9745	0.9745	0.9796	0.9787	0.9779	0.9760	0.9760	0.9760
5		9.1	0.9810	0.9820	0.9821	0.9820	0.9830	0.9820	0.9840	0.9840	0.9820
6		11.4	0.9870	0.9890	0.9889	0.9890	0.9894	0.9898	0.9889	0.9890	0.9898
7	26	5.6	0.9617	0.9642	0.9680	0.9695	0.9685	0.9693	0.9700	0.9706	0.9700
8		6.5	0.9638	0.9660	0.9700	0.9711	0.9711	0.9702	0.9720	0.9720	0.9723
9		7.2	0.9659	0.9702	0.9723	0.9745	0.9736	0.9745	0.9753	0.9760	0.9753

(contd...)

RESULT SHEET

Table - 6.42 : Voidage Along the Height of the Riser Column for Unfinned Surface

d_p = 310 μm , d_b = 100 mm , ρ_s = 2350 kg/m^3 , L_m = 0.5 m

Serial No. of runs	Bed inventory (I) kg	Superficial velocity (U_o) m/s	Voidage along the column above the distributor at a height								
			1.1m	1.6m	2.1m	2.6m	3.1m	3.6m	4.1m	4.6m	5.1m
10	26	8.2	0.9723	0.9723	0.9779	0.9787	0.9770	0.9780	0.9781	0.9781	0.9760
11		9.1	0.9787	0.9810	0.9820	0.9810	0.9821	0.9820	0.9810	0.9820	0.9810
12		11.4	0.9870	0.9889	0.9864	0.9870	0.9872	0.9890	0.9890	0.9889	0.9898
13	32	5.6	0.9600	0.9638	0.9672	0.9680	0.9677	0.9680	0.9680	0.9693	0.9689
14		6.5	0.9638	0.9659	0.9700	0.9700	0.9694	0.9700	0.9700	0.9710	0.9723
15		7.2	0.9650	0.9689	0.9723	0.9723	0.9723	0.9736	0.9745	0.9753	0.9760
16		8.2	0.9723	0.9723	0.9753	0.9753	0.9745	0.9745	0.9745	0.9760	0.9760
17		9.1	0.9766	0.9787	0.9820	0.9820	0.9813	0.9820	0.9810	0.9820	0.9810
18		11.4	0.9850	0.9870	0.9864	0.9870	0.9864	0.9885	0.9885	0.9890	0.9889

RESULT SHEET

Table - 6.43 : Voidage Along the Height of the Riser Column for 2 - Rectangular Finned Surface

d_p = 310 μm , d_b = 100 mm , ρ_s = 2350 kg/m^3 , L_m = 0.5 m

Serial No. of runs	Bed inventory (I) kg	Superficial velocity (U_o) m/s	Voidage along the column above the distributor at a height								
			1.1m	1.6m	2.1m	2.6m	3.1m	3.6m	4.1m	4.6m	5.1m
19	20	5.6	0.9625	0.9655	0.9694	0.9702	0.9723	0.9736	0.9745	0.9749	0.9745
20		6.5	0.9660	0.9668	0.9719	0.9723	0.9745	0.9753	0.9753	0.9761	0.9761
21		7.2	0.9668	0.9702	0.9728	0.9745	0.9757	0.9761	0.9766	0.9766	0.9770
22		8.2	0.9728	0.9745	0.9765	0.9779	0.9796	0.9808	0.9808	0.9821	0.9813
23		9.1	0.9796	0.9808	0.9820	0.9834	0.9847	0.9851	0.9864	0.9850	0.9864
24		11.4	0.9860	0.9860	0.9864	0.9872	0.9906	0.9900	0.9910	0.9900	0.9898
25	26	5.6	0.9617	0.9660	0.9677	0.9693	0.9715	0.9723	0.9723	0.9728	0.9719
26		6.5	0.9643	0.9677	0.9710	0.9700	0.9728	0.9736	0.9728	0.9745	0.9740
27		7.2	0.9655	0.9677	0.9700	0.9711	0.9749	0.9745	0.9753	0.9766	0.9760

(contd...)

RESULT SHEET

Table - 6.43 : Voidage Along the Height of the Riser Column for 2 - Rectangular Finned Surface

d_p = 310 μm , d_b = 100 mm , ρ_s = 2350 kg/m^3 , L_m = 0.5 m

Serial No. of runs	Bed inventory (I) kg	Superficial velocity (U_o) m/s	Voidage along the column above the distributor at a height								
			1.1m	1.6m	2.1m	2.6m	3.1m	3.6m	4.1m	4.6m	5.1m
28	26	8.2	0.9736	0.9745	0.9779	0.9761	0.9779	0.9781	0.9796	0.9780	0.9780
29		9.1	0.9779	0.9787	0.9813	0.9820	0.9838	0.9847	0.9850	0.9864	0.9847
30		11.4	0.9840	0.9847	0.9860	0.9864	0.9885	0.9889	0.9898	0.9885	0.9898
31	32	5.6	0.9600	0.9642	0.9668	0.9668	0.9689	0.9694	0.9702	0.9694	0.9700
32		6.5	0.9638	0.9660	0.9660	0.9677	0.9702	0.9710	0.9702	0.9711	0.9723
33		7.2	0.9643	0.9681	0.9694	0.9706	0.9736	0.9745	0.9745	0.9753	0.9765
34		8.2	0.9723	0.9736	0.9745	0.9745	0.9770	0.9787	0.9779	0.9779	0.9787
35		9.1	0.9770	0.9779	0.9796	0.9800	0.9821	0.9830	0.9817	0.9821	0.9813
36		11.4	0.9847	0.9855	0.9860	0.9860	0.9872	0.9872	0.9887	0.9889	0.9889

RESULT SHEET

Table - 6.44 : Voidage Along the Height of the Riser Column for 4 - Rectangular Finned Surface

d_p = 310 μm , d_b = 100 mm , ρ_s = 2350 kg/m^3 , L_m = 0.5 m

Serial No. of runs	Bed inventory (I) kg	Superficial velocity (U_o) m/s	Voidage along the column above the distributor at a height								
			1.1m	1.6m	2.1m	2.6m	3.1m	3.6m	4.1m	4.6m	5.1m
37	20	5.6	0.9634	0.9655	0.9672	0.9689	0.9745	0.9753	0.9749	0.9745	0.9745
38		6.5	0.9655	0.9660	0.9685	0.9700	0.9762	0.9770	0.9753	0.9762	0.9753
39		7.2	0.9660	0.9706	0.9706	0.9745	0.9770	0.9779	0.9787	0.9779	0.9770
40		8.2	0.9745	0.9753	0.9761	0.9717	0.9817	0.9821	0.9808	0.9820	0.9820
41		9.1	0.9808	0.9808	0.9796	0.9810	0.9864	0.9868	0.9864	0.9850	0.9850
42		11.4	0.9872	0.9889	0.9885	0.9872	0.9915	0.9910	0.9900	0.9910	0.9900
43	26	5.6	0.9617	0.9638	0.9642	0.9680	0.9728	0.9728	0.9720	0.9715	0.9711
44		6.5	0.9634	0.9655	0.9672	0.9689	0.9753	0.9762	0.9753	0.9753	0.9762
45		7.2	0.9660	0.9689	0.9706	0.9711	0.9770	0.9770	0.9761	0.9766	0.9761

(contd...)

RESULT SHEET

Table - 6.44 : Voidage Along the Height of the Riser Column for 4 - Rectangular Finned Surface

d_p = 310 μm , d_b = 100 mm , ρ_s = 2350 kg/m^3 , L_m = 0.5 m

Serial No. of runs	Bed inventory (I) kg	Superficial velocity (U_o) m/s	Voidage along the column above the distributor at a height								
			1.1m	1.6m	2.1m	2.6m	3.1m	3.6m	4.1m	4.6m	5.1m
46	26	8.2	0.9711	0.9711	0.9753	0.9761	0.9800	0.9813	0.9791	0.9808	0.9813
47		9.1	0.9787	0.9808	0.9796	0.9796	0.9847	0.9850	0.9847	0.9834	0.9834
48		11.4	0.9864	0.9885	0.9881	0.9868	0.9898	0.9890	0.9890	0.9894	0.9894
49	32	5.6	0.9600	0.9638	0.9670	0.9670	0.9715	0.9723	0.9728	0.9711	0.9711
50		6.5	0.9634	0.9655	0.9659	0.9680	0.9723	0.9728	0.9736	0.9720	0.9723
51		7.2	0.9643	0.9677	0.9694	0.9710	0.9762	0.9770	0.9753	0.9761	0.9762
52		8.2	0.9710	0.9710	0.9723	0.9745	0.9770	0.9877	0.9780	0.9796	0.9796
53		9.1	0.9760	0.9780	0.9787	0.9790	0.9830	0.9821	0.9830	0.9821	0.9813
54		11.4	0.9847	0.9855	0.9860	0.9864	0.9881	0.9889	0.9890	0.9809	0.9890

RESULT SHEET

Table - 6.45 : Voidage Along the Height of the Riser Column for 8 - Rectangular Finned Surface

d_p = 310 μm , d_b = 100 mm , ρ_s = 2350 kg/m^3 , L_m = 0.5 m

Serial No. of runs	Bed inventory (I) kg	Superficial velocity (U_o) m/s	Voidage along the column above the distributor at a height								
			1.1m	1.6m	2.1m	2.6m	3.1m	3.6m	4.1m	4.6m	5.1m
55	20	5.6	0.9617	0.9634	0.9660	0.9750	0.9800	0.9796	0.9800	0.9804	0.9808
56		6.5	0.9625	0.9660	0.9723	0.9780	0.9821	0.9821	0.9813	0.9825	0.9830
57		7.2	0.9650	0.9680	0.9745	0.9796	0.9834	0.9830	0.9840	0.9840	0.9850
58		8.2	0.9736	0.9745	0.9780	0.9821	0.9855	0.9850	0.9864	0.9859	0.9868
59		9.1	0.9787	0.9787	0.9821	0.9864	0.9894	0.9894	0.9898	0.9894	0.9894
60		11.4	0.9820	0.9850	0.9868	0.9894	0.9920	0.9919	0.9920	0.9919	0.9923

RESULT SHEET

Table - 6.46 : Voidage Along the Height of the Riser Column for 16 - Pin Finned Surface

d_p = 310 μm , d_b = 100 mm , ρ_s = 2350 kg/m^3 , L_m = 0.5 m

Serial No. of runs	Bed inventory (I) kg	Superficial velocity (U_o) m/s	Voidage along the column above the distributor at a height								
			1.1m	1.6m	2.1m	2.6m	3.1m	3.6m	4.1m	4.6m	5.1m
61	20	5.6	0.9617	0.9660	0.9702	0.9710	0.9728	0.9736	0.9736	0.9745	0.9753
62		6.5	0.9660	0.9702	0.9723	0.9736	0.9770	0.9779	0.9779	0.9770	0.9766
63		7.2	0.9668	0.9728	0.9728	0.9753	0.9779	0.9787	0.9779	0.9779	0.9770
64		8.2	0.9736	0.9745	0.9745	0.9779	0.9813	0.9820	0.9821	0.9813	0.9808
65		9.1	0.9787	0.9808	0.9808	0.9808	0.9838	0.9850	0.9840	0.9850	0.9864
66		11.4	0.9870	0.9889	0.9894	0.9872	0.9898	0.9898	0.9894	0.9889	0.9906
67	26	5.6	0.9617	0.9651	0.9651	0.9680	0.9715	0.9719	0.9723	0.9736	0.9736
68		6.5	0.9634	0.9650	0.9680	0.9719	0.9753	0.9760	0.9766	0.9753	0.9760
69		7.2	0.9660	0.9677	0.9685	0.9736	0.9766	0.9766	0.9753	0.9770	0.9770

(contd...)

RESULT SHEET

Table - 6.46 : Voidage Along the Height of the Riser Column for 16 - Pin Finned Surface

d_p = 310 μm , d_b = 100 mm , ρ_s = 2350 kg/m^3 , L_m = 0.5 m

Serial No. of runs	Bed inventory (I) kg	Superficial velocity (U_o) m/s	Voidage along the column above the distributor at a height								
			1.1m	1.6m	2.1m	2.6m	3.1m	3.6m	4.1m	4.6m	5.1m
70	26	8.2	0.9719	0.9728	0.9728	0.9766	0.9787	0.9780	0.9796	0.9781	0.9779
71		9.1	0.9787	0.9804	0.9804	0.9796	0.9830	0.9830	0.9825	0.9825	0.9820
72		11.4	0.9894	0.9894	0.9889	0.9872	0.9885	0.9889	0.9894	0.9894	0.9898
73	32	5.6	0.9655	0.9650	0.9660	0.9677	0.9711	0.9710	0.9719	0.9736	0.9736
74		6.5	0.9642	0.9680	0.9702	0.9695	0.9723	0.9723	0.9732	0.9745	0.9745
75		7.2	0.9650	0.9680	0.9710	0.9723	0.9749	0.9757	0.9749	0.9753	0.9753
76		8.2	0.9702	0.9719	0.9719	0.9745	0.9770	0.9787	0.9779	0.9779	0.9770
77		9.1	0.9760	0.9770	0.9787	0.9804	0.9826	0.9821	0.9826	0.9821	0.9821
78		11.4	0.9855	0.9864	0.9870	0.9833	0.9872	0.9872	0.9898	0.9894	0.9898

RESULT SHEET

Table - 6.47 : Voidage Along the Height of the Riser Column for 32-Pin Finned Surface

d_p = 310 μm , d_b = 100 mm , ρ_s = 2350 kg/m^3 , L_m = 0.5 m

Serial No. of runs	Bed inventory (I) kg	Superficial velocity (U_o) m/s	Voidage along the column above the distributor at a height								
			1.1m	1.6m	2.1m	2.6m	3.1m	3.6m	4.1m	4.6m	5.1m
79	20	5.6	0.9617	0.9650	0.9681	0.9710	0.9745	0.9745	0.9757	0.9770	0.9783
80		6.5	0.9660	0.9668	0.9702	0.9736	0.9774	0.9779	0.9779	0.9783	0.9787
81		7.2	0.9668	0.9672	0.9736	0.9761	0.9783	0.9796	0.9804	0.9809	0.9813
82		8.2	0.9736	0.9745	0.9779	0.9779	0.9809	0.9813	0.9813	0.9821	0.9821
83		9.1	0.9791	0.9796	0.9808	0.9821	0.9847	0.9847	0.9855	0.9864	0.9864
84		11.4	0.9864	0.9872	0.9877	0.9872	0.9898	0.9898	0.9900	0.9900	0.9900
85	26	5.6	0.9617	0.9647	0.9660	0.9702	0.9732	0.9736	0.9753	0.9757	0.9770
86		6.5	0.9629	0.9660	0.9706	0.9723	0.9753	0.9749	0.9766	0.9766	0.9780
87		7.2	0.9650	0.9693	0.9736	0.9731	0.9770	0.9780	0.9770	0.9787	0.9787

(contd...)

RESULT SHEET

Table - 6.47 : Voidage Along the Height of the Riser Column for 32-Pin Finned Surface

d_p = 310 μm , d_b = 100 mm , ρ_s = 2350 kg/m^3 , L_m = 0.5 m

Serial No. of runs	Bed inventory (I) kg	Superficial velocity (U_o) m/s	Voidage along the column above the distributor at a height								
			1.1m	1.6m	2.1m	2.6m	3.1m	3.6m	4.1m	4.6m	5.1m
88	26	8.2	0.9723	0.9731	0.9770	0.9770	0.9796	0.9808	0.9834	0.9834	0.9850
89		9.1	0.9779	0.9791	0.9787	0.9808	0.9834	0.9834	0.9850	0.9850	0.9866
90		11.4	0.9864	0.9872	0.9868	0.9864	0.9885	0.9894	0.9898	0.9900	0.9900
91	32	5.6	0.9600	0.9642	0.9668	0.9680	0.9728	0.9715	0.9720	0.9723	0.9724
92		6.5	0.9613	0.9655	0.9693	0.9706	0.9736	0.9745	0.9753	0.9770	0.9770
93		7.2	0.9650	0.9681	0.9717	0.9726	0.9753	0.9761	0.9766	0.9780	0.9787
94		8.2	0.9723	0.9736	0.9745	0.9753	0.9779	0.9779	0.9780	0.9796	0.9809
95		9.1	0.9762	0.9770	0.9787	0.9813	0.9830	0.9834	0.9830	0.9826	0.9840
96		11.4	0.9850	0.9864	0.9872	0.9865	0.9877	0.9877	0.9883	0.9887	0.9877

RESULT SHEET

Table - 6.48 : Voidage Along the Height of the Riser Column for 1500 mm Long 4-Rectangular Finned Surface

d_p = 310 μm , d_b = 100 mm , ρ_s = 2350 kg/m^3 , L_m = 0.5 m

Serial No. of runs	Bed inventory (I) kg	Superficial velocity (U_o) m/s	Voidage along the column above the distributor at a height								
			1.1m	1.6m	2.1m	2.6m	3.1m	3.6m	4.1m	4.6m	5.1m
97	26	5.6	0.9618	0.9635	0.9655	0.9668	0.9736	0.9716	0.9725	0.9732	0.9732
98		6.5	0.9633	0.9654	0.9668	0.9694	0.9757	0.9740	0.9755	0.9765	0.9765
99		7.2	0.9667	0.9668	0.9680	0.9702	0.9780	0.9770	0.9780	0.9780	0.9780
100		8.2	0.9706	0.9730	0.9745	0.9770	0.9808	0.9810	0.9804	0.9805	0.9806
101		9.1	0.9794	0.9795	0.9790	0.9808	0.9847	0.9855	0.9868	0.9866	0.9866
102		11.4	0.9868	0.9870	0.9870	0.9872	0.9896	0.9895	0.9898	0.9895	0.9895

RESULT SHEET

Table - 6.49 : Experimental Results on CFB Heat Transfer for 85 mm Vertical Probe

L_h = 85 mm , L_H = 1.22m , L_h / D = 0.85 , A_{ht} = 0.0267 m^2 , L_m = 0.5 m
d_p = 310 μm , d_b = 100 mm, ρ_s = 2350 kg/m^3 , ρ_g = 0.9218 kg/m^3 , k_g = 0.03242W/mK
μ_g = 2.214 x $=10^{-5}$ kg/m^3 , c_{ps} = 0.703 kJ/kg K

Serial number of runs	Bed inventory(I) kg	Heat Flux (q'') W/m^2	Superficial velocity (U_o) m/s	Bed temperature (T_b) K	Voidage (ε)	Suspension density (ρ_{sus}) kg/m^3	Experimental heat transfer coefficient (h_e) W/m^2K	Predicted heat transfer coefficient (h_T) W/m^2K	% Error	Experimental Nusselt number (Nu_p)$_e$	Predicted Nusselt number(Nu_p)$_T$	Reynolds number (Re)	Residence time predicted from the expression (t_r) sec	Residence time predicted from Subbarao's correlation (RT_{sub}) sec
(1)	(2)	(3)	(4)	(5)	(6)	(7)	(8)	(9)	(10)	(11)	(12)	(13)	(14)	(15)
1	32	4500	7.2	335.30	0.9736	62.00	159.44	171.65	7.15	1.52	1.64	93.06	.01272	.01349
2			8.8	334.69	0.9804	46.00	152.82	163.17	6.42	1.46	1.56	113.97	.01042	.01102
3			10.2	335.67	0.9847	36.00	146.51	157.41	6.91	1.40	1.51	131.60	.00900	.00949
4			11.4	335.44	0.9864	32.00	136.19	153.08	11.03	1.30	1.46	147.14	.00947	.00995
5			12.5	335.23	0.9894	25.00	134.00	149.63	10.42	1.28	1.43	161.18	.00768	.00806
6	32	6000	7.2	336.94	0.9736	62.00	160.98	171.65	6.25	1.54	1.64	93.06	.01243	.01319
7			8.8	336.76	0.9804	46.00	150.99	163.17	7.54	1.44	1.56	113.97	.01072	.01133
8			10.2	336.38	0.9847	36.00	145.07	157.41	7.83	1.39	1.51	131.60	.00921	.00971
9			11.4	336.33	0.9864	32.00	141.61	153.08	7.49	1.35	1.46	147.14	.00866	.00913
10			12.5	335.44	0.9894	25.00	134.31	149.63	10.22	1.28	1.43	161.18	.00764	.00802

RESULT SHEET

Table -6.50 : Experimental Results on CFB Heat Transfer for 127.5 mm Vertical Probe

L_h = 127.5 mm, L_H = 1.83 m, L_h / D = 1.275, A_{ht} = 0.04 m^2, L_m = 0.5 m
d_p = 310 μm, d_b = 100 mm, ρ_s = 2350 kg/m^3, ρ_g = 0.9218 kg/m^3, k_g = 0.03242 W/mK
μ_g = 2.214 x $=10^{-5}$ kg/m^3, c_{ps} = 0.703 kJ/kg K

Serial number of runs	Bed inventory(I) kg	Heat Flux (q") W/m^2	Superficial velocity (U_o) m/s	Bed temperature (T_b) K	Voidage (ϵ)	Suspension density (ρ_{sus}) kg/m^3	Experimental heat transfer coefficient (h_e) W/m^2K	Predicted heat transfer coefficient (h_T) W/m^2K	% Error	Experimental Nusselt number $(Nu_p)_e$	Predicted Nusselt number $(Nu_p)_T$	Reynolds number (Re)	Residence time predicted from the expression (t_r) sec	Residence time predicted from Subbarao's correlation (RT_{sub}) sec
(1)	(2)	(3)	(4)	(5)	(6)	(7)	(8)	(9)	(10)	(11)	(12)	(13)	(14)	(15)
11	32	4500	7.2	337.39	0.9736	62.00	153.44	140.15	-9.44	1.47	1.34	93.06	.01392	.01473
12			8.8	336.87	0.9804	46.00	132.43	133.23	0.68	1.27	1.27	113.97	.01452	.01523
13			10.2	337.01	0.9847	36.00	118.35	128.52	7.91	1.13	1.23	131.60	.01467	.01530
14			11.4	336.54	0.9864	32.00	113.64	124.99	9.08	1.09	1.20	147.14	.01429	.01488
15			12.5	336.36	0.9894	25.00	111.01	122.17	9.08	1.06	1.17	161.18	.01177	.01224
16	32	6000	7.2	338.38	0.9736	62.00	155.02	140.15	-10.57	1.48	1.34	93.06	.01359	.01439
17			8.8	340.02	0.9804	46.00	132.02	133.23	0.99	1.26	1.27	113.97	.01463	.01534
18			10.2	339.74	0.9847	36.00	123.46	128.52	3.93	1.18	1.23	131.60	.01333	.01394
19			11.4	339.88	0.9864	32.00	118.64	124.99	5.08	1.13	1.20	147.14	.01296	.01353
20			12.5	339.74	0.9894	25.00	114.03	122.17	6.64	1.09	1.17	161.18	.01108	.01153

RESULT SHEET

Table -6.51 : Experimental Results on CFB Heat Transfer for 170 mm **Vertical Probe**

L_h = 170 mm , L_H = 2.44 m , L_h / D = 1.70 , A_{ht} = 0.0534 m^2 , L_m = 0.5 m

d_p = 310 μm , d_b = 100 mm, ρ_s = 2350 kg/m^3 , ρ_g = 0.9218 kg/m^3 , k_g = 0.03242 W/mK

μ_g = 2.214 x $=10^{-5}$ kg/m^3 , c_{ps} = 0.703 kJ/kg K

Serial number of runs	Bed inventory(I) kg	Heat Flux (q") W/m^2	Superficial velocity (U_o) m/s	Bed temperature (T_b) K	Voidage (ϵ)	Suspension density (ρ_{sus}) kg/m^3	Experimental heat transfer coefficient (h_e) W/m^2K	Predicted heat transfer coefficient (h_T) W/m^2K	% Error	Experimental Nusselt number (Nu_p)e	Predicted Nusselt number(Nu_p)T	Reynolds number (Re)	Residence time predicted from the expression (t_r) sec	Residence time predicted from Subbarao's correlation (RT_{sub}) sec
(1)	(2)	(3)	(4)	(5)	(6)	(7)	(8)	(9)	(10)	(11)	(12)	(13)	(14)	(15)
21	32	4500	7.2	338.02	0.9736	62.00	129.04	121.38	-6.27	1.23	1.16	93.06	.02077	.02176
22			8.8	337.72	0.9804	46.00	113.98	115.38	1.30	1.09	1.10	113.97	.02040	.02124
23			10.2	337.51	0.9847	36.00	107.04	111.30	3.82	1.02	1.06	131.60	.01838	.09908
24			11.4	338.26	0.9864	32.00	102.90	108.24	4.93	0.98	1.04	147.14	.01783	.01849
25			12.5	338.07	0.9894	25.00	98.00	105.80	7.35	0.94	1.01	161.18	.01552	.01606
26	32	6000	7.2	339.69	0.9736	62.00	118.20	121.38	2.65	1.13	1.16	93.06	.02533	.02643
27			8.8	340.02	0.9804	46.00	115.01	115.38	0.41	1.10	1.10	113.97	.0199g	.02083
28			10.2	339.88	0.9847	36.00	104.68	111.30	5.94	1.00	1.06	131.60	.01931	.02003
29			11.4	340.05	0.9864	32.00	104.55	108.24	3.41	1.00	1.04	147.14	.01721	.01786
30			12.5	339.90	0.9894	25.00	100.01	105.80	5.45	0.96	1.01	161.18	.01484	.01537

RESULT SHEET

Table - 6.52 : Experimental Results on CFB Heat Transfer for 255 mm **Vertical Probe**

L_h = 255 mm , L_H = 3.66 m , L_h / D = 2.55 , A_{ht} = 0.08 m^2 , L_m = 0.5 m
d_p = 310 μm , d_b = 100 mm, ρ_s = 2350 kg/m^3 , ρ_g = 0.9218 kg/m^3 , k_g = 0.03242 W/mK
μ_g = 2.214 x $=10^{-5}$ kg/m^3 , c_{ps} = 0.703 kJ/kg K

Serial number of runs	Bed inventory(I) kg	Heat Flux (q") W/m^2	Superficial velocity (U_o) m/s	Bed temperature (T_b) K	Voidage (ϵ)	Suspension density (ρ_{sus}) kg/m^3	Experimental heat transfer coefficient (h_e) W/m^2K	Predicted heat transfer coefficient (h_T) W/m^2K	% Error	Experimental Nusselt number $(Nu_p)_e$	Predicted Nusselt number $(Nu_p)_T$	Reynolds number (Re)	Residence time predicted from the expression (t_r) sec	Residence time predicted from Subbarao's correlation (RT_{sub}) sec
(1)	(2)	(3)	(4)	(5)	(6)	(7)	(8)	(9)	(10)	(11)	(12)	(13)	(14)	(15)
31	32	4500	7.2	340.49	0.9736	62.00	110.30	99.10	-11.26	1.05	0.95	93.06	.02959	.03077
32			8.8	341.41	0.9804	46.00	101.00	94.21	- 7.11	0.97	0.90	113.97	.02672	.02768
33			10.2	341.29	0.9847	36.00	94.98	90.88	- 4.51	0.91	0.87	131.60	.02394	.02474
34			11.4	343.41	0.9864	32.00	97.05	88.38	- 9.81	.930	0.85	147.14	.02029	.02099
35			12.5	342.23	0.9894	25.00	89.82	86.39	- 3.99	0.86	0.83	161.18	.01879	.01939
36	32	6000	7.2	348.41	0.9736	62.00	109.81	99.10	-10.76	1.05	0.95	93.06	.02989	.03107
37			8.8	348.34	0.9804	46.00	104.85	94.21	-11.20	1.00	0.90	113.97	.02457	.02551
38			10.2	348.11	0.9847	36.00	101.64	90.88	-11.85	0.97	0.87	131.60	.02062	.02136
39			11.4	347.50	0.9864	32.00	98.50	88.38	-10.94	0.94	0.85	147.14	.01964	.02033
40			12.5	345.71	0.9894	25.00	94.98	86.39	- 9.97	0.91	0.83	161.18	.01662	.01718

Table - 6.53 : Experimental Conditions of other Investigators on Heat Transfer in Circulating Fluidized Beds

Curve number	Author	Mean particle size (μm)	Vertical probe length (mm)	Bed size (diameter) (mm)	Average bed temperature (K)
1	Basu and Nag (1987)	227	25	102	311
2	Basu and Nag (1987)	87	25	102	308
3	Kobro and Brereton (1986)	170	100	200	298
4	Kobro and Brereton (1986)	250	100	200	298
5	Wu et al (1987)	188	1530	152x152 (square)	550
6	Wu et al (1989)	171	22	-do-	308
7	Wu et al (1989b)	241	1590	-do-	683
8	Sekthira et al (1988)	300	700	88	503
9	Furchi et al (1988)	269	1000 (x6)	84	303
10	Subbarao and Basu (1986b)	260	25	102	300
11	Present experiment	310	300	100	354

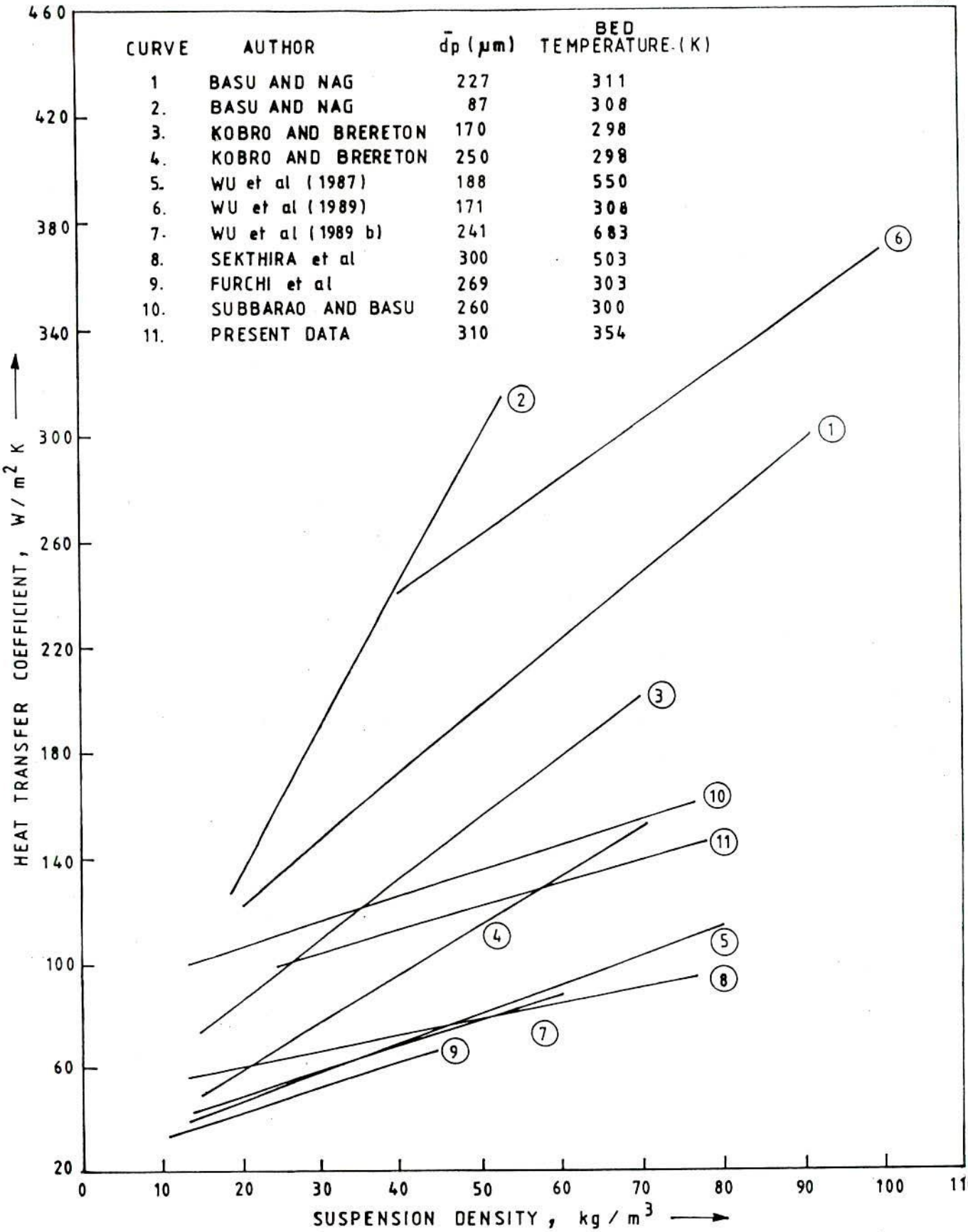

FIG. 3 COMPARISON OF PRESENT RESULTS WITH THE RESULTS OF OTHERS FOR UNFINNED SURFACE

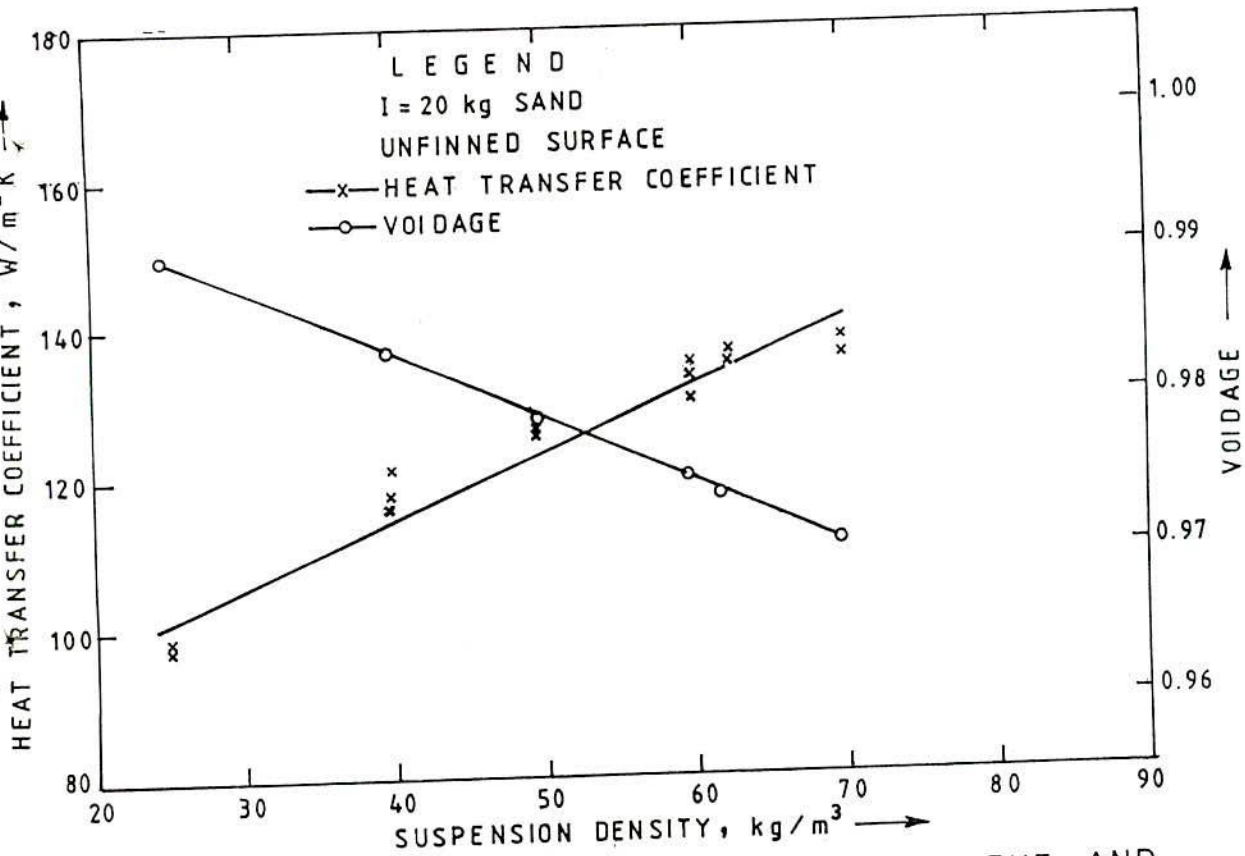

FIG. 6.2 VARIATION OF HEAT TRANSFER COEFFICIENT AND VOIDAGE WITH SUSPENSION DENSITY

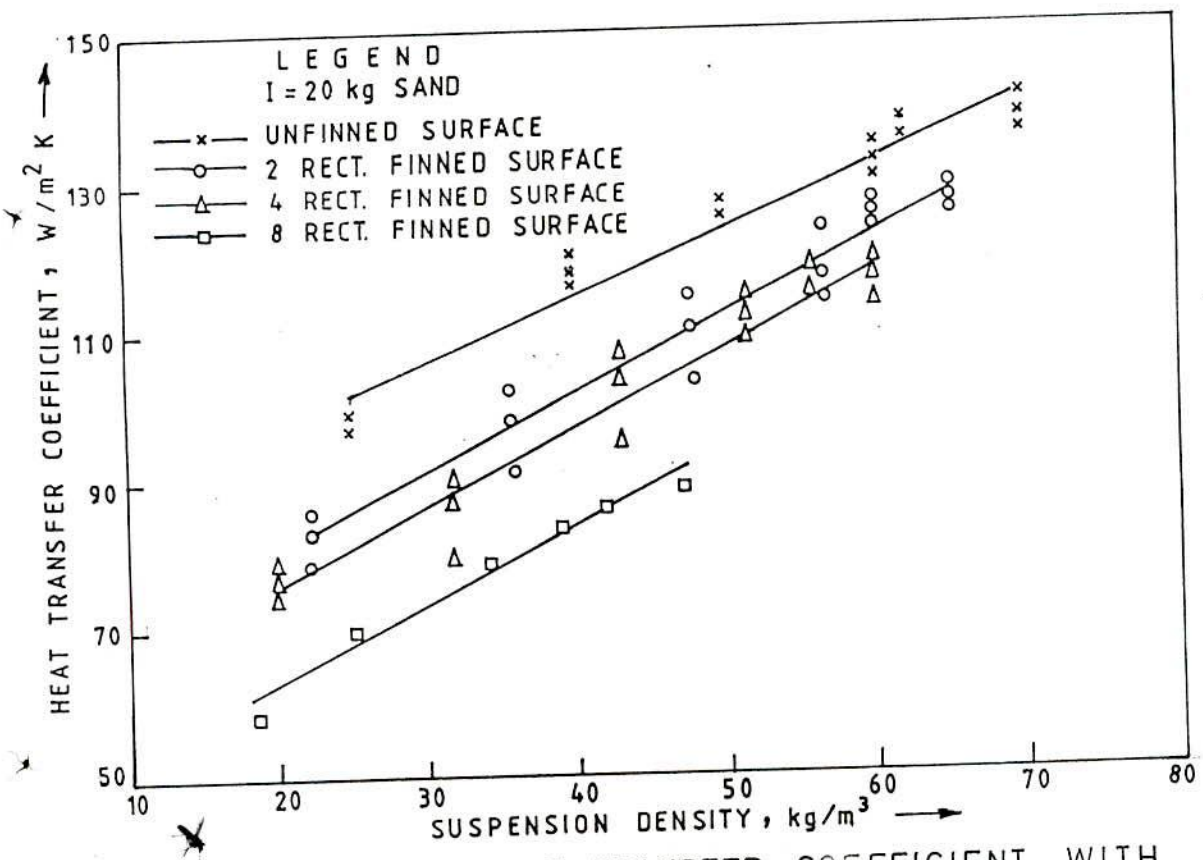

FIG. 6.3 VARIATION OF HEAT TRANSFER COEFFICIENT WITH SUSPENSION DENSITY FOR RECTANGULAR FINNED SURFACE

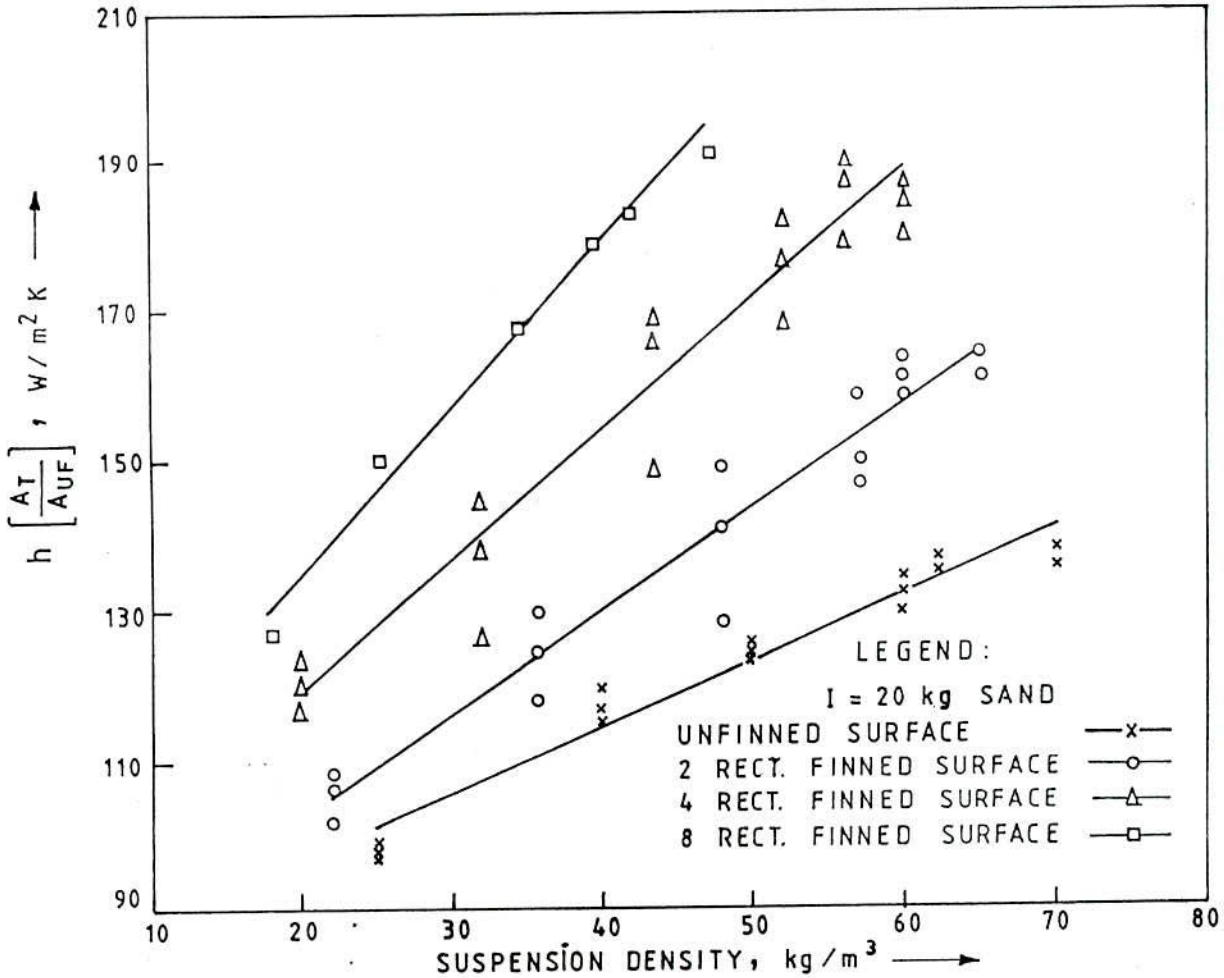

FIG. 6.4 EQUIVALENT HEAT TRANSFER COEFFICIENT OF RECTANGULAR FINS VARYING WITH SUSPENSION DENSITY

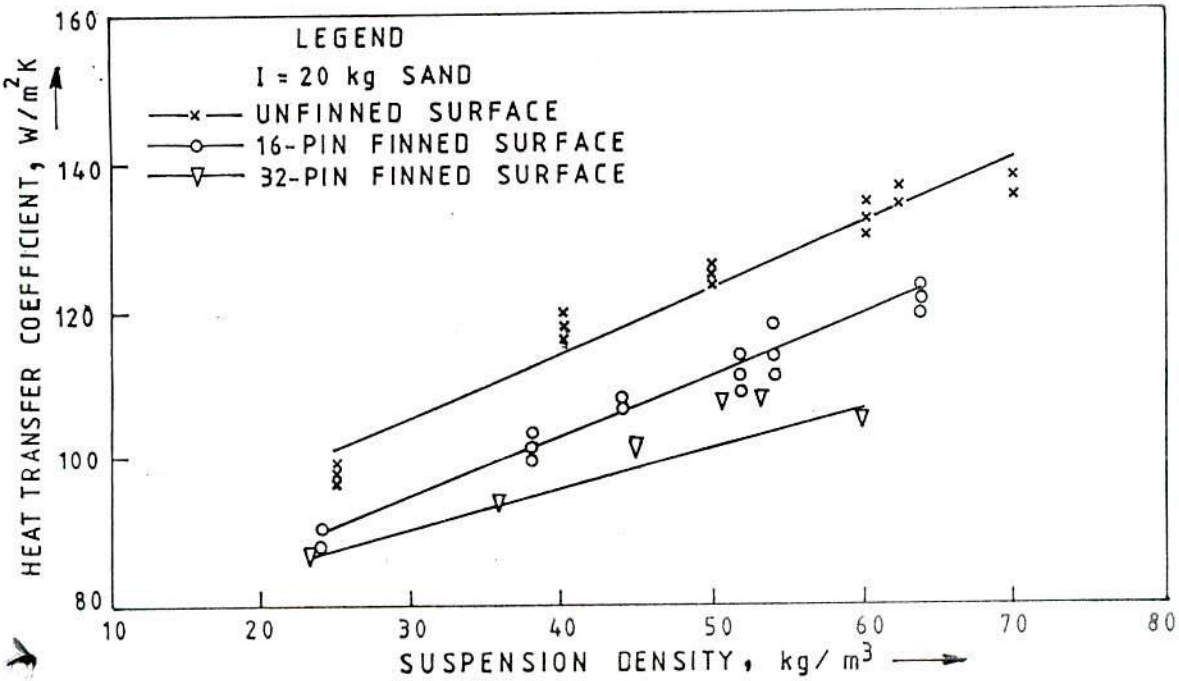

FIG. 6.5 VARIATION OF HEAT TRANSFER COEFFICIENT WITH SUSPENSION DENSITY FOR PIN FINNED SURFACE

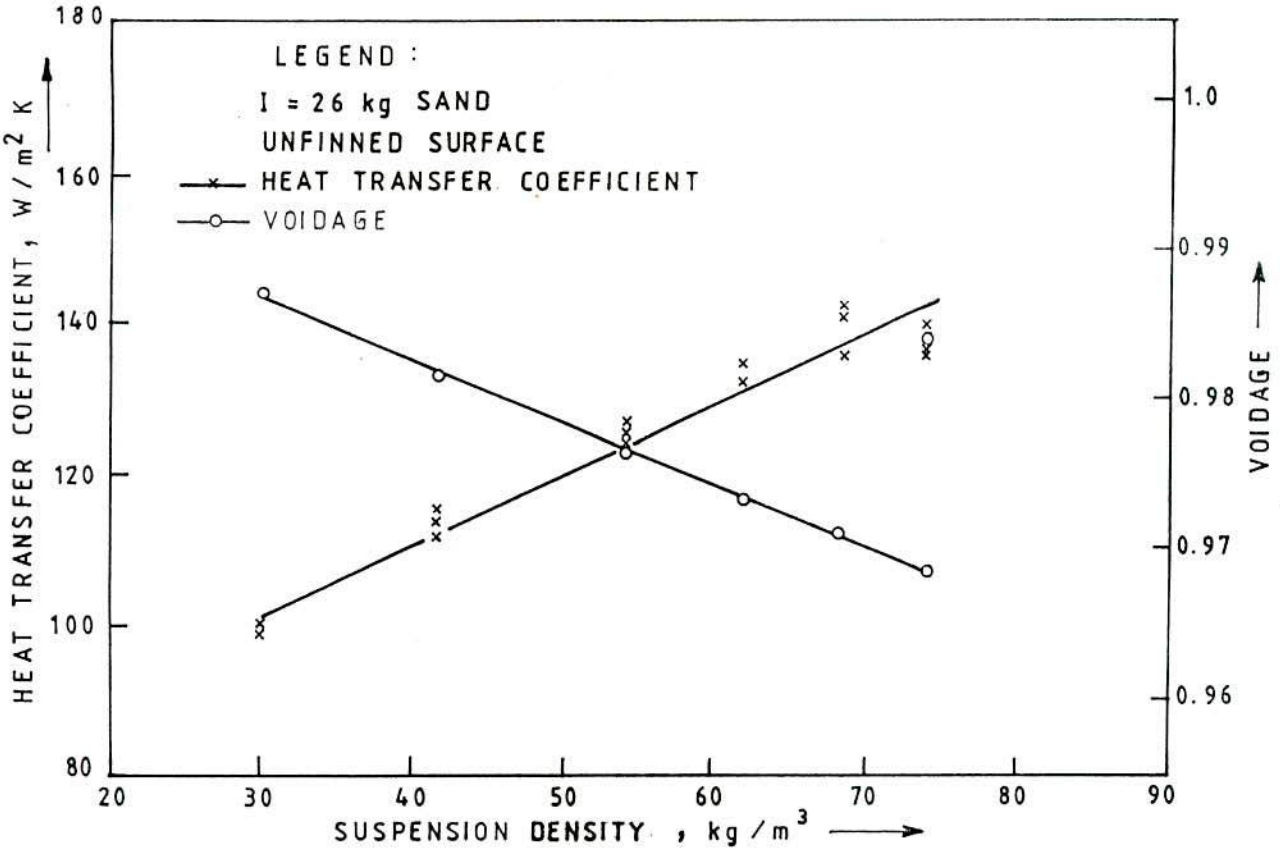

FIG.6.6 VARIATION OF HEAT TRANSFER COEFFICIENT AND VOIDAGE WITH SUSPENSION DENSITY

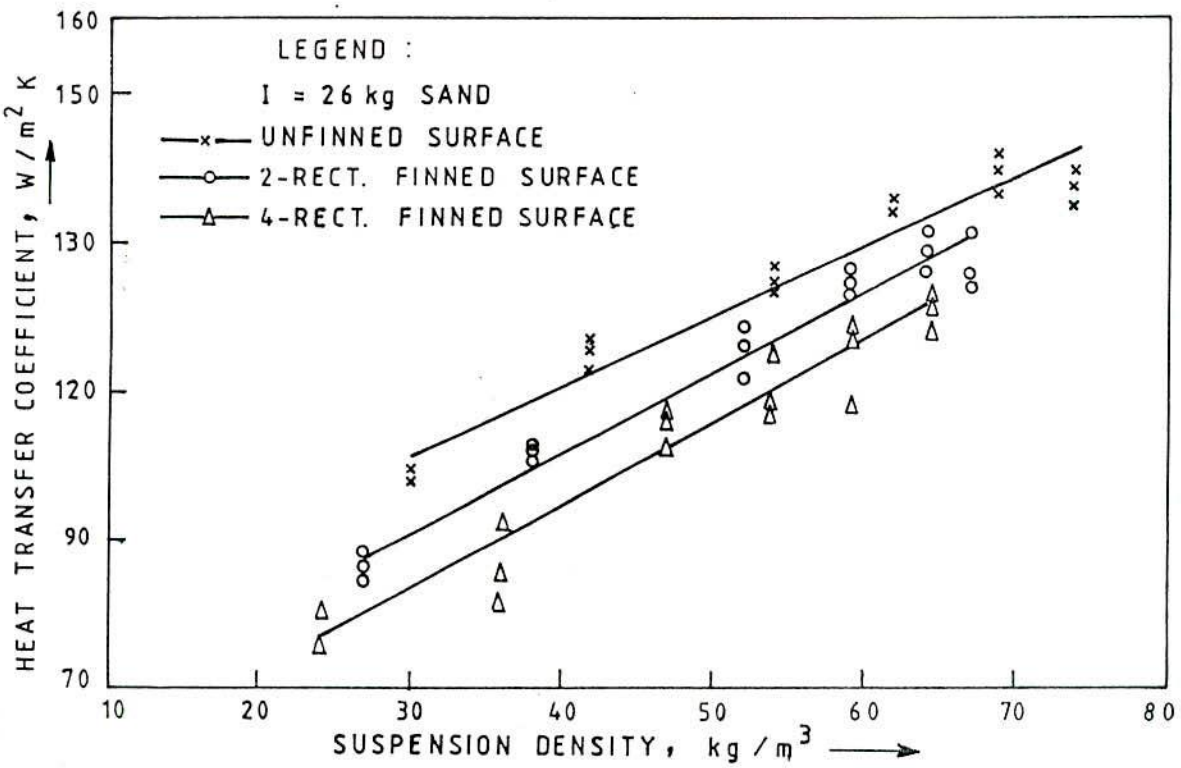

FIG.6.7 VARIATION OF HEAT TRANSFER COEFFICIENT WITH SUSPENSION DENSITY FOR RECTANGULAR FINNED SURFACE

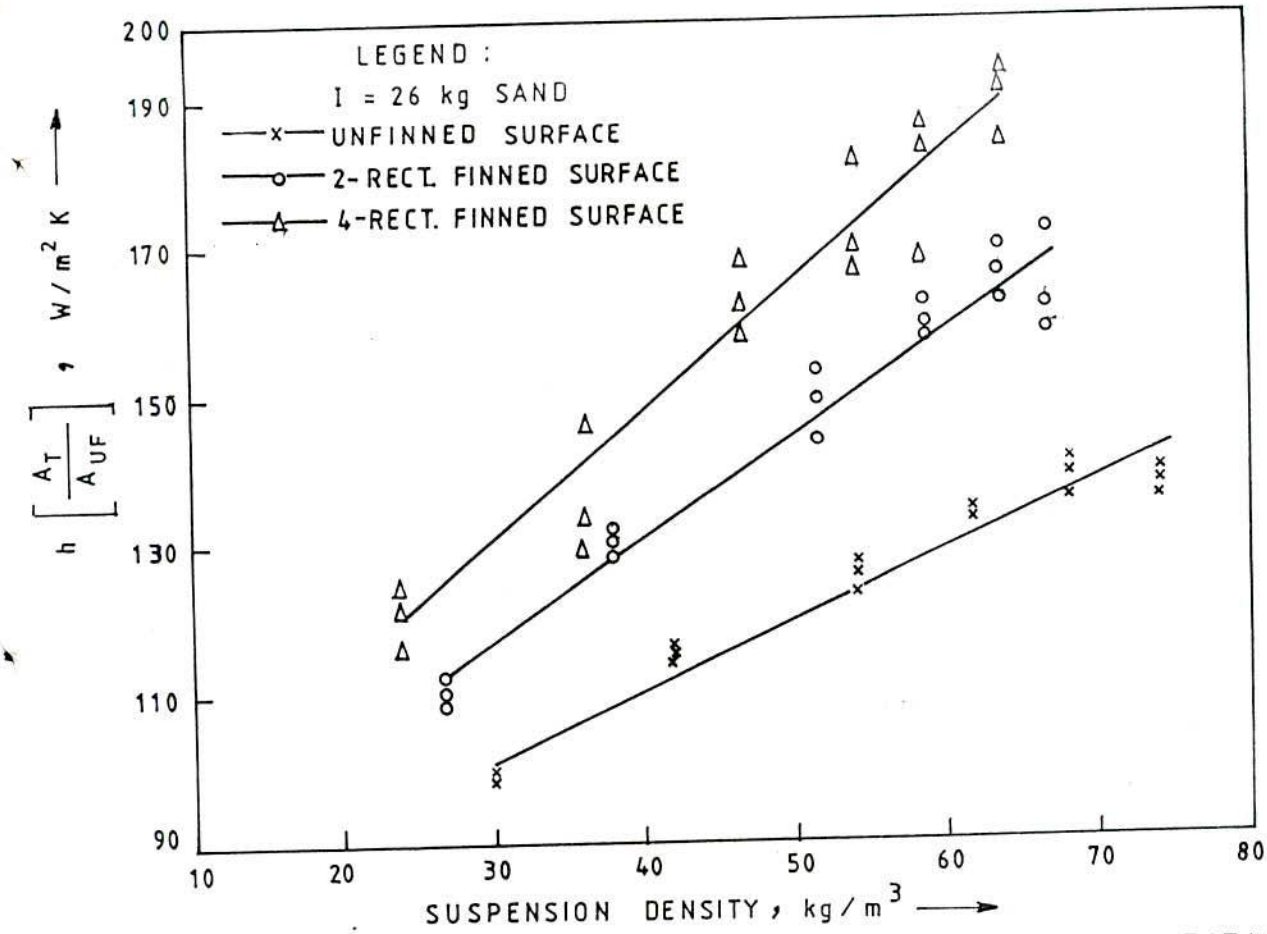

FIG.6.8 EQUIVALENT HEAT TRANSFER COEFFICIENT OF RECTANGULAR FINS VARYING WITH SUSPENSION DENSITY

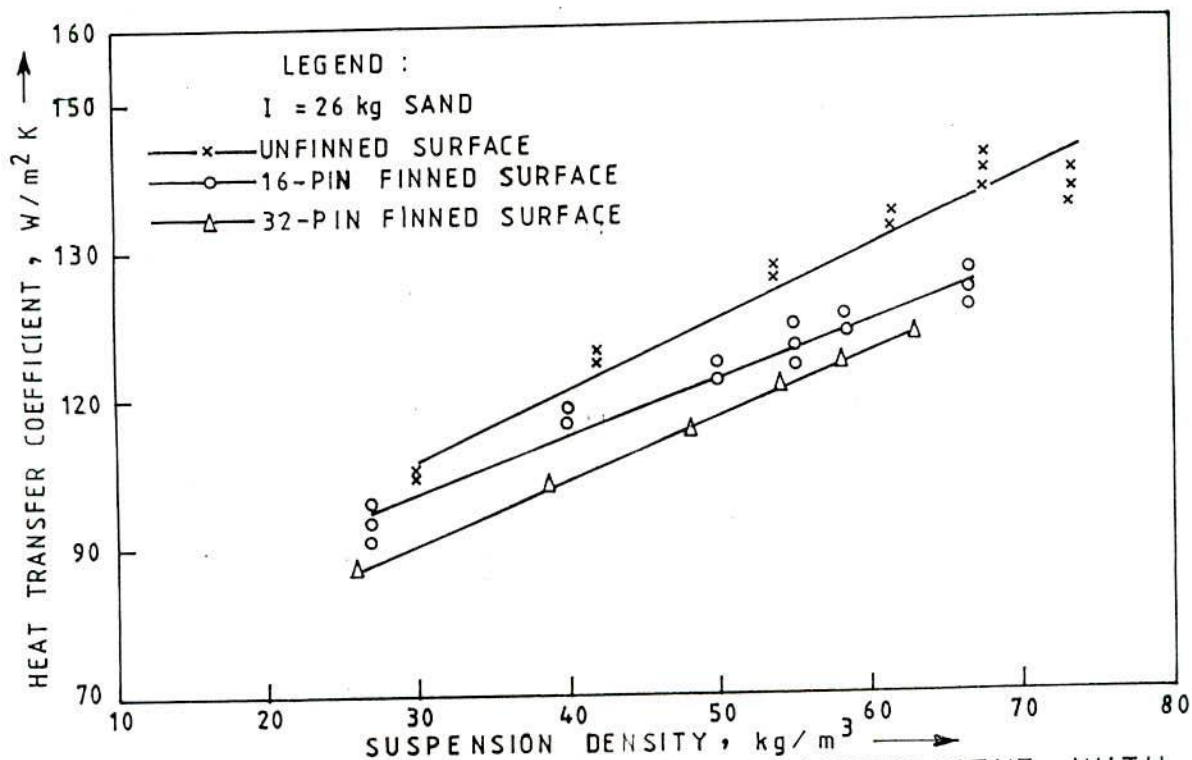

FIG.6.9 VARIATION OF HEAT TRANSFER COEFFICIENT WITH SUSPENSION DENSITY FOR PIN FINNED SURFACE

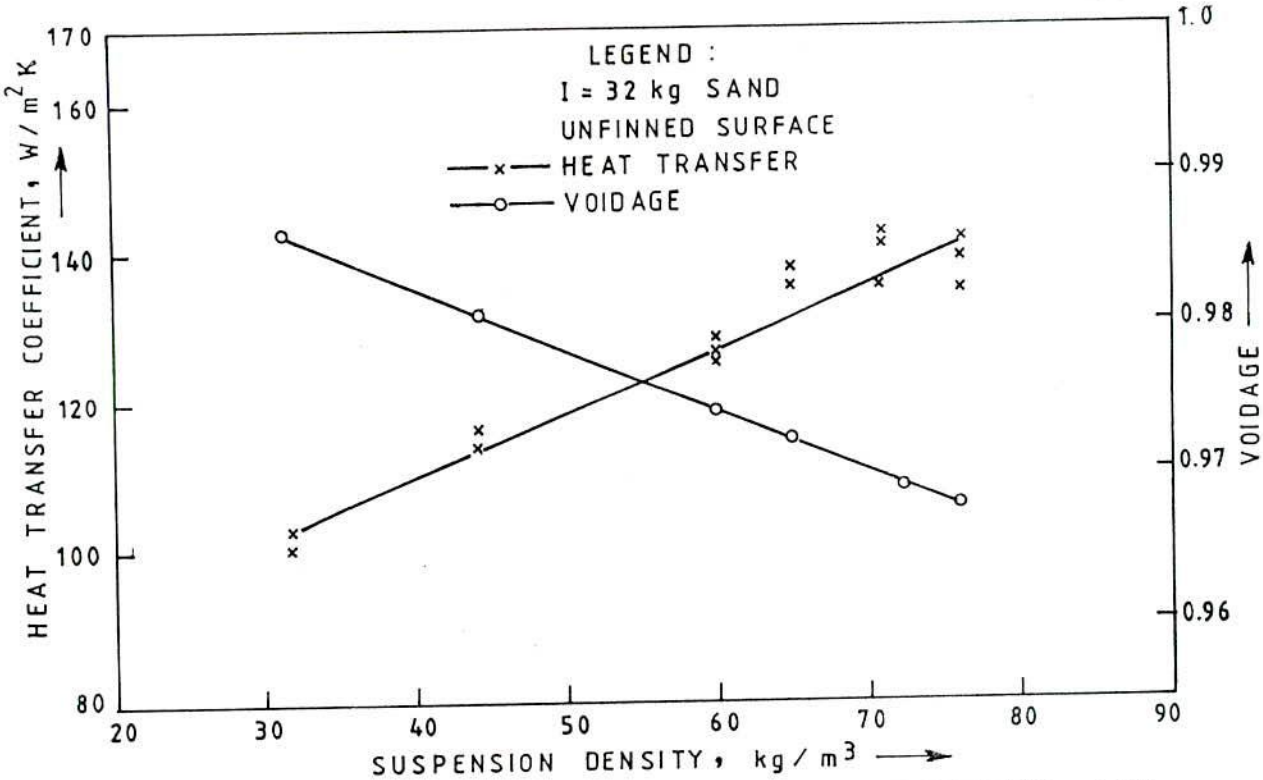

FIG.6.10 VARIATION OF HEAT TRANSFER COEFFICIENT AND VOIDAGE WITH SUSPENSION DENSITY

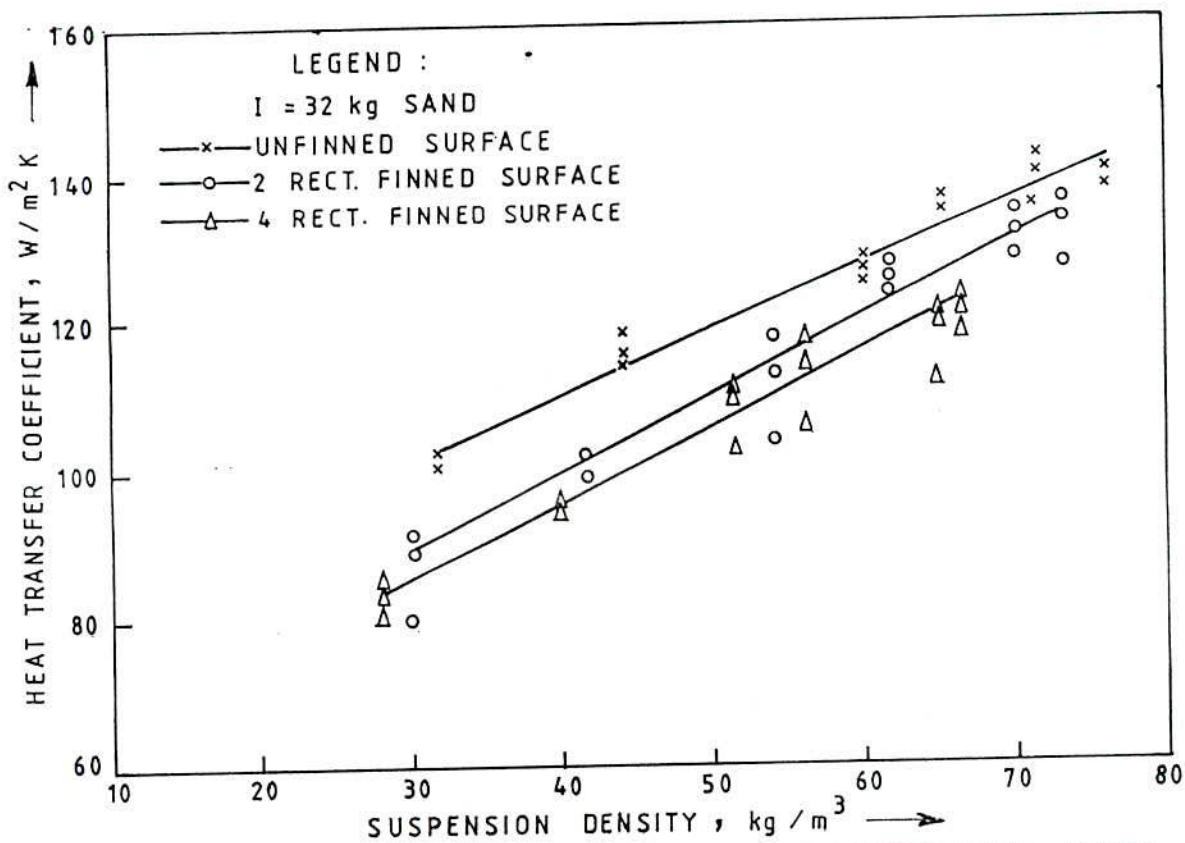

FIG.6.11 VARIATION OF HEAT TRANSFER COEFFICIENT WITH SUSPENSION DENSITY FOR RECTANGULAR FINNED SURFACE

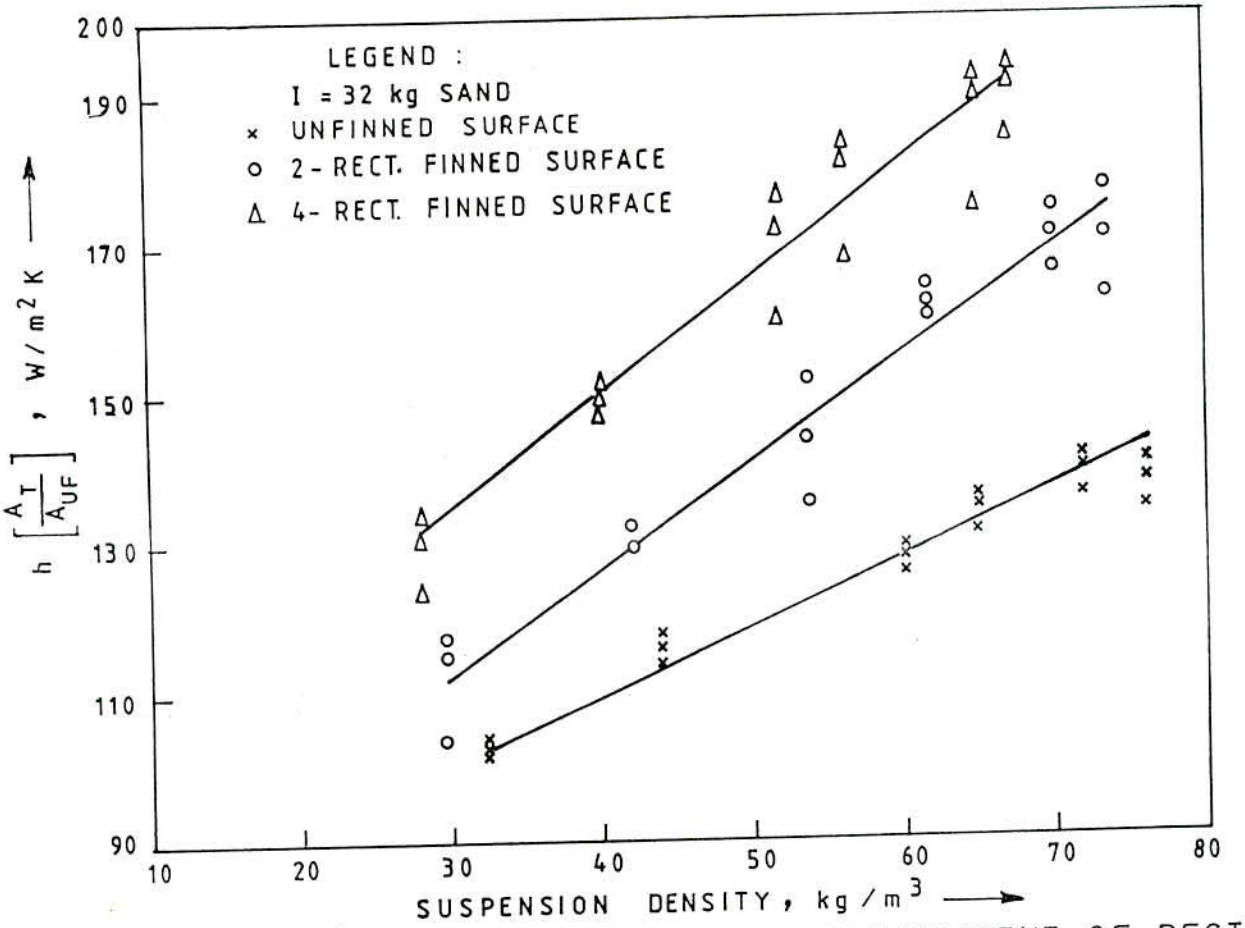

FIG. 6.12 EQUIVALENT HEAT TRANSFER COEFFICIENT OF RECTANGULAR FINS VARYING WITH SUSPENSION DENSITY

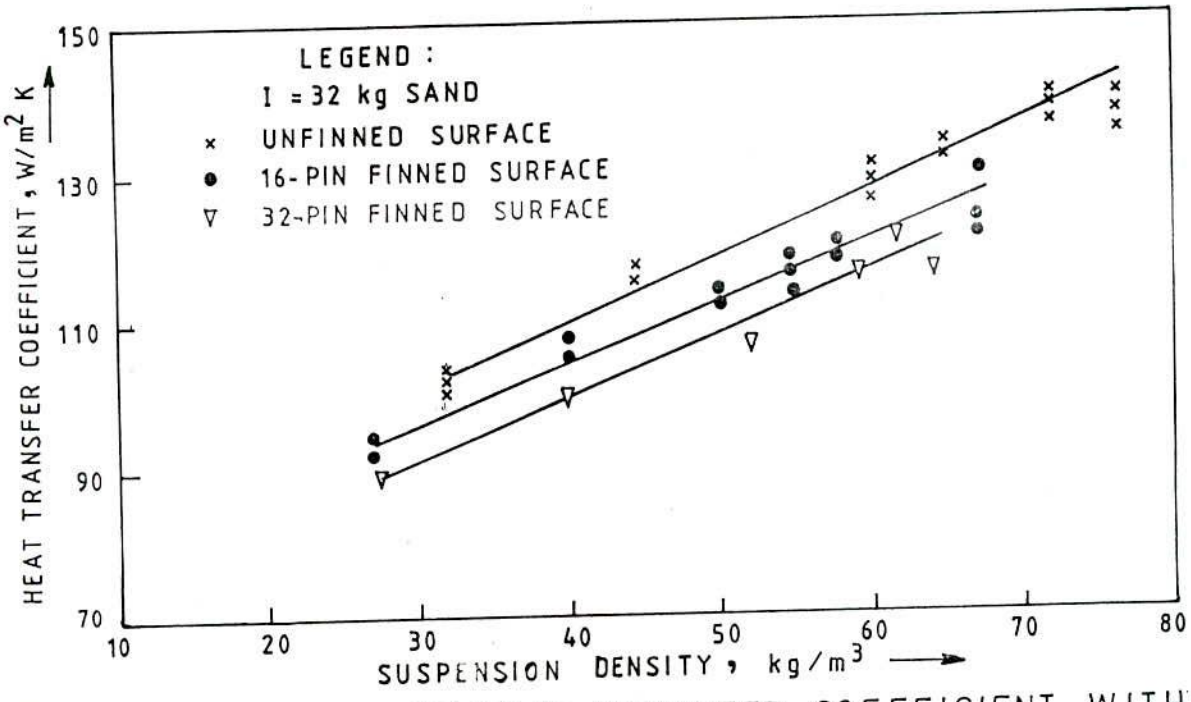

FIG. 6.13 VARIATION OF HEAT TRANSFER COEFFICIENT WITH SUSPENSION DENSITY FOR PIN FINNED SURFACE

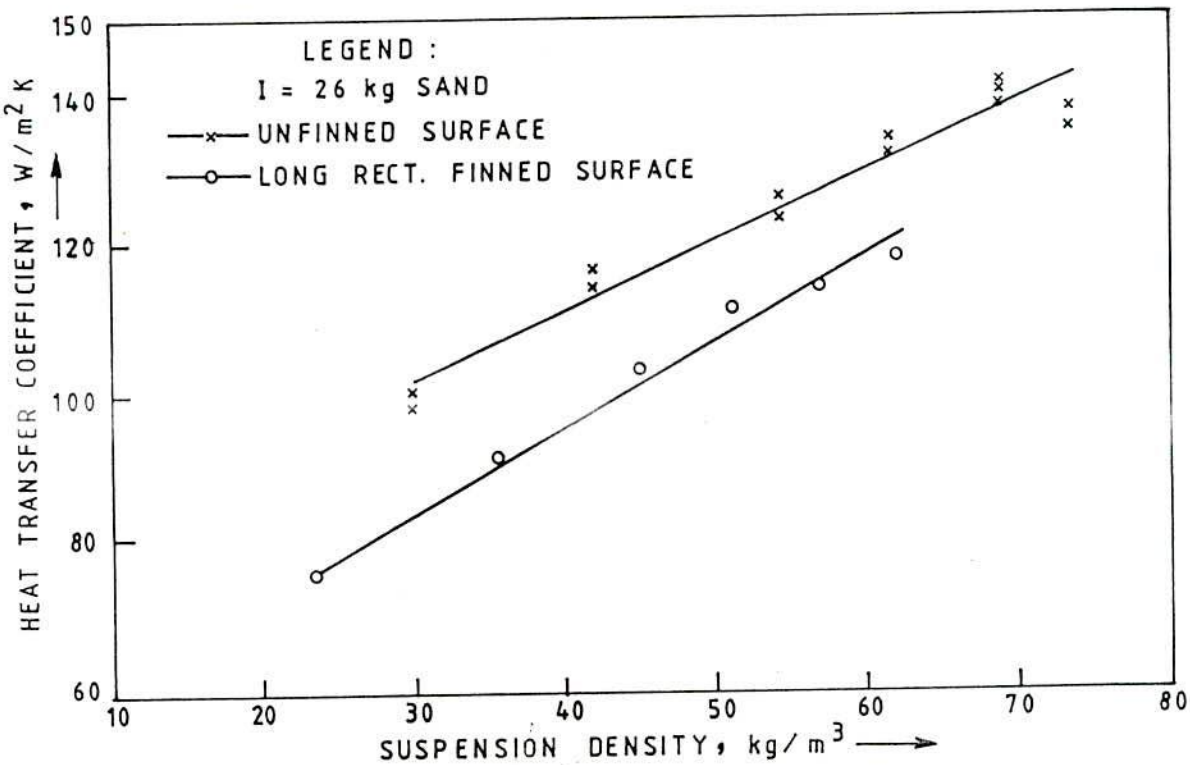

FIG.6.14 VARIATION OF HEAT TRANSFER COEFFICIENT WITH SUSPENSION DENSITY FOR 1500 mm LONG, 4-RECT. FINNED SURFACE

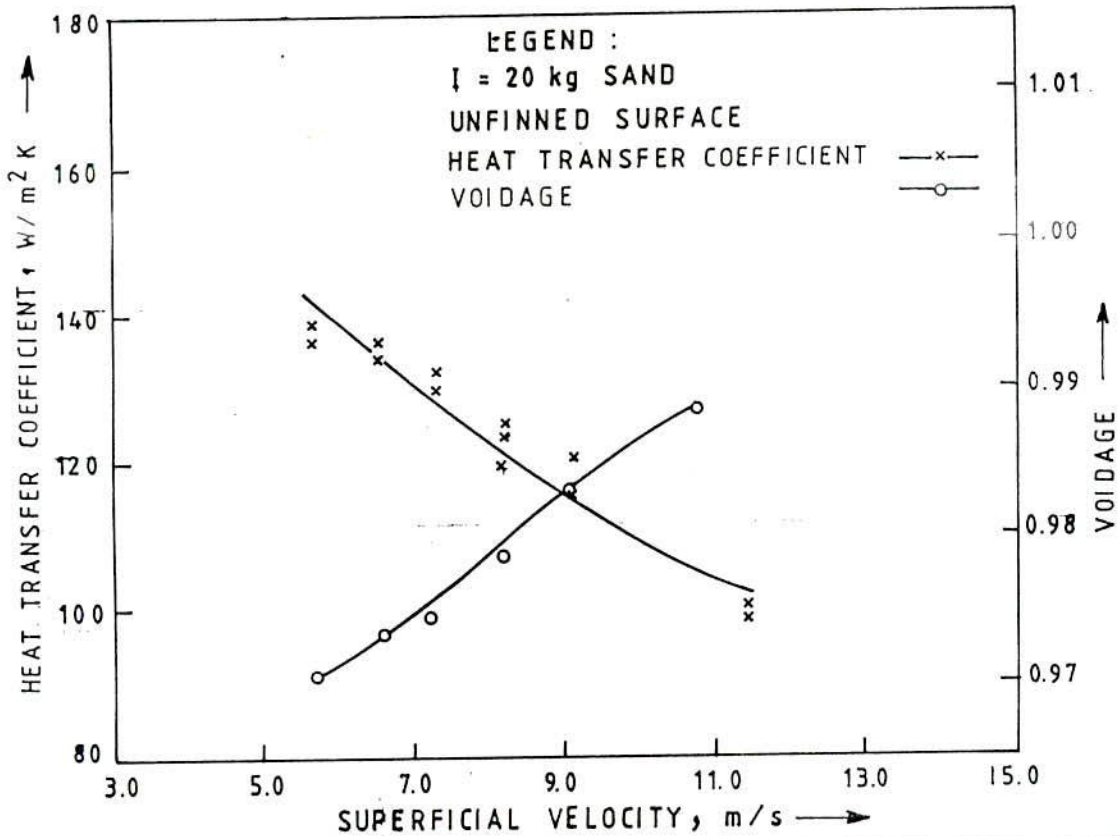

FIG.6.15 VARIATION OF HEAT TRANSFER COEFFICIENT AND VOIDAGE WITH SUPERFICIAL VELOCITY

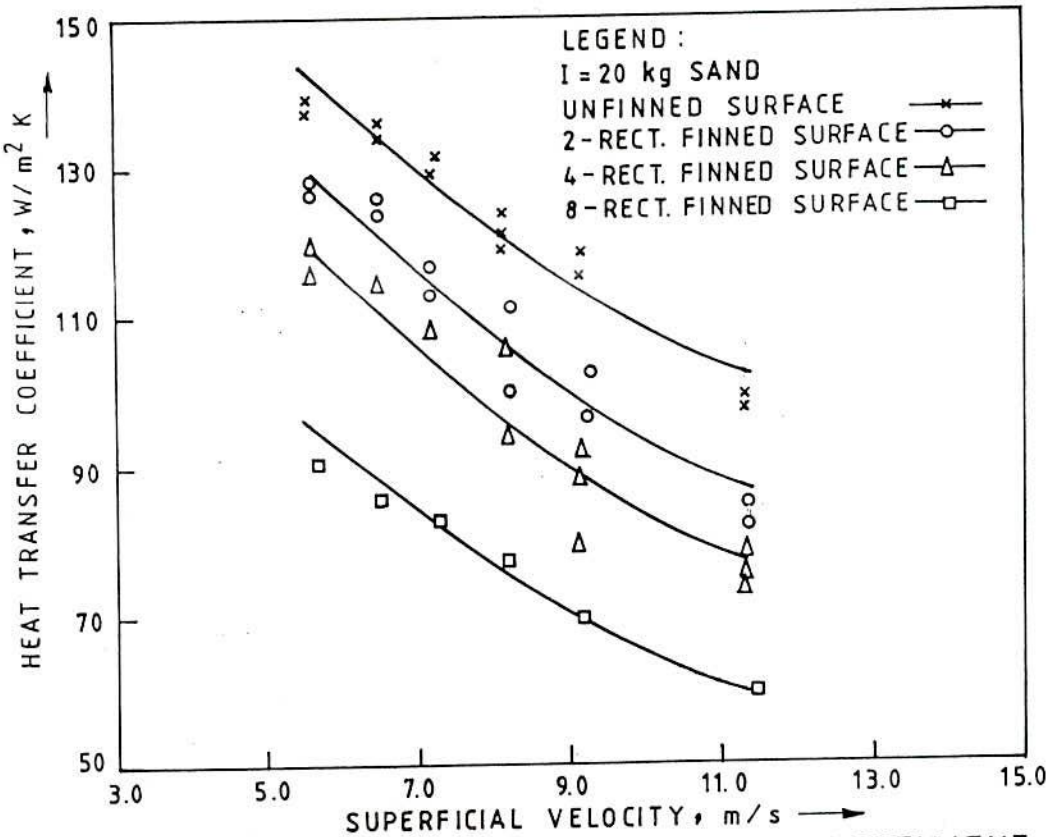

FIG.6.16 VARIATION OF HEAT TRANSFER COEFFICIENT WITH SUPERFICIAL VELOCITY FOR RECT. FINNED SURFACE

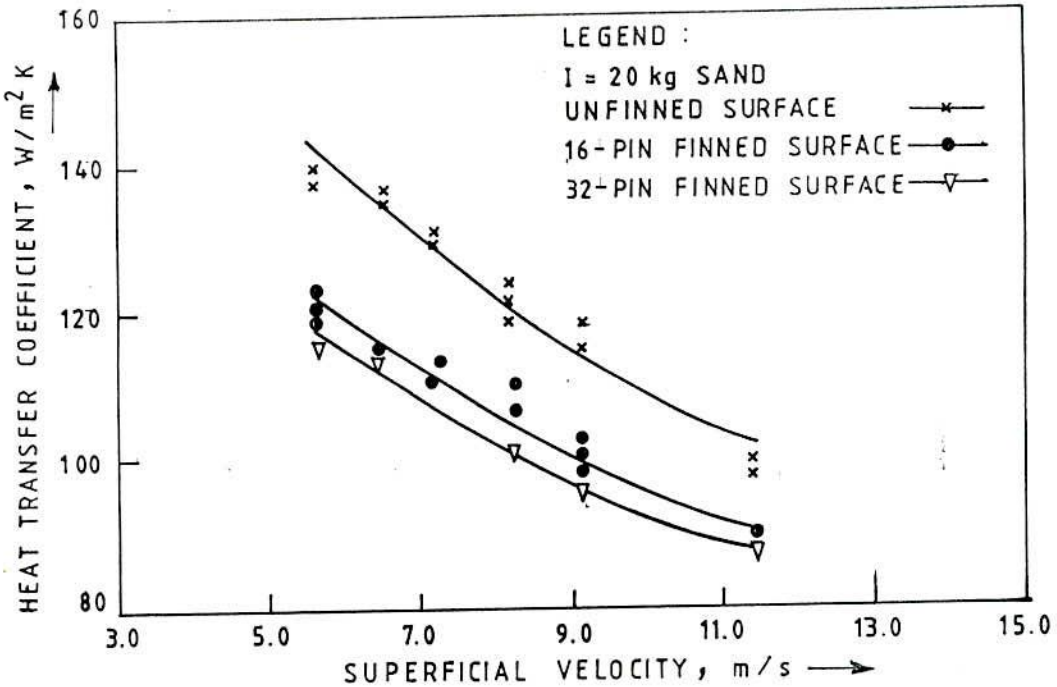

FIG.6.17 VARIATION OF HEAT TRANSFER COEFFICIENT WITH SUPERFICIAL VELOCITY FOR PIN FINNED SURFACE

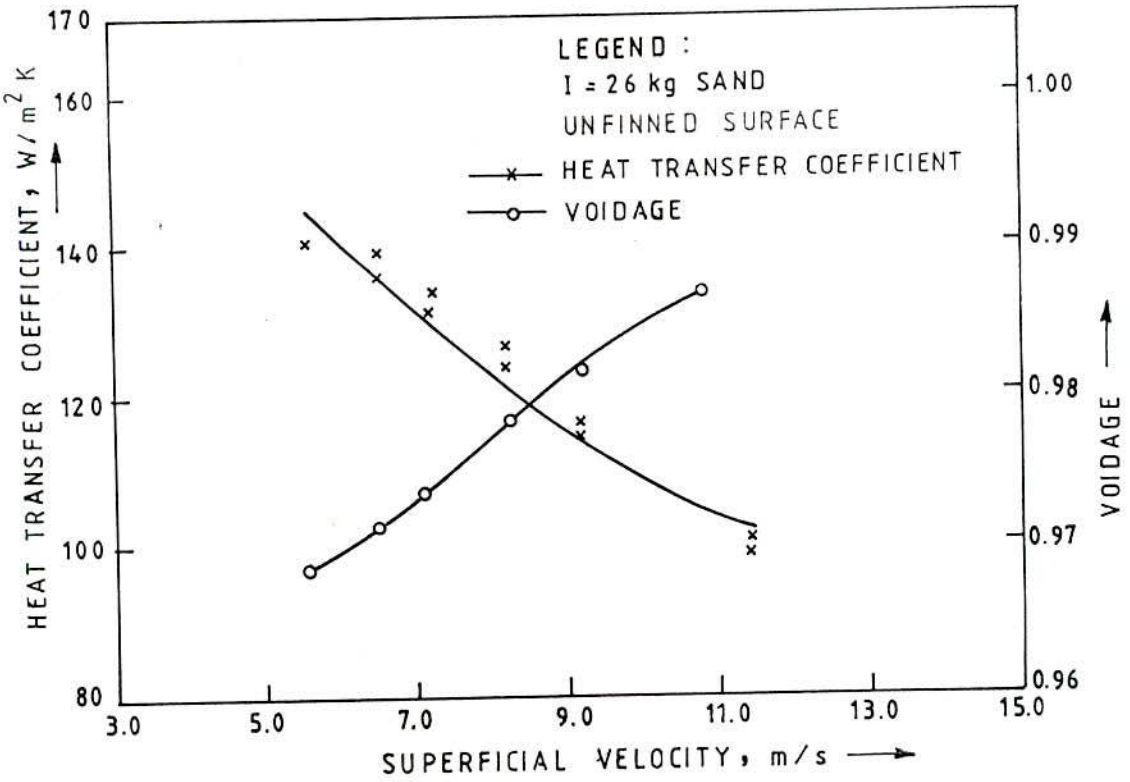

FIG. 6.18 VARIATION OF HEAT TRANSFER COEFFICIENT AND VOIDAGE WITH SUPERFICIAL VELOCITY

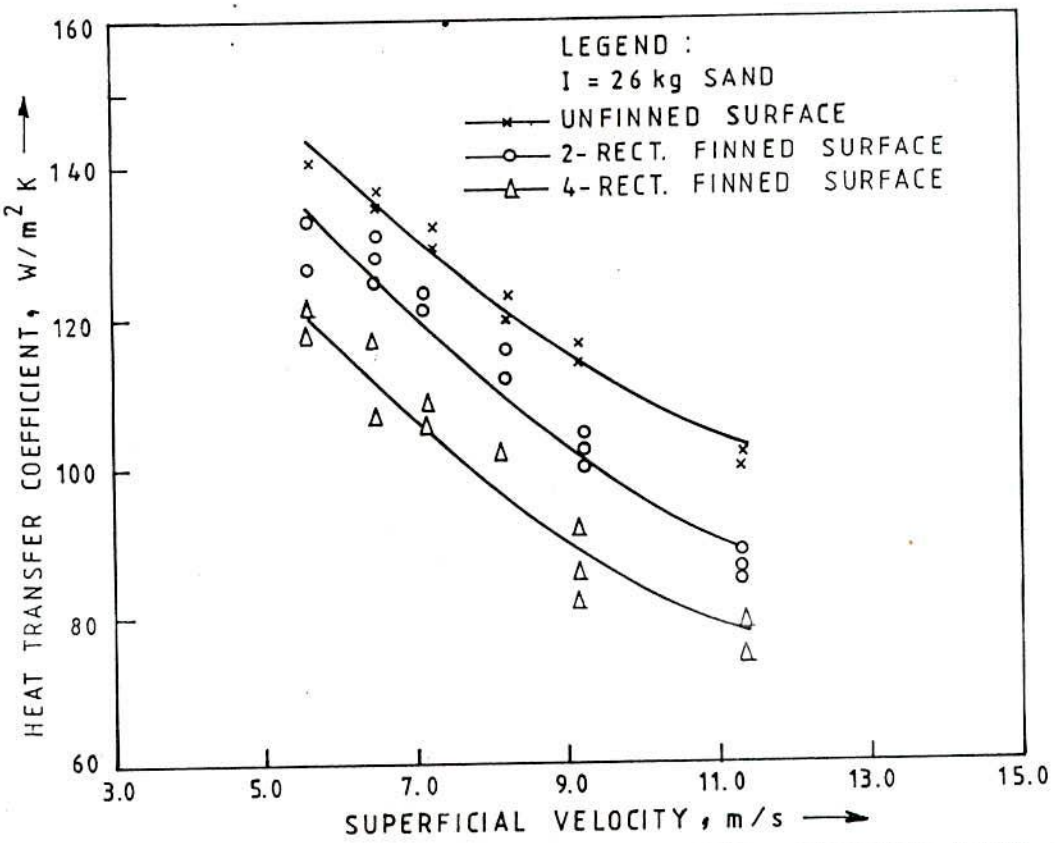

FIG. 6.19 VARIATION OF HEAT TRANSFER COEFFICIENT WITH SUPERFICIAL VELOCITY FOR RECT. FINNED SURFACE

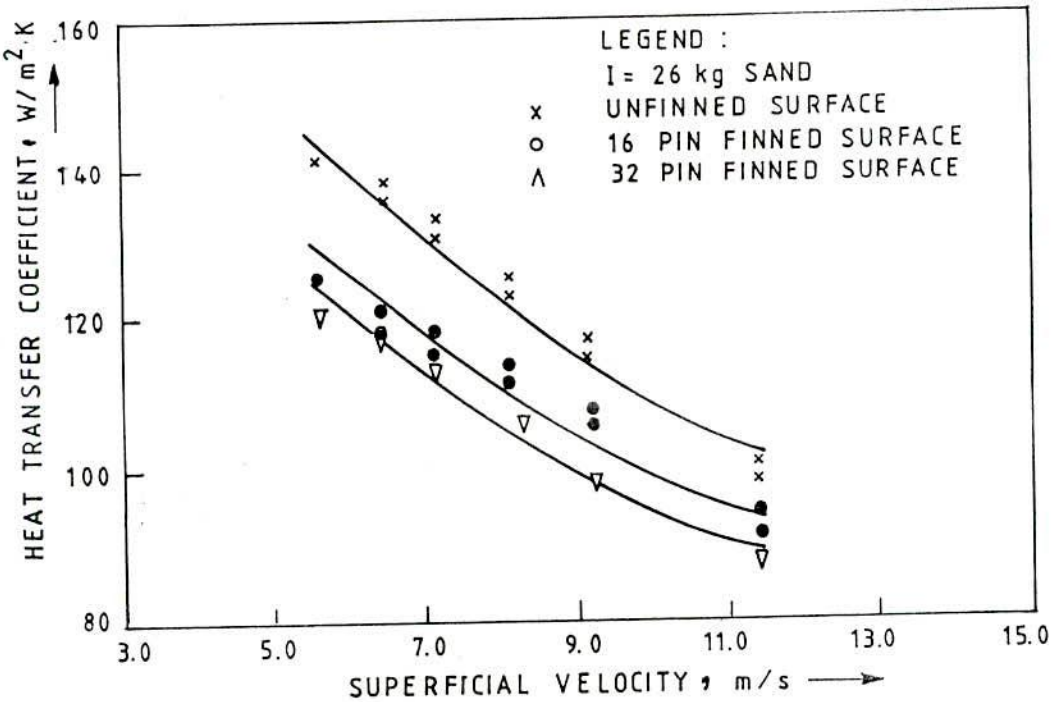

FIG.6.20 VARIATION OF HEAT TRANSFER COEFFICIENT WITH SUPERFICIAL VELOCITY FOR PIN FINNED SURFACE

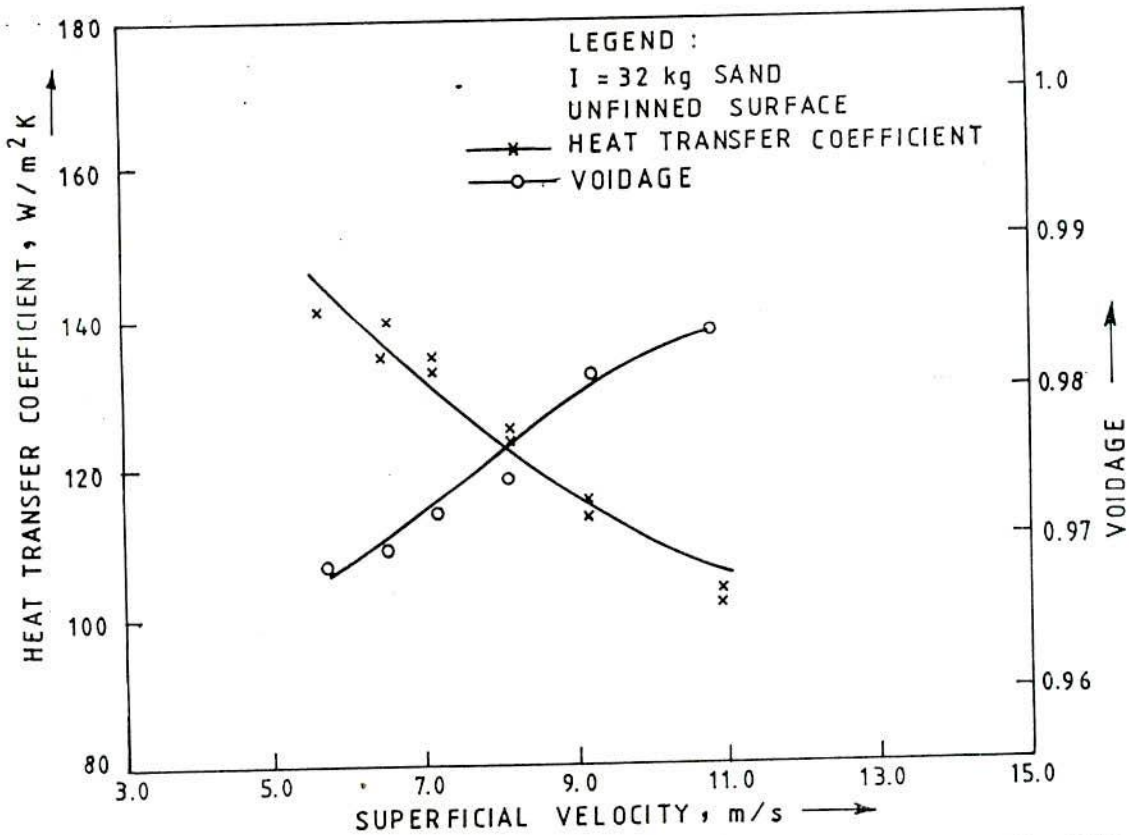

FIG.6.21 VARIATION OF HEAT TRANSFER COEFFICIENT AND VOIDAGE WITH SUPERFICIAL VELOCITY

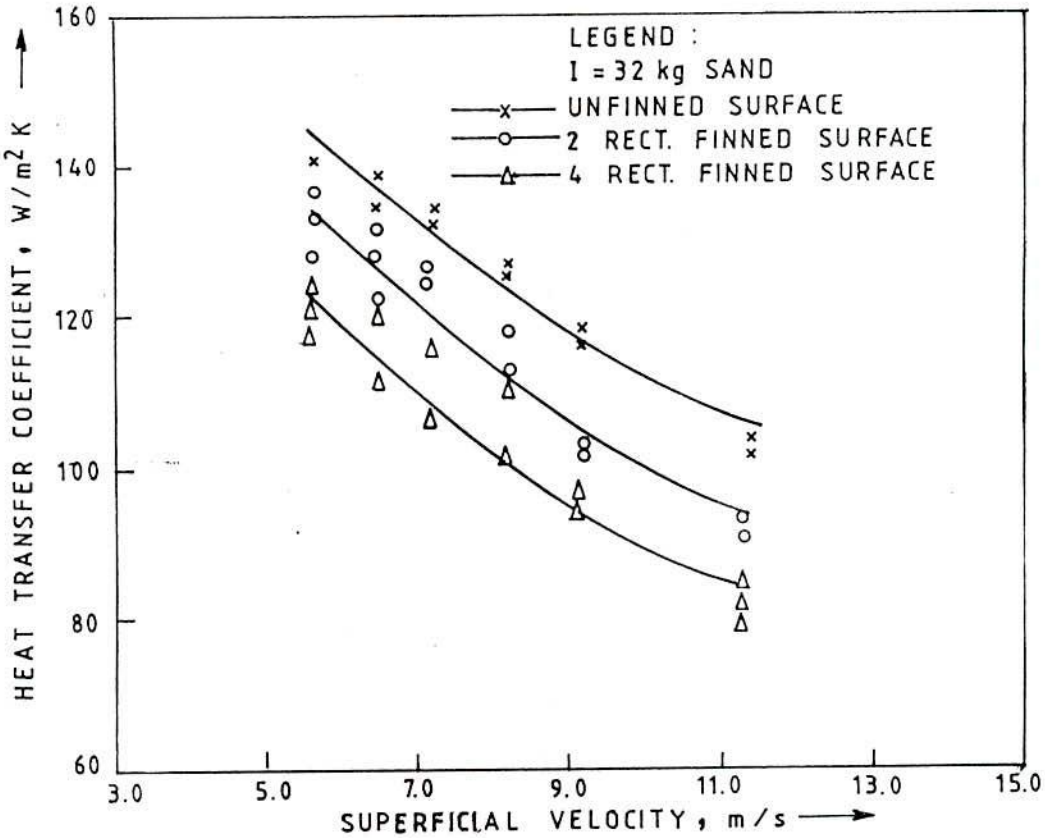

FIG. 6.22 VARIATION OF HEAT TRANSFER COEFFICIENT WITH SUPERFICIAL VELOCITY FOR RECT. FINNED SURFACE

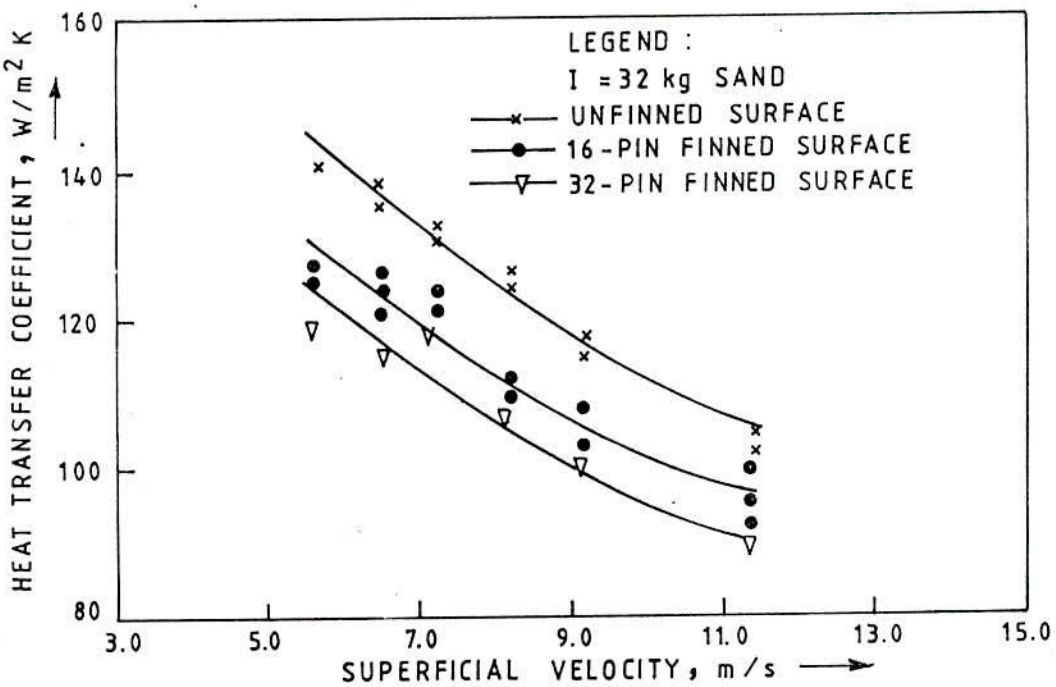

FIG. 6.23 VARIATION OF HEAT TRANSFER COEFFICIENT WITH SUPERFICIAL VELOCITY FOR PIN FINNED SURFACE

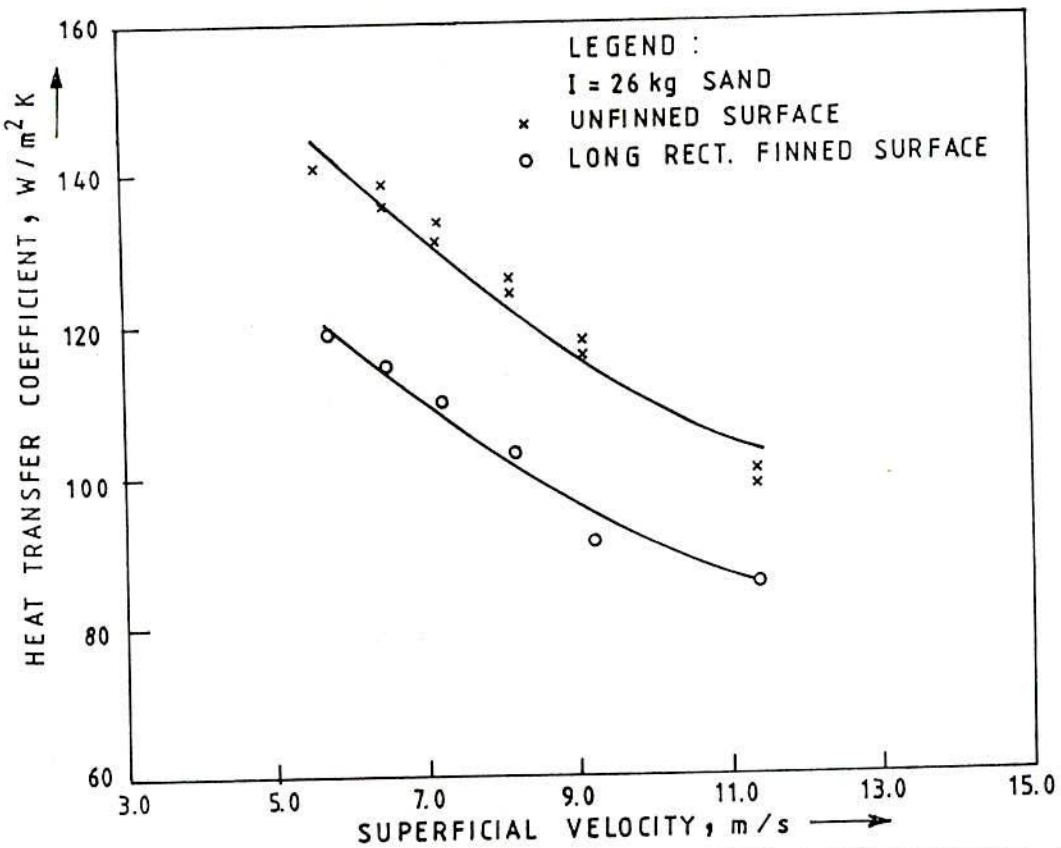

FIG.6.24 VARIATION OF HEAT TRANSFER COEFFICIENT WITH SUPERFICIAL VELOCITY FOR 1500 mm LONG 4-RECT. FINNED SURFACE

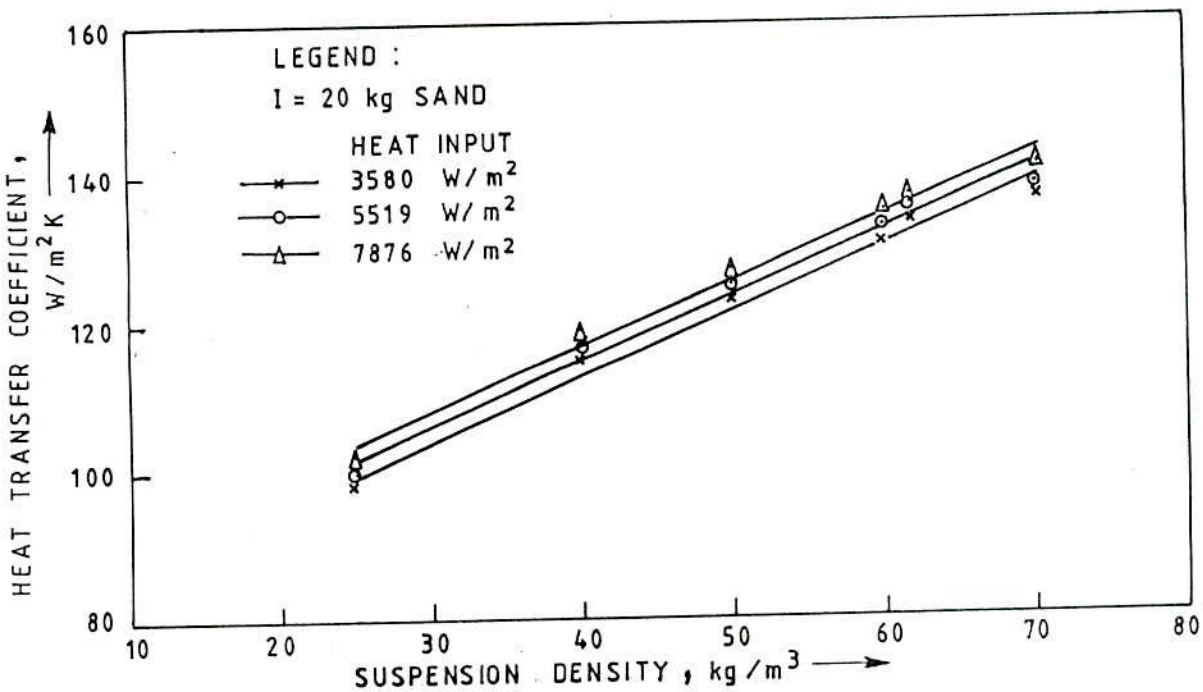

FIG.6.25 EFFECT OF HEAT INPUT ON HEAT TRANSFER COEFFICIENT FOR UNFINNED SURFACE

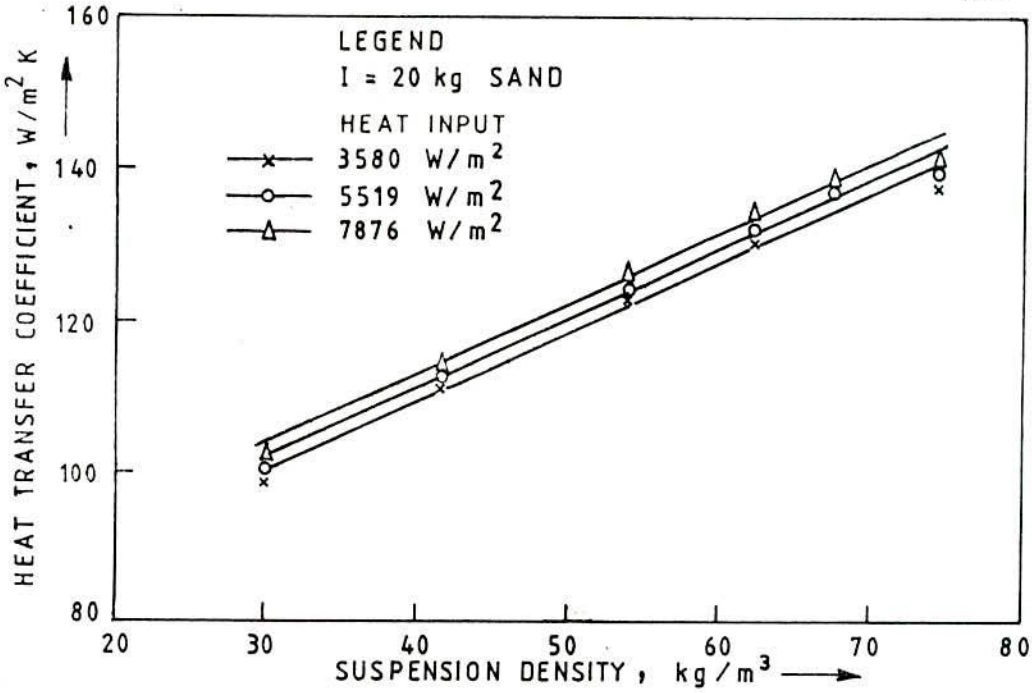

FIG. 6.26 EFFECT OF HEAT INPUT ON HEAT TRANSFER COEFFICIENT FOR 2-RECT. FINNED SURFACE

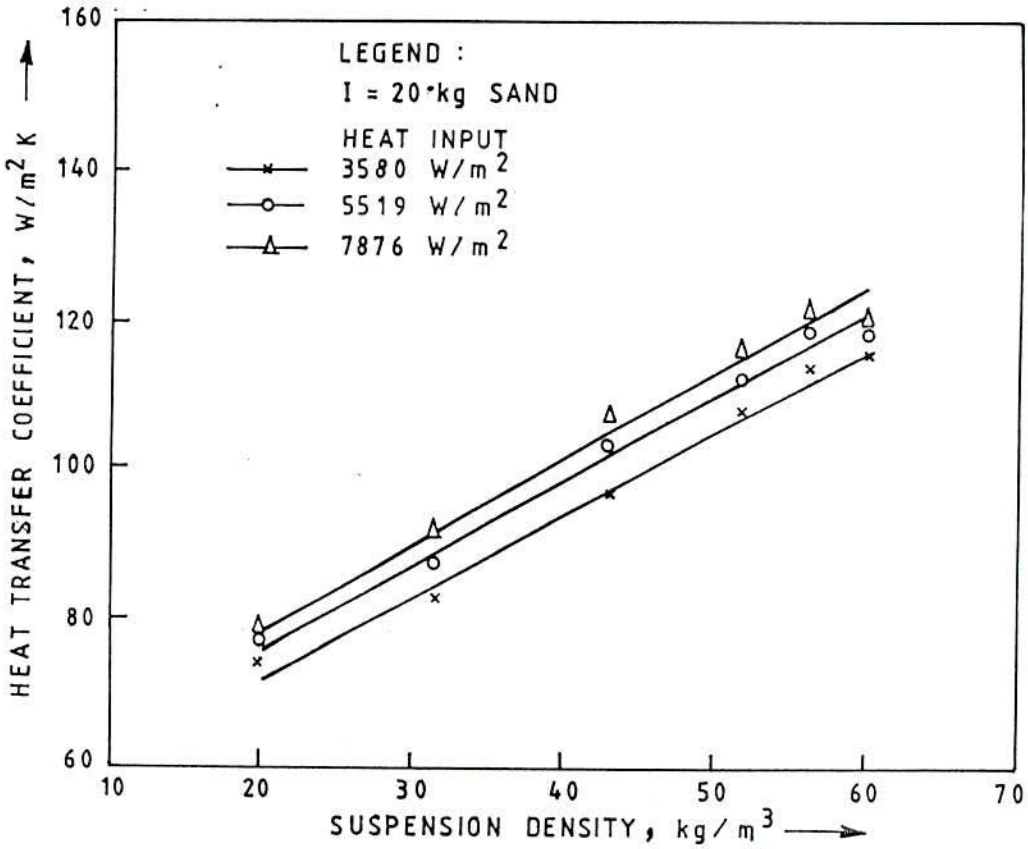

FIG. 6.27 EFFECT OF HEAT INPUT ON HEAT TRANSFER COEFFICIENT FOR 4-RECT. FINNED SURFACE

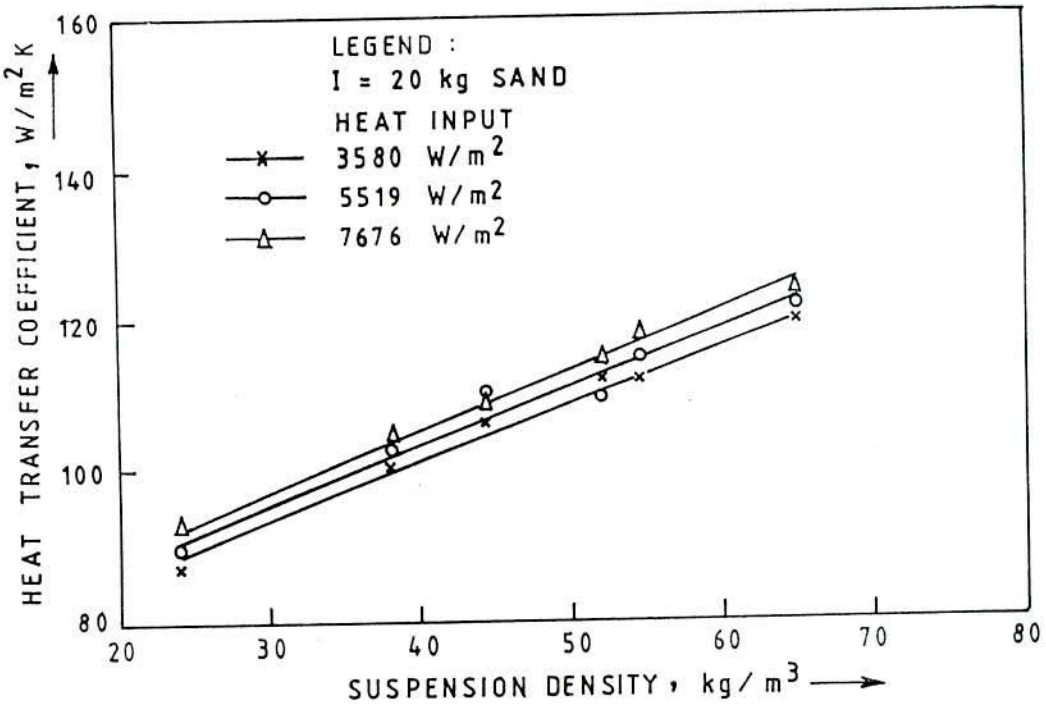

FIG. 6.28 EFFECT OF HEAT INPUT ON HEAT TRANSFER COEFFICIENT FOR 16-PIN FINNED SURFACE

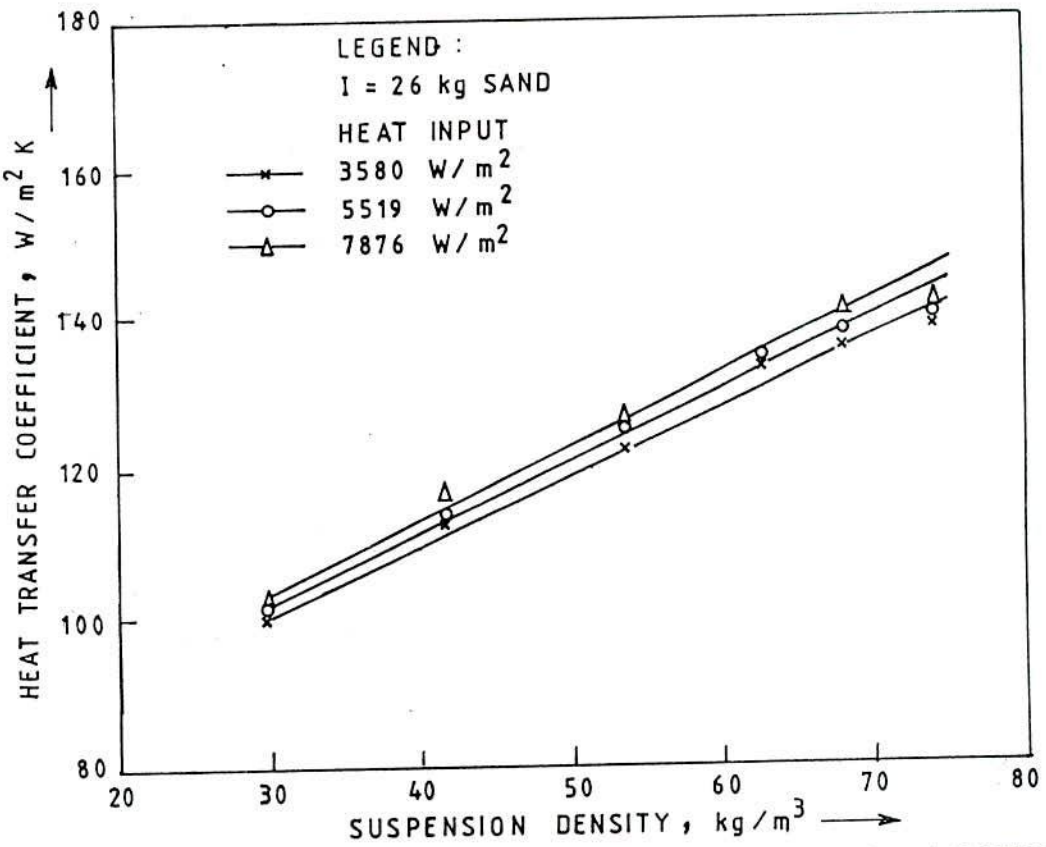

FIG. 6.29 EFFECT OF HEAT INPUT ON HEAT TRANSFER COEFFICIENT FOR UNFINNED SURFACE

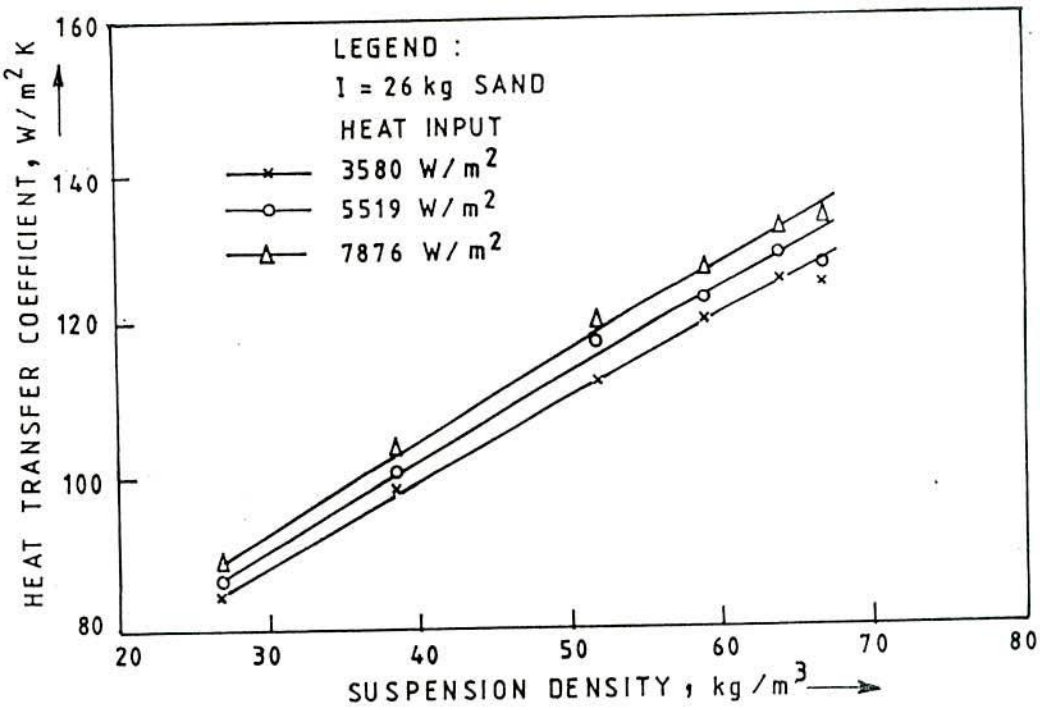

FIG. 6.30 EFFECT OF HEAT INPUT ON HEAT TRANSFER COEFFICIENT FOR 2-RECT. FINNED SURFACE

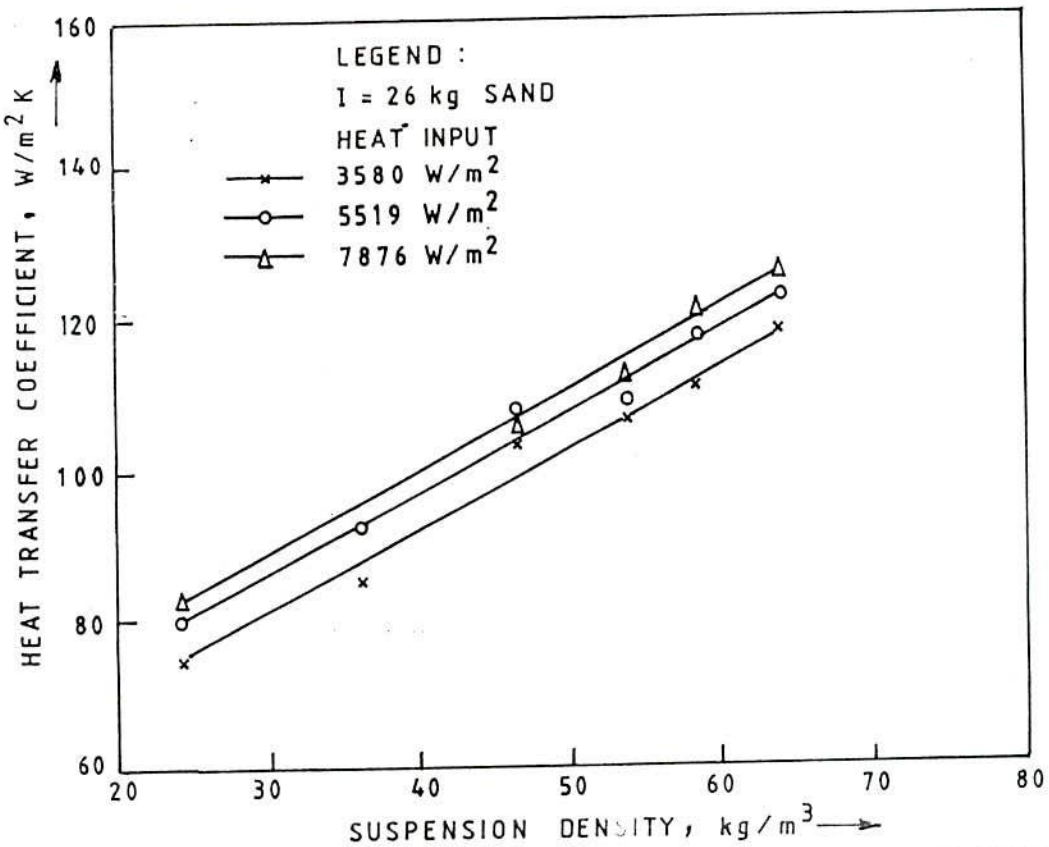

FIG. 6.31 EFFECT OF HEAT INPUT ON HEAT TRANSFER COEFFICIENT FOR 4-RECT. FINNED SURFACE

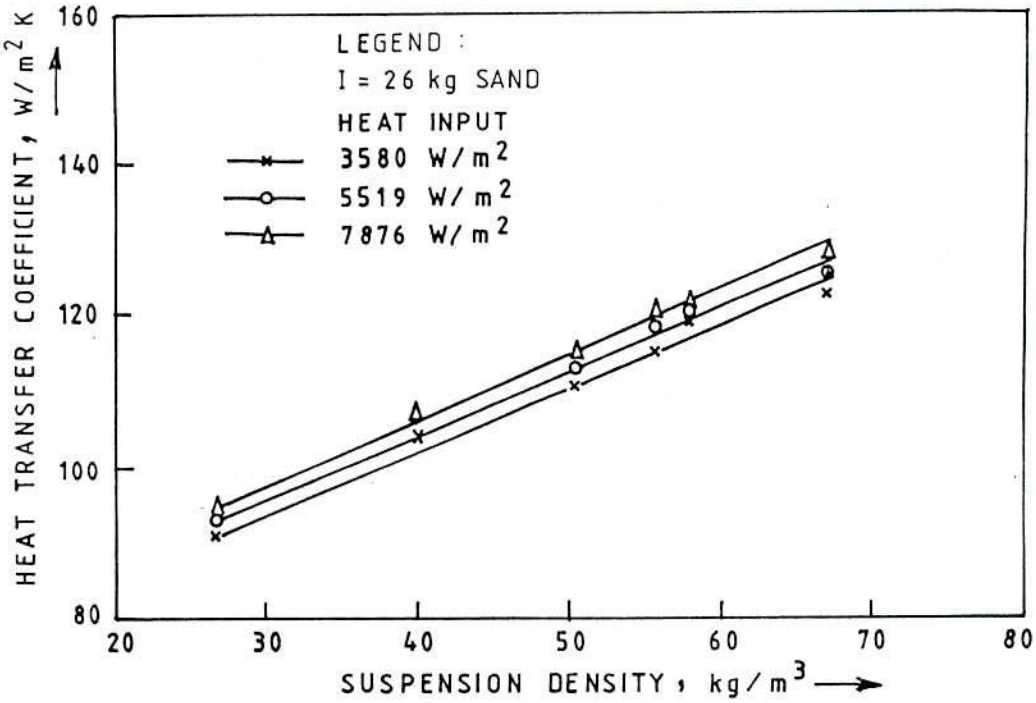

FIG.6.32 EFFECT OF HEAT INPUT ON HEAT TRANSFER COEFFICIENT FOR 16-PIN FINNED SURFACE

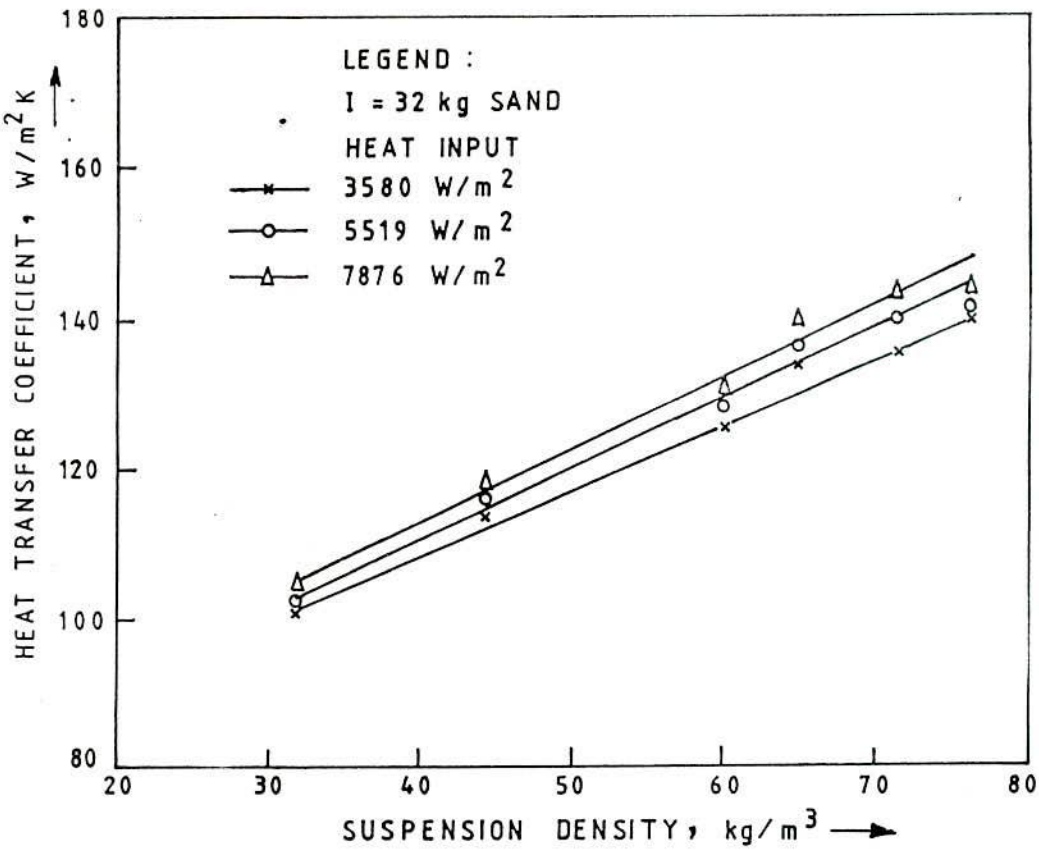

FIG.3.33 EFFECT OF HEAT INPUT ON HEAT TRANSFER COEFFICIENT FOR UNFINNED SURFACE

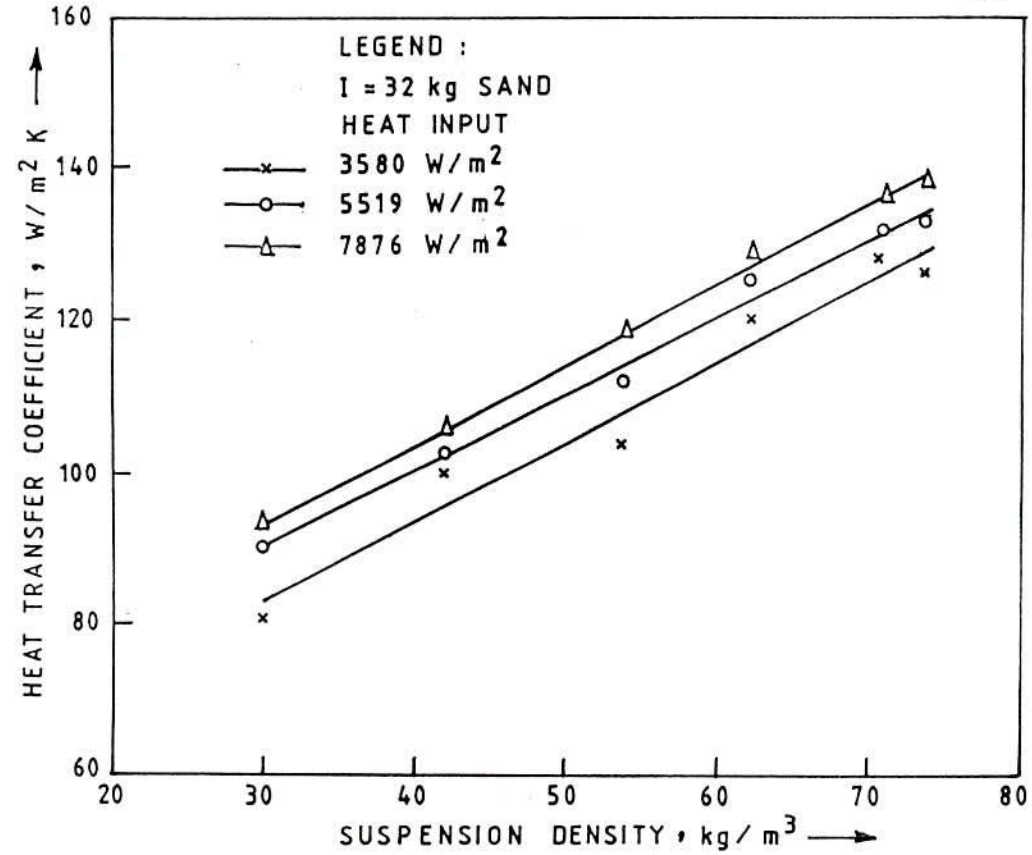

FIG. 6.34 EFFECT OF HEAT INPUT ON HEAT TRANSFER COEFFICIENT FOR 2-RECT. FINNED SURFACE

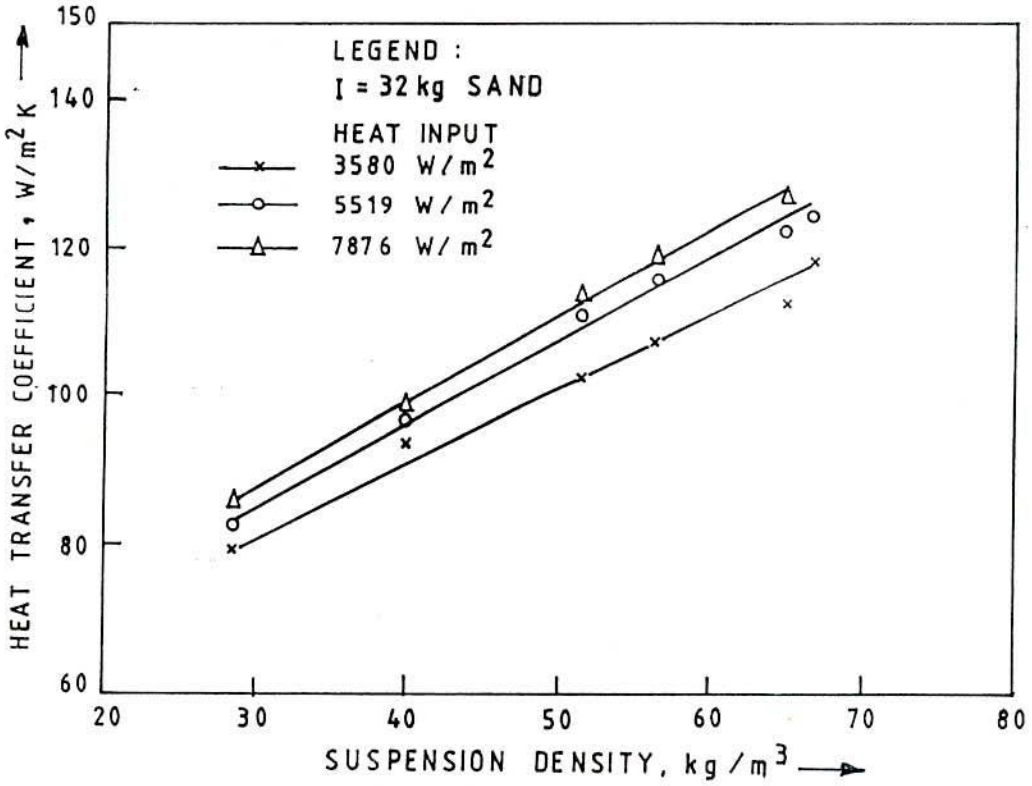

FIG. 6.35 EFFECT OF HEAT INPUT ON HEAT TRANSFER COEFFICIENT FOR 4-RECT. FINNED SURFACE

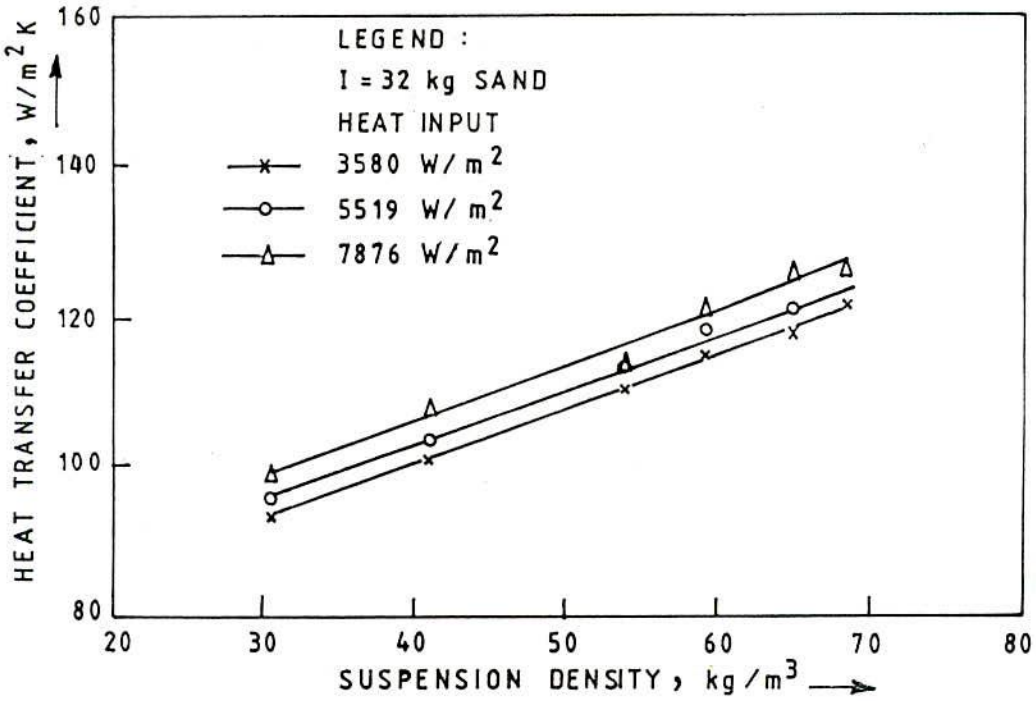

FIG.6.36 EFFECT OF HEAT INPUT ON HEAT TRANSFER COEFFICIENT FOR 16-PIN FINNED SURFACE

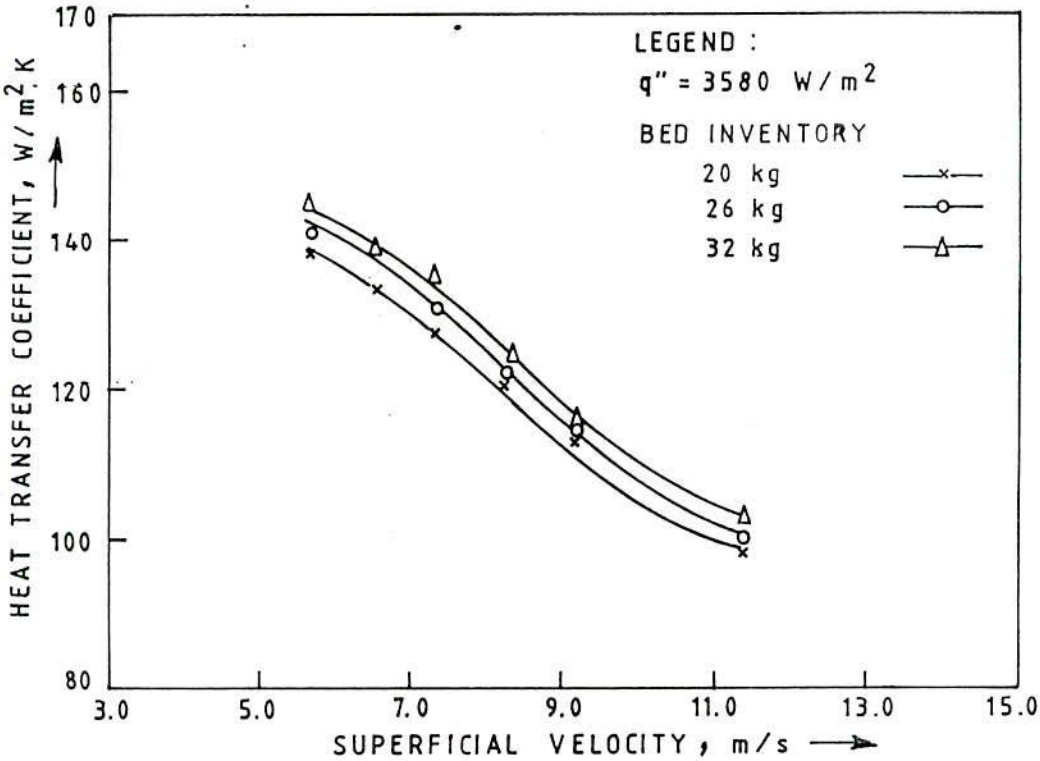

FIG.6.37 EFFECT OF BED INVENTORY ON HEAT TRANSFER COEFFICIENT FOR UNFINNED SURFACE

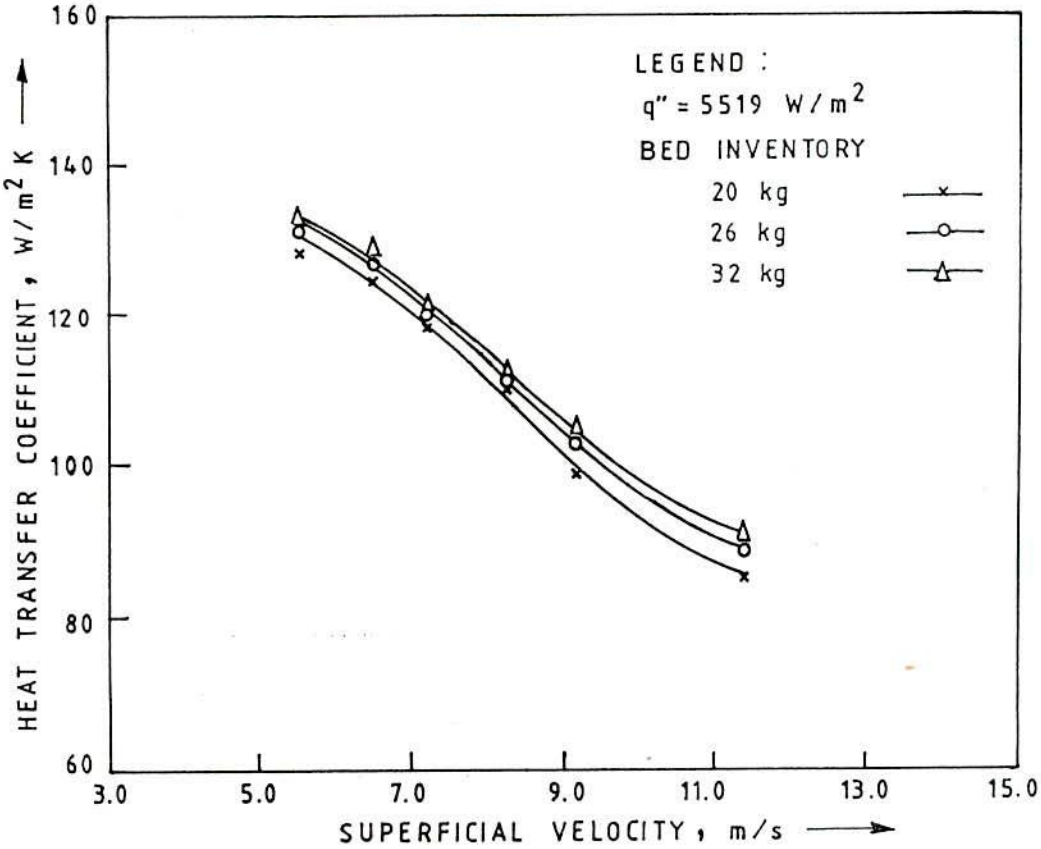

FIG.6.38 EFFECT OF BED INVENTORY ON HEAT TRANSFER COEFFICIENT FOR 2-RECT. FINNED SURFACE

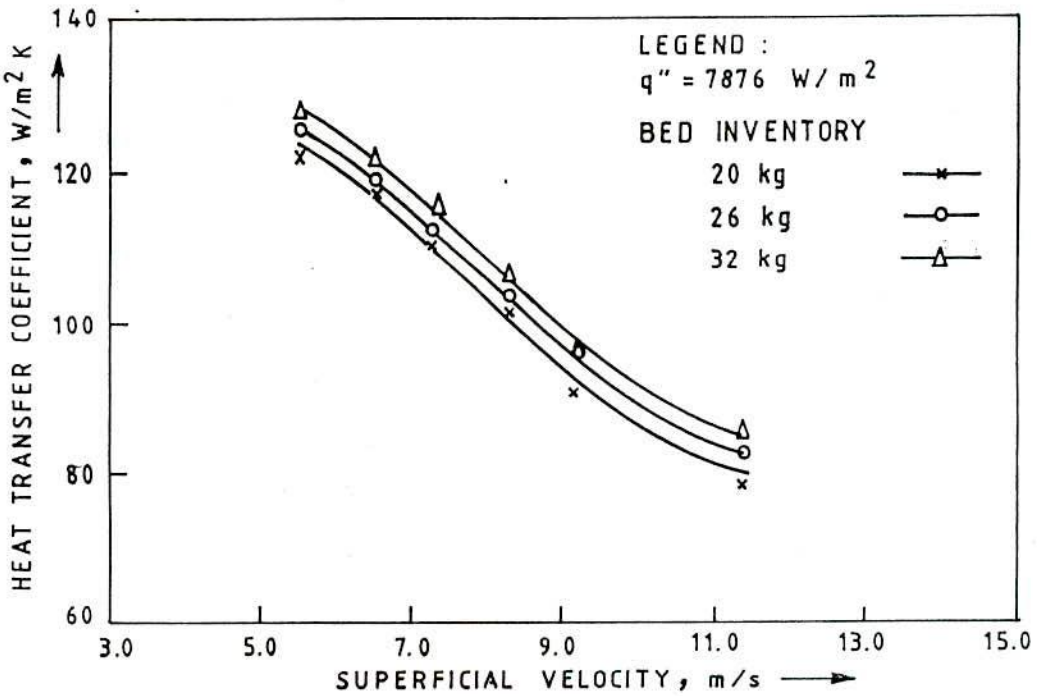

FIG.3.39 EFFECT OF BED INVENTORY ON HEAT TRANSFER COEFFICIENT FOR 4-RECT. FINNED SURFACE

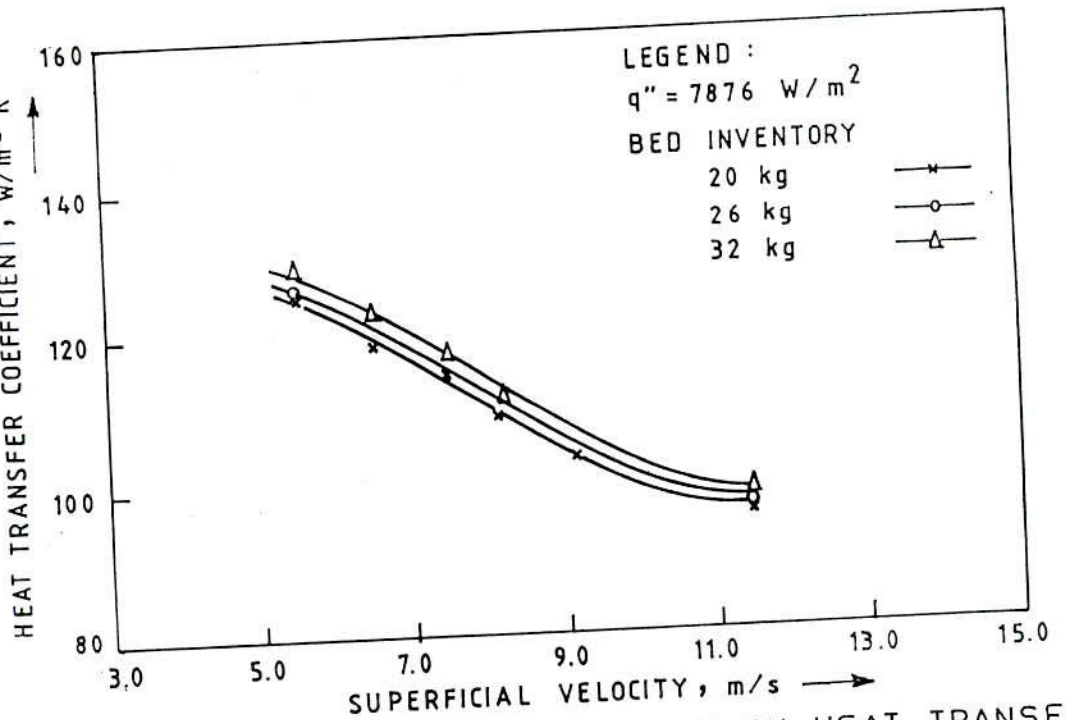

FIG.6.40 EFFECT OF BED INVENTORY ON HEAT TRANSFER COEFFICIENT FOR 16-PIN FINNED SURFACE

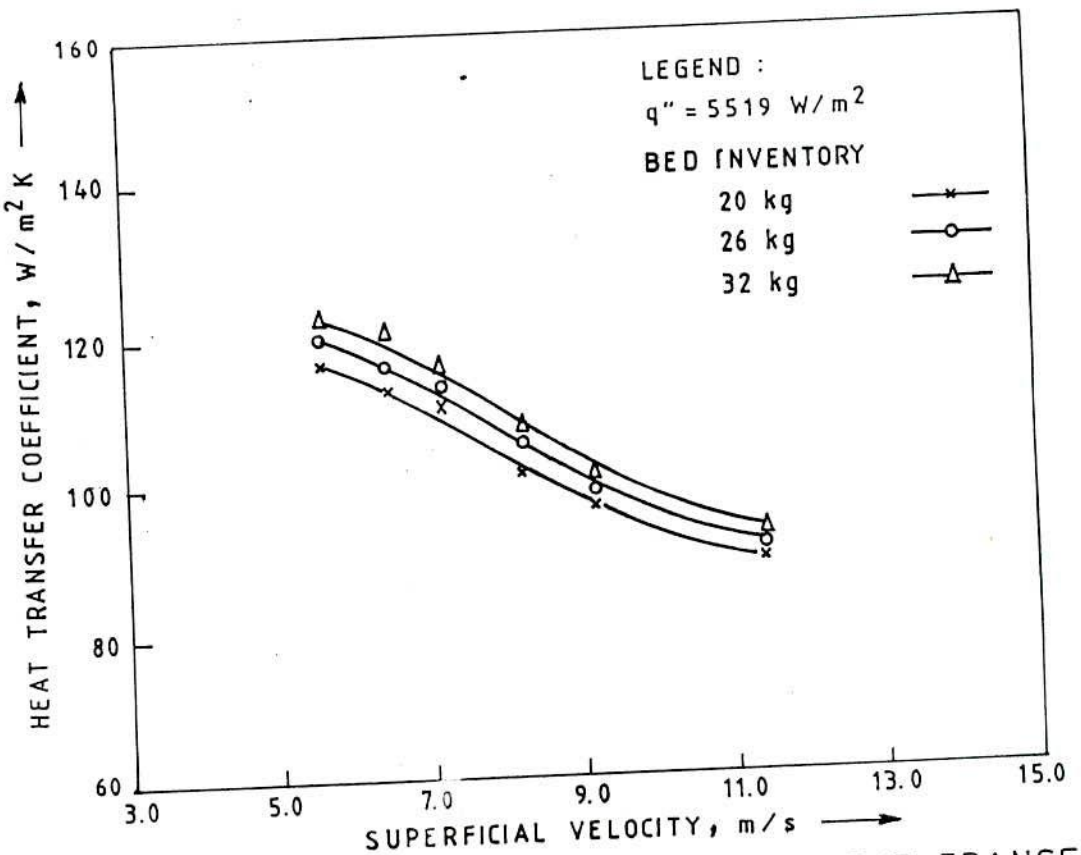

FIG.6.41 EFFECT OF BED INVENTORY ON HEAT TRANSFER COEFFICIENT FOR 32-PIN FINNED SURFACE

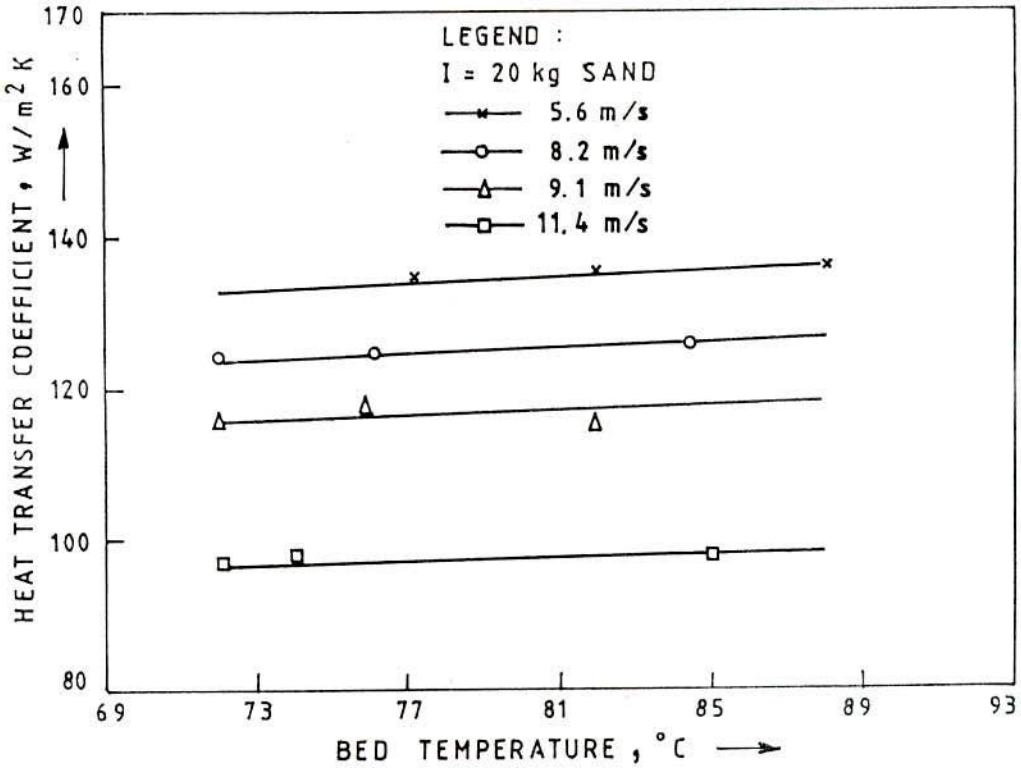

FIG. 6.42 EFFECT OF BED TEMPERATURE ON HEAT TRANSFER COEFFICIENT FOR UNFINNED SURFACE

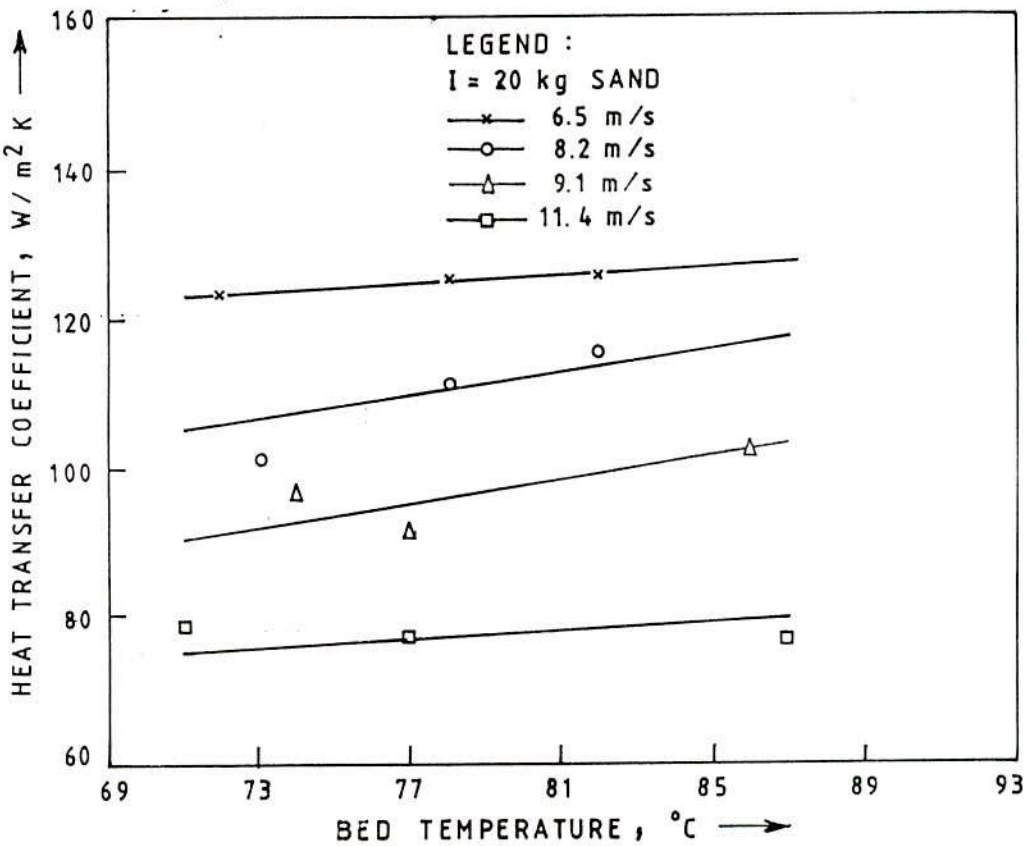

FIG. 6.43 EFFECT OF BED TEMPERATURE ON HEAT TRANSFER COEFFICIENT FOR 2-RECT. FINNED SURFACE

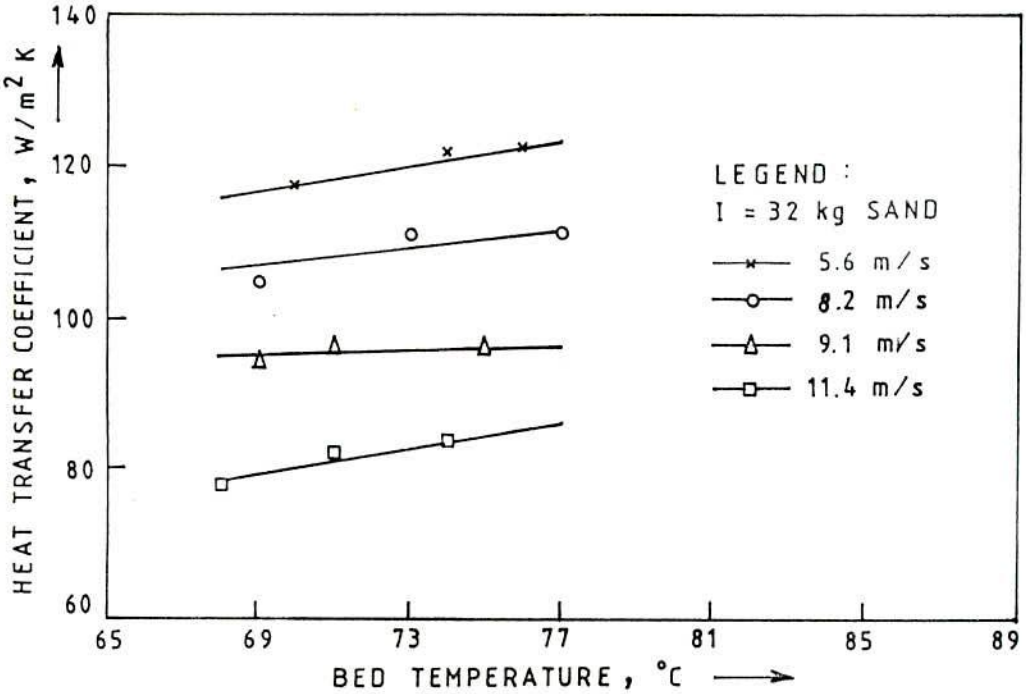

FIG. 6.44 EFFECT OF BED TEMPERATURE ON HEAT TRANSFER COEFFICIENT FOR 4-RECT. FINNED SURFACE

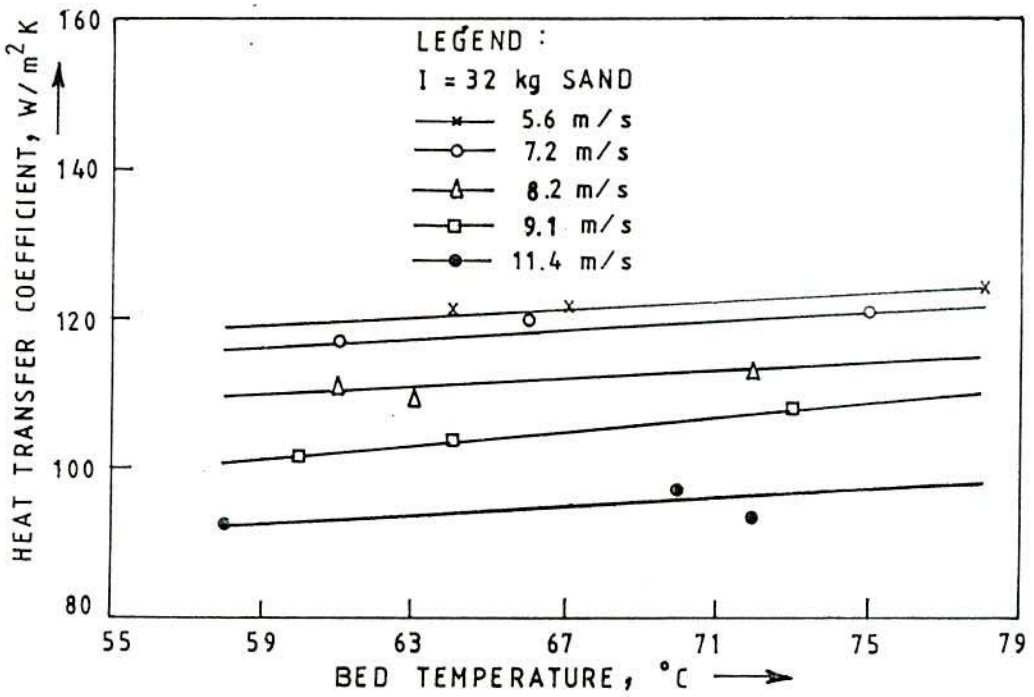

FIG. 6.45(a) EFFECT OF BED TEMPERATURE ON HEAT TRANSFER COEFFICIENT FOR 16-PIN FINNED SURFACE

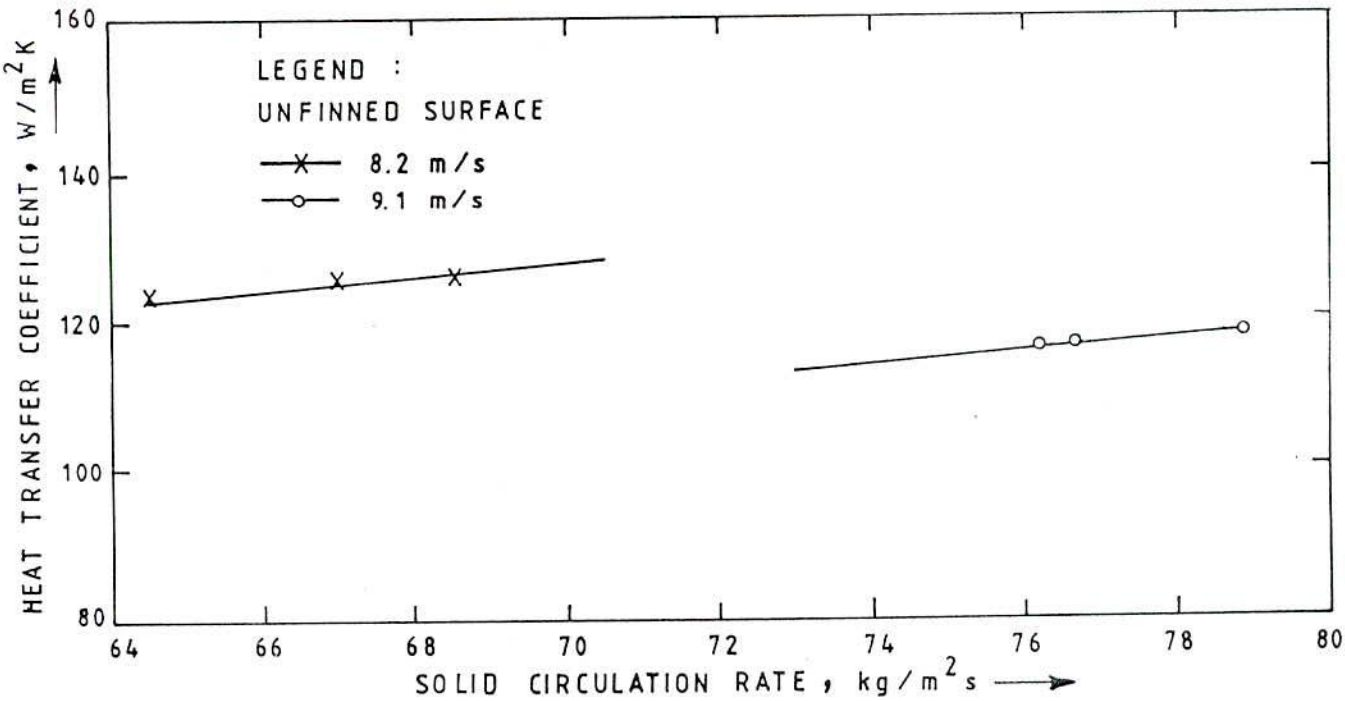

FIG. 6.45 (b) EFFECT OF SOLID CIRCULATION RATE ON HEAT TRANSFER COEFFICIENT FOR UNFINNED SURFACE

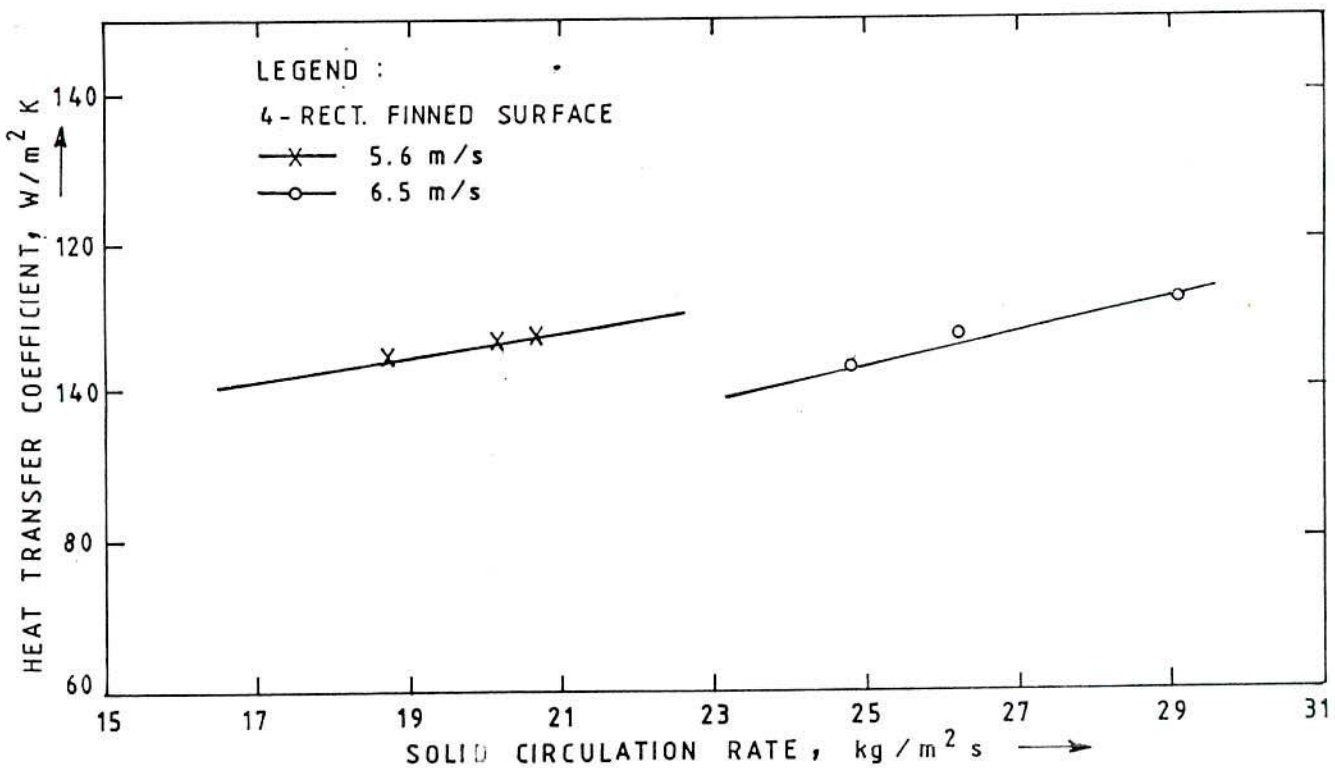

FIG. 6.45 (c) EFFECT OF SOLID CIRCULATION RATE ON HEAT TRANSFER COEFFICIENT FOR RECT. FINNED SURFACE

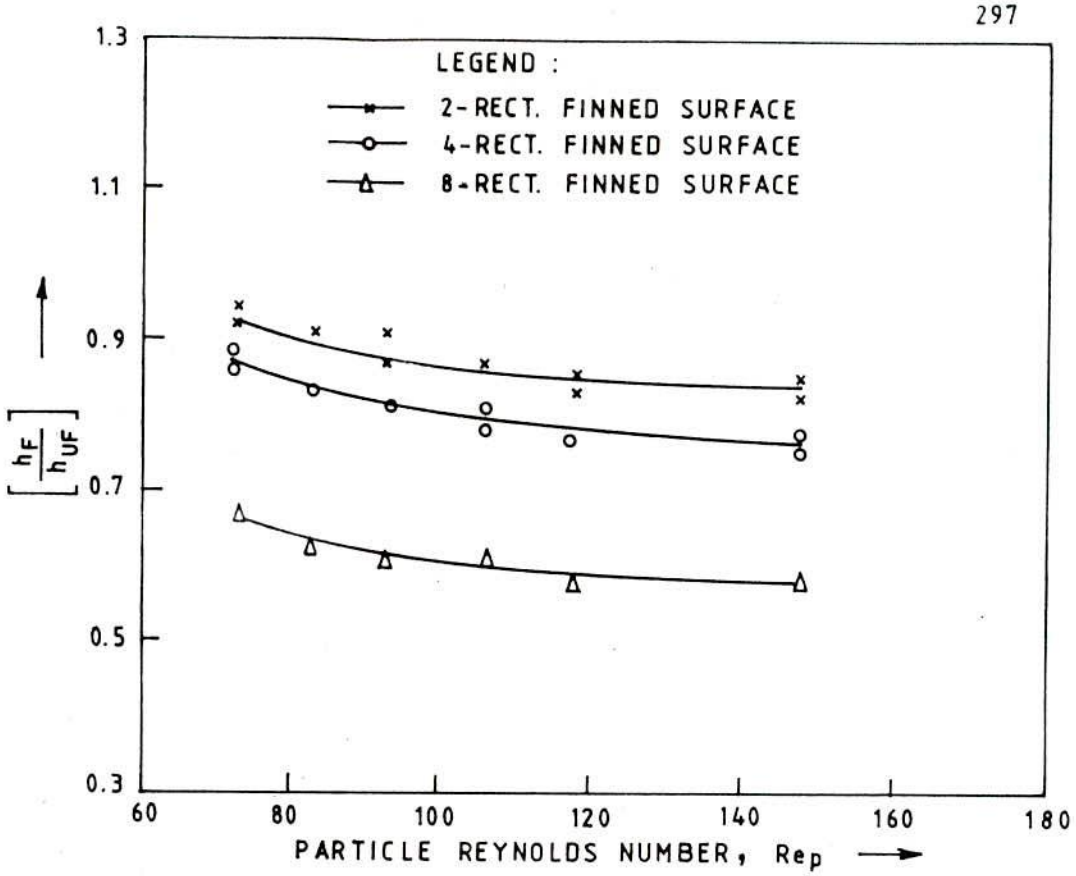

FIG. 4 EFFECT OF Re_p ON THE RATIO OF HEAT TRANSFER COEFFICIENTS FOR FINNED AND UNFINNED SURFACES.

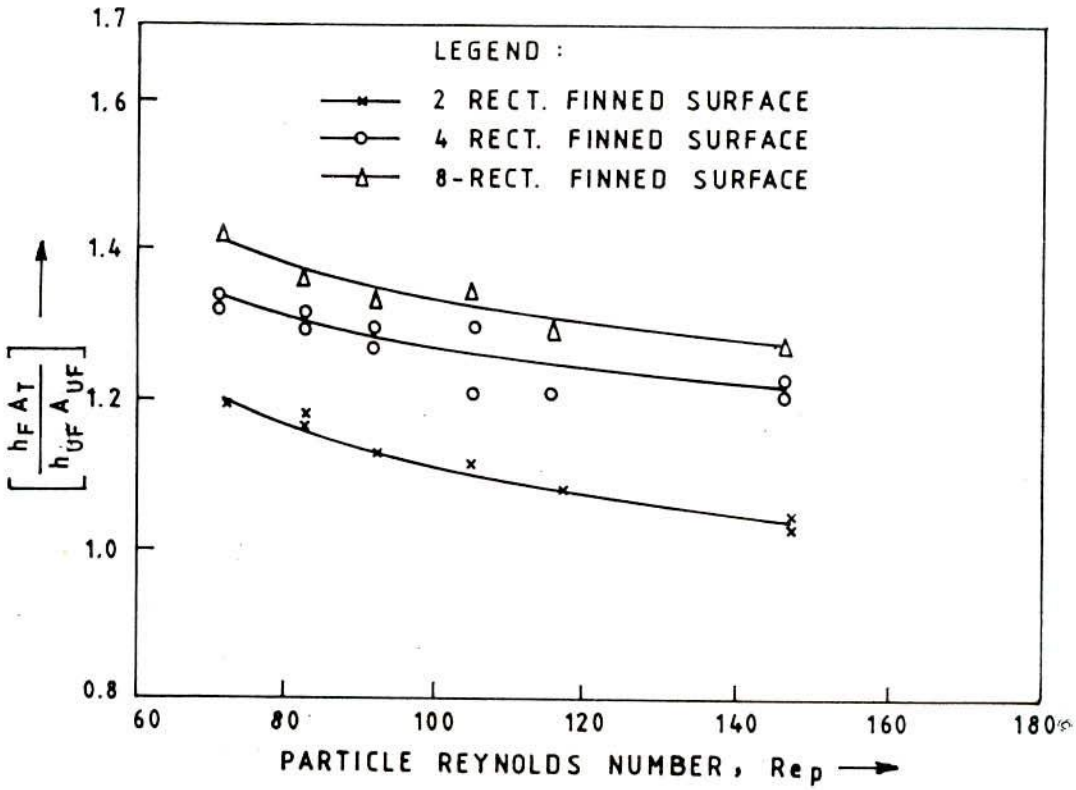

FIG. 5 EFFECT OF Re_p ON CAPACITY FUNCTION.

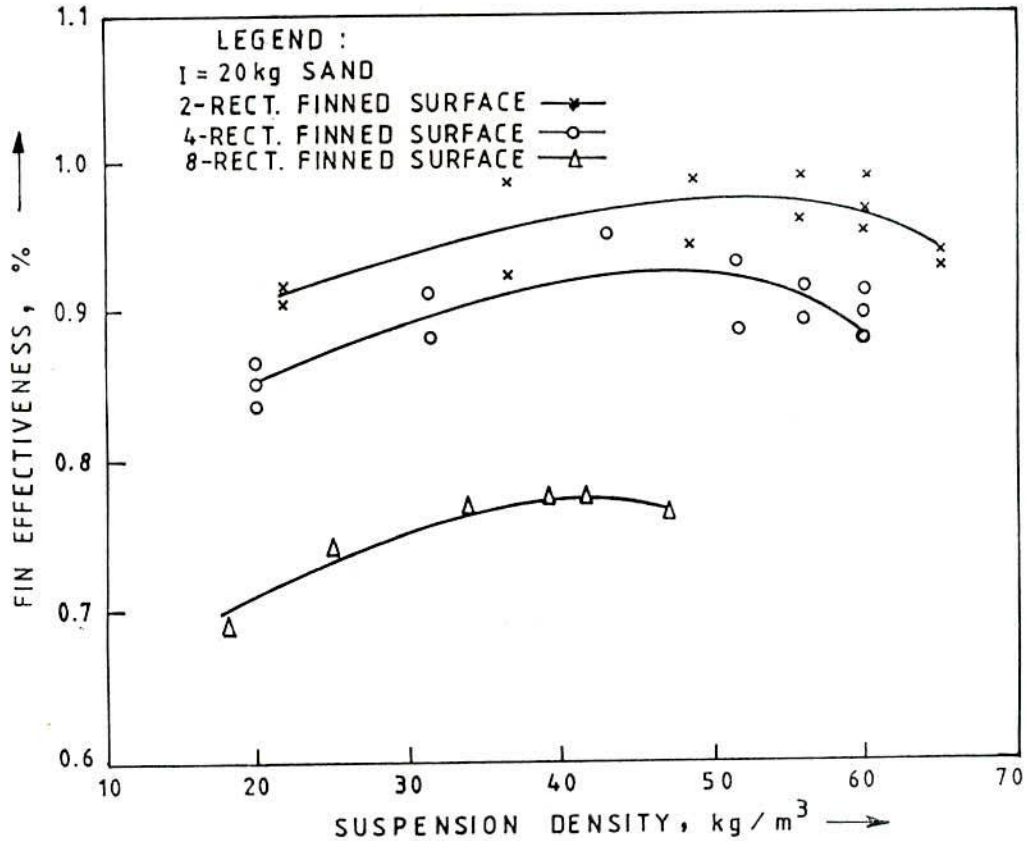

FIG. 6.48 EFFECTIVENESS OF RECTANGULAR FIN AS A FUNCTION OF SUSPENSION DENSITY

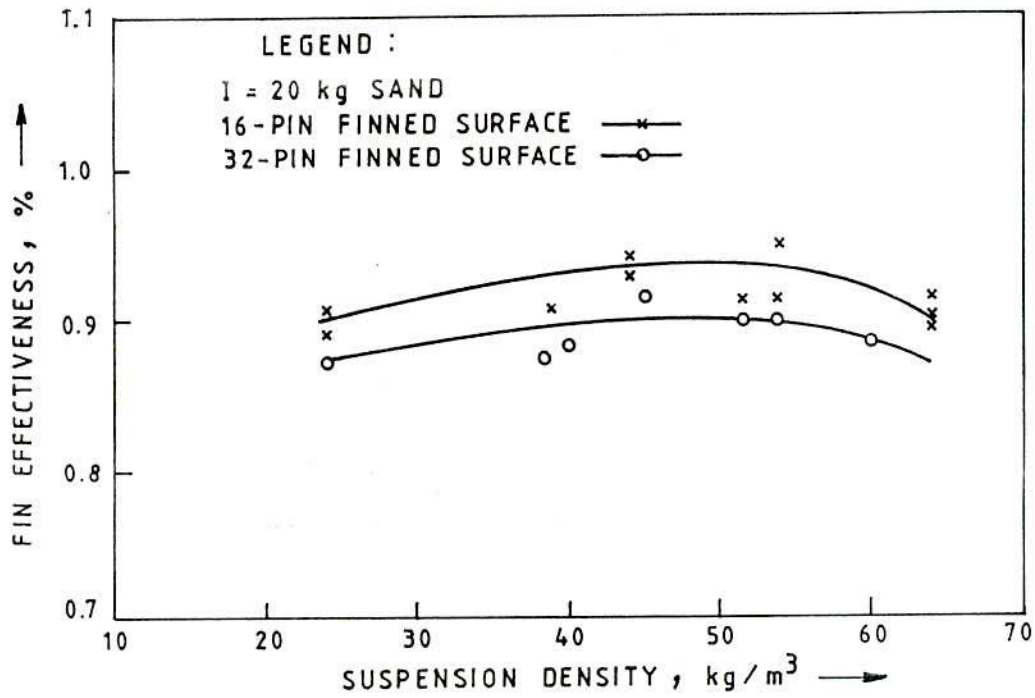

FIG. 6.49 EFFECTIVENESS OF PIN FIN AS A FUNCTION OF SUSPENSION DENSITY

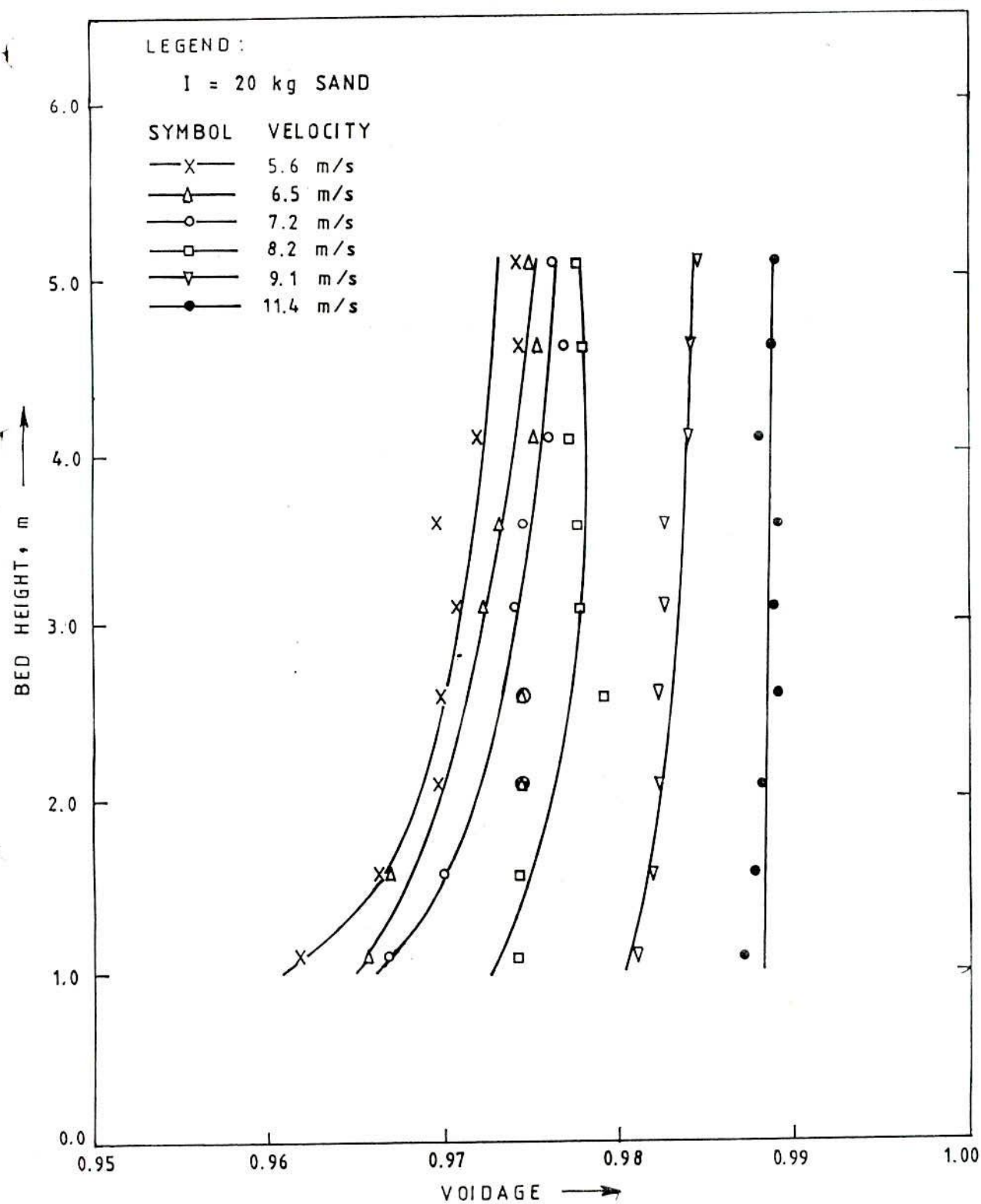

FIG.6.50 AXIAL VOIDAGE PROFILE FOR UNFINNED SURFACE

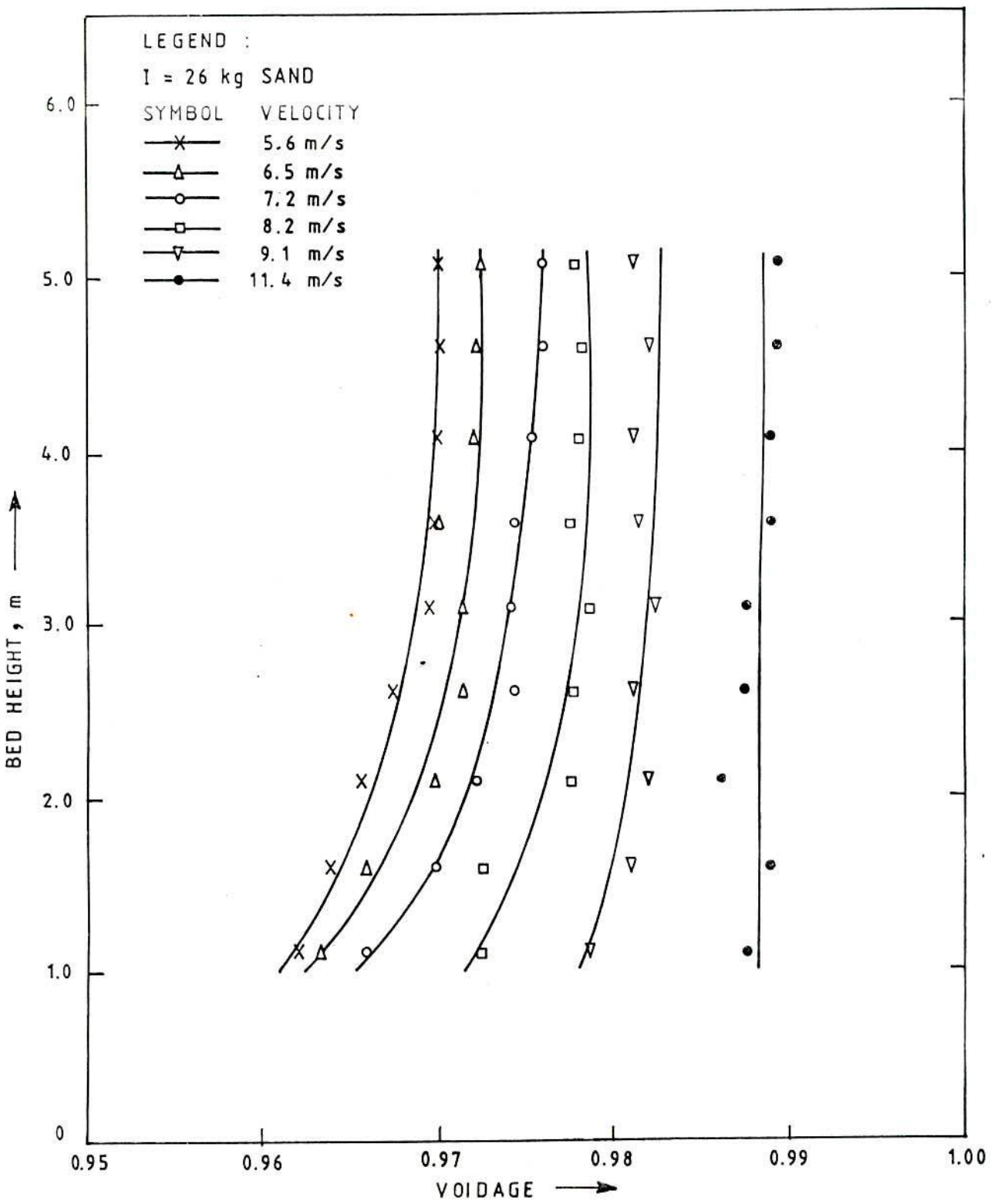

FIG. 6.51 AXIAL VOIDAGE PROFILE FOR UNFINNED SURFACE

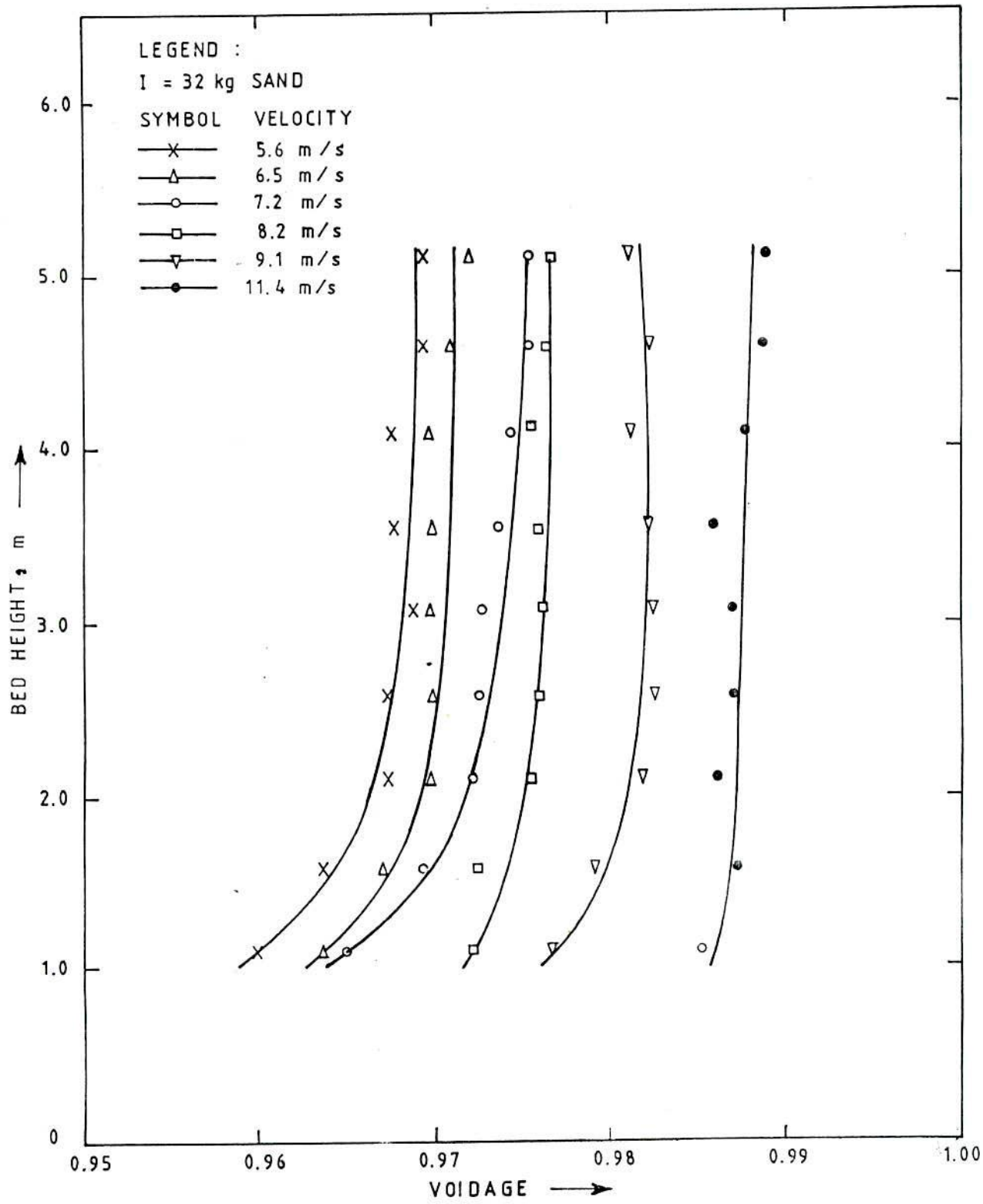

FIG. 6.52 AXIAL VOIDAGE PROFILE FOR UNFINNED SURFACE

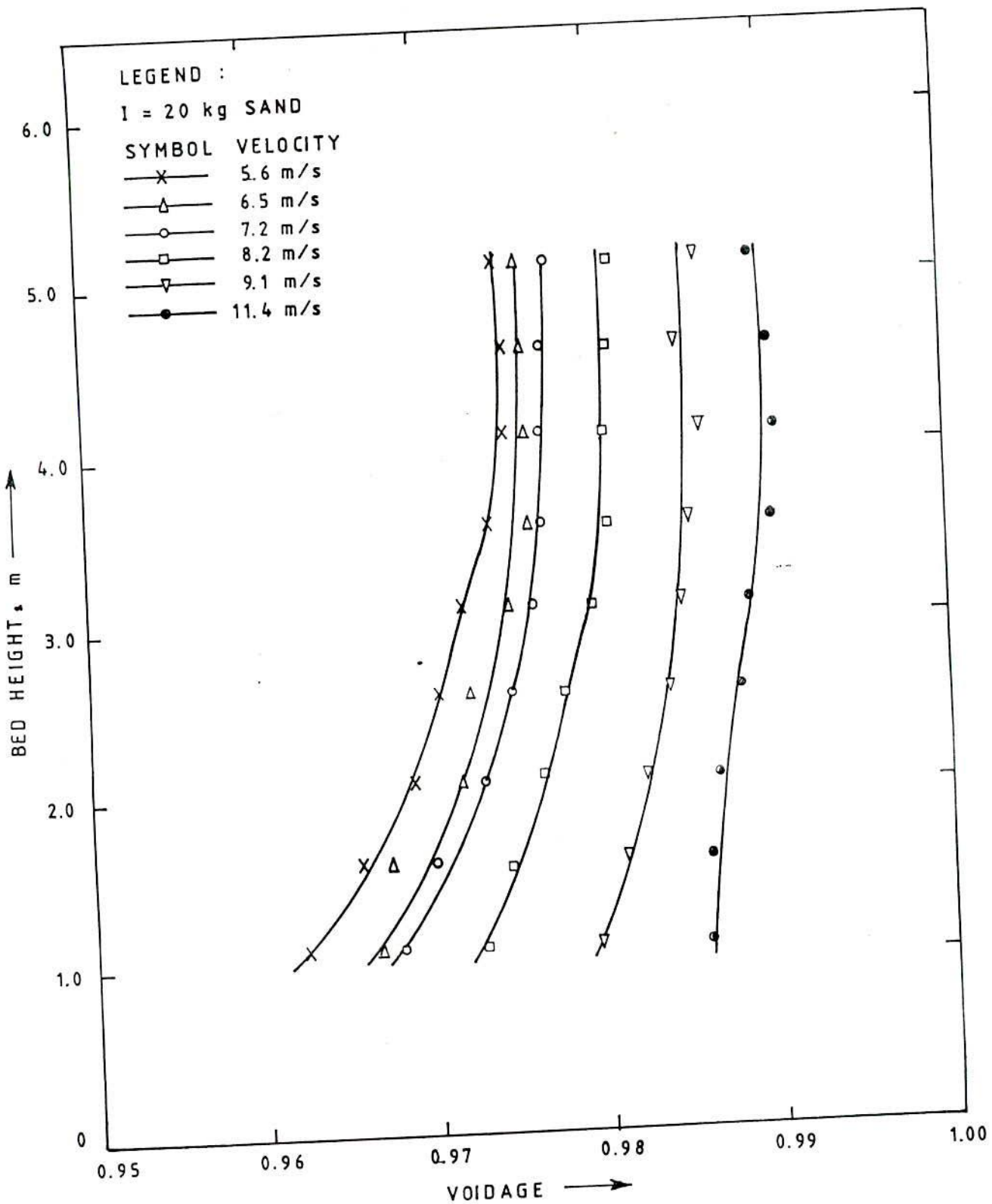

FIG. 6.53 AXIAL VOIDAGE PROFILE MEASURED IN PRESENCE OF 2-RECTANGULAR FINS

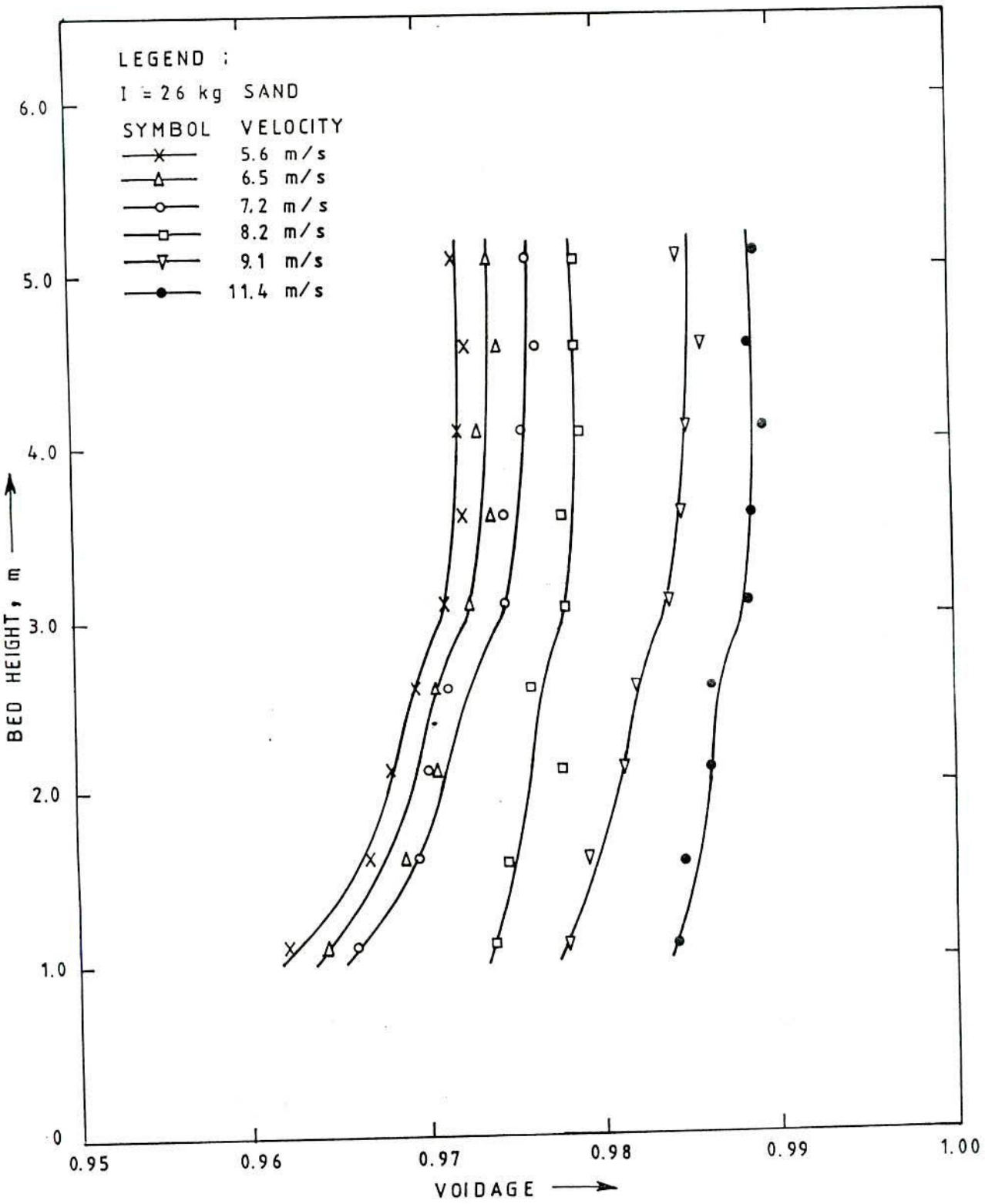

FIG. 6.54 AXIAL VOIDAGE PROFILE MEASURED IN PRESENCE OF 2-RECTANGULAR FINS

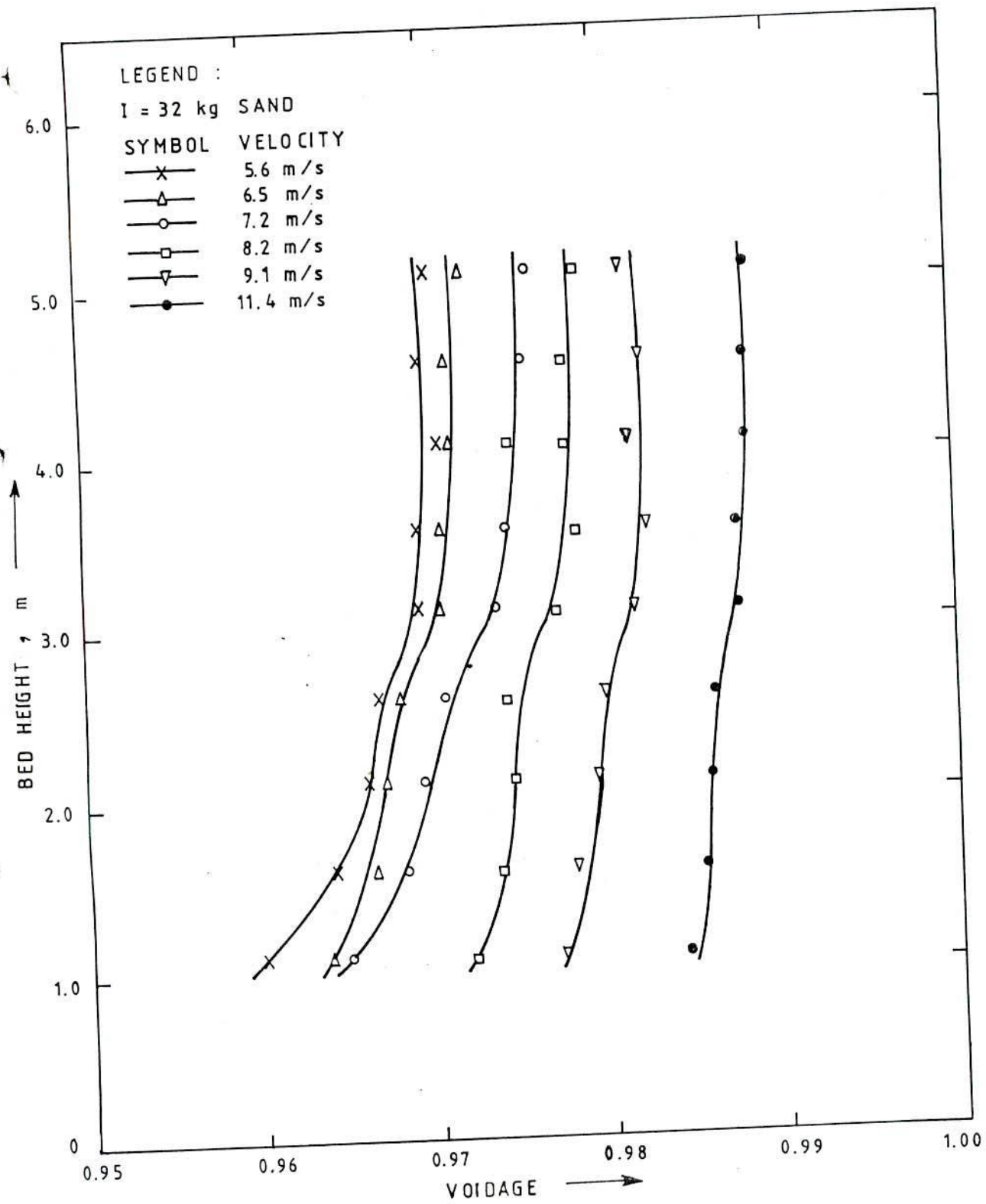

FIG. 6.55 AXIAL VOIDAGE PROFILE MEASURED IN PRESENCE OF 2-RECTANGULAR FINS

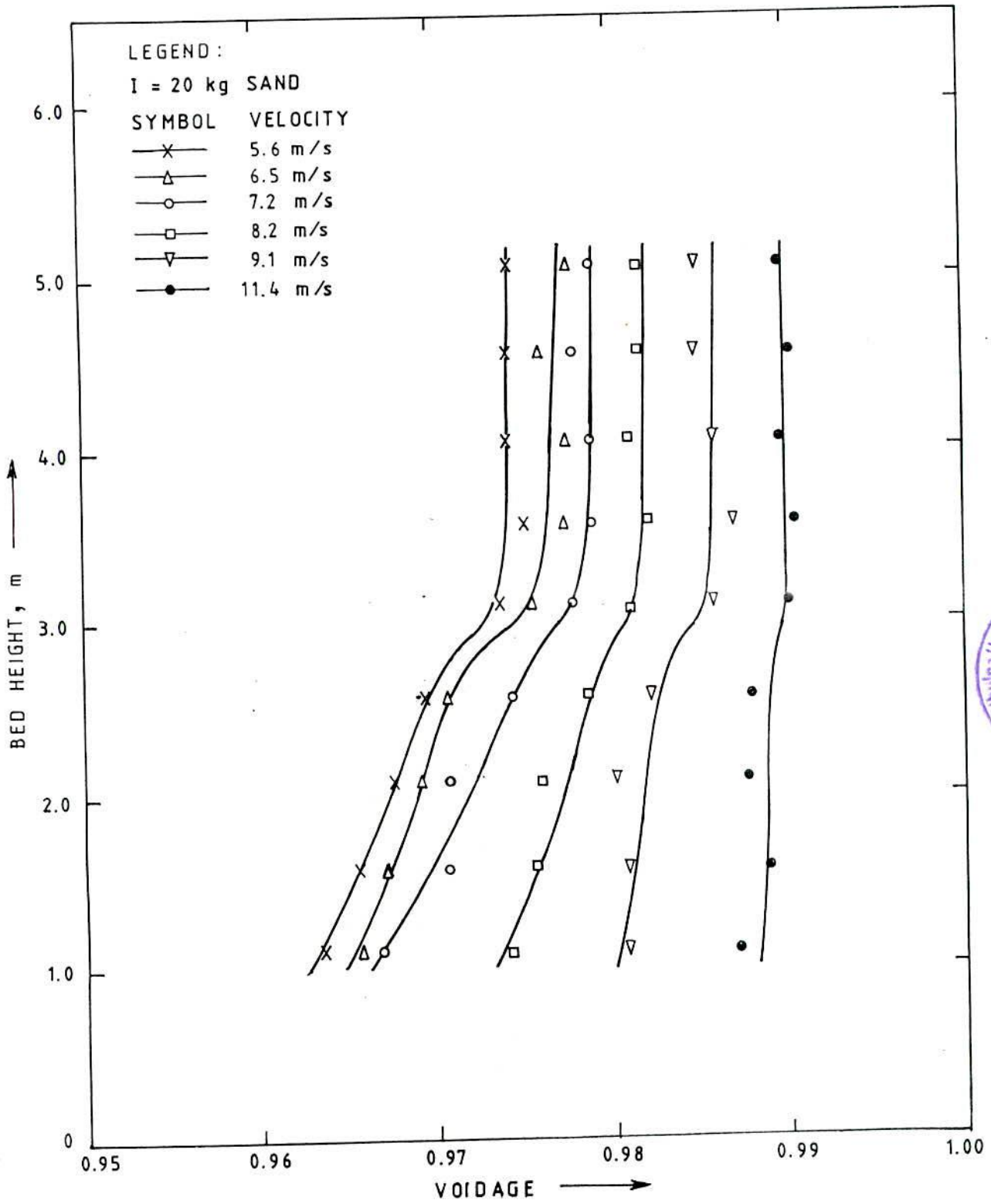

FIG. 6.56 AXIAL VOIDAGE PROFILE MEASURED IN PRESENCE OF 4-RECTANGULAR FINS

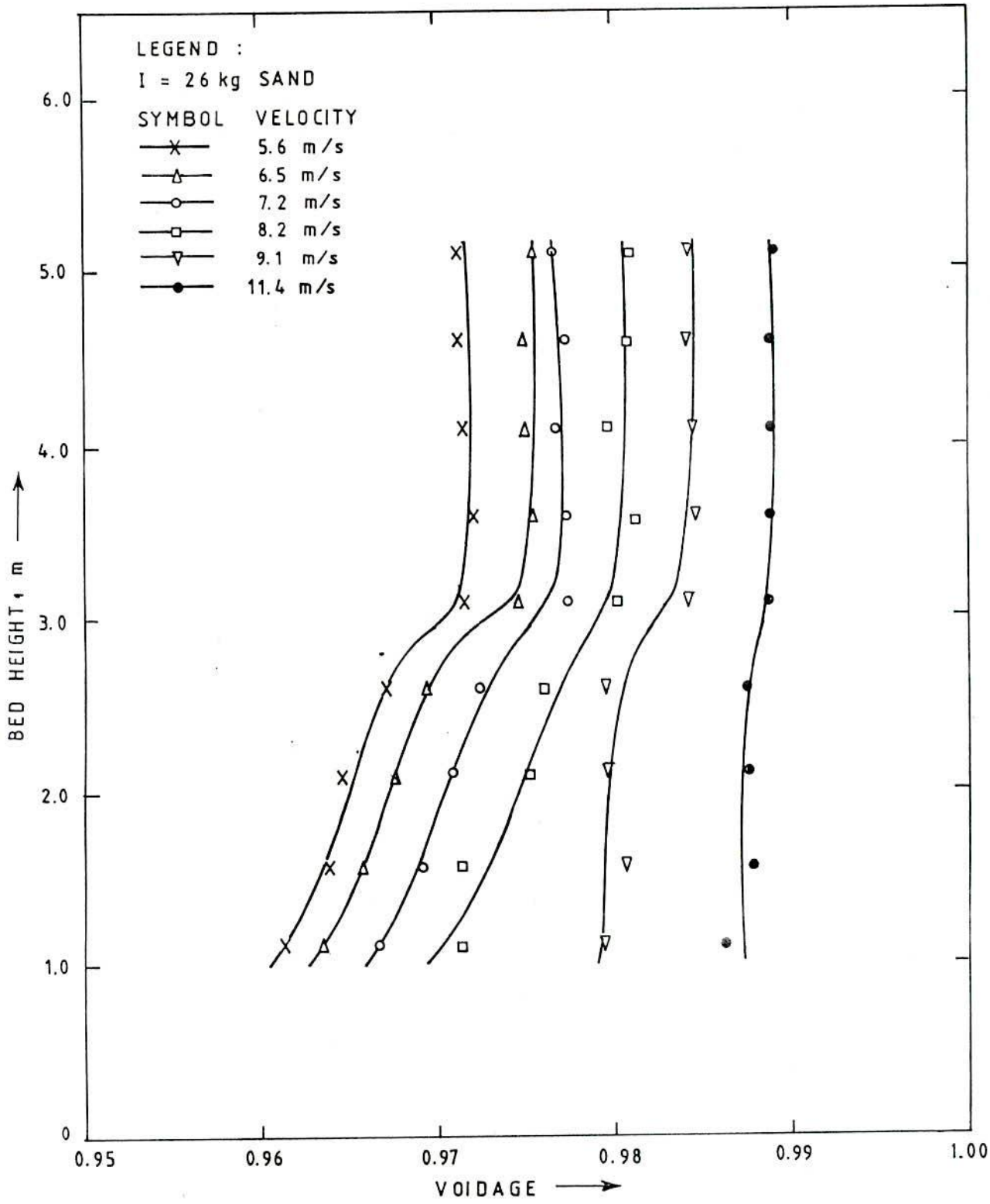

FIG. 6.57 AXIAL VOIDAGE PROFILE MEASURED IN PRESENCE OF 4-RECTANGULAR FINS

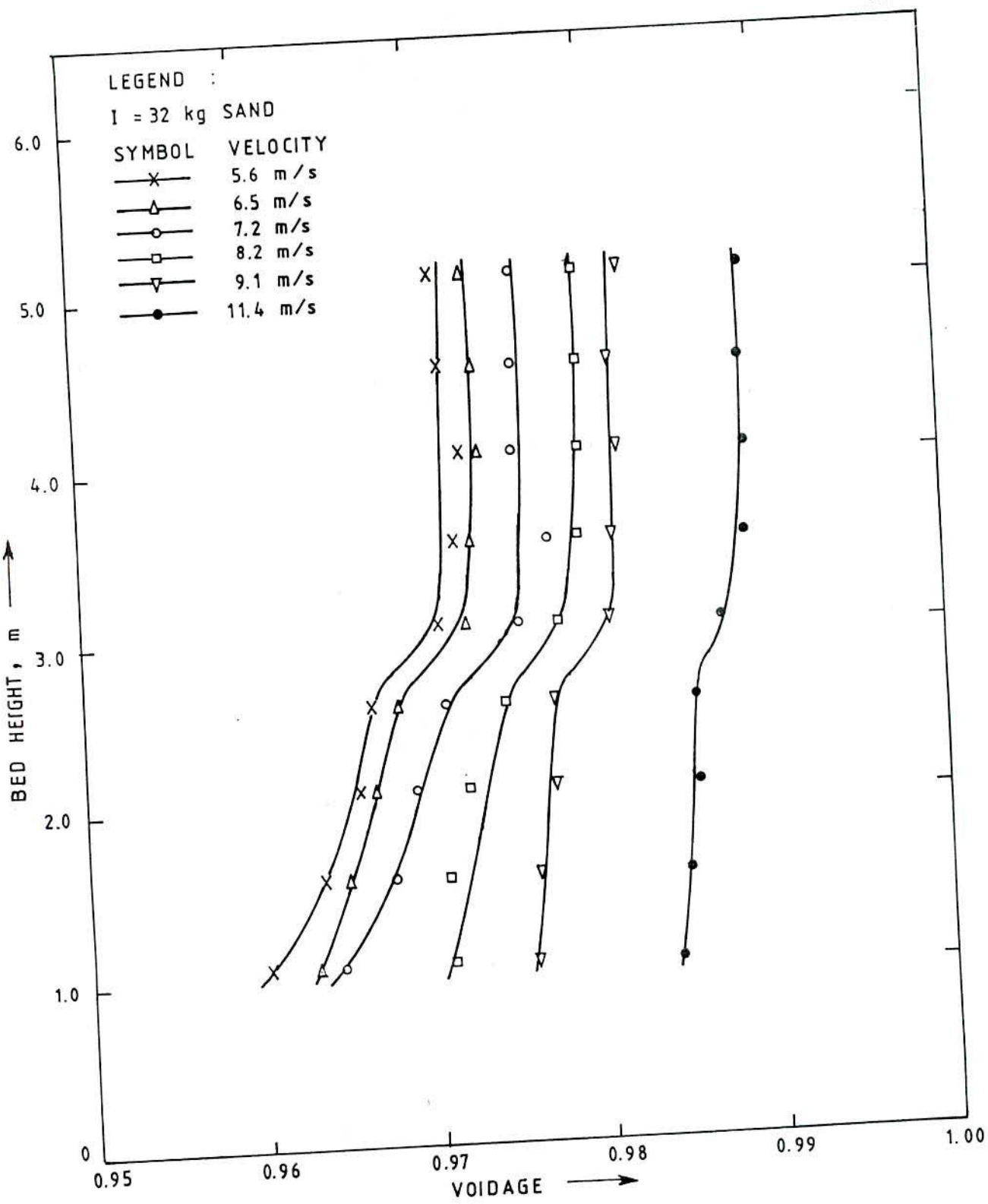

FIG. 6.58 AXIAL VOIDAGE PROFILE MEASURED IN PRESENCE OF 4-RECTANGULAR FINS

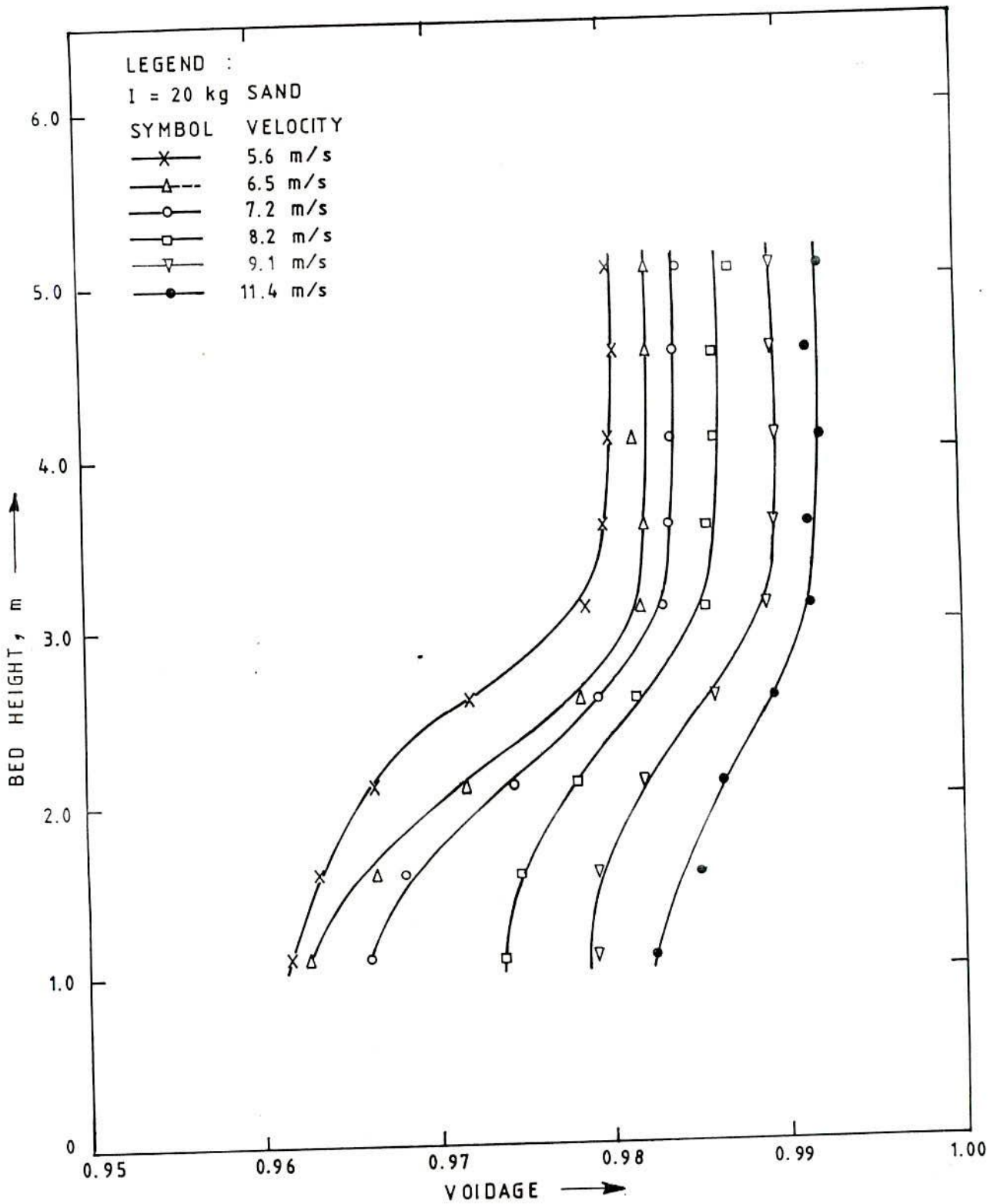

FIG. 6.59 AXIAL VOIDAGE PROFILE MEASURED IN PRESENCE OF 8-RECTANGULAR FINS

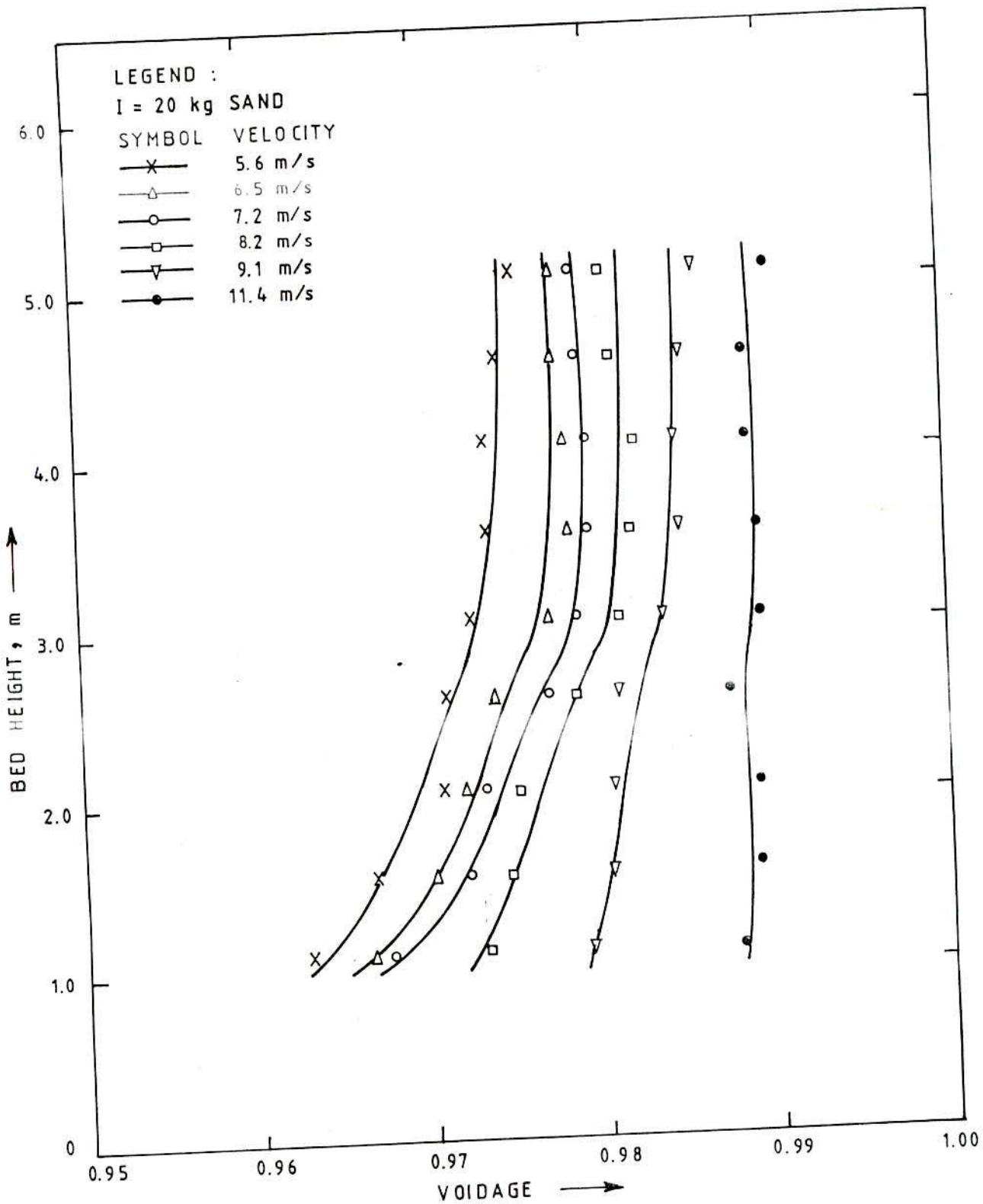

FIG. 6.60 AXIAL VOIDAGE PROFILE MEASURED IN PRESENCE OF 16-PIN FINS

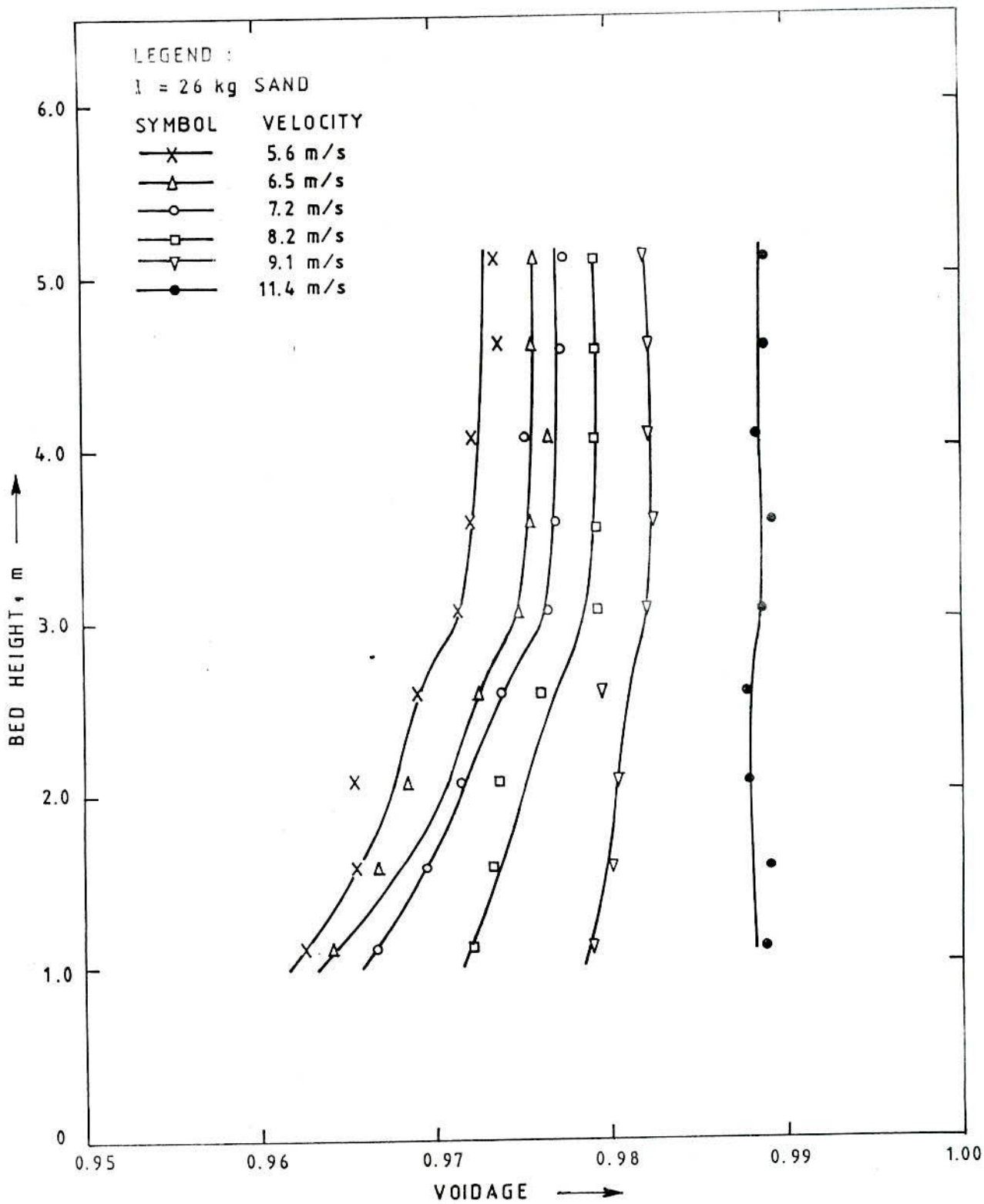

FIG. 6.61 AXIAL VOIDAGE PROFILE MEASURED IN PRESENCE OF 16-PIN FINS

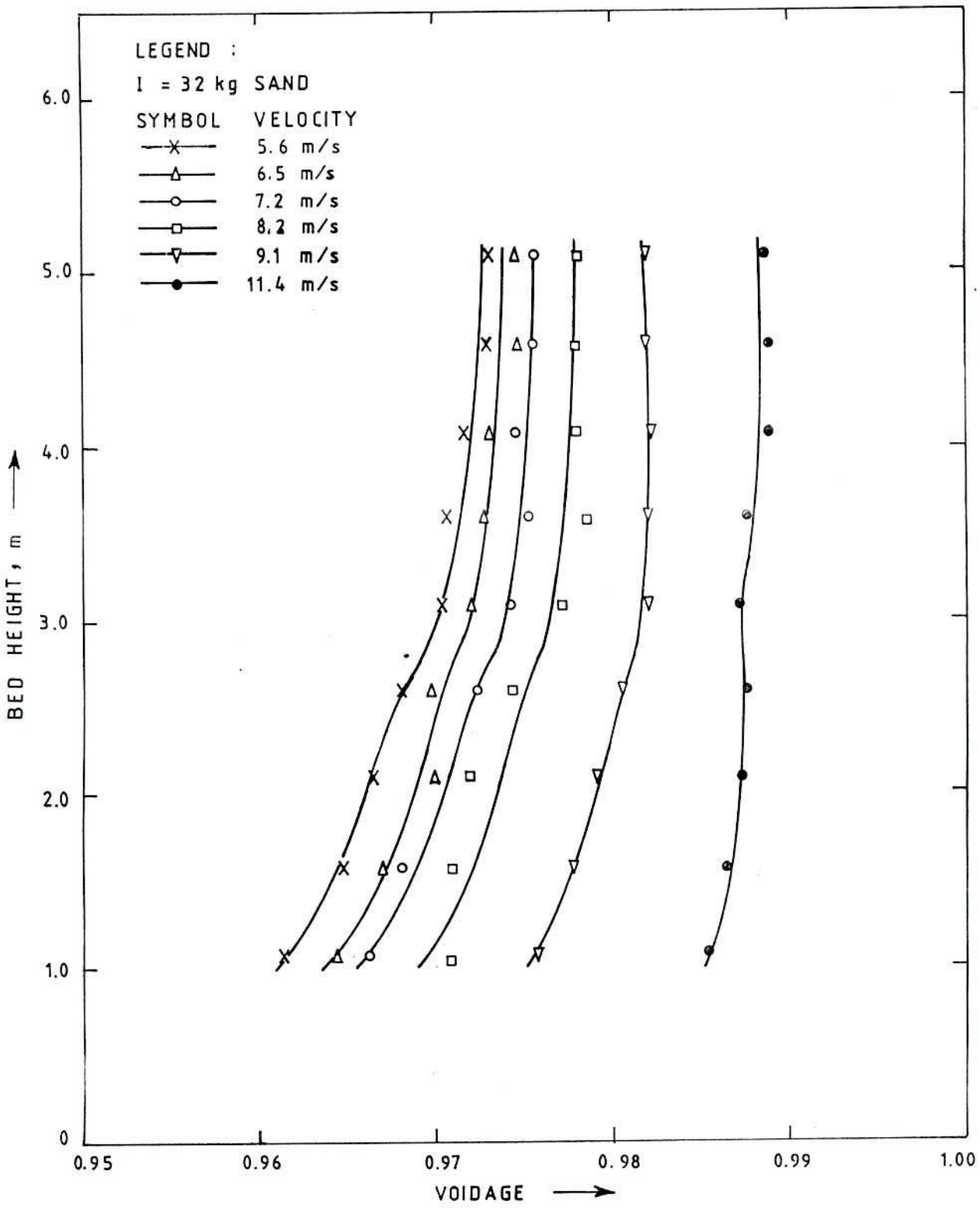

FIG. 6.62 AXIAL VOIDAGE PROFILE MEASURED IN PRESENCE OF 16-PIN FINS

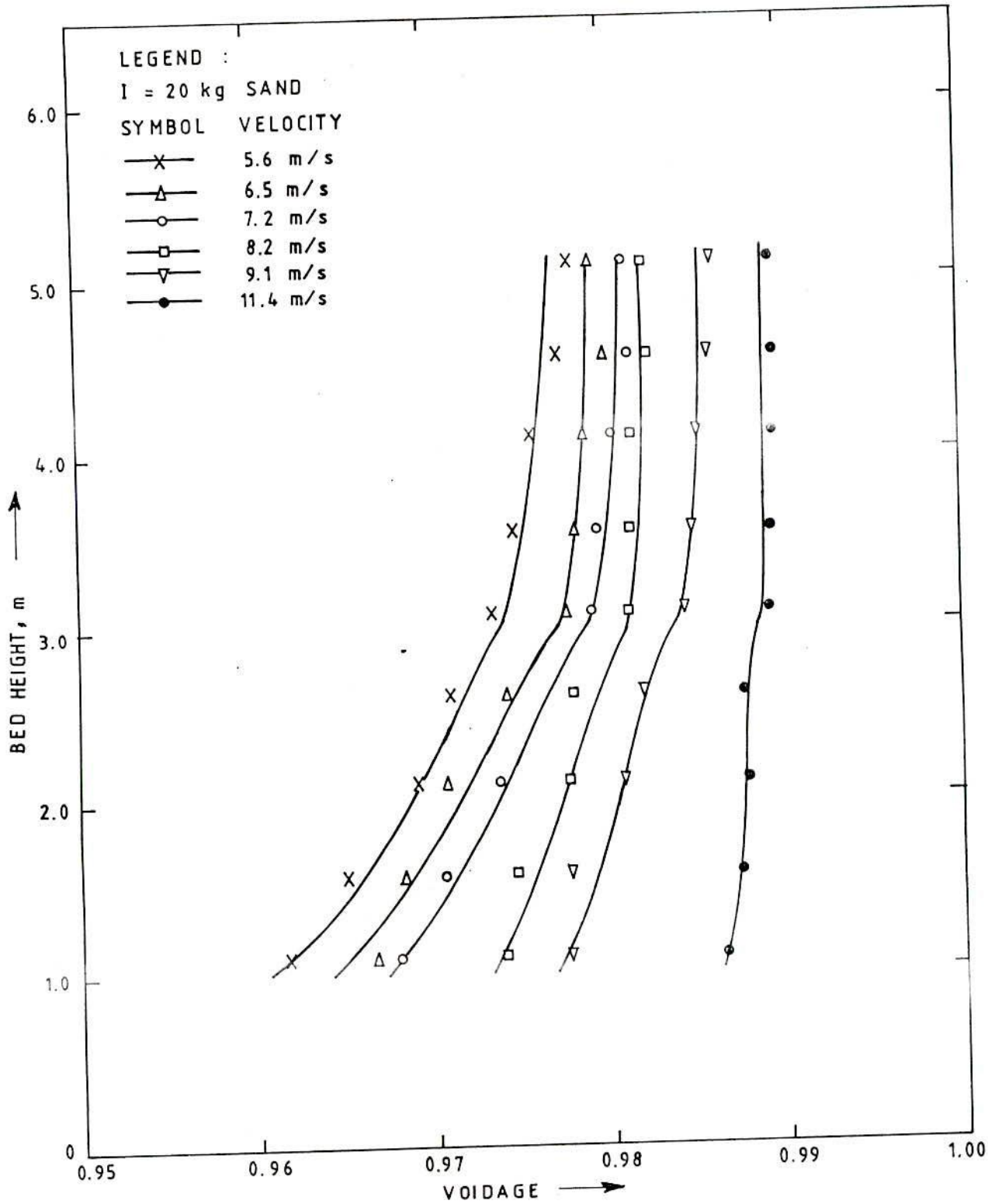

FIG. 6.63 AXIAL VOIDAGE PROFILE MEASURED IN PRESENCE OF 32-PIN FINS

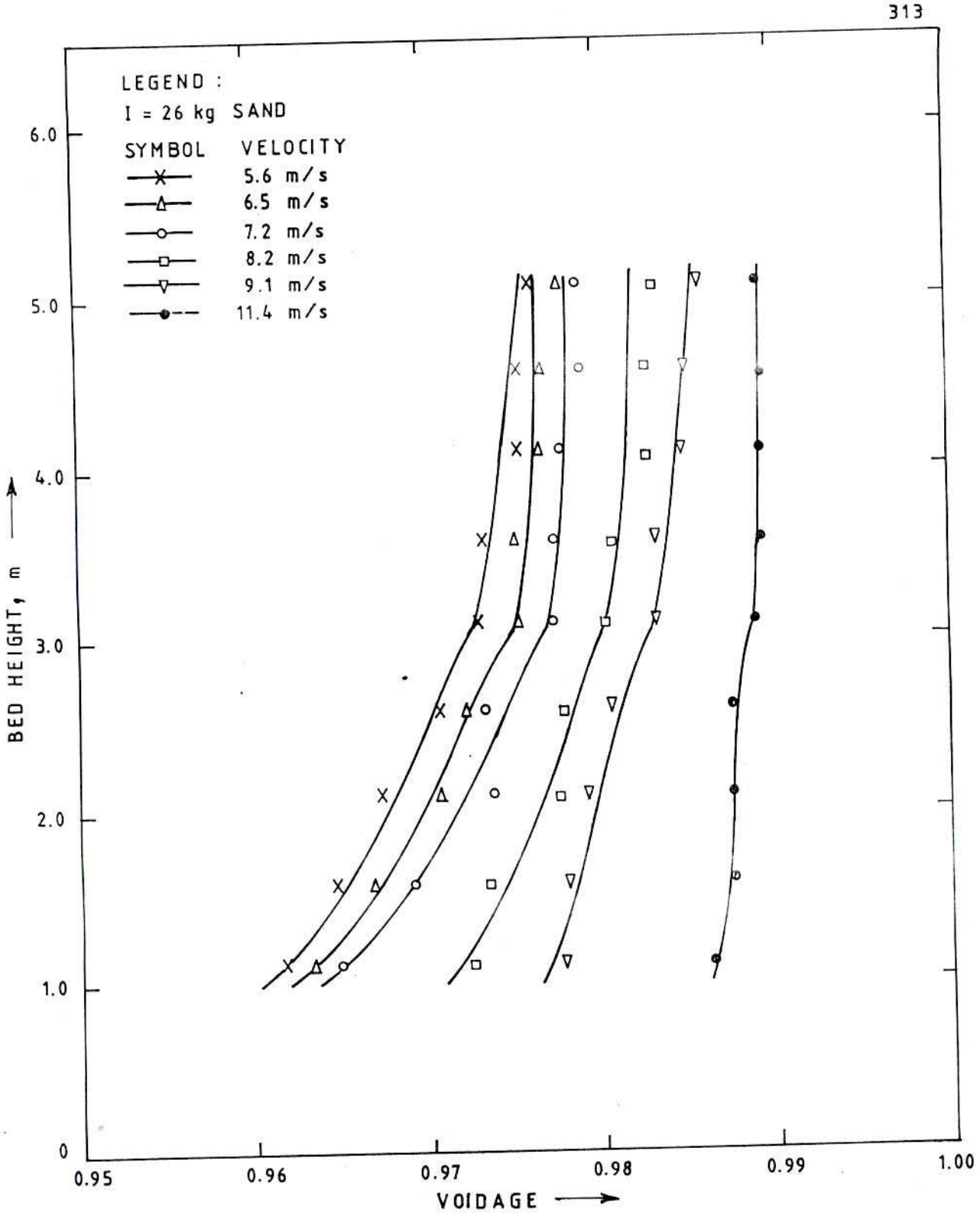

FIG. 6.64 AXIAL VOIDAGE PROFILE MEASURED IN PRESENCE OF 32-PIN FINS

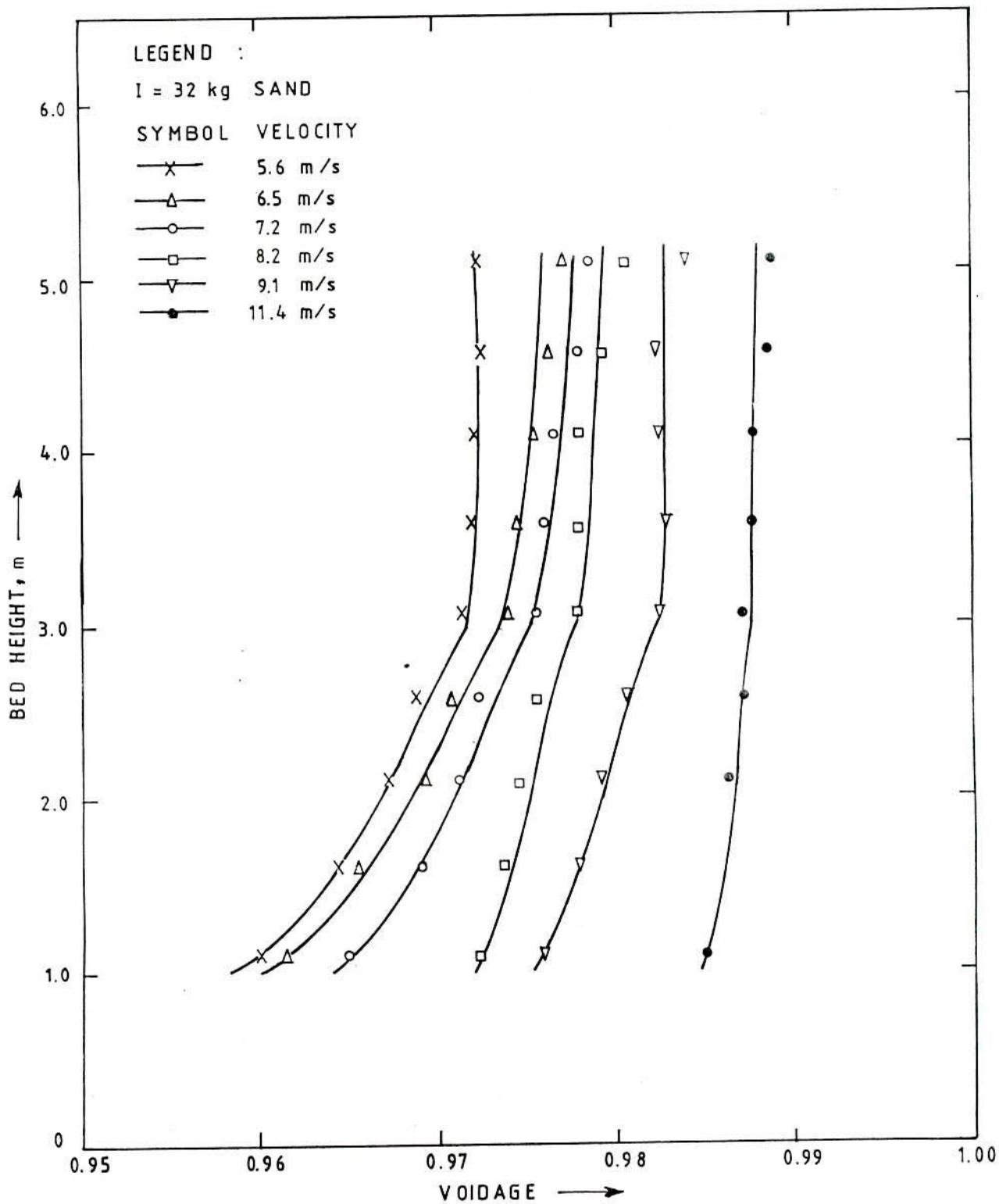

EIG. 6.65 AXIAL VOIDAGE PROFILE MEASURED IN PRESENCE OF 32-PIN FINS

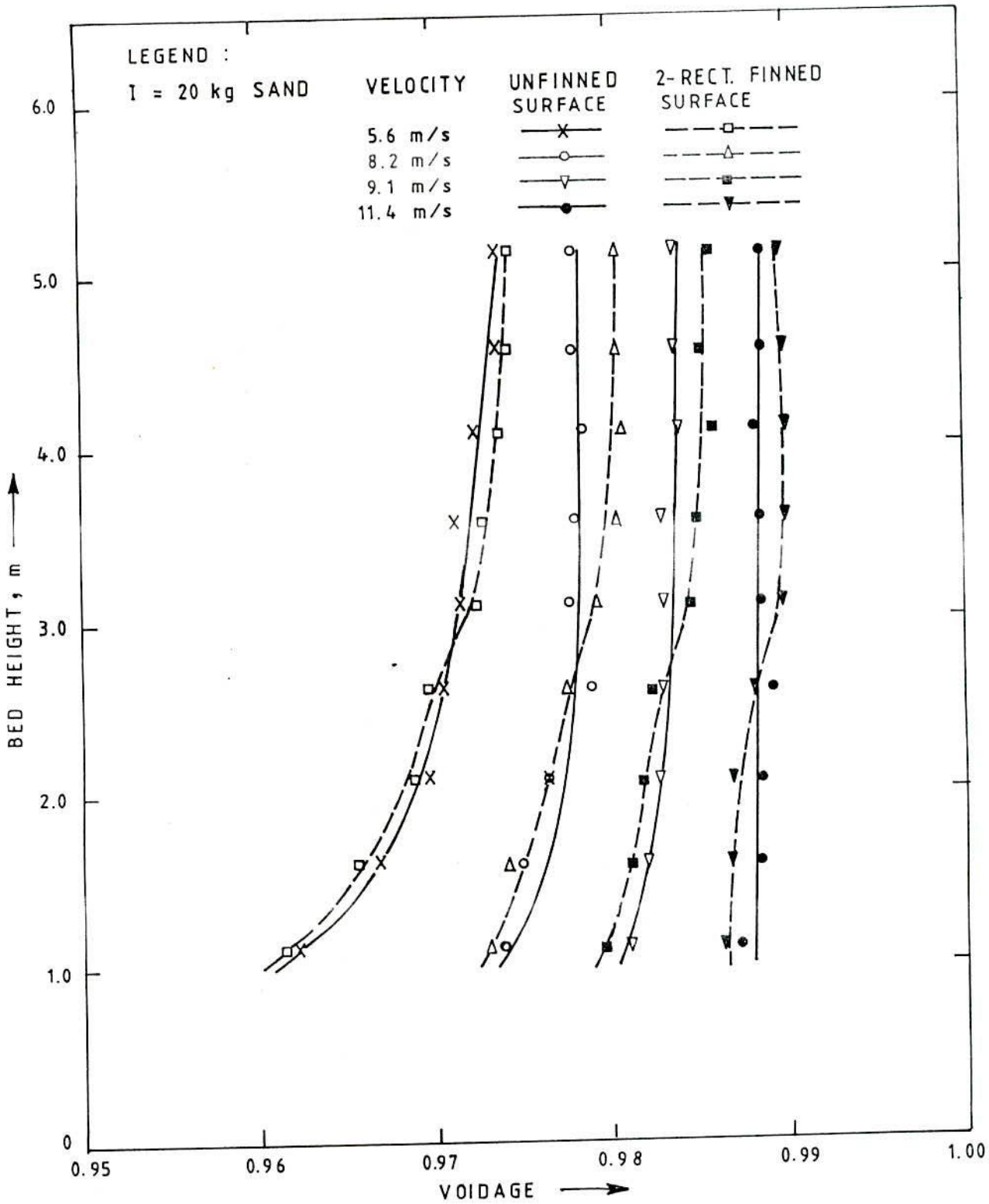

FIG. 6.66 COMPARISON OF VOIDAGE ALONG THE HEIGHT FOR 2-RECT FINNED AND UNFINNED SURFACES

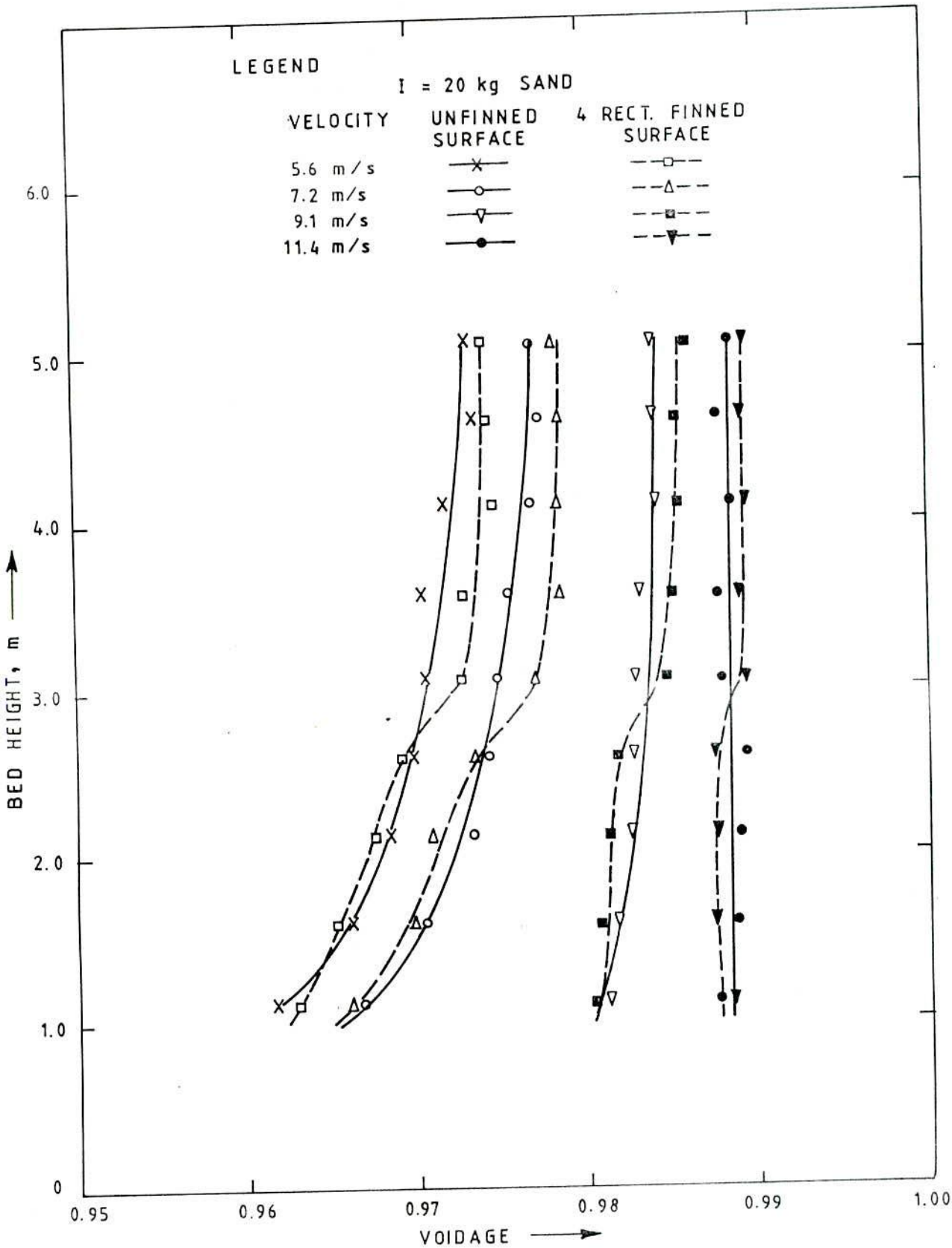

FIG. 6.67 COMPARISON OF VOIDAGE ALONG THE HEIGHT FOR 4-RECT. FINNED AND UNFINNED SURFACES

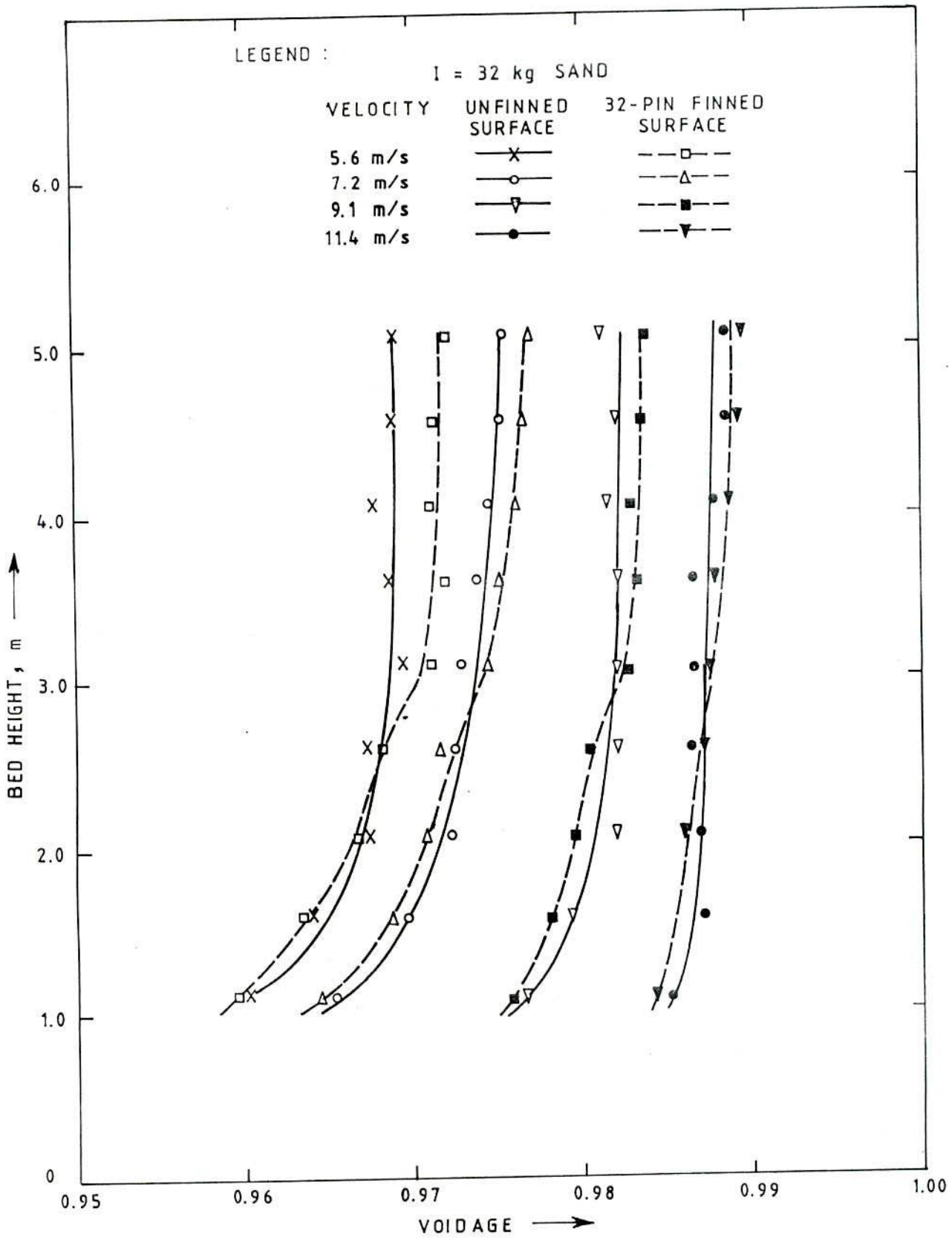

FIG. 6.68 COMPARISON OF VOIDAGE ALONG THE HEIGHT FOR 32-PIN FINNED AND UNFINNED SURFACES

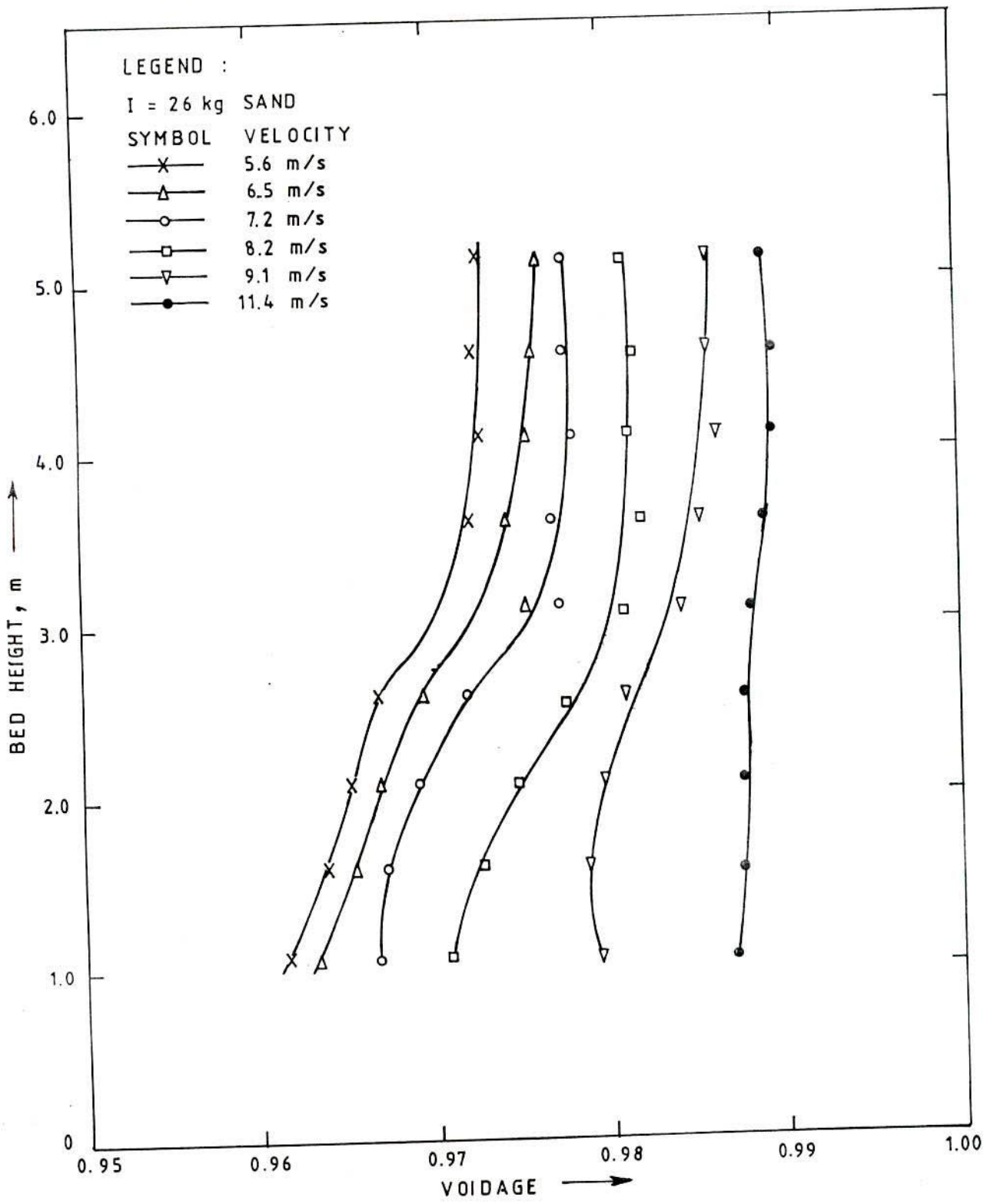

FIG.6.69 VOIDAGE ALONG THE HEIGHT OF THE COLUMN FOR 1500 mm LONG 4-RECTANGULAR FINNED SURFACE

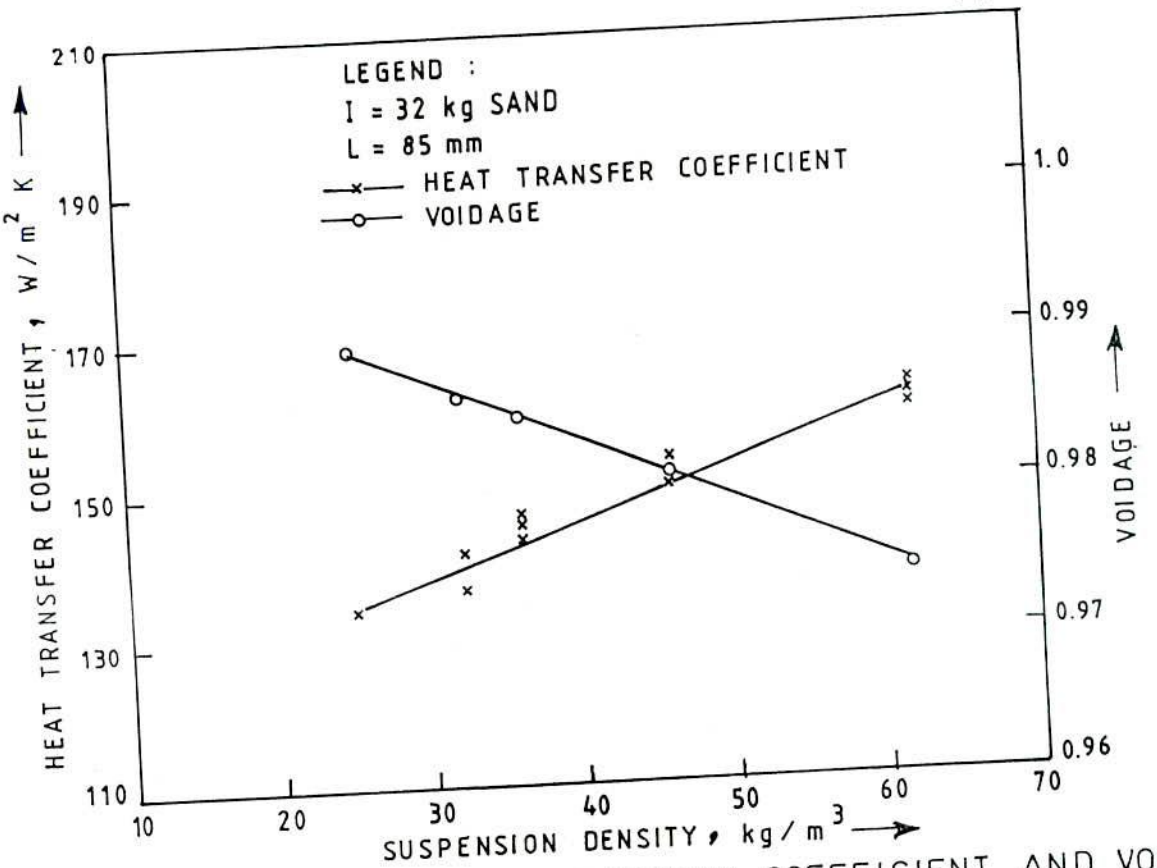

FIG. 6.70 VARIATION OF HEAT TRANSFER COEFFICIENT AND VOIDAGE WITH SUSPENSION DENSITY FOR 85 mm PROBE

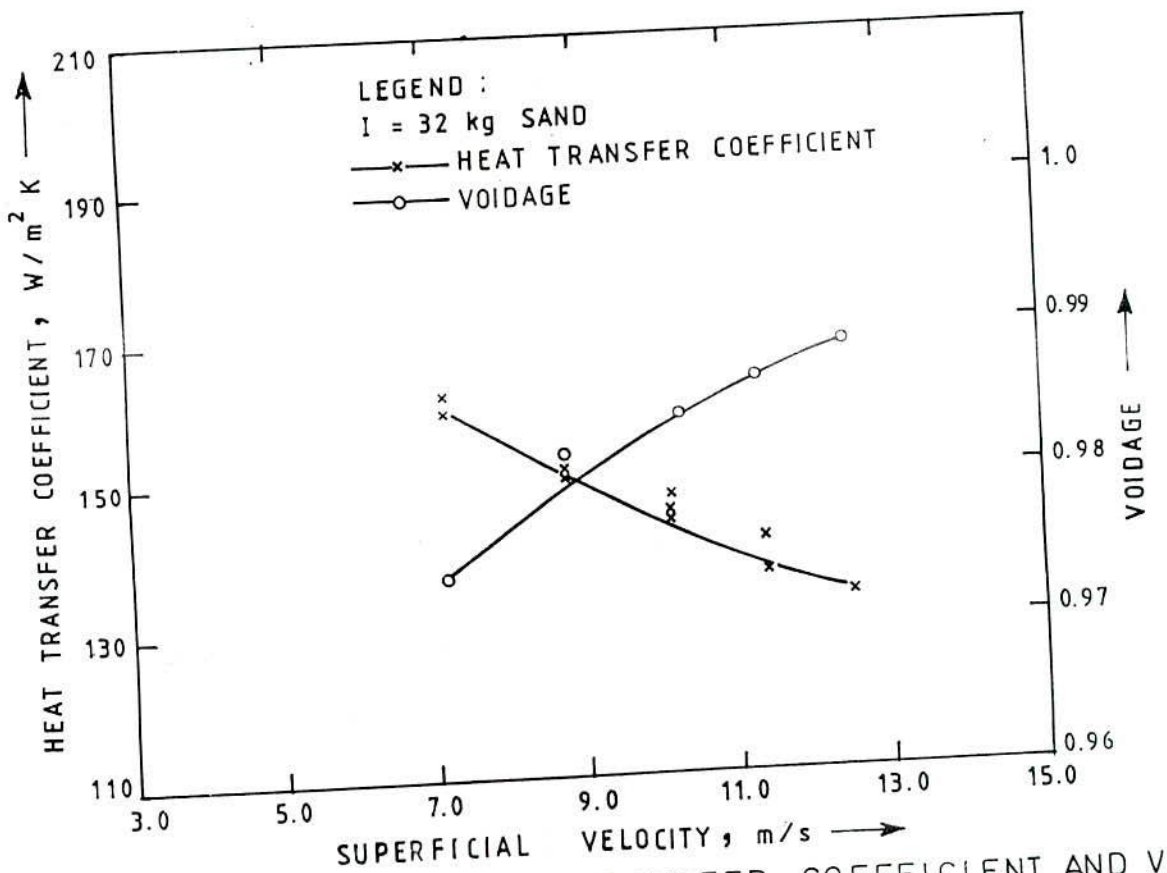

FIG. 6.71 VARIATION OF HEAT TRANSFER COEFFICIENT AND VOIDAGE WITH SUPERFICIAL VELOCITY FOR 85 mm PROBE

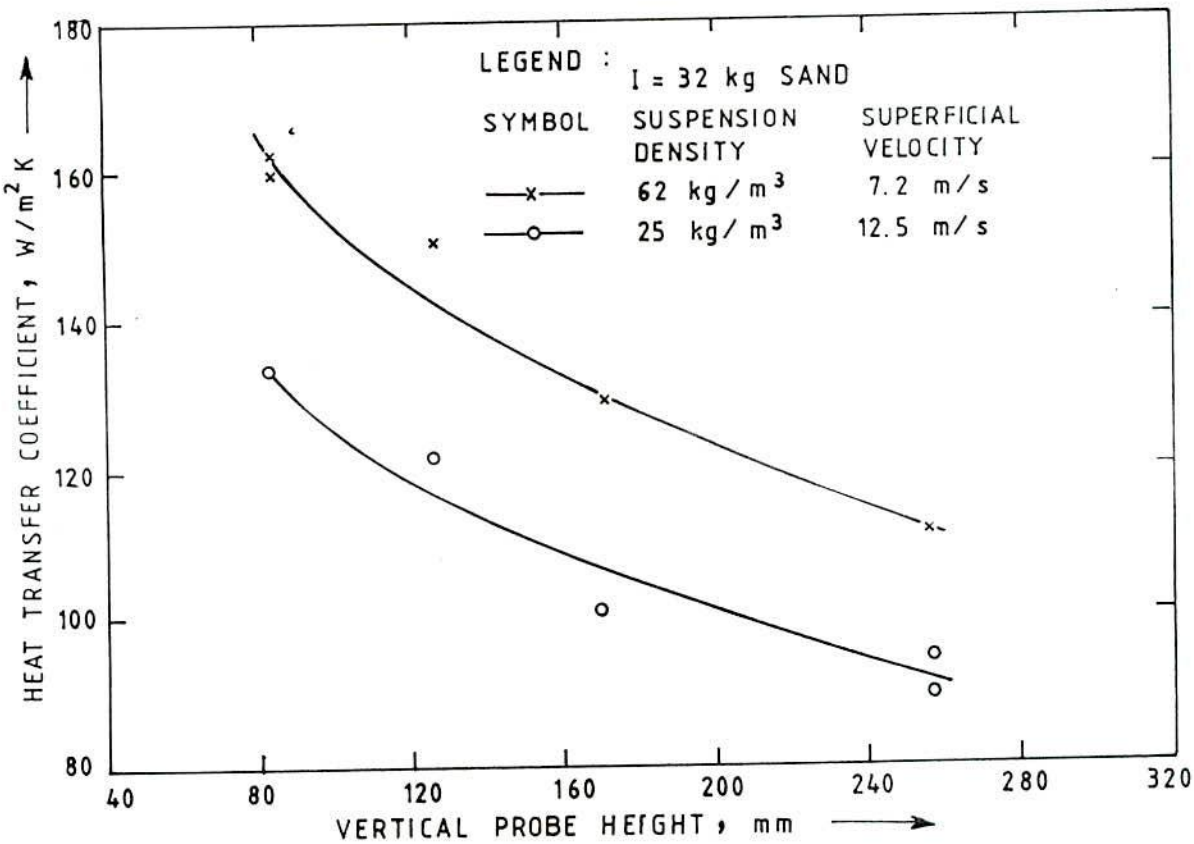

FIG.6.72 EFFECT OF VERTICAL PROBE HEIGHT ON HEAT TRANSFER COEFFICIENT

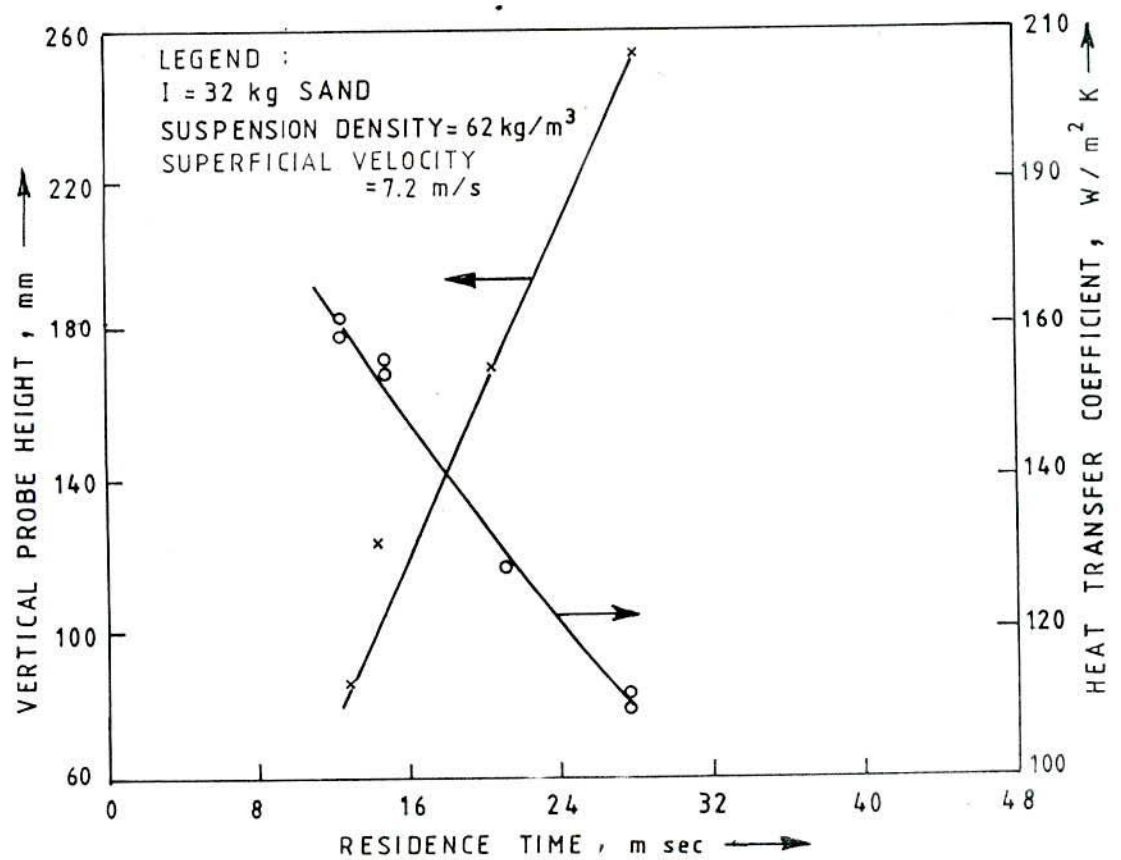

FIG.6.73 EFFECT OF RESIDENCE TIME ON HEAT TRANSFER COEFFICIENT AND PROBE HEIGHT

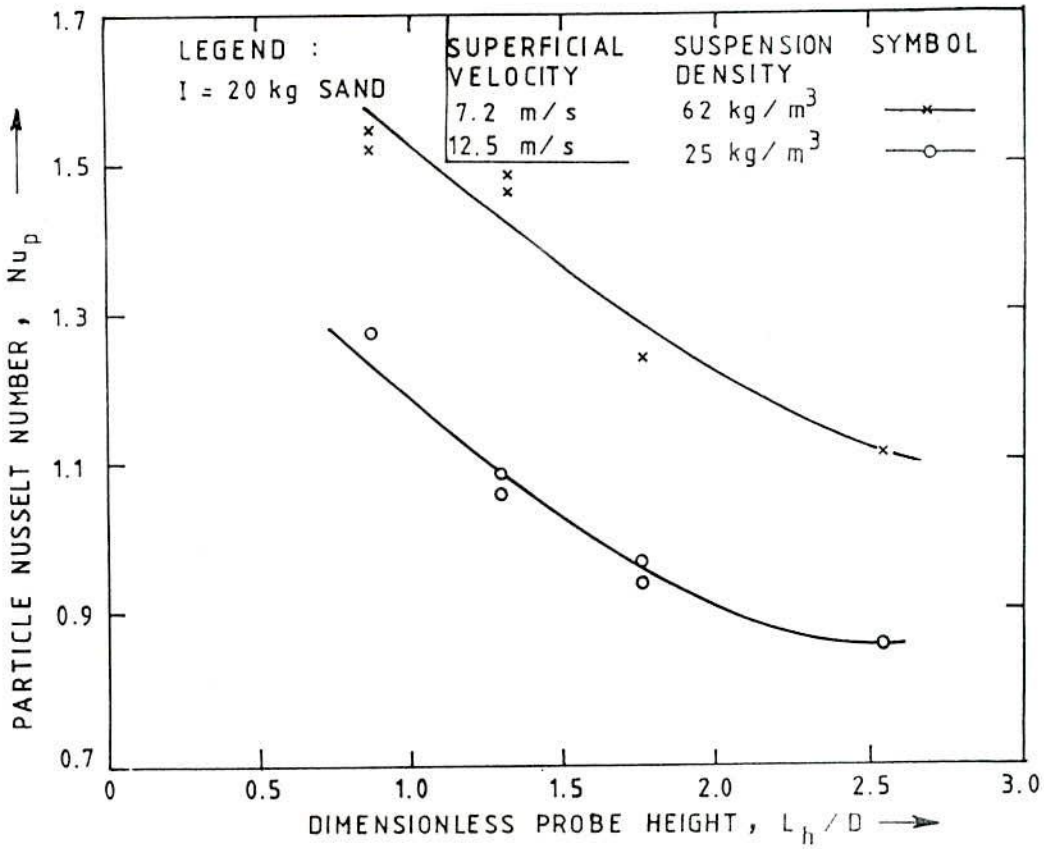

FIG. 6.74 EFFECT OF DIMENSIONLESS PROBE HEIGHT ON PARTICLE NUSSELT NUMBER

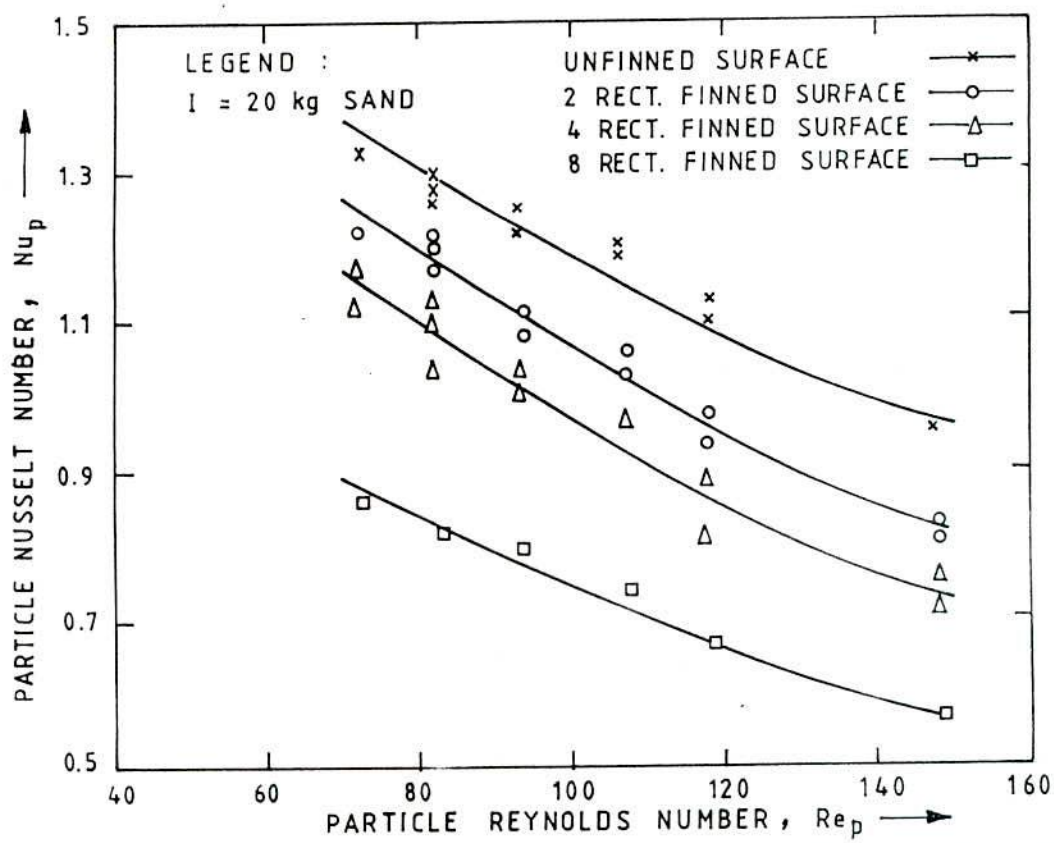

FIG. 6.75 VARIATION OF Nu_p WITH Re_p FOR RECTANGULAR FINNED AND UNFINNED SURFACES

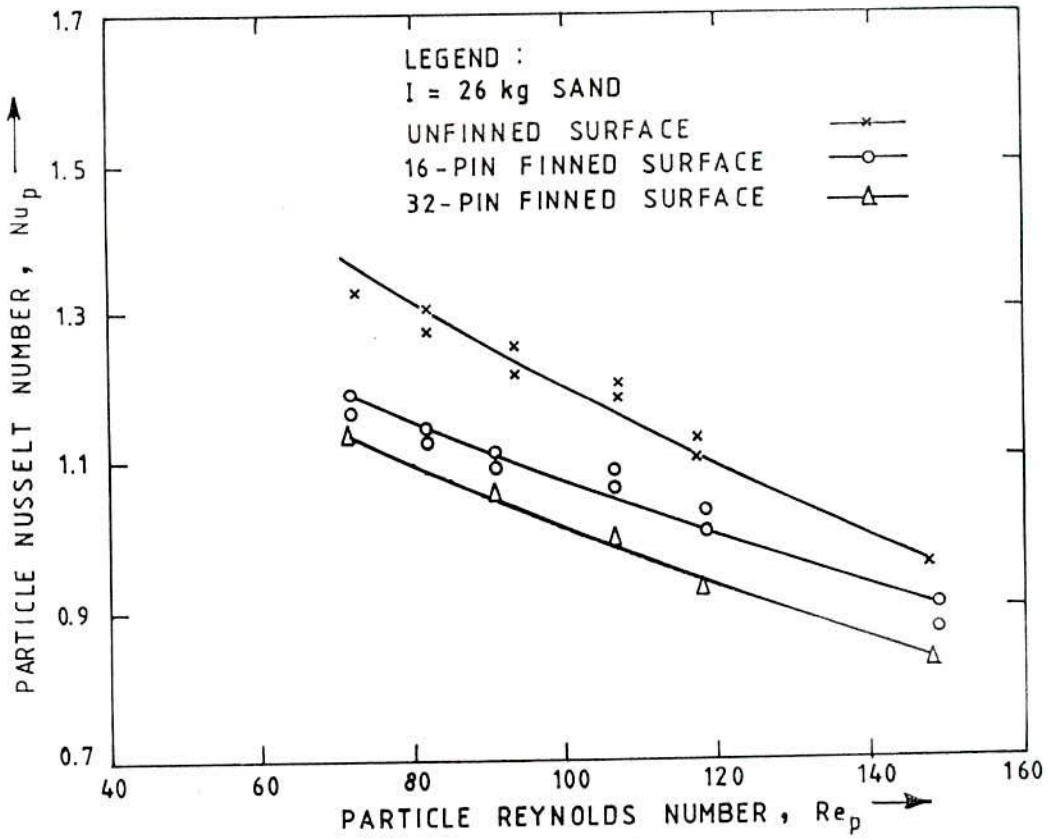

FIG. 6.76 VARIATION OF Nu_p WITH Re_p FOR PIN FINNED AND UNFINNED SURFACES

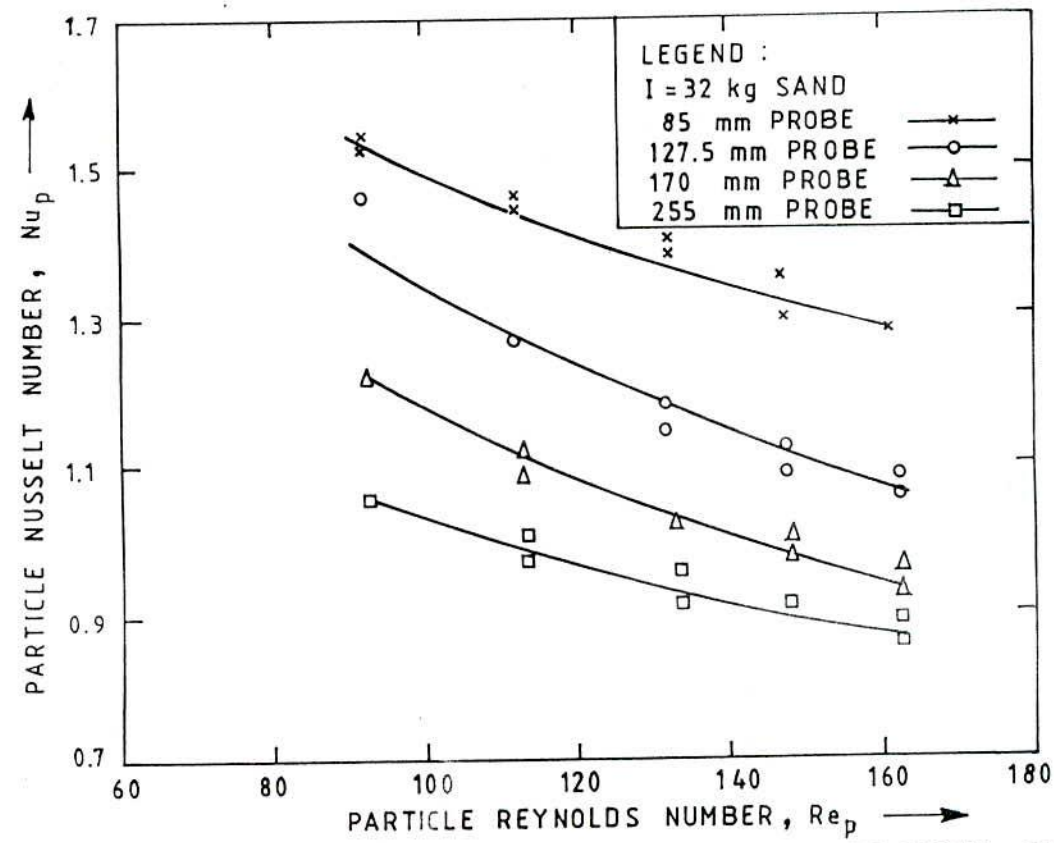

FIG. 6.77 VARIATION OF Nu_p WITH Re_p FOR PROBES OF DIFFERENT VERTICAL HEIGHTS

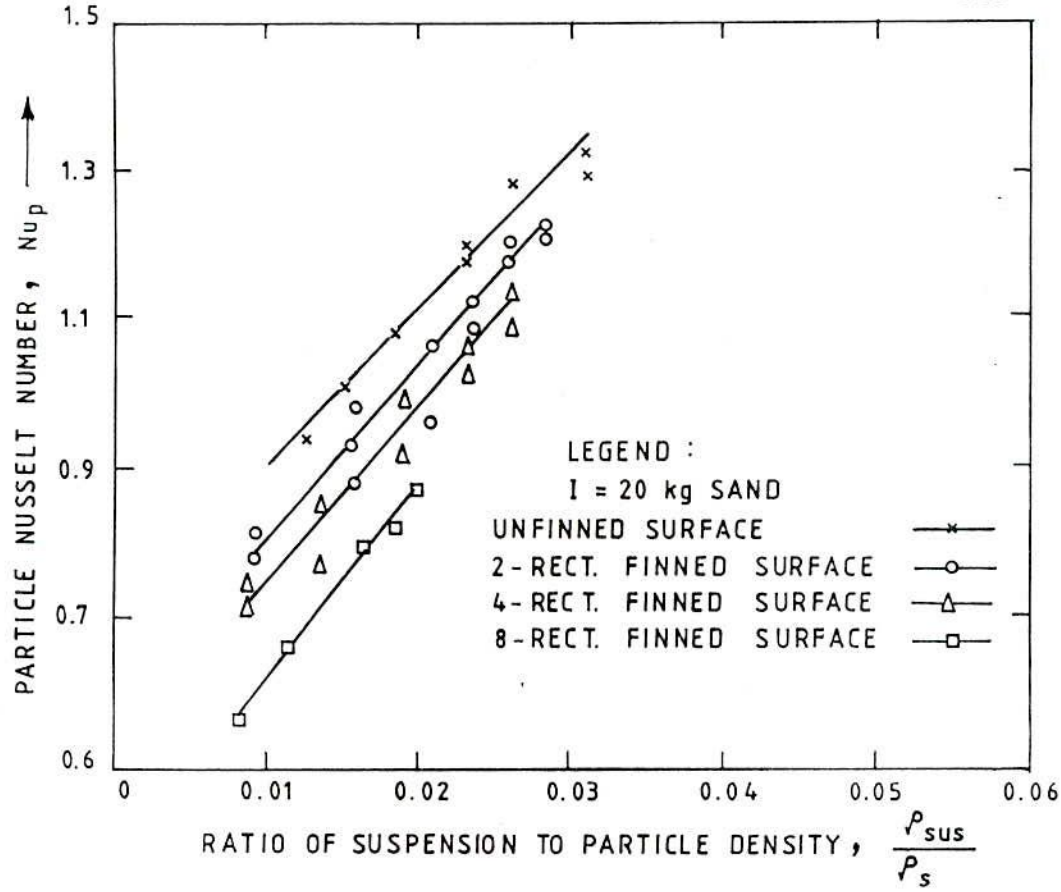

FIG. 6.78 VARIATION OF Nup WITH THE RATIO OF SUSPENSION TO PARTICLE DENSITY FOR RECT. FINNED SURFACE

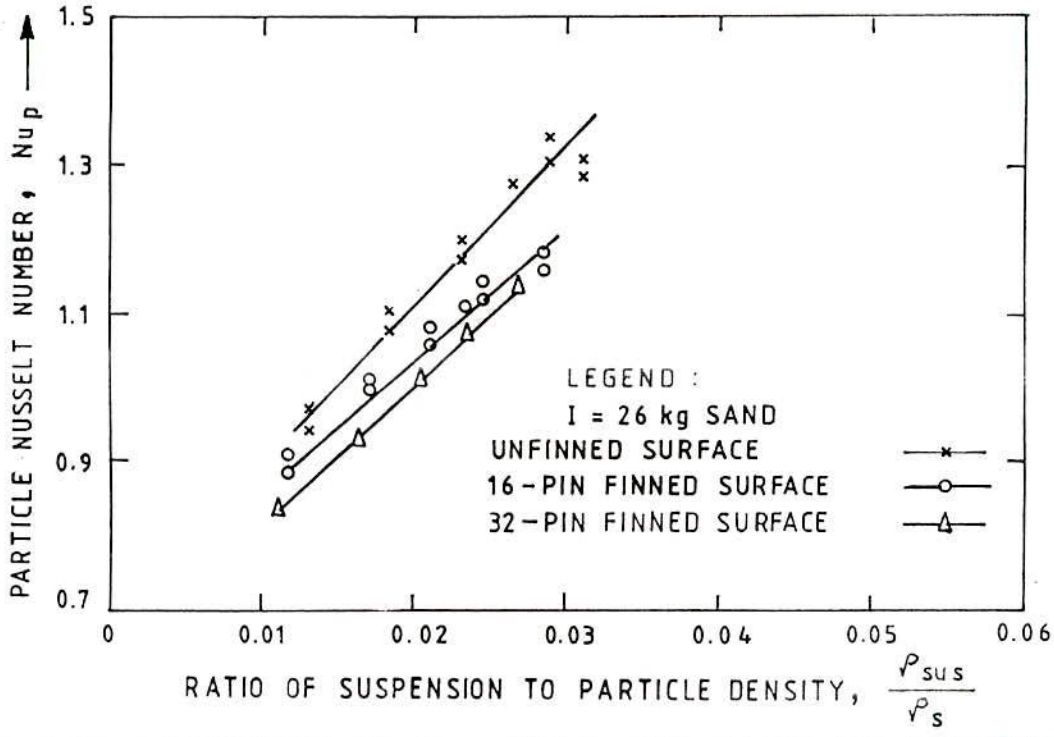

FIG.6.79 VARIATION OF Nup WITH THE RATIO OF SUSPENSION TO PARTICLE DENSITY FOR PIN FINNED SURFACE

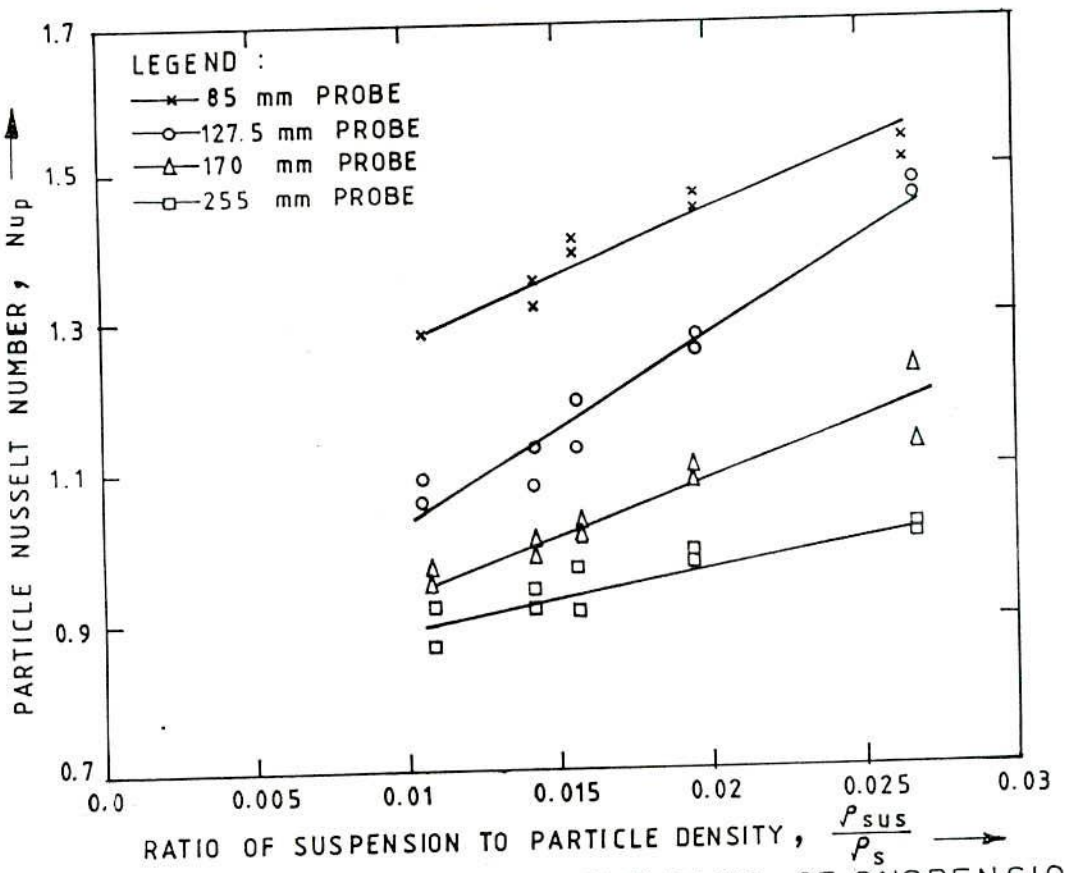

FIG. 6.80 VARIATION OF Nu_p WITH THE RATIO OF SUSPENSION TO PARTICLE DENSITY FOR PROBES OF DIFFERENT VERTICAL HEIGHTS

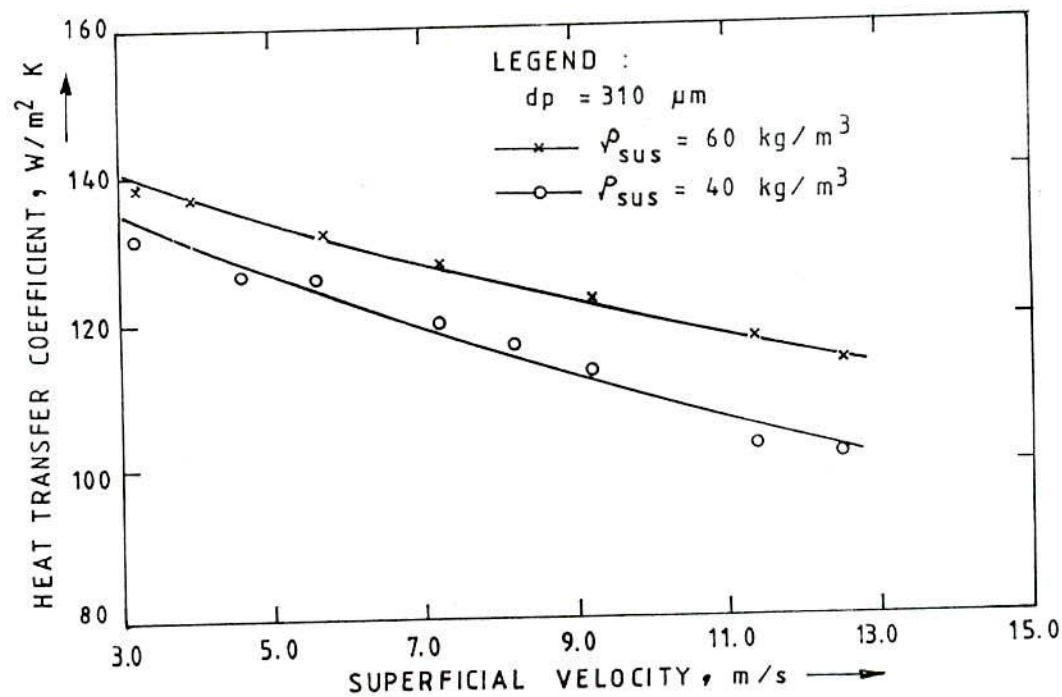

FIG. 6.81 EFFECT OF SUPERFICIAL VELOCITY ON HEAT TRANSFER COEFFICIENT PREDICTED FROM THE EMPIRICAL MODEL

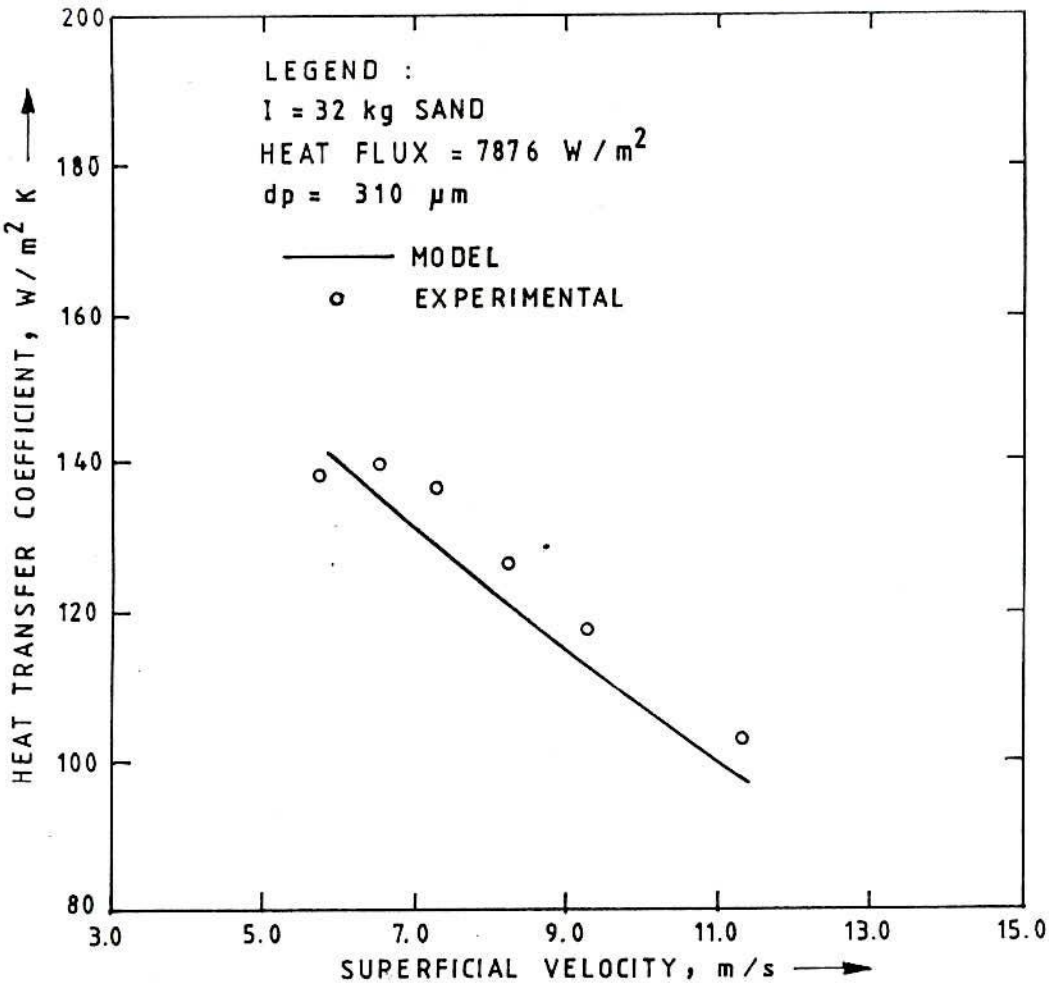

FIG. 6.82 EXPERIMENTAL RESULTS AND PREDICTED VALUES OF HEAT TRANSFER COEFFICIENT FROM THE EMPIRICAL MODEL

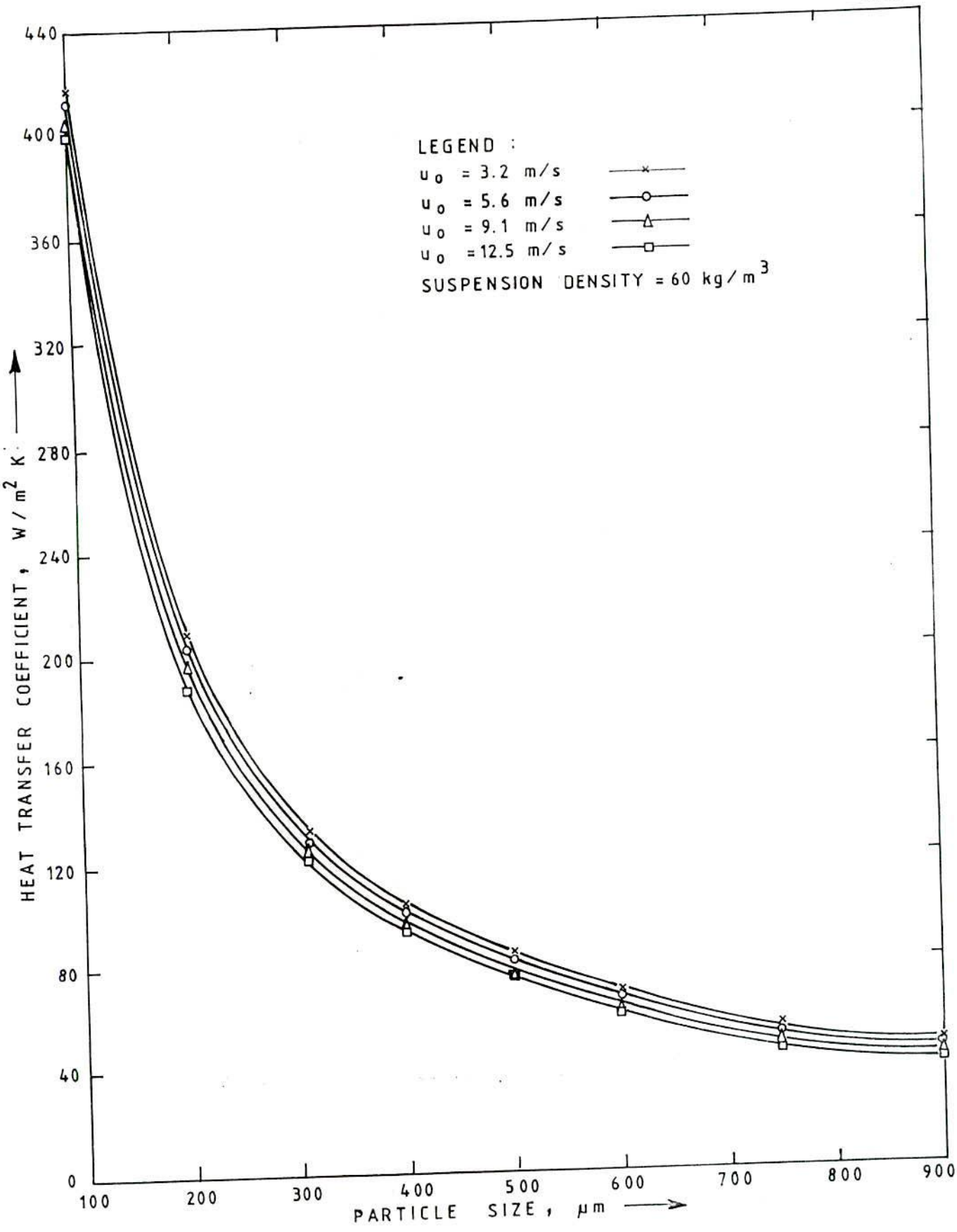

FIG.6.83 EFFECT OF PARTICLE SIZE ON HEAT TRANSFER COEFFICIENT AS COMPUTED FROM THE EMPIRICAL MODEL

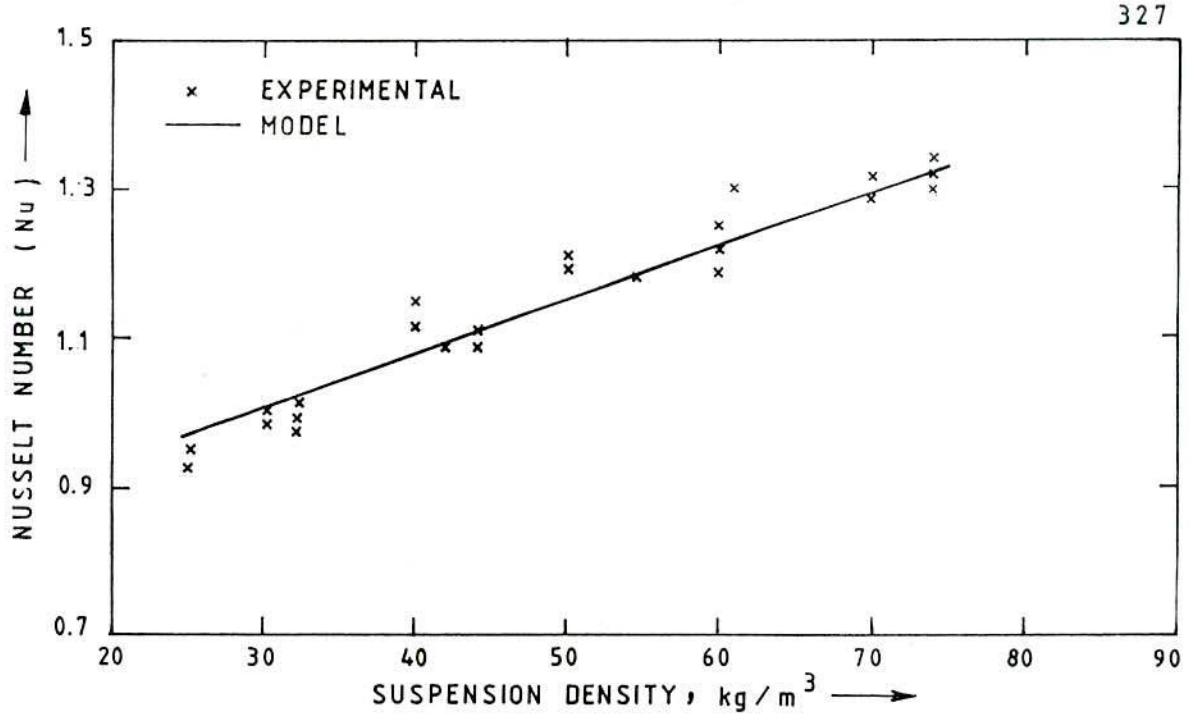

FIG. 6.84 COMPARISON OF EXPERIMENTAL RESULTS WITH THOSE PREDICTED FROM THE EMPIRICAL MODEL

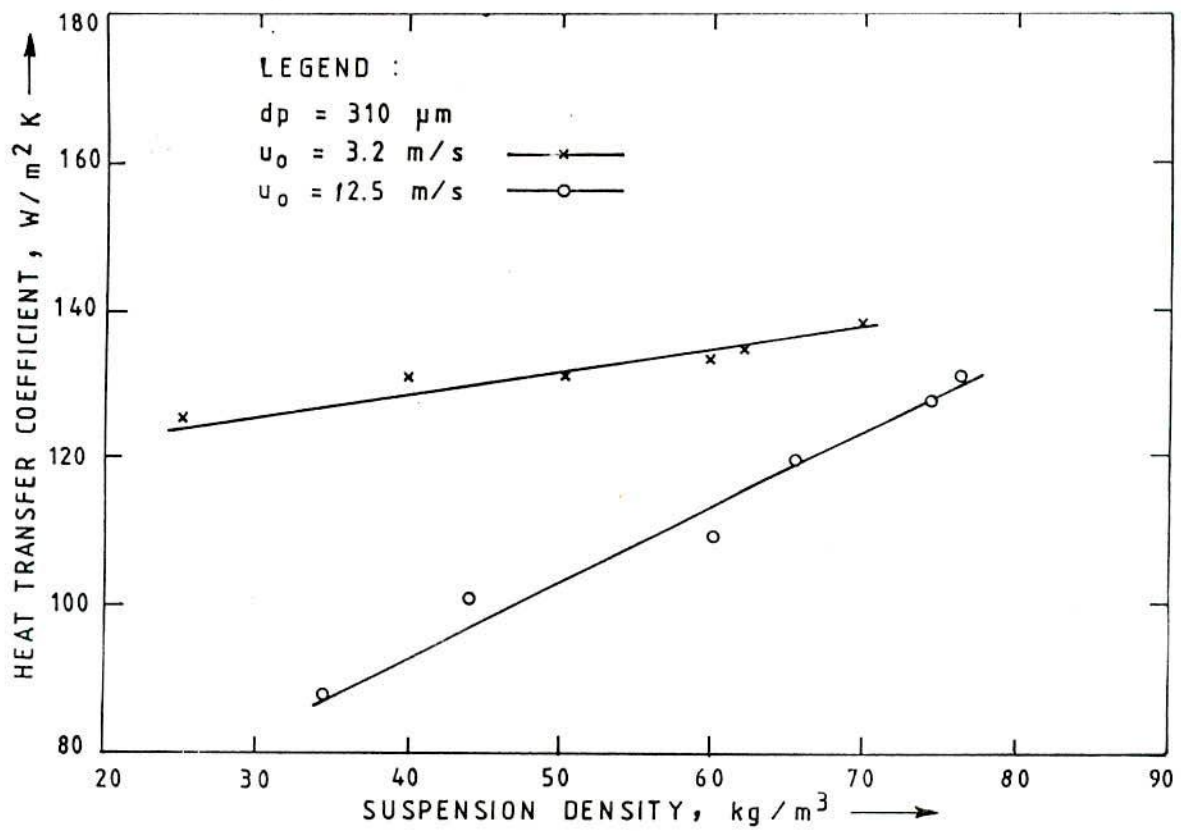

FIG. 6.85 EFFECT OF SUSPENSION DENSITY ON HEAT TRANSFER COEFFICIENT PREDICTED FROM THE EMPIRICAL MODEL

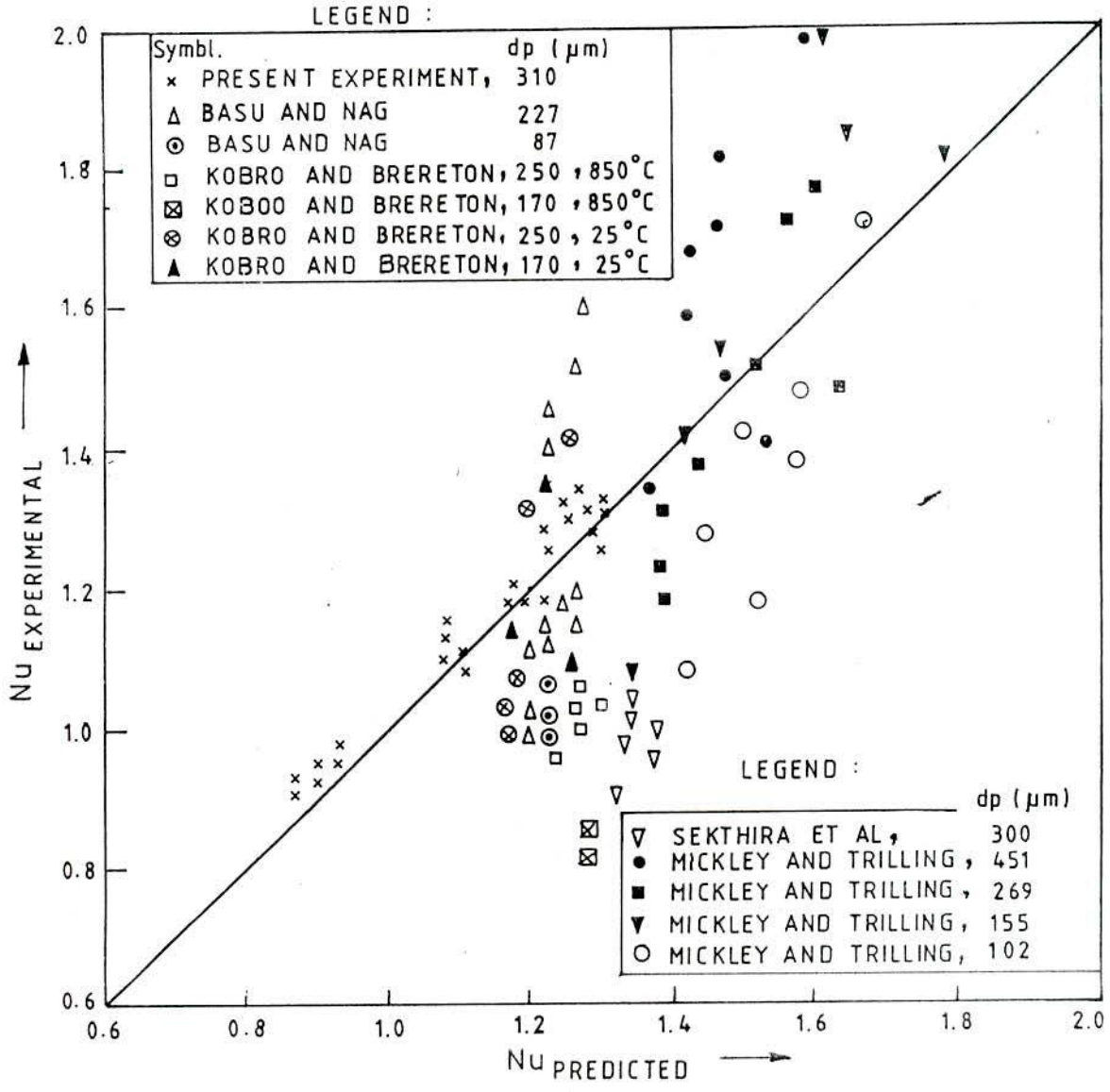

FIG. 6.86 COMPARISON OF PREDICTED VALUES FROM EMPIRICAL MODEL WITH EXPERIMENTAL RESULTS OF OTHERS

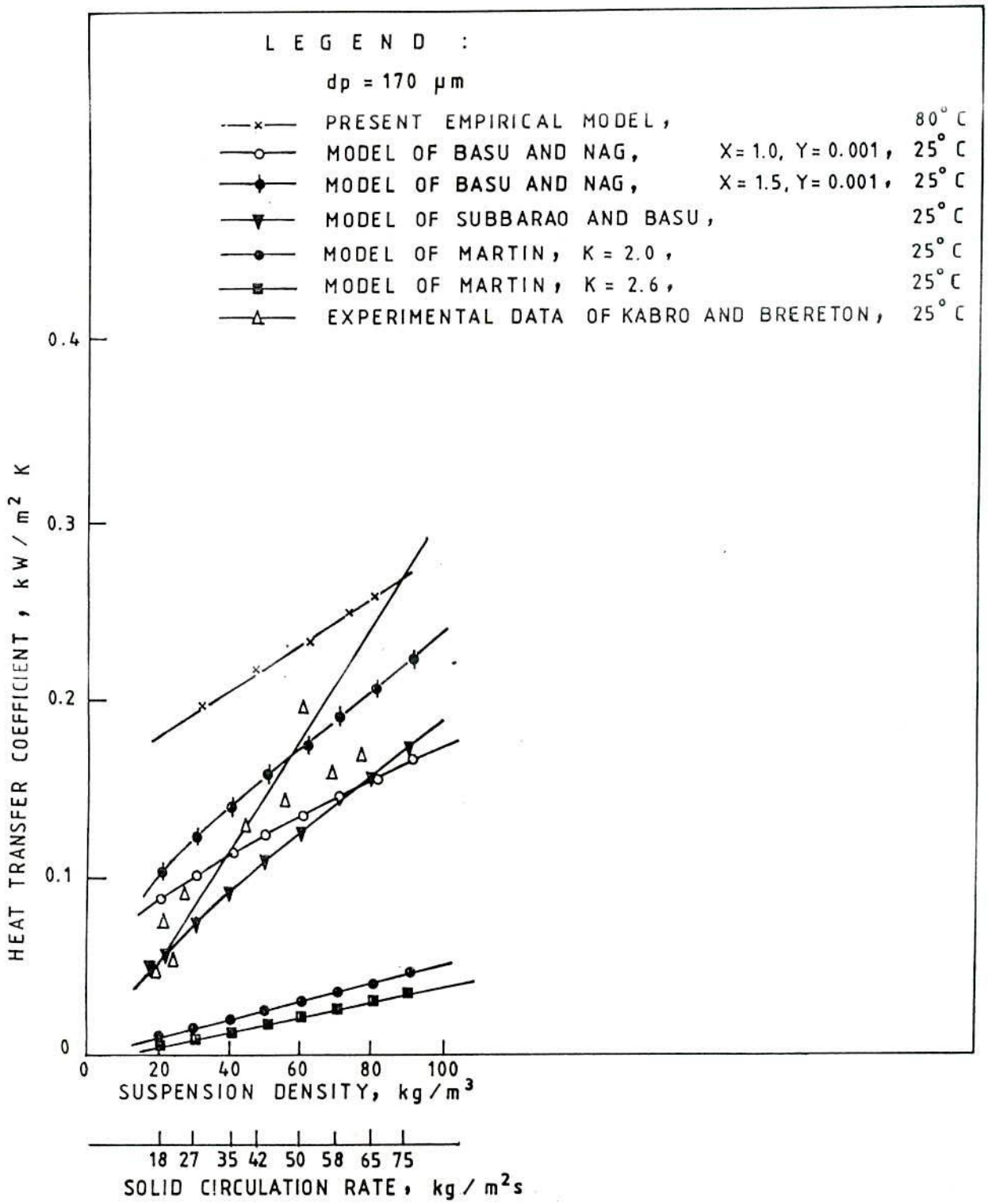

FIG. 6.87 COMPARISON OF PREDICTED VALUES WITH EXPERIMENTAL DATA OF KOBRO AND BRERETON [8] FOR 170 μm PARTICLES FOR COLD BEDS

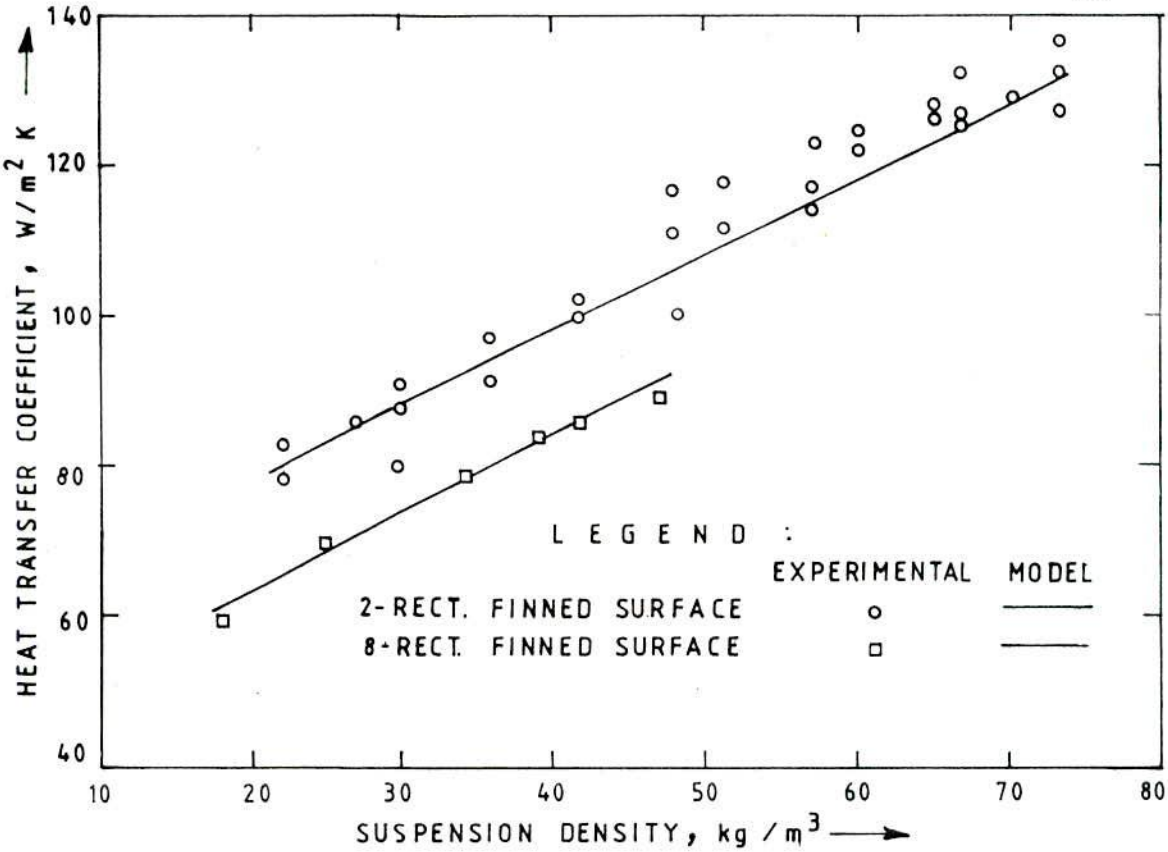

FIG. 6 COMPARISON OF PREDICTED VALUES FROM THE MODEL WITH EXPERIMENTAL RESULTS FOR 2 AND 8 RECTANGULAR FINNED SURFACES

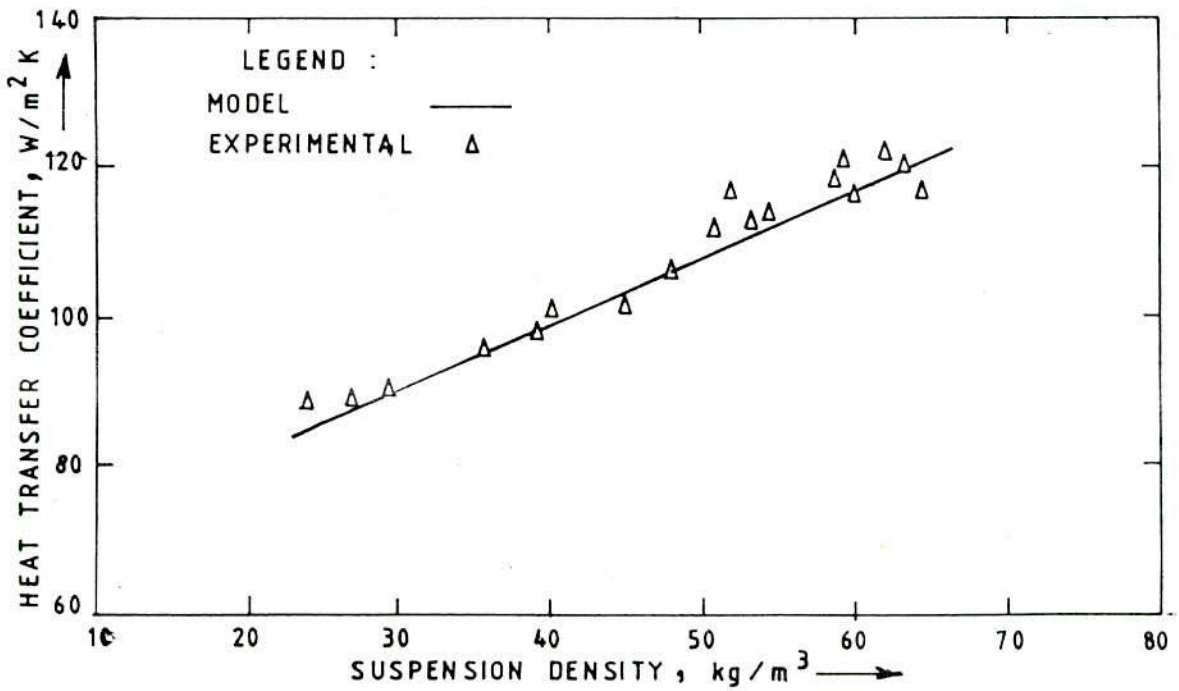

FIG. 7 COMPARISON OF PREDICTED VALUES FROM THE MODEL WITH EXPERIMENTAL RESULTS FOR 32-PIN FINNED SURFACE

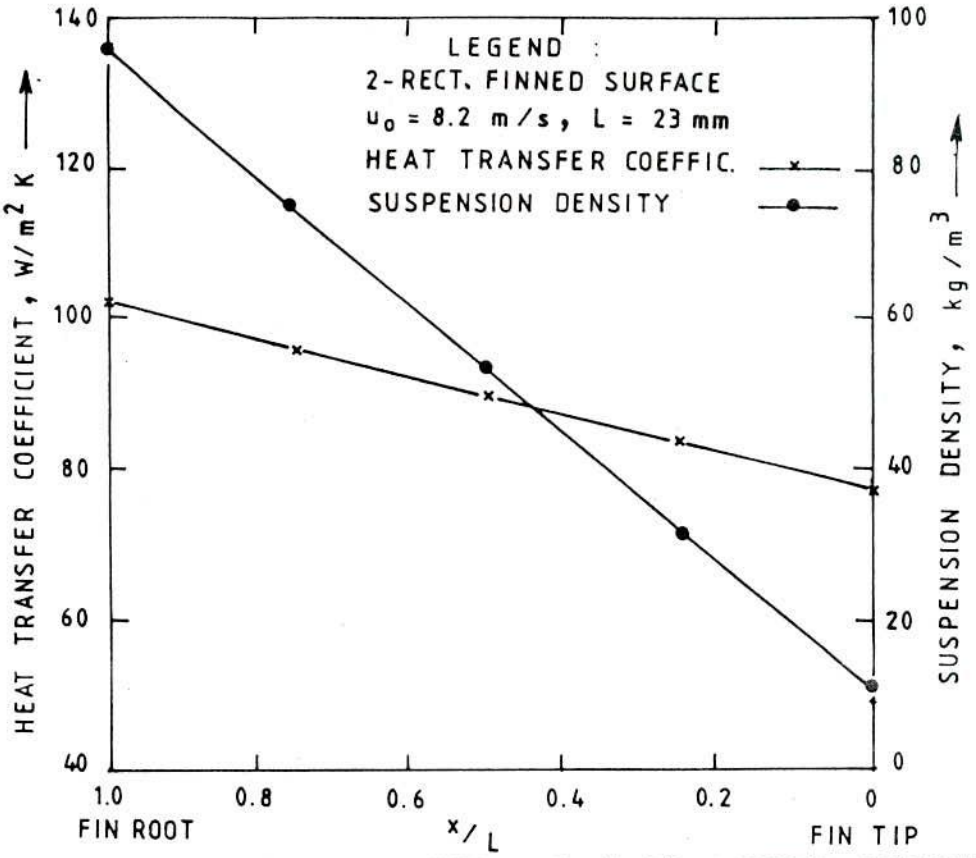

FIG. 8 VARIATION OF COMPUTED HEAT TRANSFER COEFFICIENT AND SUSPENSION DENSITY FROM THE ROOT TO THE TIP OF THE FIN (FROM MATHEMATICAL MODEL)

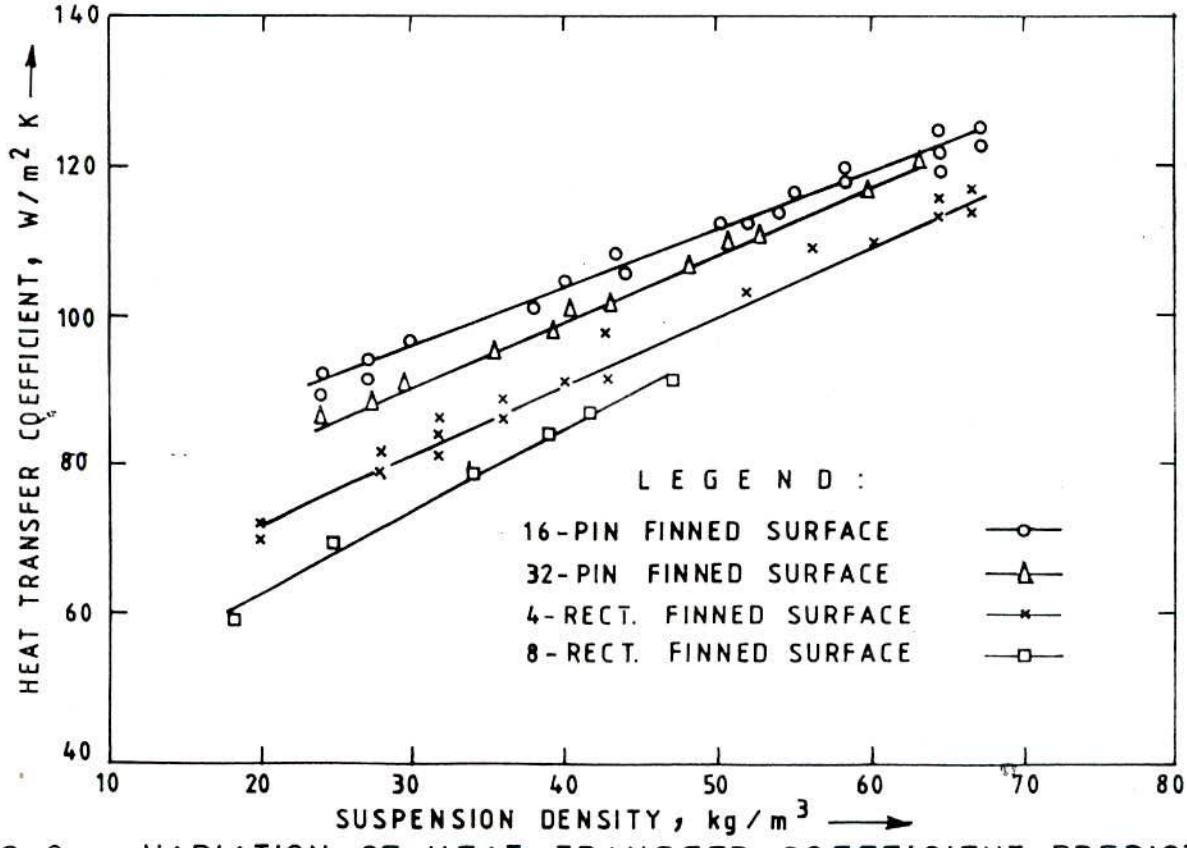

FIG. 9 VARIATION OF HEAT TRANSFER COEFFICIENT PREDICTED FROM THE MATHEMATICAL MODEL WITH SUSPENSION DENSITY

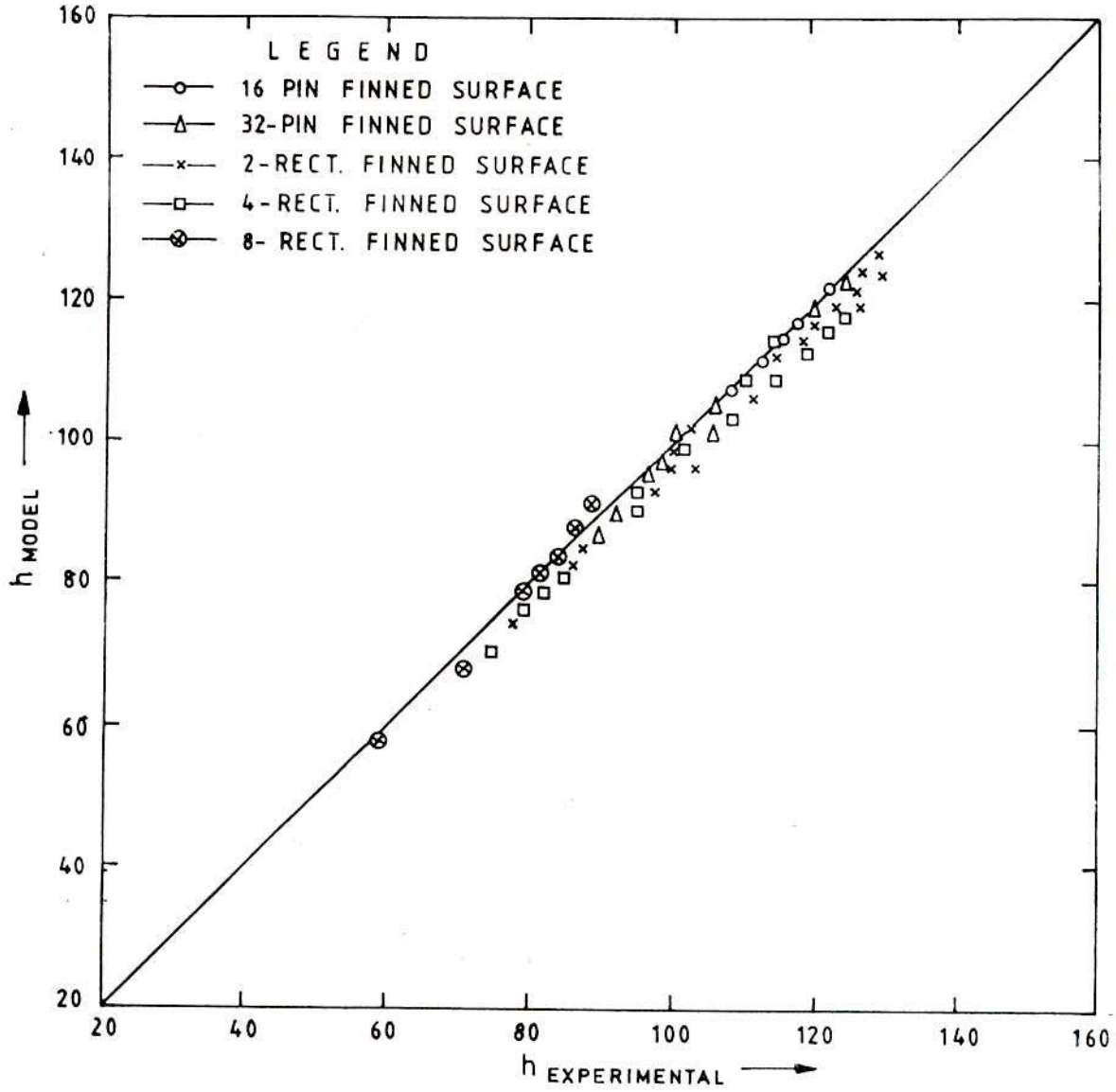

FIG. 10 COMPARISON OF PREDICTED RESULTS FROM MATHEMATICAL MODEL WITH THOSE OF PRESENT EXPERIMENTS

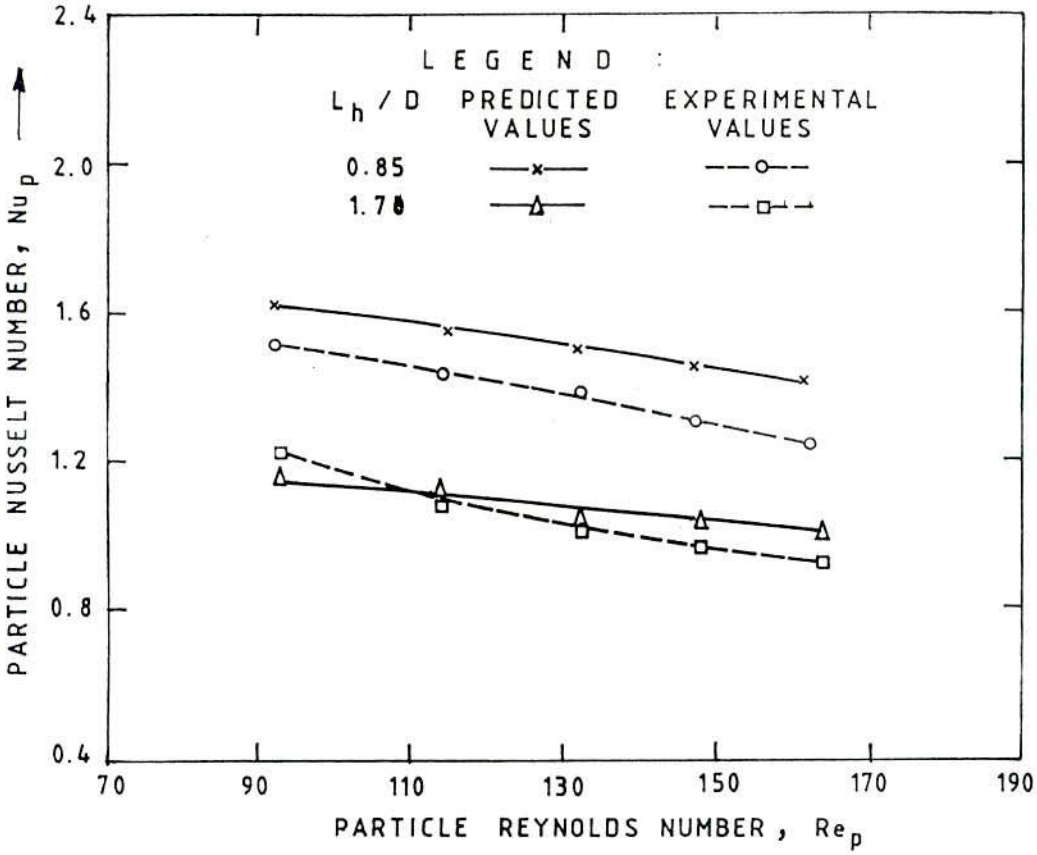

FIG. 6.93 COMPARISON OF EXPERIMENTAL RESULTS WITH THOSE PREDICTED FROM THE EMPIRICAL CORRELATION

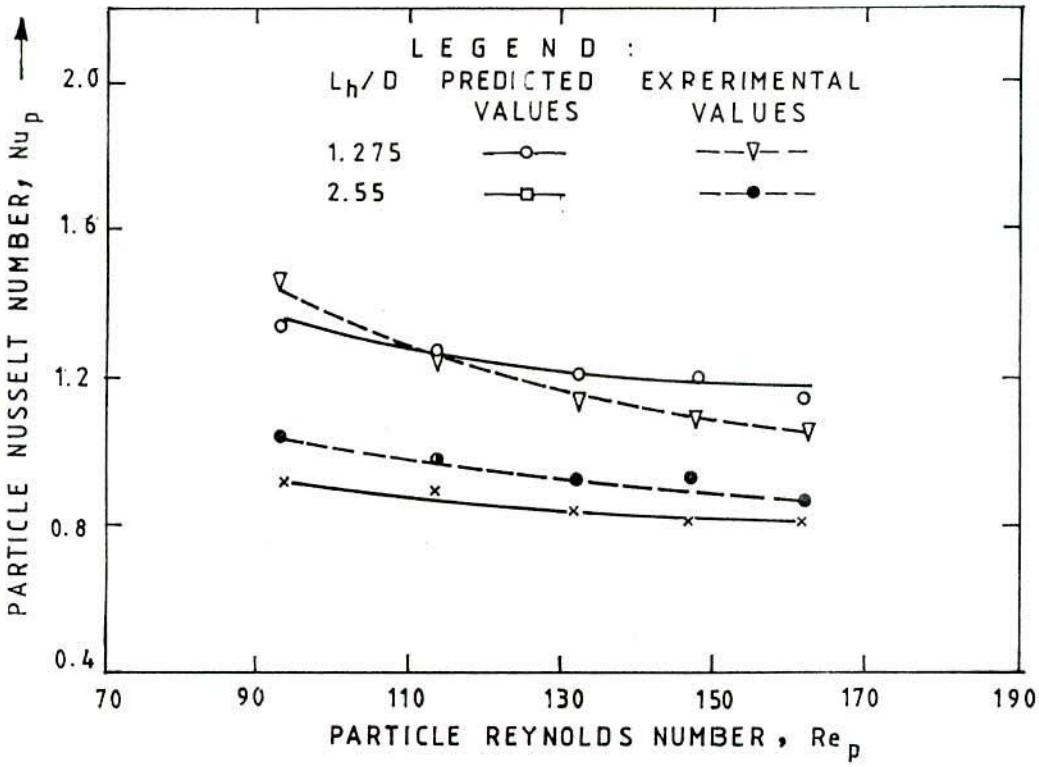

FIG. 6.94 COMPARISON OF EXPERIMENTAL RESULTS WITH THOSE PREDICTED FROM THE EMPIRICAL CORRELATION

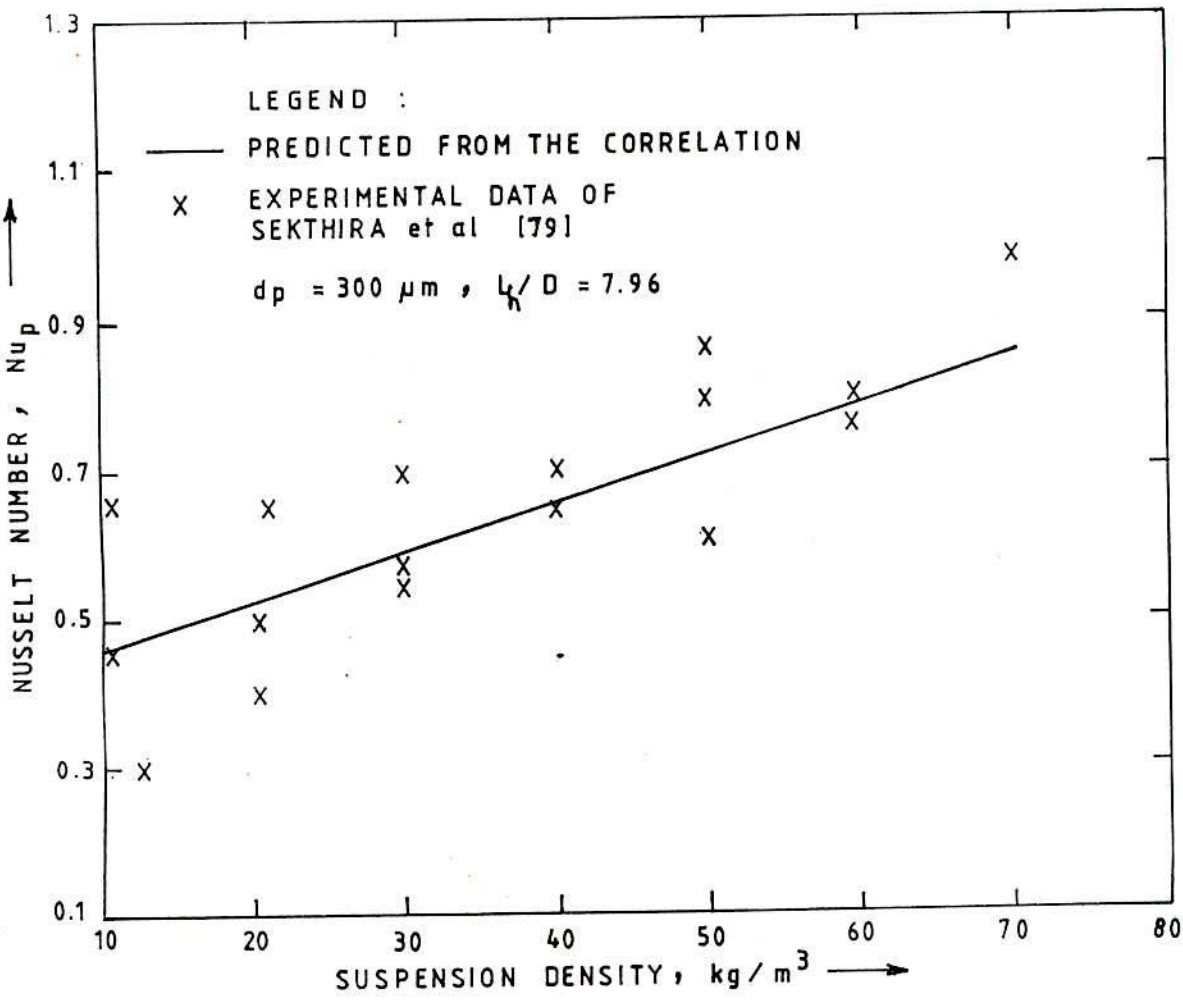

FIG. 6.95 COMPARISON OF PREDICTED VALUES FROM THE CORRELATION WITH THE EXPERIMENTAL DATA OF SEKTHIRA et al [79]

CHAPTER - VII

DISCUSSION OF RESULTS

The results obtained from the present investigation are discussed in two major sections. Under the first section discussion is limited to the experimental observations concerning the effects of various CFB parameters on heat transfer and hydrodynamics in circulating fluidized beds, while the second part deals with the theoretical aspects of the investigation, i.e., the prediction of heat transfer from the proposed models and correlations and its comparison with the experimental values.

Part-I : Discussion on Experimental Observations

It is already stated in Art. 5.2 that the experiments were divided into three parts (1) Heat transfer from bare (unfinned) surface, (2) Heat transfer from finned surfaces and (3) Heat transfer from probes of different vertical heights. So the discussion in this section has further been sub-divided as given below :

(i) Heat transfer from bare or unfinned surface,

(ii) Heat transfer in presence of finned surface,

(iii) Performance of fins in CFB,

(iv) Effectiveness of fins in CFB,

(v) Effect of fin on bed hydrodynamics,

(vi) Study of heat transfer from probes of different vertical heights,

(vii) Experimental data in non-dimensional form

7.1 Heat Transfer from Bare (Unfinned) Surface

Heat transfer data of circulating fluidized beds, with fins are not available in literature. So to form a basis of comparison as well as to check the reliability of the measuring techniques employed, heat transfer was first measured on plane or unfinned surface, and the observed data were compared with the results of other investigators who measured the same on plane walls under similar conditions. Figure 6.1 shows some previously published heat transfer results obtained on plane or unfinned surfaces in circulating fluidized beds together with those of the present work. In each case sand particles were used as the bed material and all reported results fall within the mean particle size range from 87 to 310 micron and the suspension density range from 0 to 100 kg/m^3. Some relevant experimental details of these published studies are summarized in Table - 6.53. In spite of the different operating conditions and different equipment used in these studies, it is observed that the heat transfer coefficient increases with the increase in suspension density.

The present data (curve no. 11) were obtained from a 300 mm long, 100 mm I.D. bed and for 310 micron sand particle under constant heat flux condition. The data (curve no. 1 and 2) of Basu and Nag [39] were collected from a 102 mm bed for 87 and 227 micron sand particles at room temperature and for 25 mm probe. The data (curve no. 3 and 4) of Kobro and Brereton [8] were for 170 and 250 micron sand particles in a 200 mm bed and at room temperature. The data (curve no. 5, 6 and 7) of Wu et al [38,80,81] were collected for 188, 171 and 241 micron sand particles and from a 152 x 152 mm square bed. Sekthira et al [79] obtained data (curve no. 8) from seven 100 mm long test sections of 88 mm I.D. bed. Furchi et al [78] obtained data (curve no. 9) from six 1000 mm long water jackets of 84 mm I.D. bed for 269 micron particle size at room temperature, and Subbarao and Basu [71] used a 25 mm heat transfer probe in a 102 mm diameter bed with 260 micron sand particles (curve no. 10).

The data of Basu and Nag [39] and Wu et al [81] are higher than other values presumably due to their use of small size probes and fine particles. The data of Wu et al [38, 80], Furchi et al [78] and Sekthira et al [79] were collected from longer heat transfer probes and showed lower heat transfer results. It has been shown by some investigators [39, 40] that longer heat transfer surfaces experience lower heat transfer rates due to the cooling of solids. Also as explained later in Art. 7.6 that

the effect of particle size is muted for such long surfaces. This is apparent from the overlapping of data of 188 micron [80] with those of 300 micron [79] particles both being carried out for long heat transfer surfaces. Kobro and Brereton [8] and Subbarao and Basu [71] used small probes and relatively large particles and therefore report relatively higher values of heat transfer coefficients.

Present results on bare tube surface fall in the same range of previous data and show similar trends of variation with suspension density. This adds to the confidence for further experiments using fins on the present test rigs.

7.1.1 Effect of operating variables on heat transfer for unfinned surface

The operating variables considered are suspension density, superficial velocity, heat input, bed inventory, bed temperature and solid circulation rate.

(a) Suspension density

Measured heat transfer coefficients and voidages for 310 micron sand particles for unfinned surface are plotted in Figs. 6.2, 6.6 and 6.10. The suspension density is found to be a dominating factor influencing the heat transfer coefficient in circulating fluidized beds. The heat conduction from cluster is much higher than that from the gas. Therefore, the heat transfer coefficient increases with the increase in

suspension density. This effect is in agreement with Kobro and Brereton [8], Basu and Nag [39], Wu et al [80, 81] and Mickley and Trilling [125]. A monotonic decrease of voidage is seen with the increase of suspension density.

(b) Superficial velocity

The effect of superficial velocity on heat transfer coefficient and voidage for unfinned surface is shown in Figs. 6.15, 6.18 and 6.21. With the increase of fluidization velocity the solid concentration in the bed decreases as a result of which the heat transfer coefficient decreases. This result is in agreement with the result of Basu and Nag [39], Sekthira et al [79] and Mickley and Trilling [125].

(c) Heat input

The effect of heat input on heat transfer coefficient for unfinned surface is shown in Figs. 6.25, 6.29, and 6.33. It is observed from all the diagrams that heat transfer coefficient increases with the increase of heat input to the bed.

(d) Bed inventory

The effect of bed inventory on heat transfer coefficient for unfinned surface has been shown in Fig. 6.37. The heat transfer coefficient is found to increase with the

increase in bed inventory. The marginal effect of bed inventory on heat transfer coefficient is also observed by Basu et al [73].

(e) Bed temperature

The effect of suspension temperature on heat transfer coefficient for unfinned surface is shown in Fig. 6.42. The heat transfer coefficient is found to increase with the increase in bed temperature due to increase in the value of gas thermal conductivity, which agrees well with that of Sekthira et al [79].

7.2 Heat Transfer in Presence of Finned Surface

Five finned test sections have been examined, three of which had rectangular fins and the remaining two had pin fins. The average heat transfer coefficient was determined for each operating condition at steady state from the measured heat flux rate and the temperatures of the inside wall and the bed suspension. Heat transfer coefficients on finned surfaces were expressed on the basis of total (area of fins + bare surface) heat transfer area. The effect of fins on various CFB parameters are discussed below.

7.2.1 Effect of suspension density on heat transfer coefficient

The variation of overall heat transfer coefficient with suspension density is plotted in Figs. 6.2 to 6.14. The suspension densities used are the cross-sectional average values estimated from the measured pressure drop data. The lines shown in the figures are the least-square best-fit lines.

(a) Rectangular fins

The variation of heat transfer coefficient with suspension density for rectangular finned surfaces is shown in Figs. 6.3, 6.7 and 6.11. The heat transfer coefficient was found to increase with the increase in suspension density in the same fashion as it did for unfinned surfaces. This suggests that the heat transfer to fins is governed by the same physical mechanism as on plane walls without fins. As the solid particles come at random in contact with the heat transfer surface, there is transient heat conduction which is the dominating mode of heat transfer between the fluidized bed and the wall. Higher is the suspension density, larger would be the number of particles per unit volume and hence higher would be the heat transfer coefficient. Figures 6.3, 6.7 and 6.11 show that the unfinned surface has the highest heat transfer coefficient, which decreases with the increase in the number of fins at a particular suspension density. Although

the downflowing solids in the dense annulus at the wall tend to accumulate at the top of the rectangular fins, at the bottom it is highly void so that the average suspension density around a fin is somewhat less, which results in a low heat transfer coefficient.

The fins are, however, used to provide more surface area. So, when the ratio (A_T/A_{UF}) of total heat transfer surface area with fins (A_T) to the bare surface area without fins (A_{UF}) is multiplied with the heat transfer coefficient and these values are plotted against suspension density (Figs. 6.4, 6.8 and 6.12), it is observed that the equivalent heat transfer coefficients are now higher for finned surfaces than those of unfinned surface. Therefore, the increase in surface area due to the fins more than nullifies the decrease in heat transfer coefficient, and as the number of fins increases, the overall heat transfer increases.

The additions of two, four and eight rectangular fins have increased the heat transfer area by about 28, 56 and 112 percent, decreased the heat transfer coefficient by 15, 19 and 32 percent but increased the total heat transfer by about 25.6, 51.5 and 103 percent respectively.

(b) Pin fins

The variation of heat transfer coefficients with suspension density for 16 and 32 pin finned surfaces is shown in Figs. 6.5, 6.9 and 6.13. The heat transfer coefficient for pin finned surface was found to increase linearly with the increase in suspension density in the same way as for the rectangular finned surface. Here it is also observed that the heat transfer coefficient is decreased with increase in the number of fins i.e., with the decrease of fin gap. Although the heat transfer coefficient somewhat decreased with the use of fins (Figs. 6.5, 6.9, 6.13), the total heat transfer increased due to the increase in the surface area.

The addition of 16 and 32 number of pin fins have increased the heat transfer area by about 6 and 12 percent, decreased the heat transfer coefficient by about 10 and 15 percent but increased the total heat transfer by about 5.4 and 11.0 percent respectively.

Priebe and Genetti [112] and Chen and Withers [114] also observed reduction in heat transfer coefficient when fins were used on tubes immersed in bubbling fluidized beds.

From the data of the present experiments it is observed that the reduction of heat transfer coefficient due to addition of fins is in the range of 10-32 percent and the rate of reduction is higher for pin finned surface than that of rectangular finned surface.

(c) Long fins

The effect of suspension density on heat transfer coefficient for 1500mm long four rectangular finned surface has been shown in Fig. 6.14. It also shows the same nature of increasing heat transfer coefficient with the increase of suspension density.

7.2.2 Effect of superficial velocity on heat transfer coefficient

The variation of heat transfer coefficient with superficial velocity is shown in Figs. 6.16, 6.19 and 6.22 for rectangular finned surface, in Figs. 6.17, 6.20 and 6.23 for pin finned surface and in Fig. 6.24 for long rectangular finned surface. In all the cases it is observed that the heat transfer coefficient decreases with the increase in superficial velocity. With the increase of gas velocity, more particles are entrained and move upward with the gas and less number of particles move towards the wall to cohere and fall in strands along the wall. So, the particle convective heat transfer, which is the dominant mode at low temperature, decreases. This results in a decrease of the overall heat transfer coefficient with the increase of superficial velocity. This effect is in agreement with the result of Basu and Nag [39], Sekthira et al [79] and Mickley and Trilling [125]. Due to the down flowing solid particles along the wall, although the top surface of the fin has some accumulated particles on it, the bottom surface has a low suspension

density. Therefore, the average heat transfer coefficient over the entire fin surface gets reduced by a small amount. However, the increase in surface area due to fins augments the total heat transfer from the test section as mentioned earlier.

7.2.3 Effect of heat input on heat transfer coefficient

The effect of heat input on heat transfer coefficient is shown in Figs. 6.25 to 6.36, where heat transfer coefficient is plotted versus the suspension density. The third parameter on the plot is the heat flux, i.e., the power input to the heater divided by the heat transfer area of the tube. Three curves for three heat inputs have been drawn in each figure. In all the cases of finned and unfinned surfaces, it is observed that the curves for three heat inputs show the similar nature of increasing heat transfer coefficient with increasing suspension density and increasing heat transfer coefficient with increasing heat flux.

7.2.4 Effect of bed inventory on heat transfer coefficient

The effect of bed inventory on heat transfer coefficient has been shown in Figs. 6.37 to 6.41, where heat transfer coefficient is plotted against the superficial velocity. The third parameter on the plot is the bed inventory. Three curves for three bed inventories of 20, 26 and 32 kg sand have been plotted in each figure. The bed inventory has shown marginal effect on heat transfer coefficient in all the cases

of unfinned, rectangular and pin finned surfaces. Higher bed inventory causes higher bed suspension density which attributes to higher heat transfer coefficients.

7.2.5 Effect of bed temperature on heat transfer coefficient

The present experiments were performed at low bed temperture ranging from 330 to 365 K (Figs. 6.42 to 6.45(a)). Within the range of present experiments the influence of bed temperatures on heat transfer coefficient is found to be negligible as observed by the flat nature of all the curves, although they show increasing trend. Sekthira et al [79] also observed the same nature of effect of bed temperature in their experiments with plane surface.

7.2.6 Effect of solid circulation rate on heat transfer

The effect of bed density on heat transfer in circulating fluidized bed is well documented [8,12,39]. The suspension density at a particular location in a CFB can be changed by changing the fluidization velocity and solid circulation rate. For a given superficial velocity, the suspension density can be increased by increasing the circulation rate of solid. These effects are evident from the Figs. 6.45(b) and 6.45(c) for unfinned and rectangular finned surfaces respectively. It shows that the heat transfer coefficient increases when solid circulation rate is increased, i.e., when the suspension density is increased which is expected. The

data of solid circulation rate for unfinned, rectangular and pin-finned surfaces are shown in Tables 6.1 to 6.15.

7.3 Performance of Fins in CFB

It is observed from Figs. 6.4, 6.8 and 6.12 that the equivalent heat transfer coefficient calculated on the basis of base area, is consistently higher than that of plane (unfinned) wall surface at all suspension densities. This demonstrates the enhancement of heat transfer through the use of extended surfaces or fins. A measure of fin tube performance is the ratio of the heat transfer coefficient for finned surface compared to that obtained on an unfinned surface under identical CFB conditions. When this ratio is unity, exceeds unity or even just a substantial fraction of unity, one may expect the fin tube to provide higher heat transfer duty per unit length than an unfinned surface [114]. Figure 6.46 shows the plot of this ratio (h_F/h_{UF}) as a function of particle Reynolds number (Re_p). Data from three test sections, with rectangular fins, having different fin gaps have been plotted in this figure. Each curve represents the result obtained for a particular finned test section, operating with the same fluidized condition and similar particle size. Some interesting points are indicated by these graphs. First one can look at the value of coefficient ratio, which is relatively high, being above 0.6 for the great majority of the cases, and infact for one of the

finned tube test sections, the coefficient ratio approaches near to unity (above 0.9). Second, from a comparison of the three curves, it is evident that increasing fin count, i.e., decreasing fin gap causes a definite decrease in the ratio of heat transfer coefficients. Third, it is obvious from Fig. 6.46 that the heat transfer coefficient ratio decreases with the increase of Re_p , or in other words superficial velocity. As the number of fins is increased, the solid movement becomes restricted, and with the increase of superficial velocity more solids are swept away from the test section, and for both the cases the suspension density is decreased in the test section resulting in lower heat transfer coefficient ratio.

The capacity function ($A_T h_F / A_{UF} h_{UF}$) is a direct measure of the heat transfer capability for a finned surface relative to the unfinned surface occupying the same superficial bed volume. Figure 6.47 is a diagrammatic presentation of this function for the various finned tubes tested under this investigation. For each finned tube, the capacity function is plotted against particle Reynolds number (Re_p). The third parameter here is the fin count. It is observed that with the increase in the number of fins, i.e., with the increase of heat transfer area, the curve shifts upward as expected. For the conditions presented in Fig. 6.47, the values of the average capacity functions were

approximately 1.1, 1.25 and 1.32 for two, four and eight rectangular finned tubes respectively. This represents a substantial increase in heat transfer capability over the unfinned surface ranging from 25 to 103 percent.

7.4 Effectiveness of Fin in CFB

It is well known that the total heat transfer increases with the increase in heat transfer area. Therefore, addition of a large number of fins yields higher heat transfer. But heat transfer does not increase exactly in proportion to the surface area added through fins. The actual gain is proportional to the additional surface area times the effectiveness of fin. The fin effectiveness is defined as the ratio of actual heat transfer through the fin to the maximum heat transfer through the fin. The maximum heat transfer will occur when all surfaces of the fin will be at the same temperature as the base of the fin and the heat transfer coefficient over the entire surface of the fin will be the same as that over its base. A reasonable approximation of the maximum heat transfer will be the product of actual fin area, the heat transfer coefficient measured for the plane wall and the temperature difference between the bed suspension and the base wall of the fin. This was done in the present experiments.

The fin effectiveness is calculated for two, four and eight rectangular finned surfaces and plotted against suspension density in Fig. 6.48 and the same is calculated for

sixteen and thirty two number of pin-finned surfaces and plotted against suspension density in Fig. 6.49. In both the cases the fin effectiveness is found to increase with the suspension density, though the data are somewhat scattered. The increasing tendency is clear both for rectangular and pin-finned surfaces, but a decreasing tendency of the effectiveness is observed beyond a suspension density of about 45 and 55 kg/m^3 for rectangular and pin-finned surfaces respectively.

A significant difference between fins on circulating fluidized bed and that on conventional heat exchanger is that in the later case of the local heat transfer coefficient on the fin surface is not significantly different from that on the base, because both are exposed to similar hydrodynamic conditions. In a circulating fluidized bed, a thin layer of solids frequently slides down the wall. The bulk density of the solids drops away from the wall. So the body of the fin extending away from the wall comes in contact with reducing concentration of down-flowing solids. Higher the suspension density, thicker the down flowing layer of solids and hence greater portion of the fin is exposed to the higher concentration of solids. So the fin should be more effective at higher suspension density when larger fraction of its surface is exposed to solids. But it will have a saturation limit, beyond which an increased solid concentration may not increase the heat transfer

proportionately because the solid mobility between adjacent fins is affected. This may be the reason why the fin effectiveness in this investigation is found to decrease beyond the suspension density of 45 and 55 kg/m^3 for rectangular and pin finned surfaces respectively. Further, with the increase of fin count in both the cases, the effectiveness is found to decrease due to the increased hindrance of particles by the fins as observed in Figs. 6.48 and 6.49. The most important observation is that heat transfer is increased with the installation of increasing number of fins and in all the cases the fin effectiveness is found in the range of 70 to 95 percent.

7.5 Effect of Fins on Bed Hydrodynamics

The voidages were estimated from the pressure drop data along the height of the riser column for unfinned as well as finned surfaces. The voidage profiles for unfinned, rectangular and pin finned surfaces are plotted in Figs. 6.50 to 6.65. The comparison of voidage profile of unfinned surface with those of 2,4 - rectangular and 32-pin finned surfaces is shown in Figs. 6.66, 6.67 and 6.68 respectively. In each case six profiles have been drawn for six superficial velocities. It is observed that the voidage increases with the increase of superficial velocity. Although the voidage generally increases along the height of the column, a change in gradient of axial voidage profile near the level of the finned

section was noted at all velocities. Since the fins hindered the particles moving downward, the voidage increased at the test section and then remained almost unaltered. When the fins were absent, then beyond the bubbling bed regime itself, the voidage remained fairly constant.

The voidage tended to decrease near the finned section. The particles were hindered and decelerated by the presence of projected fins. This may have caused the decrease in bed voidage near the fins. Similar lowering of voidage just below a projected surface is also observed in commercial boilers. This inflection in the voidage profile is less pronounced at higher velocities due to the lower solid concentration in the column. In commercial situations such an effect on the hydrodynamics may not be present because the fins will be continuous and will be present along the entire length of the wall.

To study the effect of continuous fin on hydrodynamics, four 1500 mm long, continuous rectangular fins were fitted uniformly at 90^{o} apart to the inner surface of the test rig (at the top) and the results are plotted in Fig. 6.69. It is observed that the long finned surface experiences slightly higher voidage than that of unfinned surface, although both the profiles are similar in nature.

7.6 Study of Heat Transfer from Probes of Different Vertical Heights

It is already mentioned in Art. 5.2.5 that four probes having vertical heights of 85, 127.5, 170 and 255 mm were tested. The results obtained from the experimental data are plotted in Figs. 6.70 to 6.74. Data taken from 85 mm long test section has been plotted in Fig. 6.70 showing the effect of suspension density on heat transfer coefficient and voidage. The heat transfer coefficient is found to increase and voidage is found to decrease with the increase in suspension density. Figure 6.71 shows the variation of heat transfer coefficient and voidage with superficial velocity for the same probe. Like many other workers [39,79], it is also observed here that heat transfer coefficient decreases and voidage increases with the increase in superficial velocity.

It has been confirmed that the structure of the circulating fluidized bed consists of a dilute central core of solids and a dense wall region [29, 149].

The tendency of the solid to stay in the wall on its way down to the bed makes the vertical height of the probe a deciding factor in CFB heat transfer. This fact is illustrated in Fig. 6.72, where the heat transfer coefficient is plotted against the vertical height of the probe for fixed bed density. Here two curves for suspension densities of 62

and 25 kg/m^3 have been drawn. In both the cases the heat transfer coefficient is found to drop rapidly with the increase in the vertical height of the probe. As the layer of particles sweep down along the heat transfer surface, it gradually approaches thermal equilibrium with the surface, since there is little renewal of particles in this layer. This reduces the driving force for heat transfer, thus producing a lower average heat transfer coefficient. This is confirmed from the observations of Wu et al [38,80], Furchi et al [78] and Sekthira et al [79], who obtained lower values of heat transfer coefficients by using longer probes. If the heating surface is short, particle clusters will exchange heat with it for a very short period of time. So the thermal resistance between the wall and the first layer of particles will govern heat transfer. Therefore, the particle size will play a dominant role on the heat transfer rate. In case of long heating surfaces, the clusters exchange heat with the wall for long periods of time and therefore the heat conduction into the particle cluster, which is less sensitive to the particle size, dominates the process [40].

Figure 6.73 shows the effect of vertical height of the probe on the residence time of the particles and in turn, the effect of residence time on heat transfer coefficient. The figure is drawn for 62 kg/m^3 bed density. It is observed that with the increase in vertical height of the probe,

the residence time is increased sharply and with the increase of residence time, the heat transfer coefficient is decreased. As the vertical height of the probe increases, the particles stay longer in flowing past over it, and more layersof particles in the cluster are involved in transient heat transfer, resulting in more cooling of particles and lower heat transfer coefficient.

The particle Nusselt number (Nu_p) defined by $h\, d_p/kg$ is plotted against dimensionless probe height, L_h/D in Fig. 6.74 at two different superficial velocities. It is observed that the value of Nu_p decreases with the increase in L_h/D as well as superficial velocity.

The values of cluster residence time calculated from the derived expression (Eq. 3.22) and that calculated from Subbarao's cluster model [155] are presented in Tables 6.49 to 6.52.

7.7 Experimental Data in Non-dimensional Form

Proper non-dimensionalization of experimental data may extend the applicability of the results for general use. Some of the experimental results are shown in non-dimensional form and plotted in Figs. 6.75 to 6.80. The variations of Nu_p with Re_p for unfinned, rectangular and pin-finned surfaces are shown in Figs. 6.75, 6.76 and 6.77 respectively. In all the cases it is found that Nu_p decreases

with the increase of Re_p . It is explained earlier that with the increase of Re_p the bed density is decreased, as a result, Nu_p is also decreased. The variation of Nu_p with the ratio of suspension to particle (solid) density is shown in Figs. 6.78 to 6.80. It is observed that Nu_p increases with the increase of the ratio of suspension to particle density.

Part-II : Discussion on Predicted Results

Under this section, the predicted results from the proposed models and correlation as they compare with the actual values obtained from experiments are subject for discussion. This discussion is sub-divided into three parts :

(i) Prediction of heat transfer from the empirical model for bare tube surfaces.

(ii) Prediction of heat transfer from the analytical model for finned surfaces.

(iii) Prediction of heat transfer from empirical correlation.

7.8 Prediction of Heat Transfer from the Empirical Model for Bare Tube Surfaces

The model takes into consideration all the parameters which are relevant to heat transfer in a circulating fluidized bed. It was tested with the experimental data having a velocity

range from 3.2 to 12.5 m/s, the particle size varying from 100 to 900 μm, the suspension density in the range from 10 to 100 kg/m^3 and the bed temperature varying from 305 to 1123 K. The results predicted from the model Eq. (4.19) and those from the present experiments as well as those of other investigators are shown in Figs. 6.81 to 6.87.

The predicted results of heat transfer coefficients from the model have been plotted against superficial velocity in Fig. 6.81. Here two curves for suspension densities of 40 and 60 kg/m^3 show similar trends of decreasing heat transfer coefficient with increasing superficial velocity and increasing heat transfer coefficient with increasing suspension density for the same superficial velocity. This was also observed from the experimental data of many other workers [39, 80].

Heat transfer coefficients predicted from the model and the experimentally determined values are plotted against superficial velocity in Fig. 6.82, which demonstrates fair agreement. With the increase of superficial velocity, more particles are entrained and move upward with the gas and less number of particles move towards the wall to cohere and fall in strands along the wall. So the particle convective component decreases which results in a decrease of overall heat transfer coefficient with the increase of superficial velocity.

Figure 6.83 shows the effect of particle size on heat transfer coefficients estimated from the model. Four curves have been drawn for velocities of 3.2, 5.6, 9.1 and 12.5 m/s keeping the suspension density constant at 60 kg/m^3 in each case. The heat transfer coefficients are found to decrease with the increase in particle size. This prediction is supported by the observations of Kobro and Brereton [8], Basu and Nag [39], Sekthira et al [79] and Mickley and Trilling [125]. It is further observed that all the four curves are very close and they almost merge. This supports the observation of Wu et al [80] about the negligible effect of superficial velocity on heat transfer coefficient for a fixed suspension density in the bed.

Experimentally determined values of Nusselt number and those predicted from the model under the same operating conditions are plotted against suspension density in Fig.6.84. A good agreement is demonstrated.

The variation of heat transfer coefficient predicted from the model with suspension density for two velocities of 3.2 and 12.5 m/s has been shown in Fig. 6.85. In both the cases the heat transfer coefficient is found to increase with the increase in suspension density as observed by many workers [8, 38, 39].

The present experimental results as well as the results of other workers who carried out their experiments over a wide range of velocity, recycle rate, bed density, particle size and bed temperature are compared with those predicted from the model. In order to facilitate easy comparison of predicted results with experimental values, all data are plotted in Fig. 6.86, with the measured Nusselt number and the theoretical prediction as the coordinates. The values computed from the present model correspond to the operating conditions in each case. Although most of the values are seen to cluster around the 45^{o} line which is the line of perfect agreement, the predicted values from the data of Basu and Nag [39] are above and those of Kabro and Brereton [8] and Sekthira et al [79] are generally below the line. The deviation did not exceed beyond $\pm$ 30 percent.

The present model successfully predicts all the effects of physical variables on heat transfer. This demonstrates the correctness of physical modelling of the process of heat transfer in a circulating fluidized bed. A dearth of experimental data over a wider range of operating conditions prevented a comprehensive comparison of model predictions. Figure 6.87 shows a comparison of few data. The heat transfer coefficient is plotted as a function of bed density, varying upto 100 kg/m^3 at room temperature. Heat transfer

coefficients at these operating conditions were computed using the present model, models of Martin [65], Subbarao and Basu [156] and Basu and Nag [8] at room temperature and at 170 μm particle size. The solid circulation rates were taken from Stromberg [72] as indicated on the x-axis. The values predicted from Martin's model (using constant K = 2 and 2.6) are an order of magnitude lower than the experimental ones. The model proposed by Subbarao and Basu [156] did not consider radiation and under estimated the gas convective component. The net effect of their approximations is an under prediction of heat transfer rates for beds at room temperature. The model of Basu and Nag [39] suffers from the uncertainity of getting proper expression of residence time. The prediction from the present model seems to be quite reasonable but it provides values of heat transfer coefficient somewhat higher than those of the experimental data of Kobro and Brereton [3].

The proposed model successfully determines the effects of all the variables pertinent to heat transfer in circulating fluidized beds. It is simple and easy to use. The strong dependence of heat transfer coefficient on suspension density and particle size is clearly demonstrated by the model. It also indicates that once a particular suspension density in the bed is established, the effect of superficial velocity is not significant.

7.9 Prediction of Heat Transfer from the Analytical Model for Finned Surfaces

The model takes into consideration the basic principle of heat transfer from the finned surface together with the observations of Glicksman [12], Li et al [149], Yang et al [150] and Tung et al [186]. The predicted results from the model have been presented in Tables 6.30 to 6.40 and shown in Figs. 6.88 to 6.92.

Heat transfer coefficients predicted from model-I and the experimentally determined values for 2 and 8 - rectangular and 32 pin-finned surfaces have been plotted against suspension density in Figs. 6.88 and 6.89 respectively, and good agreement is observed. For all the cases it is observed that the heat transfer coefficient increases monotonically with the suspension density.

The distribution of suspension density and heat transfer coefficient along the fin surface, predicted from the model-I have been plotted in Fig. 6.90. The dimensionless fin parameter, x/L, is considered '1' at the fin base and zero at the fin tip. It is observed that both suspension density and heat transfer coefficient decrease from the base to the tip of the fin. This is supported by the experimental observations of Li et al [149], Tung et al [186] and few others.

The variation of heat transfer coefficient predicted from the model-I with suspension density for 4 and 8 rectangular and 16 and 32 pin-finned surfaces has been shown in Fig. 6.91. In all the cases, the predicted values of heat transfer coefficients are found to increase with the increase in suspension density. It is further observed that with the increase in the number of fins, the curve shifts downward showing lower values of heat transfer coefficient both for pin finned and rectangular finned surfaces, which agrees fairly well with the experimental observations.

Heat transfer data in CFB with fins not being available, the heat transfer coefficient predicted from model-I have been compared with the present experimental values of 2, 4, 8 rectangular, 16 and 32 number of pin finned surfaces (Fig. 6.92). For comparison of predicted values with the experimental ones, all data are plotted with the measured heat transfer coefficient and the theoretical predicted value as the coordinates. The value computed from model-I corresponds to the operating conditions prevailing in each case. Most of the values are seen to cluster below the 45^{o} line. It demonstrates that the predicted value is somewhat an underestimation of the actual value. The maximum deviation observed is about 8 percent.

7.10 Prediction of Heat Transfer from the Empirical Correlation

The predicted values from the empirical correlation have been compared with those of present experimental results with four probes having vertical heights in the range of 85 to 255 mm and particle Reynolds number in the range of 93 to 161. Figures 6.93 and 6.94 show the predicted values from the correlation together with the computed values from the experiments for the dimensionless probe heights, L_h/D, of 0.85, 1.7 and 1.275, 2.55 respectively. It is observed from the figures that for the lowest value of L_h/D (0.85), the predicted values are higher and for the highest value of L_h/D (2.55), the predicted values are lower than those of experimental results. For L_h/D equal to 1.7 and 1.275 both computed and predicted values seem to merge showing very little deviations. The maximum deviation from the whole range of the experiments was found to be about $\pm$ 11 percent. Agreement of predicted and experimental values of Nu_p is thus quite close.

The predicted values from the correlation have been compared with the experimental results of Sekthira et al [79] who used a dimensionless probe height, L_h/D, equal to 7.96 in Fig. 6.95 and a good agreement is observed.

CHAPTER - VIII

CONCLUSION

The major conclusions drawn from the present investigation are summarised below :

(1) The general characteristics of heat transfer in a circulating fluidized bed are quite similar for finned and unfinned surfaces.

(2) There is a positive dependence of heat transfer coefficient on suspension density, heat input, bed inventory and bed temperature and a negative dependence on superficial velocity.

(3) Addition of fins decreases the heat transfer coefficient but increases the heat transfer capability. The heat transfer coefficients for finned tube are generally in the range of 0.68 to 0.9 times that of bare tubes under similar fluidized condition.

(4) An increase in the number of fins decreases the heat transfer coefficient. However, it increase the total heat transfer.

(5) In CFB fin effectiveness is a function of suspension density. It increases, reaches a maximum and then

decreases. The fin effectiveness is observed to be in the range of 70 to 95 percent.

(6) Addition of fins in CFB changes the bed hydrodynamics. The voidage tends to increase at the finned section due to the hindrance of downflowing particles by the fins.

(7) Heat transfer coefficient is found to decrease with the increase of vertical height of the probe and vice versa.

(8) The residence time of particles on the wall calculated on the basis of experimental data is smaller for short probe and increases with the increase of vertical height of the probe.

(9) An empirical correlation has been suggested to evaluate heat transfer from the probes of different vertical heights. Prediction from the correlation has been verified with the experimental results for the dimensionless probe heights (L_h/D) in the range of 0.85 to 7.96.

(10) An empirical model for predicting heat transfer in a hot CFB incorporating all the concerned variables has been proposed and it has been verified with the experimental data of the present work as well as those of others.

(11) An analytical model for predicting heat transfer from finned surfaces in a cold CFB has been developed, both for long and short fins. Heat transfer coefficients evaluated from the predicted equation for long fins have been compared with the present experimental data and are found to be in good agreement.

Scope for Further Research

There is great scope for continuation of the work as given below :

The present study was performed at low bed temperature. It needs to be further explored at actual CFB boiler furnace temperature which is in the range of 800 - 900^{o}C.

To optimize fin geometry elaborate work is required to be performed for different fin shapes, fin heights, fin gaps, particle sizes and various other operating parameters.

The experiments can be extended to measure local heat transfer coefficients along the height of the riser column with the help of Gordon type heat flux sensor.

The measurement of elutriation and attrition and their effects on CFB heat transfer could be studied.

Studies on heat transfer and hydrodynamics in the return leg could be made.

Studies could further be made with multiple number of cyclone separators and also with impact separators without, or in addition to, the cyclone.

Bed material and their sizes may be varied to study their effect on heat transfer in CFB with finned surfaces.

The study of the effect of vertical probe height on heat transfer coefficient could further be extended for finned surfaces as well.

Experimental facilities could be developed for estimating cluster residence time and its effect on heat transfer.

A separate solid storage column in the return leg could be used to vary more conveniently the bed density.

The design of a proper air distributor system to widen the range over which it can be operated without fear of unsatisfactory fluidizing condition needs further experimental work.

More work with long continuous rectangular fins on membrane tube walls could be initiated.

To visualize the flow structure and further hydrodynamic study, a model of plexiglass riser column can be used.

Studies on various aspects of combustion of coal in CFB could be undertaken.

APPENDIX - A

Evaluation of Constants of Empirical Model

The expression of Z is given in Eq. (4.7) as

$$Z = a + bX$$

where 'a' and 'b' are constants which can further be expressed as

$$a = A_o + A_1 Y$$

and

$$b = B_o + B_1 Y$$

where constants A_o, A_1, B_o and B_1 have been evaluated from the present experimental data of unfinned surface. The parameters X and Y are given in Eqs. (4.3) and (4.5), viz.

$$X = \left(Pr \; \frac{c_{ps}}{c_{pg}} \; \frac{k_s}{k_g} \; \frac{\rho_g}{\rho_g} \; \varepsilon \right)$$

and

$$Y = \left(Ar \; \frac{U_o}{18U_T} \; \frac{U_o}{U_{mf}} \; \frac{d_b}{d_p} \; \frac{L_h}{d_b} \right)$$

The properties of the fluidizing and fluidized materials were evaluated [185] at a temperature of arithmetic mean of bed and surface.

(i) Fluidizing gas = air

(ii) Fluidized material = sand

(iii) Average bed temperature $= \left(\frac{72 + 92}{2} \right)^{\circ}C$

$= 355$ K

(iv) Average surface temperature = $\left(\frac{100 + 168}{2}\right)^{o}C$
= 407 K

(v) Average bulk temperature = 381 K

(a) Properties of air at 381 K :

density (ρ_g) = 0.9218 kg/m^3

specific heat (c_{pg}) = 1.0123 kJ/kg K

viscosity (μ_g) = 2.214×10^{-5} kg/ms

thermal conductivity (k_g) = 0.03242 W/mK

Prandtl number (Pr) = 0.69131

(b) Properties of sand at 381 K :

density (ρ_s) = 2350 kg/m^3

specific heat (c_{ps}) = 0.703 kJ/kg K

thermal conductivity (k_s) = 108.15 W/mk

mean particle size (d_p) = 310×10^{-6} m

Evaluation of minimum fluidizing velocity (U_{mf}) :

Here, the correlation of Grace [15] is used which is of the form

$$U_{mf} = 7.5 \times 10^{-4} \left(\frac{\rho_s - \rho_g}{\mu_g}\right) (d_p)^2 \times g$$

$$= 7.5 \times 10^{-4} \left(\frac{2350 - 0.9218}{2.214 \times 10^{-5}}\right) \times (310 \times 10^{-6})^2 \times 9.81$$

$$= 0.075 \text{ m/s}$$

Evaluation of terminal velocity (U_T)

For $0.4 < Re < 500$ Kunii and Levenspiel [20] suggested

$$U_T = \left(\frac{4}{225} \frac{(\rho_s - \rho_g)^2 g^2}{\rho_g \mu} \right)^{1/3} d_p$$

where d_p is the smallest particle size present in appreciable quantity (Table 5.2) which is $d_p = 217 \times 10^{-6}$ m

Therefore,

$$U_T = \left(\frac{4}{225} \frac{(2350 - 0.9218)^2 \times (9.81)^2}{(0.9218 \times 2.214 \times 10^{-5})} \right)^{1/3} \times 217 \times 10^{-6}$$

$$= 1.54 \text{ m/s}$$

The properties of fluidizing and fluidized materials are assumed constant. So,

$$X = \left(Pr \frac{c_{ps}}{c_{pg}} \frac{k_s}{k_g} \frac{\rho_s}{\rho_g} \varepsilon \right)$$

$$= \left(\frac{0.703}{1.0123} \cdot \frac{108.15}{0.03242} \cdot \frac{2350}{0.9218} \right) Pr \, \varepsilon$$

$$= (5905963.5) Pr \, \varepsilon$$

and

$$Y = \left(Ar \frac{U_o}{18U_T} \frac{U_o}{U_{mf}} \frac{d_b}{d_p} \frac{L_h}{d_b} \right)$$

$$= \left(Ar \frac{U_o^2}{U_{mf} U_T} \frac{L_h}{d_b} \right)\left(\frac{d_b}{18 d_p} \right)$$

$$= \left(\frac{0.1}{18 \times 310 \times 10^{-6}} \right)\left(Ar \frac{U_o^2}{U_{mf} U_T} \frac{L_h}{d_b} \right)$$

$$= (17.92115)\left(Ar \frac{U_o^2}{U_{mf} U_T} \frac{L_h}{d_b} \right) \times 10^{-6}$$

Table - A.4.1 : Values of X and Z

U_o (m/s)	ε	X	Z $(Nu_e)^*$
	0.9207	3962805	1.28905
5.6	0.9685	3952546	1.28905
	0.9677	3944032	1.33638
	0.9736	3978606	1.30062
6.5	0.9711	3962805	1.34882
	0.9694	3962805	1.30062
	0.9745	3978606	1.24506
7.2	0.9736	3978606	1.27777
	0.9723	3969919	1.28905
	0.9787	3995980	1.19401
8.2	0.9770	3995111	1.18425
	0.9745	3978606	1.19401
	0.9830	4005275	1.11196
9.1	0.9821	4009358	1.08710
	0.9813	4009358	1.08710
	0.9894	4037938	0.9278
11.4	0.9872	4029772	0.93975
	0.9864	4029685	0.96471

* Nu_e experimental Nusselt number

For six superficial velocities used in the present experiments the following six expressions for Z can be written as

$$Z_1 = a_1 + b_1X_1 \quad .. (A.1)$$

$$Z_2 = a_2 + b_2X_2 \quad .. (A.2)$$

$$Z_3 = a_3 + b_3X_3 \quad .. (A.3)$$

$$Z_4 = a_4 + b_4X_4 \quad .. (A.4)$$

$$Z_5 = a_5 + b_5X_5 \quad .. (A.5)$$

$$Z_6 = a_6 + b_6X_6 \quad .. (A.6)$$

where 'a' and 'b' are constants which can further be expressed in terms of Y for which

$$a = A_o + A_1Y \quad .. (A.7)$$

$$b = B_o + B_1Y \quad .. (A.8)$$

This problem can be solved in two steps. In the first step, using the data of the present experiments. (Tables 6.27 to 6.29) and Table A.4.1, and applying the technique of least square the constants were evaluated which are shown in Table A.4.2.

Table A.4.2 : Values of Y and constants (a,b)

U_o (m/s)	a	b	Y
5.6	7.97036	-0.16859×10^{-5}	1740900.3
6.5	16.66261	-0.38611×10^{-5}	2345441.2
7.2	6.57678	-0.13319×10^{-5}	2877814.6
8.2	44.23346	-1.07825×10^{-5}	3732720.8
9.1	38.593004	-0.93681×10^{-5}	4597064.4
11.4	18.94288	-0.44614×10^{-5}	7214521.3

In the second step, using the values of the coefficients (a,b) as determined and with the help of Table A.4.2 and applying the least square technique as before, the constants A_o, A_1, B_o and B_1 have been evaluated as follows :

$$A_o = 4.4805 \qquad B_o = -8.0314 \times 10^{-7}$$

$$A_1 = 1.85178 \times 10^{-7} \qquad B_1 = -4.6841 \times 10^{-14}$$

APPENDIX - B

Specifications of Measuring Instruments and Heaters

The operating ranges and accuracy limits of the measuring instruments and heaters are given below :

(1) Digital D.C. Microvoltmeter

Model : AGRONIC - 113

Make : India

Range : 0.1 μv to 1000 V in 6 ranges

Accuracy : $\pm$ 0.1 % of full scale $\pm$ 1 digit

Power required : 230 V, AC , $\pm$ 10 % , 50/60 Hz

(2) Source heater :

(i) Pilz - Heizbandage (Tape heater)

No : S25/050

Length : 5 m

Width : 25 mm

Capacity : 1250 W

Voltage : 220 V

Make : GMDH, W.Germany

(ii) Tape heater :

Cat. No : GL 91.06

Length : 3.66 m

Width : 25 mm

Capacity : 600 W

Voltage : 230 V

Make : Toshniwal, India

(iii) Tape heater :

Cat. No.	:	GL 91.05
Length	:	2.44 m
Width	:	25 mm
Capacity	:	400 W
Voltage	:	230 V
Make	:	Toshniwal, India

(iv) Tape heater :

Cat. No.	:	GL 91.04
Length	:	1.83 m
Width	:	25 mm
Capacity	:	300 W
Voltage	:	230 V

(v) Tape heater :

Cat. No.	:	GL 91.03
Length	:	1.22 m
Width	:	25 mm
Capacity	:	200 W
Voltage	:	230 V
Make	:	Toshniwal, India

(3) Guard heater :

Pilz - Heizbandage (Tape heater)

No.	:	SiS / 052
Length	:	5.2 m
Width	:	27 mm
Capacity	:	780 W
Voltage	:	220 V
Make	:	GMDH, W. Germany

APPENDIX - C

Design of Distributor

The distributor was made following the design outline given by Kunii and Levenspiel [20], Botlerill [35] and Basu [191]. It is a straight hole orifice type of distributor. The design considerations are given below :

Diameter of particle, d_p = 1 mm

Bed inventory, I = 30 kg

Operating velocity, U_{op} = 3.25 m/s

Voidage at minimum fluidization, ε_{mf} = 0.5

Diameter of the bed, D = 0.1 m

X-sectional area of the inlet of the windbox,

$$A_i = \frac{\pi}{4} (7.62 \times 10^{-2})^2 = 4.56 \times 10^{-3} \text{ m}^2$$

X-sectional area of the bed, $A_b = \frac{\pi}{4} (0.1)^2$

$$= 7.854 \times 10^{-3} \text{ m}^2$$

Density of solid particle (sand), ρ_s = 2350 kg/m^3

Density of air, ρ_g = 1.165 kg/m^3

Acceleration due to gravity, g = 9.81 m/s^2

Height of the bed at minimum fluidization

$$H_{mf} = \frac{\Delta p}{(1 - \varepsilon_{mf})\ \rho_s g} = \frac{(I.g\ /\ A_b)}{(1 - \varepsilon_{mf})\ \rho_s g} = \frac{I}{A_b \rho_s (1 - \varepsilon_{mf})}$$

$$= \frac{30}{(1 - 0.5) \times 7.854 \times 10^{-3} \times 2350} = 3.25 \text{ m}$$

(i) Bed pressure drop (Δp_b) :

$$\Delta p_b = \rho_s g\ H_{mf}\ (1 - \varepsilon_{mf})$$

$$= 2350 \times 9.81 \times 3.25 \times (1 - 0.5)$$

$$= 37461.94 \ \text{N/m}^2$$

(ii) Orifice diameter, (d_{or}) :

$$d_{or} = 3\ d_p = 3 \times 1 \times 10^{-3} = 3 \times 10^{-3} \text{ m}$$

(iii) Minimum distributor pressure drop for uniform distribution ($\Delta\ p_D$) :

$$\Delta p_D = \Delta p_b \left[0.01 + 0.2 \left[1 - \exp\left(\frac{-D}{2 \times H_{mf}}\right) \right] \right]$$

$$= 37461.94 \left[0.01 + 0.2 \left[1 - \exp\left(\frac{-0.1}{2 \times 3.25}\right) \right] \right]$$

$$= 489 \ \text{N/m}^2$$

(iv) Rearrangement resistance (Δp_R) :

$$\Delta p_R = \rho_g \left(\frac{(U_{op} \cdot (A_b/A_i))^2}{2\,g} \right)$$

$$= 1.165 \frac{(3.25 \times 1.72)^2}{2 \times 9.81}$$

$$= 1.86 \text{ N/m}^2 < \frac{\Delta p_D}{100}$$

For stable and uniform fluidization, the condition of $\Delta p_R < (\Delta p_D/100)$, is satisfied.

(v) Thickness of the distributor plate (t) :

$$t = 6 \text{ mm} = 6 \times 10^{-3} \text{ m} \quad \text{(selected)}$$

(vi) Orifice discharge coefficient (c_D) :
[Qureshi and Creasy (1979)]

$$c_D = 0.82 \left(\frac{t}{d_{or}} \right)^{0.13}$$

$$= 0.82 \times \left(\frac{6 \times 10^{-3}}{3 \times 10^{-3}} \right)^{0.13} = 0.897$$

(vii) Gas velocity through the orifice (U_{or})

$$U_{or} = c_D \left(\frac{2 \times \Delta p_D}{\rho_g} \right)^{1/2}$$

$$= 0.897 \left(\frac{2 \times 489}{1.165} \right)^{1/2}$$

$$= 26.23 \text{ m/s}$$

(viii) Number of orifices per square meter of distributor (N_{or}) :

$$N_{or} = \frac{U_{op}}{U_{or}} \times \frac{4}{\pi d_{or}^2}$$

$$= \frac{3.25}{26.23} \times \frac{4}{\pi \times (3 \times 10^{-2})^2}$$

$$= 17528.82 \ \frac{1}{m^2}$$

(ix) Total number of holes on perforated distributor

$$= N_{or} \times A_b$$

$$= 17528.82 \times 7.854 \times 10^{-3}$$

$$= 138$$

(x) Pitch of the orifices on the perforated plate

$$= \frac{1}{(N_{or})^{1/2}} = \frac{1}{(17528.82)^{1/2}}$$

$$= 7.55 \text{ mm} = 8 \text{ mm}$$

(xi) The open area in the distributor

$$= \frac{\pi}{4}(3 \times 10^{-3})^2 \times 138 = 9.76 \times 10^{-4} \ m^2$$

(xii) Percent opening $= \frac{9.76 \times 10^{-4}}{7.854 \times 10^{-3}} = 12.42 \ \%$

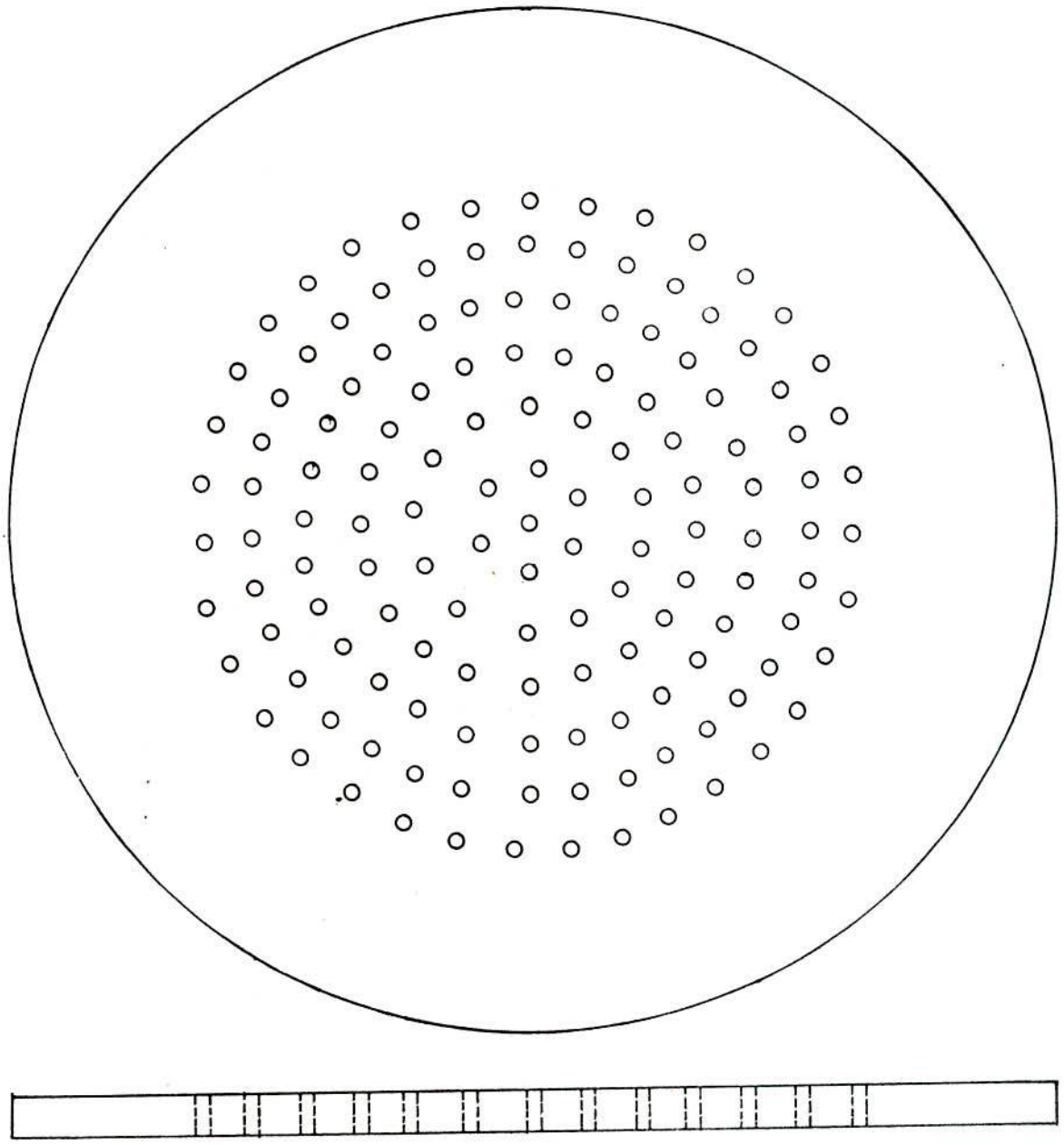

DIAMETER OF ORIFICE (d_o)	= 3 mm
PITCH	= 8 mm
THICKNESS OF DISTRIBUTOR PLATE	= 6 mm
TOTAL NUMBER OF HOLES	= 138
PERCENT OPENING	= 12.4 %

FIG. C 5.1 DETAILS OF THE DISTRIBUTOR

REFERENCES

1. Beer, J.M., 'The Fluidized Combustion of Coal', Proc. 6th International Symposium on Combustion, p. 439, (1976).

2. Dry, R.J. and LaNauze, R.D., 'Combustion in Fluidized Beds', Chemical Engineering Progress, p.31-47, July, (1990).

3. Beisswenger, H., Darling, S., Plass, L. and Wechster, A., 'Burning Multiple Fuels and Following Load in the Lurgi/Combustion Engineering Circulating Fluid-bed Boiler', Proc. 8th Int. Conf. on Fluid Bed Combustion, Houston, March, (1985).

4. Yerushalmi, J., 'An Overview of Commercial Circulating Fluidized Bed Boilers' in Circulating Fluidized Bed Technology, Ed. P. Basu, Pergamon Press, Canada, p. 97-104, (1986).

5. LaNauze, R.D., 'Combustion in Fluidized Beds' Ch.-I Advanced Combustion Methods, Ed. F.J. Weinberg, Academic Press, London (1986).

6. Gaglia, B.N. and Hall, A, 'Comparison of Bubbling and Circulating Fluidized Bed Industrial Steam Generation', Proc. 9th Int. Conf. on Fluidized Bed Combustion, Boston, May, (1987).

7. Hasatani, M., Furusawa, T. and Horio, M., (Ed.) 'Preface', Proc., 2nd SCEJ Symposium on Circulating Fluidized Beds, Tokyo, Japan, June, (1988).

8. Kobro, H. and Brereton, C., 'Control and Fuel Flexibility in Circulating Fluidized Beds', in Circulating Fluidized Bed Technology, Ed. P. Basu, Pergamon Press, Canada, p.263-272, (1986).

9. Herbertz, H., Lienhard, H., Barner, H.E. and Hansen, P.L., 'Effect of Fuel Quality on Solids Management in CFB Boilers', Proc. Tenth International Conference on Fluidized Combustion, San Francisco, ASME, Vol.I, p. 1-6, (1989).

10. Seshamani, M., Taylor, T. and Watanabe, S., 'Foster Wheeler Circulating Fluidized Bed Boilers', Proc. Third SCEJ Symposium on Circulating Fluidized Bed, Tokyo, Soc. of Chem. Engrs., Japan, p.142-152, June, (1989).

11. Grace, J.R., 'Heat Transfer in Circulating Fluidized Beds', in Circulating Fluidized Bed Technology, Ed. P. Basu, Pergamon Press, Canada, p.63-81, (1986).

12. Glicksman, L.R., 'Heat Transfer in Circulating Fluidized Beds', in Circulating Fluidized Fed Technology-II, Ed. P. Basu and J.F. Large, Pergamon Press, Canada, p.13-29, (1988).

13. Basu, P. and Large, J.F., Ed., Circulating Fluidized Bed Technology-II, Pergamon Press, (1988).

14. Basu, P. and Hasatani, M., Ed., Circulating Fluidized Bed Technology-III, being published by Pergamon Press.

15. Grace, J.R., 'Hydrodynamics of Gas Fluidized Beds', in Fluidized Bed Boilers : Design and Application, Ed. P. Basu, Pergamon Press, Canada, p. 13-30, (1984).

16. Zenz, F.A. and Othmer, D.F., 'Fluidization and Fluid-Particle Systems', Reinhold, New York, (1960).

17. Jahnig, C.E., Campbell, D.L. and Martin, H.Z., 'History of Fluidized Solids Developments at Exxon', in Fluidization, Ed. J.R. Grace and J.M. Matsen, Plenum, New York, (1980).

18. Squires, A.M. 'Contributions Towards a History of Fluidization', Joint Meeting of A.I.Ch.E. and Chem. Ind. and Engg., Soc. China, Beijing, Sept. 20-22, (1982).

19. Squires, A.M., 'The Story of Fluid Catalytic Cracking', in Circulating Fluidized Bed Technology, Ed. P. Basu, Pergamon Press, Canada, p. 1-19, (1986).

20. Kunii, D. and Levenspiel, O., 'Fluidization Engineering', John Wiley, New York, (1969).

21. Yates, J.G., Fundamentals of Fluidized Bed Chemical Processes, Butterworths, London, (1983).

22. Davidson, J.F., Clift, R. and Harrison, D., Fluidization , 2nd Edition, Academic Press, London, (1985).

23. Van Swaaij, W.P.M. and Afgan, N.H., Ed. Heat and Mass Transfer in Fixed and Fluidized Beds, Hemisphere Publishing Corporation, U.S.A., (1986).

24. Radovanovic, M., Ed., Fluidized Bed Combustion, Hemisphere Publishing Corporation, U.S.A. (1986).

25. Geldart, D., Ed. , Gas Fluidization Technology, John Wiley, Chichester, (1986).

26. Howard, J.R., Fluidized Bed Technology, Adam Hilger, Bristol and New York, (1989).

27. Pell, M., Gas Fluidization, Elsevier Science Publishers, (1990).

28. Yerushalmi, J. and Avidan, A., in Fluidization 2nd Edition, Ed. J.F. Davidson, R. Clift and D. Harrison, Academic Press, London, (1985).

29. Geldart, D. and Rhodes, M.J., 'From Minimum Fluidization to Pneumatic Transport - A Critical Review of the Hydrodynamics', in Circulating Fluidized Bed Technology, Ed. P. Basu, Pergamon Press, Canada, p. 21-32, (1986).

30. Kwauk, M., Ningde, W., Youchu, L., Bingyu, C. and Zhiyuan, S., 'Fast Fluidization at ICM', in Circulating Fluidized Bed Technology, Ed. P. Basu, Pergamon Press, Canada, (1986).

31. Matsen, J., 'The Rise and Fall of Recurrent Particles: Hydrodynamics of Circulation', in Circulating Fluidized Bed Technology-II, Ed. P. Basu and J.F. Large, Pergamon Press, Canada, p. 3-11, (1988).

32. Horio, M., 'Hydrodynamics of Circulating Fluidization - Present Status and Research Needs' Preprints for 3rd International Conference on Circulating Fluidized Beds, Nagoya, Japan, p. (PL4-1) - (PL4-11), Oct. 15-18, (1990).

33. Gelperin, N.I. and Einstein, V.G., 'Heat Transfer in Fluidized Beds', Fluidization, Ed. J.F. Davidson and D. Harrison, Academic Press, New York, p.471-540, (1971).

34. Baskakov, A.P., 'Heat Transfer in Fluidized Beds : Radiative Heat Transfer in Fluidized Beds', in Fluidization, 2nd Edition, Ed. J.F. Davidson, R. Clift and D. Harrison, Academic Press, London, (1985).

35. Botterill, J.S.M., 'Fluid Bed Heat Transfer', Academic Press, London, (1975).

36. Gutfinger, C. and Abuaf, N., 'Heat Transfer in Fluidized Beds', in Advances in Heat Transfer, Ed. J.P. Hartnett and T.F. Irvine, Jr., Vol. 10, p.167-217, (1974).

37. Saxena, S.C., Grewal, N.S., Gabor, J.D., Zabrodsky, S.S. and Galershtein, D.M., 'Heat Transfer Between a Gas Fluidized Bed and Immersed Tubes', in Advances in Heat Transfer, Ed. J.P. Hartnett and T.F. Irivine, Jr., Vol. 14, p.149-247, (1978).

38. Wu, R.L., Grace, J.R., Lim, C.J. and Brereton,C.M.H. 'Suspension-to-Surface Heat Transfer in a Circulating Fluidized Bed Combustor', A.I.Ch.E.J., Paper No. P01873, (1989b).

39. Basu, P. and Nag, P.K., 'An Investigation into Heat Transfer in Circulating Fluidized Beds', Int. J. Heat Mass Transfer, Vol. 30, No.11, p.2399-2409, (1987).

40. Basu, P., 'Heat Transfer in High Temperature Fast Bed', Chemical Engineering Science,Vol. 45, No.10, p. 3123-3136, Sept. (1990).

41. Leckner, B., 'Heat Transfer in Circulating Fluidized Bed Boilers', Preprints for 3rd Int. Conf. on Circulating Fluidized Beds, Nagoya, Japan, p.(PL5-1) - (PL5-9), Oct. 15-18, (1990).

42. Hoy, H.R. and Kaye, W.G., 'Work by the NCB on the Development of Atmospheric and Pressurized Fluidized Bed Combustion', J. Inst. Energy, 86, June, (1979).

43. Kullendroff, A. and Andersson, S., 'A General Review on Combustion in Circulating Fluidized Beds', in Circulating Fluidized Bed Technology, Ed. P. Basu, Pergamon Press, Canada, p. 83-96, (1986).

44. Basu, P., Ed., Circulating Fluidized Bed Technology, Pergamon Press, Canada, (1986).

45. Dow, W.M. and Jakob, M., 'Heat Transfer Between a Vertical Tube and Fluidized Air-Solid Mixture', Chem. Eng. Progress, Vol. 47, p. 637-684, (1951).

46. Leva, M. and Grummer, M., Chem. Eng. Progr., Vol. 48, p. 307, (1952).

47. Levenspiel, O. and Walten, J.S., 'Bed to Wall Heat Transfer in Fluidized Systems', Chem. Eng. Prog., Symposium Series, Vol. 50, No.9, p.1, (1954).

48. Wasen, D.T. and Ahluwalia, M.S., 'Consecutive Film and Surface Renewal Mechanism for Heat and Mass Transfer from a Wall', Chem. Eng. Sci., Vol. 24, p. 1535,(1969).

49. Van Heerden, C., Nobel, P. and Van Krevelen, D.W., 'Mechanism of Heat Transfer in Fluidized Beds', Ind. Eng. Chem., Vol. 45, No. 6, p. 1237, (1953).

50. Mickley, H.S. and Fairbanks, D.F., 'Mechanism of Heat Transfer to Fluidized Beds', A.I.Ch.E. Journal, Vol. 1, p. 374-384, (1955).

51. Glicksman, L.R., 'Heat Transfer in Fluidized Bed Combustors', in Fluidized Bed Boilers : Design and Application, Ed. P. Basu, Pergamon Press, Canada, p. 63-100, (1984).

52. Dunsky, V.D., Zabrodsky, S.S. and Tamarin, A.I., 'On the Mechanism of Heat Transfer Between a Surface and a Bed of Moving Particles', Proc. 3rd International Conf., Vol. 4, A.I.Ch.E., p. 193-297, (1966).

53. Baskakov, A.P., 'The Mechanism of Heat Transfer Between a Fluidized Bed and a Surface', Int. Chem. Eng., Vol.4, p. 320-324, (1964).

54. Patel, R.D., U.S. Atomic Energy Commission, ANL-7353, (1967).

55. Yoshida, K., Kunii, D. and Levenspiel, O., 'Heat Transfer Mechanisms Between Wall Surface and Fluidized Bed', Int. Journal of Heat and Mass Transfer, Vol. 12, p. 529-536, (1969).

56. Kubie, J. and Broughton, J., 'A Model of Heat Transfer in Gas Fluidized Beds', Int. J. Heat Mass Transfer, Vol. 18, p. 289-299, (1975).

57. Wunschmann, J. and Schlunder, E.V., Trans. Int. Conf. of Heat Transfer, CT2.1, p.49, (1975).

58. Zabrodsky, S.S., 'Hydrodynamics and Heat Transfer in Fluidized Beds', MIT Press, Cambridge, Massachusetts, (1966).

59. Botterill, J.S.M. and Williams, J.R., 'The Mechanism of Heat Transfer to Gas-Fluidized Beds', Transactions of the Institution of Chemical Engineers, Vol. 41, p. 217, (1963).

60. Botterill, J.S.M., Butt, M.H.D., Cain, G.L. and Redish, K.A., 'The Effect of Gas and Solids Thermal Properties on the Rate of Heat Transfer to Gas-Fluidized Beds', International Symposium on Fluidization, Eindhoven, Ed. A.A.H. Drinkenburg, Netherlands University Press, Amsterdam, p. 442-457, (1967).

61. Ziegler, E.N. and Brazelton, W., 'Mechanism of Heat Transfer to a Fixed Surface in a Fluidized Bed', Ind. Eng. Chem. Fundamental, Vol. 3, No. 2, 196, (1964).

62. Gabor, J.D., 'Wall-to-Bed Heat Transfer in Fluidized and Packed Beds', Chemical Engineering Progress Symposium Series, Vol. 66, No. 105, p. 76-86, (1970a).

63. Decker, N.A. and Glicksman, L.R., 'Comduction Heat Transfer at the Surface of Bodies Immersed in Gas Fluidized Beds of Spherical Particles, A.I.Ch.E. Symposium Series, Vol. 77, No. 208, p. 341-349, (1981).

64. Martin, H., Chem. Ing. Tech., Vol. 52, p. 199-209, (1980).

65. Martin, H., 'Heat Transfer Between Gas Fluidized Beds of Solid Particles and the Surface Immersed in Heat Exchanger Elements', Chem. Eng. Process, Vol. 18, p. 157-223, (1984).

66. Kolar, A.K., Grewal, N.S. and Saxena, S.C., 'Investigation of Radiative Contribution in a High Temperature Fluidized Bed Using the Alternate-Slab Model', Int. J. Heat Mass Transfer, Vol. 22, p. 1695-1702, Pergamon Press, U.K., (1979).

67. Kolar, A.K., Grewal, N.S., Saxena, S.C. and Gabor, J.D., 'On Gabor's Alternate-Slab Model', Numerical Heat Transfer (1980).

68. Yoshida, K., Ueno, T. and Kunii, D., Chem. Eng. Sci., Vol. 29, p. 77, (1974).

69. Gabor, J.D., 'Wall to Bed Heat Transfer in Fluidized and Packed Beds', Chem. Engng. Symp. Ser. 66 (105), 76, (1970).

70. Kiang, K.O., Lin, K.T., Nack, H. and Oxley, J.H., 'Heat Transfer in Fast Fluidized Beds', Fluidization Technology-II, Ed. D.C. Kearns, Hemisphere Publishing, (1976).

71. Subbarao, D. and Basu, P., 'Heat Transfer in Circulating Fluidized Beds', in Circulating Fluidized Bed Technology, Ed. P. Basu, Pergamon Press, Canada, p. 281-286, (1986).

72. Stromberg, L., 'Experiences of Coal Combustion in a Fast Fluidized Bed', Arch. Combustion, Vol. 1, p. 95 - 107, (1981).

73. Basu, P., Nag, P.K., Chen, B.H. and Shao, M., 'Effect of Operating Variables on Bed to Wall Heat Transfer in a Circulating Fluidized Bed', Chem. Eng. Comm., Vol. 61, p. 227-237, (1987).

74. Fraley, L.D., Lin, Y.Y., Hsiao, K.H. and Solbakken, A., 'Heat Transfer Coefficient in Circulating Fluidized Bed Reactor', ASME, Paper 83-ht-92, Scattle, (1983).

75. Wu, R.L., Lim, C.J., Chaouki, J. and Grace, J.R., 'Heat Transfer From a Circulating Fluidized Bed Membrane Walls', A.I.Ch.E. Symposium, Miami Beach, (1986).

76. Feugier, A., Gaulier, C. and Martin, G., 'Some Aspects of Hydrodynamics, Heat Transfer and Gas Combustion in Circulating Fluidized Beds', Proc. Int. Conference on Fluidized Bed Combustion, (1987).

77. Andersson, B.A., Johnson, F. and Leckner, B., 'A Probe for Heat Flow Measurements in Fluidized Bed Boilers, IEA AFBC Technical Meeting, May, (1987).

78. Furchi, J.C.L., Goldstein, Jr., L., Lombardi, G. and Mohseni, M., 'Experimental, Local Heat Transfer in a Circulating Fluidized Bed', in Circulating Fluidized Bed Technology-II, Ed. P. Basu and J.F. Large, Pergamon, Press, Canada, p. 263-270, (1988).

79. Sekthira, A., Lee, Y.Y. and Genetti, W.E., 'Heat Transfer in a Circulating Fluidized Bed', Paper presented at 25th National Heat Transfer Conference, Houston, TX, USA, July 24-27, (1988).

80. Wu, R.L., Lim, C.J., Chaouki, J. and Grace, J.R., 'Heat Transfer from a Circulating Fluidized Bed to Membrane Water Wall Cooling Surfaces', A.I.Ch.E., Journal, Vol. 33, No. 11, (1987).

81. Wu, R.L., Lim, C.J. and Grace, J.R., 'The Measurement of Instantaneous Local Heat Transfer Coefficients in a Circulating Fluidized Bed', The Canadian Journal of Chemical Engineering, Vol. 67, p. 301-307, April, (1989).

82. Sens, P.F. and Wilkinson, J.K., Fluidized Bed Combustor Design Construction and Operation, Elsevier Applied Science, London, (1988).

83. Bi, H. T., Jin, Y., Yu, Z. Q. and Bi, D. R., 'An Investigation on Heat Transfer in Circulating Fluidized Bed', Preprints for 3rd Int. Conf. on Circulating Fluidized Beds, Nagoya, Japan, p.(5-2-1) - (5-2-12), Oct. 15-18, (1990).

84. Zheng, Q., Wang, X. and Li, X., 'Heat Transfer in Circulating Fluidized Beds', Preprints for 3rd Int. Conf. on Circulating Fluidized Beds, Nagoya, Japan, p. (5-7-1) - (5-7-12), Oct. 15-18, (1990).

85. Liu De-Chang, Yang He-Ping, Wang Yang-Liang and Lin Zhi-jie, 'Experimental Studies of Heat Transfer in Circulating Fluidized Beds', Preprints for 3rd Int. Conf. on Circulating Fluidized Bed, Nagoya, Japan, Oct. 15-18, (1990).

86. Wen, C.Y. and Miller, E.N., 'Heat Transfer in Gas Solid Transport Line', Ind. Eng. Chem., Vol. 53, p. 51-53, (1961).

87. Baskakov, A.P. and Supron, V.M., 'The Determination of Convective Component of the Coefficient of Heat Transfer to a Gas in a Fluidized Bed', Int. Chem. Eng., Vol. 12, p. 53, (1972).

88. Baskakov, A.P., Vitt, O.K., Kirakosyan, V.A., Maskaev, V.K. and Filippovsky, N.F., 'Investigation of Heat Transfer Coefficient Pulsations and of the Mechanism of Heat Transfer From a Surface Immersed into a Fluidized Bed', Proc. Int. Symp., Fluid. Appl., Cepadues Editions Toulouse, p. 293, (1974).

89. Gabor, J.D., 'Heat Transfer to Particle Beds with Gas Flows Less Than or Equal to That Required for Incipient Fluidization', Chem. Eng. Sci., Vol. 25, p. 979, (1970b).

90. Botterill, J.S.M. and Denloye, A.O.O., 'A Theoretical Model of Heat Transfer to a Packed or Quiescent Fluidized Bed', Chem. Eng. Sci. Vol. 33, p. 509, (1987b).

91. Decker, N.A. and Glicksman, L.R., 'A Simplified Model for Heat Transfer from a Cylinder Immersed Within a Packed Bed', Chem. Eng. Sci., Vol. 35, p. 831, (1980).

92. Botterill, J.S.M. and Denloye, A.O.O., A.I.Ch.E 69th Annual Meeting, Paper No. 103e, Part-II, (1976).

93. Sathi, N., Liu, D.C., Yang, L.D. and Saxena, S.C., 'Heat Transfer Between a Vertical Tube and Air Fluidized Bed at Moderate Temperature', Int. J. Heat and Mass Transfer, Vol. 9, No. 5, p. 395, (1982).

94. Kharchenko, N.V. and Makhorin, K.E., J. Eng. Phys (English Translation), Vol. 7, p. 11, (1964).

95. Ilchenko, A.I. and Makhorin, K.E., Khim. Prom. No. 6, p. 443, (1967).

96. Botterill, J.S.M., Powder Technology, Vol. 14, p. 19, (1970).

97. Zabrodsky, S.S., 'Heat and Mass Transfer in Disperse Systems', Nauka i Tekh, Minsk., (1965).

98. Dunsky, V.D. and Tamarin, A.I., 'Heat and Mass Transfer in Disperse Systems', Nauka i Tekh, Minsk, (1965).

99. Vedamurthy, V.M. and Sastri, V.K.M., 'An Analysis of the Conductive and Radiative Heat Transfer to the Walls of Fluidized Bed Combustors', Int. J. Heat and Mass Transfer, Vol. 17, p.1, (1974).

100. Vedamurthy, V.M. and Sastri, V.M.K., 'An Experimental Study of the Influence of Bed Parameters on Heat Transfer in a Fluidized Bed Combustor', Future Energy Production System, Vol. II, Ed. J.C. Denton and N.H. Afgan, Hemisphere Publication Corporation, p. 589, (1976).

101. Basu, P., 'Bed-to-Wall Heat Transfer in a Fluidized Bed Coal Combustor', A.I.Ch.E. Sym., Vol. 74, No. 176, p. 187, (1978).

102. Flamant, G., 'Combined Radiative and Conductive Transient Heat Transfer Between a Wall and a Fluidized Bed', C.N.R.S., Laboratorie d'Energe'tique Solaine, B.P.5 - 66120, FONT-ROMEU-ODEILLO, FRANCE.

103. Petrie, J.C., Freeby, W.A. and Buckham, J.A., 'In Bed Heat Exchangers', Chemical Engineering Progress, Vol. 64, No. 7, p. 45-51, (1968).

104. Bartel, W.J., Genetti, W.E. and Grimmett, E.S., 'Heat Transfer from a Horizontal Discontinuous Finned Tube in a Fluidized Bed', Chem. Eng. Prog. Symp. Ser., Vol. 67, No. 116, p. 85-89, (1971).

105. Genetti, W.E., Schmall, R.A. and Grimmet, E.S., 'The Effect of Tube Orientation on Heat Transfer with Bare and Finned Tubes in a Fluidized Bed', A.I.Ch.E. Sym. Ser., Vol. 67, No. 116, 1971, p. 90-96, (1971).

106. Ziegler, E.N., Koppel, L.B. and Brazelton, W.T., 'Effect of Solid Thermal Properties on Heat Transfer to Gas Fluidized Beds', Industrial and Engineering Chemistry Fundamentals, Vol. 3, p. 324-328, (1964).

107. Elliot, D.E., Heaby, E.M. and Roberts, A.G., 'Fluidized Bed Heat Exchangers', Institute of Fuel, Paris, June (1971).

108. Gelperin, N.I., Einshtein, V.G. and Toskelbaev, I.N., Khin. Tekhnol. Tops., Masel 2, 42, (1972).

109. Bartel, W.J. and Genetti, W.F., 'Heat Transfer from a Horizontal Bundle of Bare and Finned Tubes in An Air Fluidized Bed', Chem. Eng. Progress Symposium Series, Vol. 68, No. 128, p. 84, (1973).

110. Natusch, H.J. and Blenke, H., Verfahrenstechnik, Vol.7, p. 293, (1973).

111. Gelperin, N.I., Einshtein, V.G., Toskubaev, I.N. and Ryspacu, Jr., N.S., TITChT, Vyp., Vol.1, p. 165 (1974).

112. Priebe, S.J. and Genetti, W.E., 'Heat Transfer from a horizontal bundle of Extended Surface Tubes to an Air Fluidized Bed', A.I.Ch.E. Sym. Ser, Vol. 73, No. 161, p. 38-43, (1977).

113. Genetti, W.E. and Kratovil, M.T., 83rd Natl. Meet A.I.Ch.E., Paper No. 4(b), (1977).

114. Chen, J.C. and Withers, J.G., 'An Experimental Study of Heat Transfer from Plain and Finned Tubes in Fluidized Beds', A.I.Ch.E. Sym. Ser, No. 174, Vol. 74, p. 327-333, (1978).

115. Staub, F.W., Kuwata, M., Ku, A.C. and Wood, R.T., 'Modelling of Flow Behaviour and Finned Tube Performance in the Turbulent Flow Regime', Proc. 6th Int. Conf., Flow Bed Combustion, Atlanta, Ga., Vol.3, April 9-11, p. 784-790, (1980).

116. Wood, R.T., Kuwata, M. and Staub, F.W., 'Heat Transfer to Horizontal Tube Banks in the Splash Zone of a Fluidized Bed of Large Particles', Fluidization, Proceedings of the International Fluid Conference, Henniker, N.H., Plenum Press, p. 235-242, Aug.3-8, (1980).

117. Krause, W.B. and Peters, A.R., 'Heat Transfer from Horizontal Serrated Finned Tubes in An Air Fluidized Bed of Uniformly Sized Particles', ASME, Journal of Heat Transfer, Vol. 105, p. 319-324, May, (1983).

118. Jakob, A. and Osberg, L. Canadian Journal of Chemical Engineering, Vol. 35, p. 5, (1957).

119. Richardson, J.F. and Mitson, A.E., Trans. Inst. Chem. Eng. (London), Vol. 36, p. 270, (1958).

120. Wen, C.Y. and Leva, M., A.I.Ch.E. Journal, Vol. 2, p. 482, (1956).

121. Gaffney, B.J. and Drew, T.B., Ind. Eng. Chem., Vol.42, p. 1120, (1950).

122. Wunder, R. and Mersmann, A., 'Heat Transfer Between Gas Fluidized Beds and Vertical Surfaces', German Chem. Eng. Journal, Vol. 2, No. 4, p. 242-248, (1979).

123. Baskakov, A.P., Berg,B.V., Vilt, O.K., Filippovsky, N.F., Kirakosyan, V.A., Goldobin, T.L. and Maskaev, V.B., Powder Technology, Vol. 8, No. 5/6, p. 273-282, (1973).

124. Decker, N. and Glicksman, L.R., 'Heat Transfer in Large Fluidized Beds', Int. J. Heat Mass Transfer, Vol. 26, No. 9, p. 1307-1320, (1983).

125. Mickley, H.S., and Trilling, C.A., 'Heat Transfer Characteristics of Fluidized Beds', Ind. Engg. Chem., Vol. 41, p. 1135-1147, (1949).

126. Wen, C.Y., King, D.F. and Shang, J., Proc. DOE/WVO Conference on Fluidized Bed Combustion System and Operation, Morgantown, p. 165-216, (1980).

127. Grewal, N.S. and Saxena, S.C., 'Effect of Distributor Design on Heat Transfer from an Immersed Horizontal Tube in a Fluidized Bed', Chem. Eng. J. Vol. 18, p.197, (1979).

128. Yerushalmi, J., Cankurt, N.T., Geldart, D. and Liss, B., 'Flow Regions in Vertical Gas-solid Contact System', A.I.Ch.E. Sym. Ser., Vol. 74, No. 176, p. 1-13, (1978).

129. Yerushalmi, J. and Cankurt, N.T., 'High Velocity Fluid Beds', CHEMTECH, Vol. 8, p. 564-571, (1978).

130. Yerushalmi, J. and Cankurt, N.T., 'Further Studies of the Regimes of Fluidization', Powder Technology, Vol.24, p. 187-205, (1979).

131. Weinstein, H., Graff, R.A., Meller, M. and Shao, M.J., in Fluidization , Ed. D. Kunii and R. Toei, Engineering Foundation, Paper Presented at the 1982 Annual A.I.Ch.E Meeting, Los Angeles, California, (1983).

132. Gajdos, L.J. and Bierl, T.W., Topical Report Submitted to US Department of Energy, NTIS No. FE-2449-6, (1978).

133. Hartge, E.U., Li, Y. and Werther, J., 'Analysis of the Local Structure of the Two-Phase Flow in Fast Fluidized Bed', in Circulating Fluidized Bed Technology, Ed. P. Basu, Pergamon Press, Canada, p. 153-159, (1986).

134. Matsen, J.M., in Fluidization Technology, Ed. D.K. Keairns, Hemisphere Publishing Co., Washington, Vol.II, p. 136, (1976).

135. Saxton, A.L. and Worley, A.C. Oil and Gas Journal, Vol. 68, No. 84, (1970).

136. Soo, S.L., Trezek, G.J., Dimick, R.C. and Hohnstreiter, G.F., I and E.C. Fund, Vol. 3, No. 98, (1964).

137. Horio, M., Taki, A., Hsieh, Y.S. and Muchi, I., in Fluidization, Ed. J.R. Grace and J.M. Matsen, Plenum Press, New York, p. 509, (1980).

138. Abed, R., in Fluidization IV, Ed. D. Kunii and R. Toei, Eng. Fnd., p. 137, (1983).

139. Grace, J.R. and Harrison, D., in Fluidization, I. Chem. E. (London), Sym. Ser. Vol. 105, No. 30, (1968).

140. Farrokhalaee, T. and Clift, R., in Fluidization Ed. J.R. Grace and J.M. Matsen, Plenum Press, New York, Vol. 135, (1980).

141. Whitehead, A.B., Gartside, G. and Dent, D.C., Powder Technology, Vol. 14, No. 61, (1976).

142. Abed, R., A.I.Ch.E. 74th Annual Meeting, Los Angles, Nov. 14-18, (1982).

143. Kwuak, M., Ningde, W., Youchu, L., Bingyu, C. and Zhiyuan, S., 'Fast Fluidization at ICM', in Circulating Fluidized Bed Technology, Ed. P. Basu, Pergamon Press, Canada, p. 34, (1986).

144. Brereton, C. and Stromberg, L., 'Some Aspects of the Fluid Dynamic Behaviour of Fast Fluidized Bed', in Circulating Fluidized Bed Technology, Ed. P. Basu, Pergamon Press, Canada, p. 133-143, (1986).

145. Rhodes, M.J., Laussmann, V.S. and Geldart, D., 'Measurement of Radial and Axial Flux Variation in the Riser of a Circulating Fluidized Bed', in Circulating Fluidized Bed Technology-II, Ed. P. Basu and J.F. Large, Pergamon Press, Canada, p. 155-164, (1988).

146. Horio, M., Morisita, K., Tachibana, O. and Murata, N., 'Solid Distribution and Measurement in Circulating Fluidized Beds', in Circulating Fluidized Bed Technology-II, Ed. P. Basu and J.F. Large, Pergamon Press, Canada, p. 147-154, (1988).

147. Bolton, L.W. and Davidson, J.F., 'Recirculation of Particles in Fast Fluidized Risers', in Circulating Fluidized Bed Technology-II, Ed. P. Basu and J. F. Large, Pergamon Press, Canada, p. 139-146, (1988).

148. Li, Y. and Kwauk, M., in Fluidization, Ed. J.R. Grace and J.F. Matsen, Plenum Press, London, p. 537, (1980).

149. Li, J., Tung, Y. and Kwuak, M., 'Axial Voidage Profiles of Fast Fluidized Beds in Different Operating Regions', in Circulating Fluidized Bed Technology-II, Ed. P. Basu and J.F. Large, Pergamon Press, Canada, p. 193-1204, (1988).

150. Yang, W.C., 'A Model for the Dynamics of a Circulating Fluidized Bed Loop', in Circulating Fluidized Bed Technology-II, Ed. P. Basu and J.F. Large, Pergamon Press, Canada, p. 181-192, (1988).

151. Rhodes, M.J. and Geldart, D., 'The Hydrodynamics of Recirculating Fluidized Beds', in Circulating Fluidized Bed Technology, Ed. P. Basu, Pergamon Press, Canada, p. 193-199, (1986).

152. Mickley, H.S., Fairbanks, D.F. and Hawthorn, R.D., Chem. Eng. Progr. Sym. Ser. No. 32, Vol. 57, p.51,(1961).

153. Koppel, L.B., Patel, R.D. and Holmes, J.T., A.I.Ch.E. Journal, Vol. 16, p. 456, (1970).

154. Ozkaynak, T.F. and Chen, J.C., 'Average Residence Times of Emulsion and Void Phases at the Surface of Heat Transfer Tubes in Fluidized Beds', The American Institute of Chemical Engineers, Vol. 74, No. 174, p. 334-343, (1978).

155. Subbarao, D., 'Clusters and Lean Phase Behaviour', Powder Technology, Vol. 46, p. 101-107, (1986).

156. Subbarao, D. and Basu, P., 'A Model for Heat Transfer in Circulating Fluidized Beds', Int. J. Heat Mass Transfer, Vol. 29, p. 487-489, (1986).

157. Chen, J.C., Dou, S.S. and Cimini, R.J., 'A Theoretical Model for Simultaneous Convective and Radiative Heat Transfer in Circulating Fluidized Beds', in Circulating Fluidized Bed Technology-II, Ed. P. Basu and J.F. Large, Pergamon Press, Canada, p. 255-262, (1988).

158. Biyikli, S., Tuzla, K. and Chen, J.C., 'A Phenomenological Model for Heat Transfer in Free board of Fluidized Beds', The Canadian Journal of Chemical Engineering, Vol. 67, p. 240-246, April, 1989.

159. Mahalingam, M. and Kolar, A.K., 'Heat Transfer Model For the Membrane Wall of A High Temperature Circulating Fluidized Bed', Preprints for the 3rd. Int. Conf. on Circulating Fluidized Beds, Nagoya, Japan, p.(5-4-1) - (5-4-14), Oct. 15-18, (1990).

160. Nag, P.K. and Moral, M.N.A., 'Prediction of Heat Transfer in Circulating Fluidized Beds', Preprints for the 3rd. Int. Conf. on Circulating Fluidized Beds, Nagoya, Japan, p.(5-6-1) - (5-6-18), Oct. 15-18, (1990).

161. Rhodes, M.J. and Geldart, D., 'A Model for the Circulating Fluidized Bed', Powder Technology, Vol. 53, p. 155-162, (1987).

162. Kunii, D. and Levenspiel, O., 'Flow Modelling of Fast Fluidized Beds', Preprints for the 3rd Int. Conf. on Circulating Fluidized Beds, Nagoya, Japan, p(4-7-1) - (4-7-8), Oct. 15-18, (1990).

163. Heng Zhang, Chen, Y. and Hasatani, M., Yusheng 'Mathematical Modelling for Longitudinal Voidage Distribution of Fast Fluidized Beds', Preprints for the 3rd Int. Conf. on Circulating Fluidized Beds, Nagoya, Japan, p.(4-13-1) - (4-13-6), Oct. 15-18, (1990).

164. Schlunder, E.U., Chem. Ing. Tech., Vol. 43, p. 651 - 654, (1971).

165. Genetti, W.E. and Knudsen, J.G., 'Heat Transfer in a Dilute Phase Heat Exchanger', I. Chem. Engg. Sym. Ser., Vol. 30, No. 147, (1968).

166. Ismail, S. and Chen, J.C., 'Volume Fraction of Solids in the Freeboard Region of Fluidized Beds', A.I.Ch.E. Sym. Ser., Vol. 80, p. 114-118, (1984).

167. Biyikli, S., Tuzla, K. and Chen, J.C., 'Particle Contact Dynamics on Tubes in the Freeboard Region of Fluidized Beds', A.I.Ch.E. Journal, Vol. 33, p.1225 - 1227, (1987a).

168. Bird, R.B., Stewart, W.E. and Lightfoot, E.N. 'Transport Phenomena', John Wiley and Sons, New York, p.289, (1960).

169. Wen, C.Y. and Chen, L.H., A.I.Ch.E. Journal, Vol.28, p. 117, (1982).

170. Toomey, R.D. and Johnstone, H.F. Chem. Eng. Sym. Ser. Vol. 49, p. 54, (1953).

171. Lewis, L.S., Gilliland, E.R. and Lang, P.M., CEP Sym. Ser. Vol. 58, No. 38, p. 65, (1962).

172. Leung, L.S., Chong, Y.O. and Lottes, J., Powder Technology, Vol. 49, p. 271, (1987).

173. Li, Youchu, Chemical Metallurgy, 4, 20, (1980).

174. Grace, J.R., 'Fluidized Bed Hydrodynamics', Chapter 8.1 in Handbook of Multiphase Systems, Ed. G. Hetsroni, Hemisphere, Washington, (1982).

175. Saxena, S.C. and Vogel, G.J., 'The Measurement of Incipient Fluidization Velocities in a Bed of Coarse Dolomite at Temperature and Pressure', Trans. Instn. Chem. Engrs., Vol. 55, No. 184, (1977).

176. King, D.F. and Harrison, D., 'The Dense Phase of a Fluidized Bed at Elevated Pressures', Trans. Inst. Chem. Engrs., Vol. 60, No. 26, (1982).

177. Geldart, D., 'Types of Gas Fluidization', Powder Technology, 7, p. 285-292, (1973).

178. Geldart, D., and Abrahamsen, A.R., 'Homogeneous Fluidization of Fine Powders Using Various Gases and Pressures', Powder Technol, 19, 133, (1978).

179. Stewart, P.S.B. and Davidson, J.F., 'Slug Flow in Fluidized Beds', Powder Technol., 1, 61 (1967).

180. Yerushalmi, J., Turner, D.H. and Squires, A.M., 'The Fast Fluidized Bed', I and EC Process Design and Development, Vol. 15, p. 47, Jan. (1976).

181. B.S. Code Lo42 : (1943).

182. Eckert, E.R.G. and Drake, Jr., R.M., Analysis of Heat and Mass Transfer, McGraw-Hill, Kogakusha, Japan, (1972).

183. Bennett, C.O. and Myers, J.E., Momentum, Heat and Mass Transfer, McGraw-Hill, U.S.A., (1962).

184. Hottel, H.C. and Sarofim, A.F., Radiative Transfer, McGraw-Hill, New York, (1967).

185. Özisik, M.N., Heat Transfer - A Basic Approach, McGraw-Hill, Singapore, 3rd Edition, (1988).

186. Tung, Y., Li, J. and Kwauk, M., 'Radial Voidage Profiles in Fast Fluidized Beds', in Fluidization, Ed. M. Kwauk and D. Kunii, Science Press, Beijing, p.139-145, (1988).

187. Mikhailov, M.D. and Özisik, M.N., Unified Analysis and Solutions of Heat and Mass Diffusion, John Wiley and Sons, U.S.A., (1984).

188. Arpaci, V.S., Conduction Heat Transfer, Addision-Wesley Publishing Co., U.S.A. (1966).

189. Mclachlan, N.W., Bessel Functions for Engineers, Clarendon Press, Oxford, (1955).

190. Kreith, F. and Bohn, M.S., Principles of Heat Transfer Harper and Row Publishers, New York, 4th Edition, (1986).

191. Basu, P., 'Design of Gas Distributor for Fluid Bed Boilers', in Fluidized Bed Boilers Design and Application, Ed. P. Basu, Pergamon Press, Canada, p. 45-62, (1984).

192. Myers, G.E., Analytical Methods in Conduction Heat Transfer, McGraw-Hill, U.S.A. (1971).